UNIVERSITAT DE BARCELONA

Departament d'Astronomia i Meteorologia

Broadband emission from high-energy processes in microquasars

Memòria presentada per
Valentí Bosch i Ramon
per optar al grau de
Doctor per la Universitat de Barcelona
Barcelona, gener de 2006

Programa de Doctorat d'Astronomia i Meteorologia

Bienni 2002–2004

Memòria presentada per **Valentí Bosch i Ramon** per optar al grau de Doctor per la Universitat de Barcelona

Director de la tesi

Dr. Josep Maria Paredes Poy

Dedicatori

Dedico aquesta tesi a la Rosa i a la Pilar. La primera em va precedir en el camí a través d'aquest món fantàstic que és la ciència. La segona em va iniciar en la curiositat per tot allò que veiem quan aixequem els ulls cap al cel en una nit clara.

Agraïments

Agraïments / Agradecimientos / Acknowledgments

Primer de tot, vull agrair als meus pares, en Josep i la Pilar, el seu esforç per donar-me una educació que m'ha permès encarar les dificultats i els reptes vitals amb els recursos necessaris, així també com la transmissió d'uns valors que em són referent i guia. També vull mencionar el meu germà petit, l'Eduard, pel qual sento una responsabilitat especial, sent ell una gran motivació per a mi per lluitar a la vida. Faig extensiu el meu agraïment a la resta de la meva família, especialment als meus avis, pel seu recolzament i estima incondicionals. I no puc deixar de fer esment dels bons amics que m'han envoltat sempre, els quals han aportat i aporten un gran valor a la meva existència.

El meu jo professional no seria res sense la col·laboració del meu amic i director de tesi, el doctor Josep Maria Paredes. El seus seny, experiència, coneixements, sapiència vital i, per sobre de tot, paciència amb el meu caràcter un pèl explosiu, han permès que jo pogués desenvolupar les meves capacitats de treball en el camp de l'astrofísica sense patiment, amb tranquil·litat i bon fer -principalment el seu-. La seva guia, que mai ha sigut inflexible sinó, ans al contrari, més aviat confiada en el meu criteri -quan calia-, ha sigut vital per fer que aquesta tesi hagi arribat a bon port. A més, a través d'en Josep Maria he treballat amb grans investigadors, tan joves com consolidats, els quals han aportat molt, tant al treball desenvolupat en equip com a mi mateix, a nivell professional i personal.

El doctor Gustavo Romero es uno de estos colaboradores y un gran amigo mío con el cual he aprendido mucho. Hemos mantenido extensas discusiones intelectuales tanto relacionadas con el trabajo como en un contexto de ocio, todas ellas tan profundas como estimulantes. Su participación en los trabajos realizados a lo largo de la tesis es muy importante, destacando entre otros los que desarrollamos en parte

en el Instituto Argentino de Radioastronomía (IAR), cerca de Buenos Aires, y en la Universidad Nacional de la Plata, en los años 2003 y 2005.

També de gran significació per al meu desenvolupament com a investigador ha sigut el tenir a prop una persona com el doctor Marc Ribó. Treballador incansable, rigorós i amb amplis coneixements tot i la seva joventut, en Marc, a més de col·laborador en treballs de recerca, ha sigut el meu "germà gran"durant les primeres etapes de la meva formació com a científic, dedicant moltes hores a repassar i millorar treballs nostres en els quals ell no figurava com a autor.

Another scientist that has played a role of great relevance during my scientific formation process is the doctor Felix Aharonian. Felix hosted me during my staying in the Max Planck Institut für Kernphysik (MPIfK) in Heidelberg, Germany, in 2004 and 2005, collaborating with us in several works and on-going projects. He has been a constant stimulus and a source of knowledge for me, our scientific discussions being very fruitful.

I want to acknowledge the support, which goes beyond the professional plane, given by the doctor Dmitry Khangulyan. Mitya has been a good friend and an excellent host -here I must thank also his wife, (Dr.) Natasha-. He has put under test my knowledge in physics, which appears really small when compared with his own, enriching much our scientific collaboration.

Tengo que hacer aquí también reconocimiento de la importante ayuda prestada por la doctora Marina Kaufman Bernadó, buena amiga i colega, la cual ha sido muy importante en momentos clave, destacando su casi maternal apoyo durante mi estadía en Argentina el año 2003. Mi agradecimiento va también para mi buen amigo y anfitrión el doctor Simon Vidrih, marido de Marina.

En Pol Bordas és el meu "germà petit". Incorporat al grup des de fa un any i mig, la seva presència ha sigut enriquidora per a mi en diferents aspectes: personalment és un amic, professionalment un bon company, i ha permès que comencés a fer ús de les meves dots didàctiques amb ell, cal dir que amb paciència.

Un altre membre del meu grup amb el qual també he tingut l'oportunitat de col·laborar és el doctor Josep Martí, al qual he d'agrair-li el seu tracte excel·lent, des del primer dia, així com els fruits del treball realitzat en comú.

Quiero agradecer a la doctora Paula Benaglia su apoyo durante mis viajes a

Argentina, así como su amistad. Hago extensivo este reconocimiento a la familia Paula-Gustavo-Blumina, con los cuales me he sentido como en mi propia casa.

Al doctor Diego Torres agradezco su positiva contribución en trabajos conjuntos así como las interesantes conversaciones y discusiones mantenidas alrededor del mundo -Catalunya, la China, Argentina, etcétera-.

I want to thank doctor Evgeny Derishev for his help in plasma physics and radiative processes, for his patience and disposition to spend time answering my questions, being also a friend with whom I have had very interesting discussions.

Als doctors Joan García-Sánchez i Marta Peracaula, tots dos membres del grup, agraeixo la seva ajuda en diferents moments de la tesi.

I thank doctor Indranil Chattopadhyay for the interesting conversations in science and geopolitics, keeping always in my memory those nice days in Corsica - Simon and Marc enjoyed them too-. I must acknowledge doctor Frank Rieger for nice scientific and philosophical discussions.

Agradezco al doctor Félix Mirabel su confianza y las interesantes charlas mantenidas con él durante nuestros encuentros en los más variopintos lugares del mundo en América, Europa y Asia.

Vull agrair l'ajuda del doctor Pau Reig quan m'estava barallant amb l'anàlisi de dades de raigs X del satèl·lit CHANDRA primer, i d'RXTE després. I also thank doctor Jon M. Miller for his help to treat RXTE data in a proper way, as well as for hosting me during my short staying in the Center for Astrophysics in Cambridge, USA, in 2003.

I would like to thank doctor John Kirk for our scientific discussions during my staying in the MPIfK. I also acknowledge the kind help provided by doctor Heinz Vöelk during my staying in MPIfK when he was director of the astrophysics group, in 2004. I must mention the interesting and fruitful discussions held with the PhD students and postdocs of the astrophysics group of MPIfK, which was a great environment for my scientific development.

En el temps durant el qual he desenvolupat la meva activitat al Departament d'Astronomia i Meteorologia (DAM), he compartit despatx amb diferents persones les quals voldria anomenar, tot agraint la seva companyonia durant les llargues

hores de treball en l'espai comú: el doctor David Fernández, el doctor Octavi Fors, la Maite Merino, i en Pol Bordas. De l'Octavi he de dir que em va aconsellar també en alguns aspectes de la tesi i amb qui sempre hi podia haver un breu descans tot conversant sobre els més variats temes. I also shared office during my stages in MPIfK and IAR with Olivia Tsang, doctor Gustavo E. Romero, Marianne Lemoine and doctor Dmitry Khangulyan.

Vull agrair al personal d'administració del DAM, per la seva amabilitat i ajuda en totes les qüestions burocràtiques que he hagut d'afrontar. Vull agrair especialment al JR la seva paciència amb mi sempre que l'he perseguit amb munts de dubtes.

Agraeixo a en Chema Torrelles la seva ajuda en el meu primer viatge a Estats Units. Ell va jugar un paper important en el meu primer contacte amb l'astronomia fora dels llibres.

Vull agrair als doctorands i postdocs, i d'altres membres col·laboradors i/o contractats del DAM, així com a professors titulars i catedràtics, els bons moments que he passat amb vosaltres en aquesta casa. Cal dir que la meva experiència personal ha sigut magnífica al DAM, on m'agradaria poder desenvolupar en el futur la meva tasca investigadora.

Finally, I thank different institutions that have supported my research task in any way during the development of this thesis: Ministerio de Educación y Ciencia, Universitat de Barcelona, DAM, CONICET, IAR and MPIfK.

Una llista exhaustiva de totes les persones que mereixen el meu reconeixement i agraïment seria massa llarga. Si algú no es troba representat en aquests agraïments mereix de ser-hi i mereix també una disculpa. En realitat, la quantitat de gent a qui faig extensiu el meu reconeixement, i el perquè del qual, difícilment podria ser encabida en aquesta tesi. If I missed someone in the acknowledgments, he/she deserves to be there as well as my apologies. Actually, the amount of people for whom I feel gratitude is too large making these acknowledgments hardly exhaustive -and somewhat unfair-.

Contents

Resum de la tesi: Emissió multilongitud d'ona generada per processos d'alta energia als microquàsars

Abans de començar a presentar els treballs realitzats al llarg d'aquesta tesi, anem a resumir el tema de la manera més didàctica possible. Aquest resum no pretén ser ni exhaustiu ni comprensiu a l'hora de parlar de microquàsars en general o de la tesi mateixa, sinó que vol posar sobre la taula la qüestió més important que envolta el camp de l'estudi dels microquàsars: quina física hi ha darrera de la radiació que podem observar; a més, també intenta explicar quina és la contribució que fa aquesta tesi a l'hora de respondre-la. Així, evitarem entrar en detalls tècnics relatius a les observacions i a les teories físiques aplicades, exposant tot plegat de manera esquemàtica. Per un aprofundiment en els temes tractats, una veritable introducció a la bibliografia, i un coneixement detallat de l'aportació dels treballs aquí presentats, recomanem la lectura de tota la tesi. Al final del resum llistem les conclusions principals assolides en els treballs realitzats.

Fem notar que en aquest resum farem ús del terme 'jet' per referir-nos al fluid de plasma magnetitzat, movent-se a velocitats relativistes, que caracteritza als microquàsars.

1. Una visió general sobre els microquàsars

Els microquàsars són sistemes formats per dos objectes, un d'ells pot ser una estrella d'alta massa que es troba en la seqüència principal o en fase de supergegant, o una estrella de baixa massa en fase terminal de la seva existència, l'altre pot ser una estrella de neutrons[1] o un forat negre[2]. Hi ha transferència de matèria des de la companya estel·lar cap a l'objecte compacte (sigui estrella de neutrons o forat negre). La matèria és perduda per la companya a través d'un fort vent o per superació del punt de Lagrange intern del sistema[3]. En el cas d'estrelles d'alta massa, tots dos mecanismes es poden donar, mentre que només el segon és operatiu per estrelles de baixa massa. Aquesta matèria atrapada en el pou de gravetat de l'objecte compacte no segueix un moviment rectilini cap al centre d'atracció sinó que, degut a que originalment tenia una certa velocitat tangencial, cau fent voltes i formant una mena de disc.

Quan el disc es forma, la matèria segueix caient sobre l'objecte compacte però ho fa més lentament. A mesura que cau pateix un cert fregament degut a un procés físic viscós l'origen del qual no està ben determinat. Aquest fregament dissipa energia elevant la temperatura de la matèria, que aviat es converteix en un plasma fortament ionitzat[4] que emet una part significativa de l'energia cinètica assolida amb la caiguda

[1] Antic estel que ja no produeix llum a través de reaccions de fusió nuclear en el seu nucli i que, degut a la seva gran massa, pateix una auto-compressió gravitatòria que només la pressió de degeneració dels neutrons pot aturar. La matèria de l'objecte es troba formada bàsicament per neutrons, que en les condicions de pressió, densitat i temperatura donades són estables. La densitat és tan alta, que una massa semblant a la del Sol està confinada en un espai de deu quilòmetres de radi (el radi del Sol és de $\sim 6.9 \times 10^5$ km).

[2] Quan la força nuclear forta no és prou gran com per frenar el col·lapse, l'estel mort segueix comprimint-se fins que el seu radi es tal (~ 9 km) que, a la seva superfície, la gravetat és tan forta que ni la llum pot escapar. L'objecte segueix empetitint-se fins a convertir-se en quelcom de mida $\leq 10^{-33}$ cm que té una massa igual o superior a tres vegades la del Sol, però des del moment en que la llum no pot escapar ja s'ha convertit en un forat negre. Segueix allà, i la seva gravetat té efectes sobre l'entorn (e.g. la matèria de la companya estel·lar), però cap informació (e.g. llum) pot sortir del seu interior.

[3] Sobre la línia recta que uneix els centres dels dos objectes, hi ha un punt on la gravetat generada per un i per l'altre es compensa. Si les capes externes de l'estrella companya superen aquest punt, començaran a caure sobre l'objecte compacte.

[4] Matèria en la que els àtoms han perdut alguns o tots els electrons que giren al voltant dels nuclis. Aquests electrons es mouen doncs lliurement, juntament amb els ions (el que resta de l'àtom), formant tot plegat un gas ionitzat.

cap al centre atractor, al voltant d'un 10%, en forma de raigs X. Aquests objectes, si no presenten majors peculiaritats són anomenats binàries de raigs X, ja que són sistemes binaris que emeten fortament en raigs X.

Els processos físics que tenen lloc i que expliquen l'emissió als discos de les binàries de raigs X es coneixen aproximadament. Però les binàries de raigs X no sempre presenten una radiació X amb igual distribució dels fotons en energia (i.e. presentant el mateix espectre). A vegades aquesta emissió es troba concentrada al voltant d'1 keV (fotons $\sim 10^3$ vegades més energètics que els que es poden veure) i s'anomena de cos negre, a vegades l'emissió s'estén fins 100 keV o més de manera significativa, i es diu que l'espectre segueix una llei de potència[5]. A voltes, es radia fins i tot més energia a 100 keV que a 1 keV. Es creu que aquesta emissió amb espectre de llei de potència s'origina quan la matèria del disc és poca i, escalfant-se, s'infla i modifica les seves propietats emissores, encara que això ja no està tan ben establert (per una revisió sobre aquestes qüestions, veure Barret 2004). L'origen de l'emissió en forma de llei de potència no és clar, ja que existeix l'alternativa que aquesta radiació s'origini no al disc (sigui normal o inflat, i.e. prim o gruixut), sinó a dos jets de plasma que és mouen relativísticament en tots dos sentits i en la direcció perpendicular al disc. Aquests jets s'originarien amb la participació de forts camps magnètics presents al veïnatge de l'objecte compacte. Podria ser fins i tot que una part de la radiació X s'originés en aquest disc gruixut (a vegades anomenat corona), i una part en aquests jets.

Els jets existeixen, contenen partícules relativistes i camp magnètic (per una revisió del tema, veure Mirabel & Rodríguez 1999). S'han observat fotons d'energies molt baixes (i.e. longituds d'ona molt llargues, de ràdio, amb fotons $\sim 10^{-5}$ vegades menys energètics que els visibles) originats en la interacció de les partícules relativistes amb el camp magnètic (i.e. emissió sincrotró). De fet, és la presència de jets ràdio amb velocitats properes a la de la llum el que caracteritza als microquàsars, terme l'ús del qual es va estendre fa uns 15 anys a partir dels treballs de Mirabel et al. (1992) i Mirabel & Rodriguez (1994) (veure la Fig. 1 per una representació pictòrica d'un microquàsar). Fins i tot hi ha evidències observacionals de la presència en aquests jets de partícules amb energies altíssimes (Corbel et al. 2002), i això podria explicar l'emissió molt per sobre de 100 keV (> 1 MeV o fotons $> 10^6$ vegades més energètics que els visibles, anomenats gamma) que s'ha obser-

[5]Quan representem la distribució dels fotons en funció de l'energia posant els eixos de la gràfica de manera logarítmica, s'obté una línia recta.

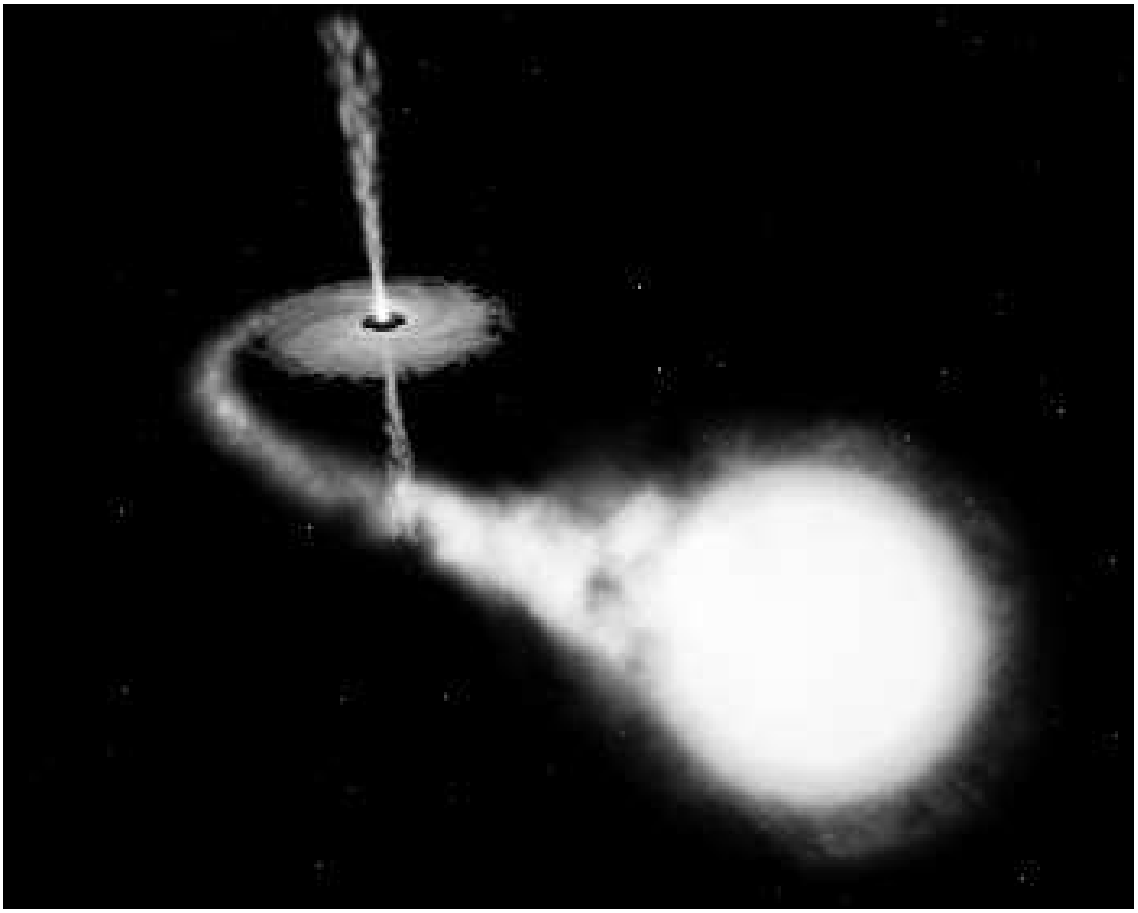

Figura 1: Representació artística d'un microquasar. No està feta a escala (http://hubblesite.org/newscenter/newsdesk/archive/releases/2002/30/).

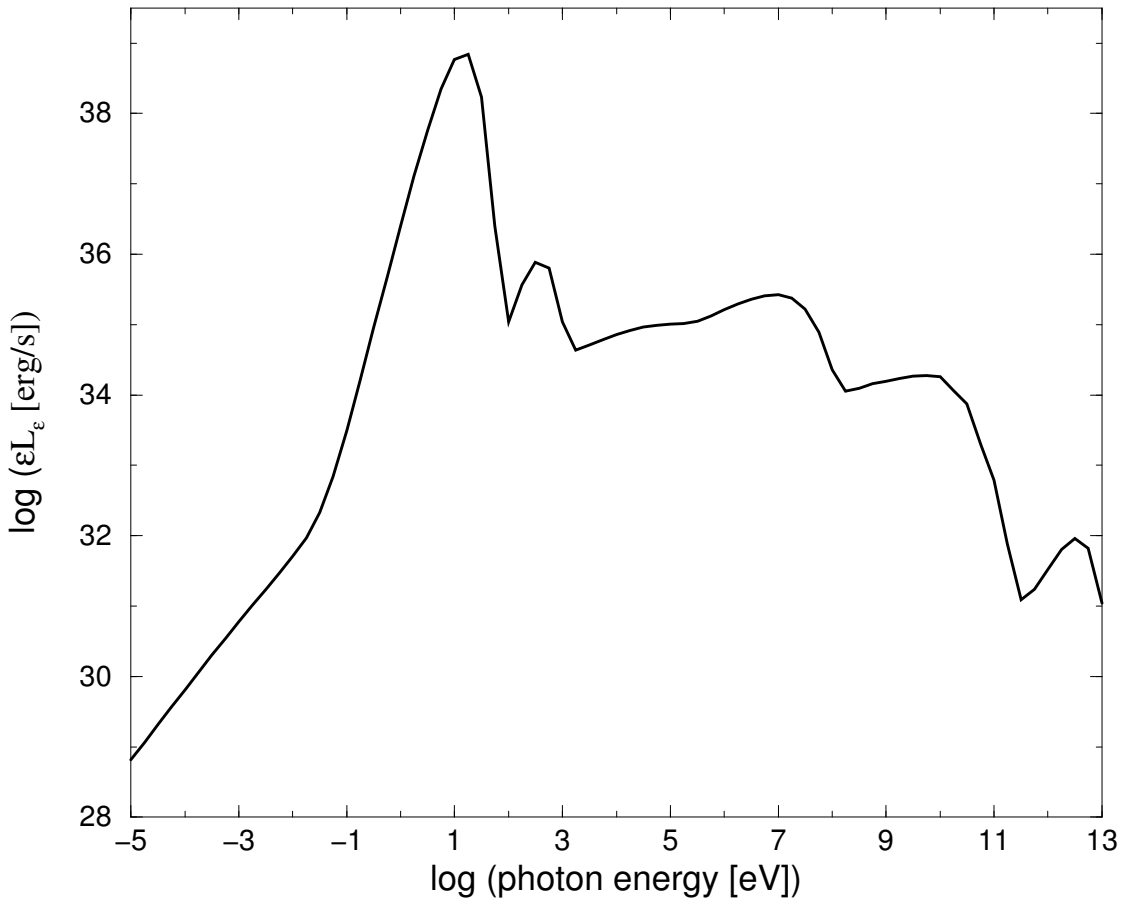

Figura 2: Representació sintètica del que seria la distribució espectral d'energia d'un microquàsar des de ràdio (10^{-5} eV) fins a raigs gamma de molt alta energia (10^{12} eV).

vat en alguns microquàsars (Paredes et al. 2000), sense poder establir encara que aquesta radiació tan energètica provingui dels jets. Se sap de l'existència d'aquestes partícules per la seva emissió sincrotró en raigs X estesa amb forma de jet (aquesta emissió X no estaria associada directament al microquàsar sinó a les regions més externes dels jets). L'emissió tan energètica, que arriba a voltes fins a TeV (Aharonian et al. 2005) (10^9 vegades més energètica que els raigs X), no presenta forma de jet, sinó que sembla provenir d'un punt dins la capacitat de resolució angular dels instruments gamma d'avui en dia. Malgrat això, és molt probable que, si hi ha partícules molt energètiques als jets i hi ha emissió d'alta energia, aquesta serà probablement emesa per aquestes partícules; a més, si hi ha emissió X estesa, també es produiran raigs X a regions de mida per sota de la capacitat resolutiva dels instruments (al cor de la font) i només caldrà establir, avui per avui, en quina quantitat. Cal, a més, trobar com aquestes partícules tan energètiques dels jets són accelerades i emeten fotons d'energies $\gg 1$ MeV. Una dificultat afegida és que, com el contingut del jet no és conegut, la naturalesa de les partícules origen d'aquests fotons d'energia $\gg 1$ MeV és incerta. S'ha d'explicar tot plegat, en la mesura que sigui possible, dins el context general conegut. Així, doncs, l'explicació de l'emissió en gamma als jets no ha de ser contradictòria amb allò observat en ràdio, i si hi ha variacions en la quantitat de radiació observada en un cert rang d'energia, això ha de ser consistent amb variacions de l'emissió en altres rangs d'energia i amb la visió o context global. És la coherència d'una visió global entre els diferents mecanismes d'emissió, encara que aproximada de moment, el que es busca amb els treballs d'aquesta tesi. Ara passem a explicar com això ha estat tractat i quines conclusions n'hem extret. A la Fig. 2, presentem una reproducció sintètica del que seria l'espectre multilongitud d'ona d'un microquàsar com els aquí estudiats.

2. Els processos físics darrera la radiació dels jets als microquàsars

Degut a que els microquàsars semblaven ser la contrapartida d'algunes fonts de raigs gamma de 100 MeV, el primer que vam investigar va ser si un conjunt d'electrons relativistes, d'energies suficientment altes i injectats a la base del jet, radiarien en el rang d'energia esmentat la seva energia de la manera observada. Les primeres investigacions van mostrar que si l'estrella companya presentava un camp de fotons prou

dens, o a la regió emissora hi havia un camp magnètic prou alt, en tots dos casos amb valors justificables i raonables, la radiació de 100 MeV podia ser fàcilment reproduïda, fos per interacció Compton invers amb fotons de l'estrella, fos per interacció auto-Compton amb fotons sincrotró emesos pels mateixos electrons. El següent pas era veure si aquesta predicció per l'emissió gamma tenia conseqüències a més baixes energies que anaven en contra d'allò observat en ràdio o en raigs X. Per exemple, l'emissió sincrotró derivada d'assumir la presència d'un camp magnètic podia violar els límits observacional a les freqüències on fos rellevant, o ser massa petita no sent capaç d'explicar les observacions. Vam estudiar en un model més complex si la radiació produïda a diferents longituds d'ona en el jet era compatible doncs amb les observacions en tot l'espectre i vam trobar, en relació amb el jet, que l'emissió gamma de 100 MeV semblava provenir de les regions més internes, que l'emissió X podia ser significativa i fins i tot dominant per IC, i que si volíem tenir emissió radio sincrotró com l'observada calia que hi hagués reacceleració de partícules. En aquest escenari més detallat vam tenir en compte la influència de la radiació del disc prim i el gruixut, cosa que va permetre explorar com contribueixen al total. Una altra conclusió interessant, recolzada també per estudis estadístics, fou que hi ha indicis que apunten als microquàsars com a contrapartides d'una bona part de les fonts gamma variables no identificades del pla galàctic.

Un cop es va veure que un model relativament senzill de jet podia predir l'emissió gamma probablement associada als microquàsars, però que hi havia mancances com la modelització acurada de l'emissió ràdio, es va anar més lluny en l'estudi teòric d'aquests objectes introduint processos d'acceleració de partícules al llarg de tot el jet per intentar reproduir de manera consistent l'emissió en tot l'espectre. A més, degut a l'existència de diferents camps de fotons, es va afegir l'efecte de l'opacitat per fotons gamma deguda als fotons ambients (de l'estrella, del disc, i fins i tot d'aquells produïts al mateix jet). Aquesta opacitat és deguda a que els fotons gamma col·lisionen amb els òptics, ultraviolats i X presents i formen parelles electró-positró que també poden radiar. L'efecte a primer ordre d'aquestes parelles també es va incloure. Un altre element innovador del model va ser l'assumpció de la presència de matèria no relativista[6] dins el fluid del jet. Aquest material, provinent del disc, seria

[6]Aquesta matèria és no relativista en el sentit que l'energia per partícula del plasma no és una part substancial de la seva energia en repòs, en el sistema de referència on el plasma estaria quiet (i.e. el del centre de masses del plasma: el del jet). En canvi, tot ell es mou a velocitats relativistes en el sistema de referència de l'observador.

qui dominaria la dinàmica del jet[7], sent la part radiativa, els electrons relativistes, una part menor. Per la presència de protons al jet, el Bremsstrahlung també es va calcular. L'acceleració es donaria degut a la dissipació d'energia per part dels protons de temperatures relativament baixes ($\sim 10^{10}$ K!) per inestabilitats en el plasma (e.g. xocs). De retruc, aquest material relativament fred confinaria el plasma relativista emissor col·limant el jet, al menys fins a una distància considerable de l'objecte compacte, a partir de la qual altres mecanismes de confinament podrien jugar un paper (e.g. el medi extern). Aquesta col·limació vindria d'una velocitat d'expansió controlada pel material fred, força menor que la velocitat en la direcció del moviment. La presència d'aquest material fred es va tractar ampliant l'escenari modelat incloent l'ejecció i el disc, encara que de manera simplista. Això va permetre tractar l'equilibri d'energia entre la matèria del disc, aquella que era ejectada i la que finalment queia a l'objecte compacte, tot plegat partint de ritmes raonables de caiguda de material del disc sobre l'objecte compacte.

El nou model de jet de microquàsar podia explicar molts dels aspectes observats als microquàsars emissors en gamma. De fet, la confirmació observacional de que aquests objectes poden arribar a emetre a energies altíssimes va arribar quan aquest model ja s'havia desenvolupat i podia explicar l'emissió fins el rang de TeV, amb un conjunt de valors pels paràmetres perfectament justificables, sense entrar a més en contradicció amb allò conegut sobre la radiació en altres bandes de l'espectre. A més es feien prediccions addicionals (presentades al llarg d'aquesta tesi i recollides al final), que poden ser contrastades observacionalment en el temps a venir. El que sembla clar en relació amb la qüestió de si els jets poden emetre teòricament en X de manera important és que la resposta és afirmativa. Observacionalment encara està per provar, però teòricament sembla raonable que l'emissió en X sigui important si hi ha, per una banda, força radiació detectada a $\sim$100 MeV, indicant que el reservori d'energia al jet és gran; a més, també hi ha emissió observada en el rang TeV, indicant que l'energia de les partícules és gran i que pot ser emesa també per sincrotró en la banda X si el camp magnètic és prou alt, cosa probable. Una altre punt a remarcar en relació amb el model és que assumeix un determinat contingut de matèria al jet, protons i electrons on una determinada part dels electrons es accelerada. També s'hi podrien encabir positrons accelerats ja que la creació de parelles electró-positró no és en contradicció amb el model mentre les parelles no superin en pressió la matèria freda. Sota la mateixa condició, l'acceleració de protons també pot tenir lloc,

[7]La pressió vindria dominada pel plasma no relativista, i.e. l'energia per partícula seria no relativista fins i tot amb la presència d'una component relativista radiativa.

encara que aquests protons relativistes no podrien transportar una gran quantitat d'energia degut a la necessitat de trobar-se dominats dinàmicament pels protons freds, i això comportaria una emissió hadrònica força minsa per la poca eficiència radiativa d'aquestes partícules. És a dir, que dins el context treballat aquí, al jet aquests protons no emetrien de forma rellevant excepte en casos molt concrets.

Explorant les regions on el jet del microquàsar desapareix d'una manera o altra, xocant o diluint-se, enmig del medi interestel·lar, es poden trobar encara interessants resultats. Ja s'ha esmentat més amunt que als jets dels microquàsars s'ha detectat la presència de partícules molt energètiques degut a la presència de radiació X estesa. A més, és probable que hi hagi partícules relativistes, protons i electrons, a grans distàncies del microquàsar on van ser generades. Tot plegat ens va portar a investigar les conseqüències radiatives d'aquestes partícules quan es trobessin amb el medi interestel·lar. Per una banda, els electrons podrien radiar per sincrotró i Compton invers la seva energia, sent detectables a prop dels microquàsars; per una altra, els protons podrien interaccionar amb regions denses del medi circumdant com per exemple núvols moleculars, generant emissió gamma així com parelles electró-positró que emetrien també en tot l'espectre per sincrotró i Bremsstrahlung. En tots dos casos, les condicions requerides no serien particularment extremes, així que seria factible obtenir informació dels microquàsars i els seus entorns degut a la presència o no de la radiació produïda per les partícules a les parts terminals dels jets. A les Figs. 3, 4 i 5, presentem les distribucions espectrals d'energia del microquàsar, l'emissió dels electrons accelerats a la part final del jet, i l'emissió dels protons i partícules secundàries que interaccionen amb núvols moleculars propers, respectivament.

A títol de comentari final, cal dir que els objectes estudiats aquí presenten unes qualitats excepcionals, difícils de trobar en altres fonts astrofísiques. Radien fortament en totes les longituds d'ona, cosa que permet fer estudis dels processos radiatius en tota la seva complexitat. També varien en escales de temps que faciliten la investigació dels mecanismes físics darrera dels canvis que es donen. Es pot dur a terme l'estudi de la distribució espacial de la radiació d'aquestes fonts proveint de molta informació física, ja que ostenten mides assolibles per la capacitat resolutiva dels nous instruments. Totes aquestes qualitats, juntament amb el fet que s'ha fet un salt qualitatiu en quant a instrumentació (i no només en observatoris de radiació electromagnètica, sinó també de partícules massives com neutrins i raigs còsmics), fan d'aquests objectes laboratoris gairebé inigualables per estudiar els processos no

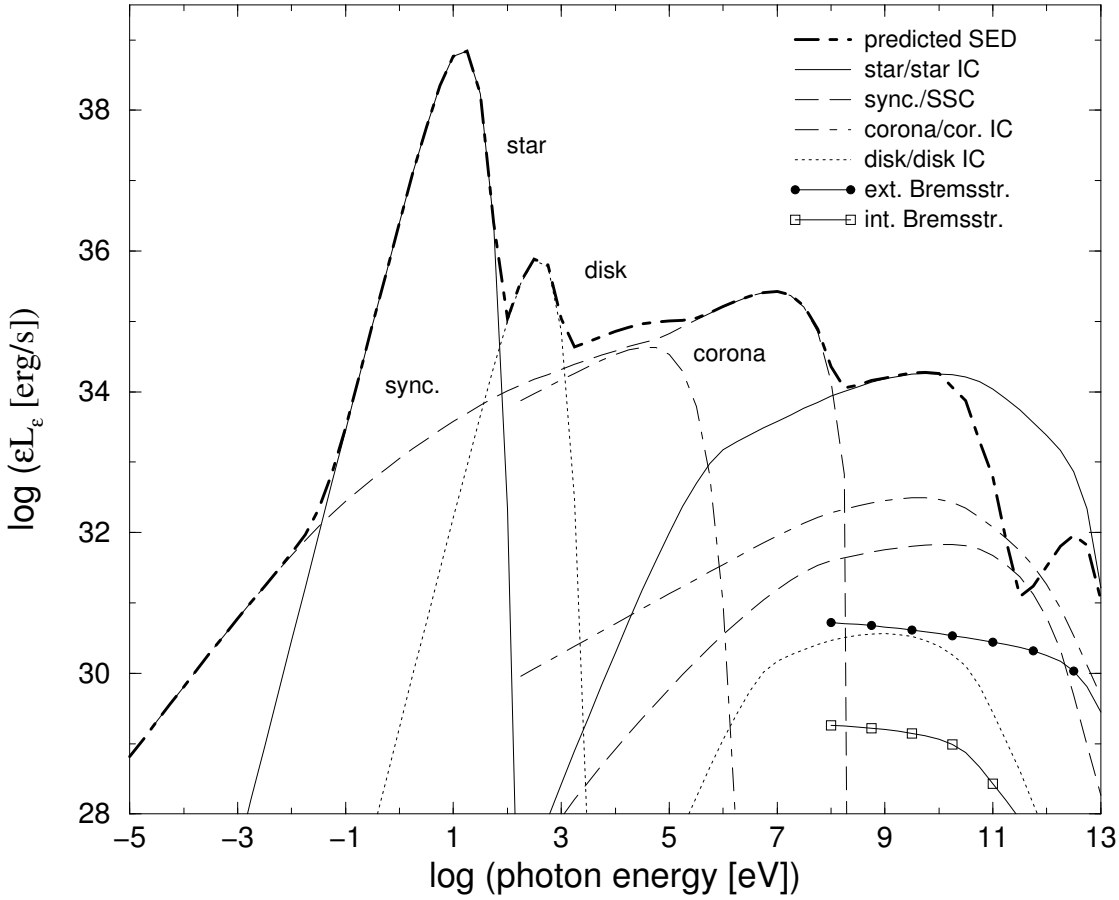

Figura 3: Distribució espectral d'energia de la radiació intrínseca d'un microquàsar des de ràdio (10^{-5} eV) fins a raigs gamma de molt alta energia (10^{12} eV). Ara es mostren les diferents components radiatives i processos físics involucrats. Per a més detalls, veure capítols posteriors.

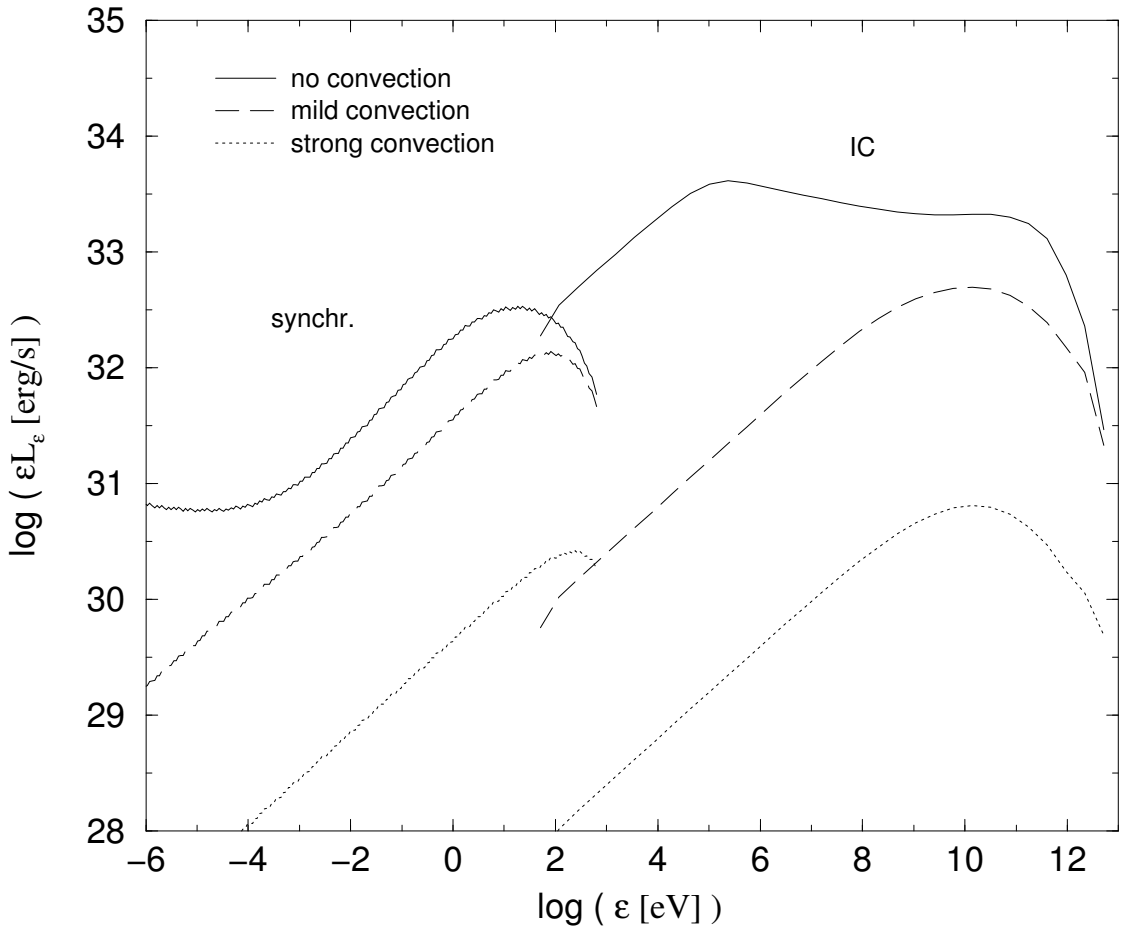

Figura 4: Distribució espectral d'energia de la radiació produïda pels electrons accelerats a la part final d'un jet i difonent-se en el medi circumdant. Per a més detalls, veure capítols posteriors.

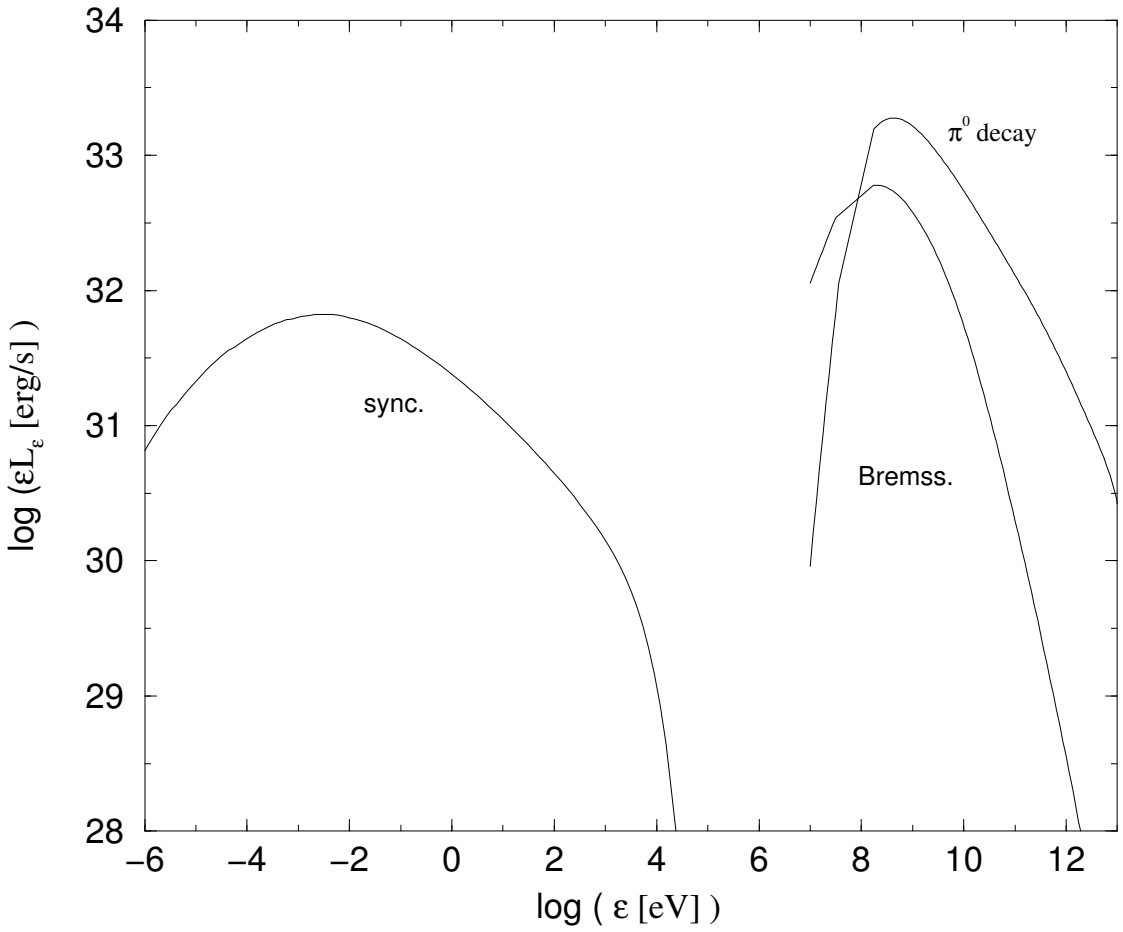

Figura 5: Distribució espectral d'energia de l'emissió generada pels protons relativistes alliberats al medi interestel·lar interaccionant amb núvols moleculars. Per a més detalls, veure capítols posteriors.

tèrmics en un rang molt ample d'energia, afegint la investigació de l'acreció, la física de plasmes i els xocs, tot plegat des d'un punt de vista comprensiu, profitós i amb una gran projecció de cara al futur.

3. Conclusions

- Podem explicar els fluxos gamma observats als microquàsars LS 5039 i LS I +61 303 assumint continguts d'energia en les partícules emissores raonables encara que més grans que aquells que serien suficients per explicar només la part ràdio. La companya d'alta massa en tots dos sistemes pot ser la font dels fotons que pateixen interacció Compton invers amb electrons d'energies similars a les necessàries per emetre en ràdio per procés sincrotró, produint la radiació gamma observada.

- Mostrem que, quan el camp magnètic es té en compte a la base del jet, l'emissió auto-Compton amb fotons sincrotró pot també explicar l'emissió gamma observada a LS 5039 i LS I +61 303.

- La variabilitat de l'emissió gamma observada als microquàsars és pot explicar a partir de variacions en la densitat de fotons estel·lars llavor del Compton invers, amb canvis en l'acreció degut a excentricitat orbital, i també degut a precessió.

- Concloem que els microquàsars podrien ser una fracció important de les fonts no identificades variables al pla galàctic.

- Trobem que el jet podria dominar en el rang dels raigs X a sistemes amb discs i corona dèbils.

- Mostrem que emissió gamma significativa fins a energies the 10^3 MeV podria ser produïda tenint en compte només la presència dels fotons provenint del disc i la corona.

- Concloem que l'acceleració dels electrons del jet quan ja es troben fora del sistema binari sembla necessària per explicar l'emissió ràdio estesa observada, tenint en compte que pèrdues d'energia significatives tenen lloc en les regions internes del jet per sincrotró, Compton invers amb l'estrella y auto-Compton amb els fotons sincrotró.

- Mostrem que l'escenari on el jet dominat per la matèria freda s'ajusta millor al fet que els jets són observats amb velocitats relativistes moderades quan el balanç d'energia accreció/ejecció és considerat, al menys per jets que no apunten cap a l'observador, ja que el jet ha de transportar prou matèria per radiar de forma observable. Per això, si la càrrega de matèria del jet és gran i l'energia disponible limitada, la velocitat d'aquest no pot ser molt relativista.

- Trobem que el mecanisme de col·limació per matèria freda sembla més consistent amb l'escenari global, més justificat des d'aquest punt de vista que per altres mecanismes de col·limació magnètica o per matèria externa.

- Podem explicar de manera elegant l'espectre multilongitud d'ona de LS 5039 des de ràdio fins a raigs gamma de molt alta energia amb la introducció d'acceleració de partícules i absorció per creació de parelles. Algunes troballes són que l'emissió X podria venir principalment del jet, que els raigs gamma d'alta energia serien observats amb més intensitat quan l'objecte compacte es troba en oposició a l'observador, que els raigs gamma de molt alta energia podrien ser fortament absorbits durant el pas pel periastre, i que la component Bremsstrahlung de l'emissió seria difícilment rellevant.

- Mostrem que la introducció d'un vent equatorial lent i anisotròpic (i la introducció de l'absorció per creació de parelles) podria explicar les característiques de la variabilitat observades a LS 5039.

- Posem de manifest que la modelització de LS 5039 apunta cap a una relació entre l'emissió ràdio òpticament prima i els fluxos aparentment poc absorbits i significatius de raigs gamma de molt alta energia, anant tots dos fets lligats a un augment dels electrons relativistes a escales del jet intermitges.

- Concloem que el model de jet dominat per matèria freda pot ser aplicat a 1E 1740.7−2942. El model descriu apropiadament l'espectre de banda ampla detectat, i prediu que raigs gamma d'alta i molt alta energia podrien ser detectables pels nous instruments treballant a aquestes energies. En relació a l'origen dels raigs X per aquesta font, semblarien dominats per la corona.

- Mostrem que, en cas que una fracció significativa dels electrons accelerats als jets dels microquàsars abandonessin el lloc d'acceleració a grans distàncies de l'objecte compacte, emissió ràdio estesa, així com raigs X i gamma en sistemes d'alta massa, podrien ser produïts, presentant aquesta emissió fluxos més aviat constants en escales de temps de l'ordre d'un any.

- Trobem que, si protons relativistes abandonessin el jet quan interactua amb el medi circumdant, el flux de raigs còsmics a les regions properes seria incrementat de forma significativa, cosa que mostra la rellevància dels microquàsars com a acceleradors de raigs còsmics.

- Concloem que, si regions de medi interestel·lar dens com núvols moleculars es trobessin a prop d'un microquàsar (i.e. pocs pc), cosa que podria ser comuna a les regions internes del pla galàctic, emissió significativa de 10^3 MeV a TeV seria generada per decaïment de pions neutres creats per col·lisions protó-protó. A més, es podria produir emissió ràdio fins a raigs X sincrotró, i raigs gamma tous produïts per Bremsstrahlung, originat tot plegat per parelles electró-positró generades en el decaïment dels pions carregats sortints de les col·lisions protó-protó. Aquestes fonts serien esteses, i no variables a escales d'alguns anys.

Per tant, el treball presentat en aquesta tesi mostra la riquesa de la física involucrada en l'estudi dels microquàsars, i posa de manifest que l'estudi del fenomen microquàsar ha de recórrer un llarg camí abans de ser comprés de manera global. En qualsevol cas, degut a les excitants perspectives en el camp teòric i observacional, el viatge cap a una bona comprensió d'aquests objectes promet grans avenços en el futur proper, havent aportat ja un primer tast a aquells que han donat els primers passos en el món de la aproximació multilongitud d'ona i multipartícula aplicada als microquàsars.

Bibliografia

Aharonian F.A., Akhperjanian A.G., Aye K.M., et al., Jul. 2005, Science, 309, 746 x

Barret D., Apr. 2004, In: AIP Conf. Proc. 703: Plasmas in the Laboratory and in the Universe: New Insights and New Challenges, 238–249 vii

Corbel S., Fender R.P., Tzioumis A.K., et al., Oct. 2002, Science, 298, 196 vii

Mirabel I.F., Rodriguez L.F., Sep. 1994, Nature, 371, 46 vii

Mirabel I.F., Rodríguez L.F., 1999, ARA&A, 37, 409 vii

Mirabel I.F., Rodriguez L.F., Cordier B., Paul J., Lebrun F., Jul. 1992, Nature, 358, 215 vii

Paredes J.M., Martí J., Ribó M., Massi M., Jun. 2000, Science, 288, 2340 x

Chapter 1

Introduction

High energy astrophysics is at the moment one of the hottest topics in physics. The most relevant theoretical problems could be solved with the help of the powerful instruments working currently or to start operating soon. From the high precision X-ray imaging and spectroscopy to the high angular resolution and sensitivity of the ground-based Cherenkov telescopes, passing through the next high-energy γ-ray satellite-borne instruments, the observational data quality is getting higher pretty fast, and the future prospects point to an even better situation of the field. Furthermore, the new data is allowing to go beyond what has been put forward during the last decades allowing, on the one hand, to better test previous models and, on the other hand, to improve them increasing their physical insight. Of course, the very connection between astrophysics and physics at high energies provides to the former discipline development with far reaching consequences in the latter field. In this context, different types of sources have become primary targets for the high energy detectors and, in the context of the multiwavelength study era, also for low energy instruments. Concretely, γ-ray astronomy showed in the past that objects such as extragalactic blazars and galactic pulsars conformed two dominant populations at that energy range. Nevertheless, all this new instrumentation is showing that new populations of γ-ray sources are to be considered and observed also in the whole spectrum (and not just in the electromagnetic one). Among these new classes of γ-ray emitters, galactic microquasars are turning out to be one of the most attractive classes.

Microquasars are X-ray binaries that present relativistic radio jets (Mirabel & Rodríguez 1999). The origin of the jets is related to the matter accreted by the

compact object, a neutron star or a black hole, from the companion star. Since these systems behave as scaled-down versions of quasars and active galactic nuclei, their study can provide us with information about their larger-scale analogs. However, the population of microquasars is still a very reduced one, with about sixteen known objects up to now (Ribó 2002, Paredes 2005). Regarding our knowledge about the physics involved in the behavior of such objects, it is necessary to go further in our observational and theoretical insight on them, increasing also the list of the known microquasars.

Particularly, the high energy processes that take place in microquasars are of great importance to understand the spectral and time properties of the observed emission from these sources. High energy processes occur in the accretion disk, formed with expelled stellar matter, as well as in the jets, and their complexity appears when looking at the comprehensive approach required for studying them. Stellar physics, accretion, magnetohydrodynamics, particle acceleration, radiative and absorption processes, relativity, all these topics play a main role if microquasar behavior is to be understood, although other subjects could enlarge the list, since this is plenty of connections with other astrophysical fields, e.g. like the microquasar-environment interaction.

Because of the complicated nature of the matter under study, historically it has been common to start with a very rough glance on the general scenario, taking by granted many assumptions that, in spite of simplifying and clarifying the questions to answer, are often quite mistaken. Nevertheless, the theoretical development is linked to and limited by the quality of the observational data, and only the increase of such quality altogether with previous modeling can lead to a more accurate choice of the assumptions in the theory. At present, the state of the field is still at the phenomenological level concerning the study of the emission and its properties in the overall spectrum. However, it seems likely that a fast development is going to occur soon in both directions the theoretical and the observational one.

In order to go further in the study of the role of high energy processes in the context of microquasars, we have considered the main elements of the scenario, altogether with their intrinsic and relational properties, studying afterward what observational features come out. Our aim has been to build physically meaningful models following a comprehensive approach, well in agreement with the phenomenology and capable of providing predictions concerning the physics underlying not only

radiative processes, but also globally other important aspects of microquasars and their environment. Therefore, we have developed, step by step, a set of models which aim at explaining different characteristics of the γ-ray emission first, and the broadband emission afterwards.

The contents of the thesis has been structured in 7 chapters. In Chapter 2, to put in context the work presented here, the description of the main microquasar characteristics and a historical review on the field are given. In Chapter 3, the physics behind the developed models is explained. It has been intended to provide with simple tools to reproduce the calculations performed by us, and which could also be applied for solving further problems. When developing more concrete models later on, we provide with additional details concerning the particular scenario. In Chapter 4, it is presented the first approach to the high energy radiative processes in microquasar jets in the context of the γ-ray sources in the Galaxy. A model for jet γ-ray emission and a model for jet high energy broadband emission are described and applied to microquasars and unidentified γ-ray sources. In Chapter 5, it is investigated the role of microquasar jets with a model where accretion, particle acceleration, and radiative and absorption processes are considered. This model is applied also to different sources to explain not only their broadband spectra, but also to explore physical properties of accretion and jets that can be inferred from theoretical considerations as well as observational data obtained by us. In Chapter 6, it is studied the relationship between microquasars, their environment and diffuse emission in the Galaxy, at different energy ranges, as well as the role of these systems as cosmic ray accelerators. Finally, in Chapter 7, the conclusions of this work are presented and discussed.

Bibliography

Mirabel I.F., Rodríguez L.F., 1999, ARA&A, 37, 409 1

Paredes J.M., Feb. 2005, In: AIP Conf. Proc. 745: High Energy Gamma-Ray Astronomy, 93–104 2

Ribó M., Nov. 2002, Ph.D. Thesis, Univesitat de Barcelona 2

Chapter 2

Microquasars in the astrophysical context

In this chapter, the topic of the thesis is put in context with the historical development of high energy astronomy as well as with the present knowledge on microquasars. Moreover, it is also pointed out the relationships between the topic of γ-ray emission and the future of the field of microquasar study. We intend to give the context in which microquasars are embedded before presenting the work of modeling the emission generated in microquasars, mainly in their jets, from radio to γ-rays, to go further in the study of the underlying physical processes. The primary motivation of such work was to explore theoretically the possibility that microquasars could be high-energy γ-ray emitters (see Chapter 4), as proposed by Paredes et al. (2000) for the source LS 5039/3EG J1824−1514 (Hartman et al. 1999). Eventually, the high energy modeling naturally became a real multiwavelength approach and, finally, we tried to provide an overall rough theoretical view on the situation. We aimed at making clear the connection between γ-rays and radiation at lower energies as well as high energy processes likely taking place in microquasars. In addition to all this, strong limitations due to lack of clear counterparts favored also the use of alternative means as population analysis. Basically, we have intended to show that there are more γ-ray source types than it was thought in the past. Moreover, among other types of sources, microquasars are a very interesting and new γ-ray population that could play a significant role in our understanding of different topics, from accretion to particle acceleration, going through magnetized plasma behavior, general relativity, and other involved subjects. The forthcoming observational input

will allow for better treatments on microquasar high energy processes and related radiation than those presented here. We hope nevertheless that some of the ideas proposed in this work will help future research in the field.

2.1 A short historical note

Microquasars were discovered in the 90s as an X-ray binary subclass (see, e.g., Mirabel et al. 1992, Mirabel & Rodriguez 1994). Nowadays, it is known that they emit in the whole energy range, and a plethora of low and high energy processes occurs there: continuum and line emission in the infrared, optical and ultraviolet bands from the companion star, its wind and the external regions of the accretion disk; continuum and line absorption up to soft X-rays due to the stellar wind and the accretion disk itself; X-ray continuum and line emission from the inner regions of the disk; radio, infrared and likely X-rays and γ-rays from the jets, etc. Nowadays, the observational and theoretical studies of the high energy processes taking place in these objects are becoming very popular among high energy astrophysicists coming from different fields (for instance active galactic nuclei, γ-ray bursts, accretion disks, pulsars, X-ray binaries or cosmic rays), in part because their initially unexpected γ-ray emitter nature.

During several decades, radiation beyond the X-ray band was considered as a very rare phenomenon. Indeed, the physical processes producing such radiation can not be thermal, since otherwise it would correspond to an extremely high temperature plasma in thermal equilibrium. In nature, very high temperature plasmas in thermal equilibrium can be found for instance in the inner regions of the accretion disk of X-ray binaries, or in the core of the stars. However, the generated radiation does not reach energies higher than hard X-rays. Therefore, non-thermal processes, i.e. acceleration of particles beyond the thermal tail, radiating under the effects of matter, photon and/or magnetic fields, seem to be required for generating emission beyond, say, 100 keV.

During the 60s and early 70s, the first γ-ray detections (the diffuse background radiation, γ-ray bursts) were performed by instruments on board satellites (e.g. Ranger 3, ORS-4 and the Vela serie). Later in the 70s , the instruments SAS-2 and COS-B allowed the scientific community to realize that high-energy γ-ray emission could play a major role in the high energy sky. Nevertheless, the end of the first

childhood for the field arrived with EGRET, a high-energy γ-ray instrument that was operating during about one decade and detected almost three hundred sources, two thirds of them without identified counterpart at other energies. Different source classes are found in the third EGRET catalog (Hartman et al. 1999). On the one hand, there are galactic populations like pulsars and supernova remnants and, on the other hand, there are extragalactic ones like active galactic nuclei. The former are concentrated in the galactic plane, and the latter appear isotropically distributed in the sky.

Nevertheless, as it is seen for instance in the work by Romero et al. (1999), among unidentified sources there are several additional potential populations of sources like massive binaries and OB associations. Moreover, the distribution of these γ-ray sources without known counterpart shows that some are concentrated towards the galactic plane, whereas others form a halo around the galactic center at mid latitudes or are distributed roughly isotropically (see Romero et al. 2004 and references therein; for the EGRET source distribution in the sky, see Fig. 2.1). Furthermore, within these particular groups of sources (laying on the galactic plane or at higher latitudes), some present variability and some are steady or dubiously variable (Nolan et al. 2003). In short, at the statistical stage of the analysis, it is already clear that several types of sources co-exist in the subset of unidentified sources of the third EGRET catalog. In Chapter 4, we will focus on the statistical study of the possible relationship between variable EGRET sources and microquasars.

It must be remarked that the success of ground-based Cherenkov astronomy is opening the population study to the very high-energy γ-ray sky (see e.g. Fig. 2.2[1]). In addition, next high-energy γ-ray instruments on board satellites will fill the gap created after EGRET disappearance between X-rays and very high-energy γ-rays. All this renders a new scenario for high energy astrophysics, where microquasars can play a significant role, as we will try to show below.

[1]Presented by Martínez, M. and elaborated by Tonello, N. during TAUP 2005 conference, held in Zaragoza, Spain, in september of 2005.

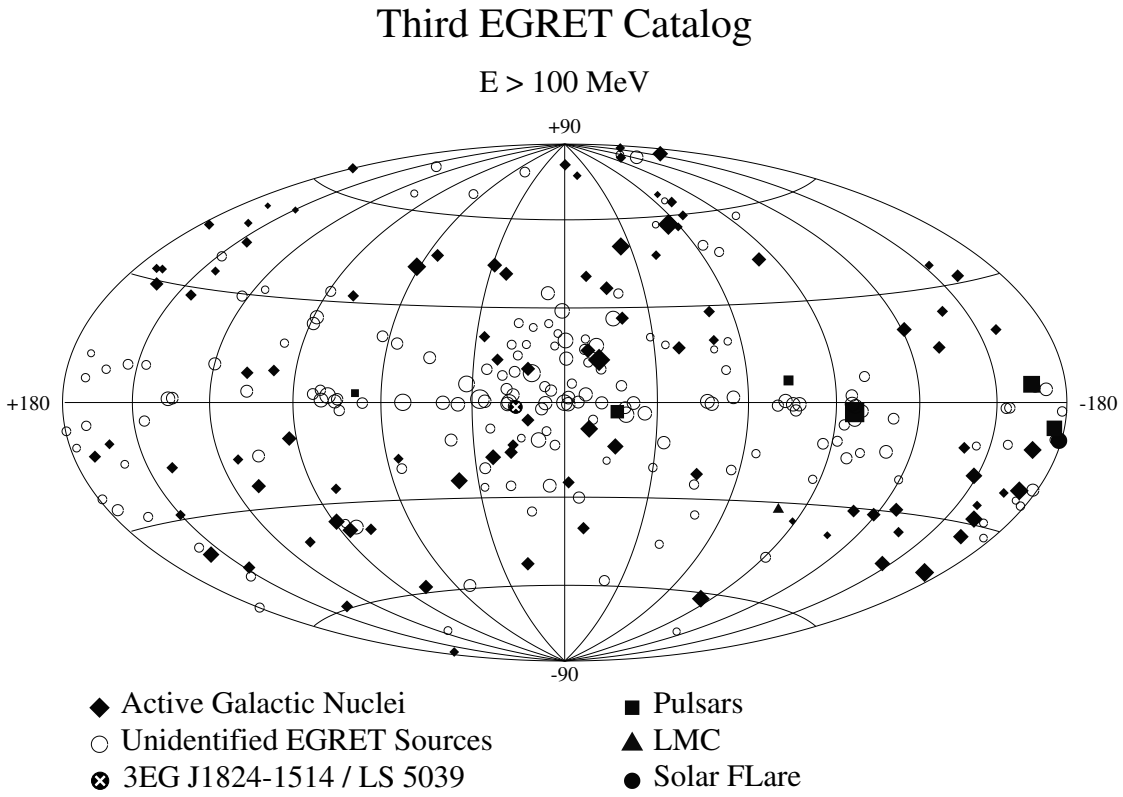

Figure 2.1: The Third EGRET source Catalog shown in galactic coordinates. The white cross inside a black circle, with galactic coordinates $l = 16.88°$ and $b = -1.29°$, indicates the location of 3EG J1824−1514, to be associated with LS 5039. Taken from Ribó (2002), which was adapted from Hartman et al. (1999).

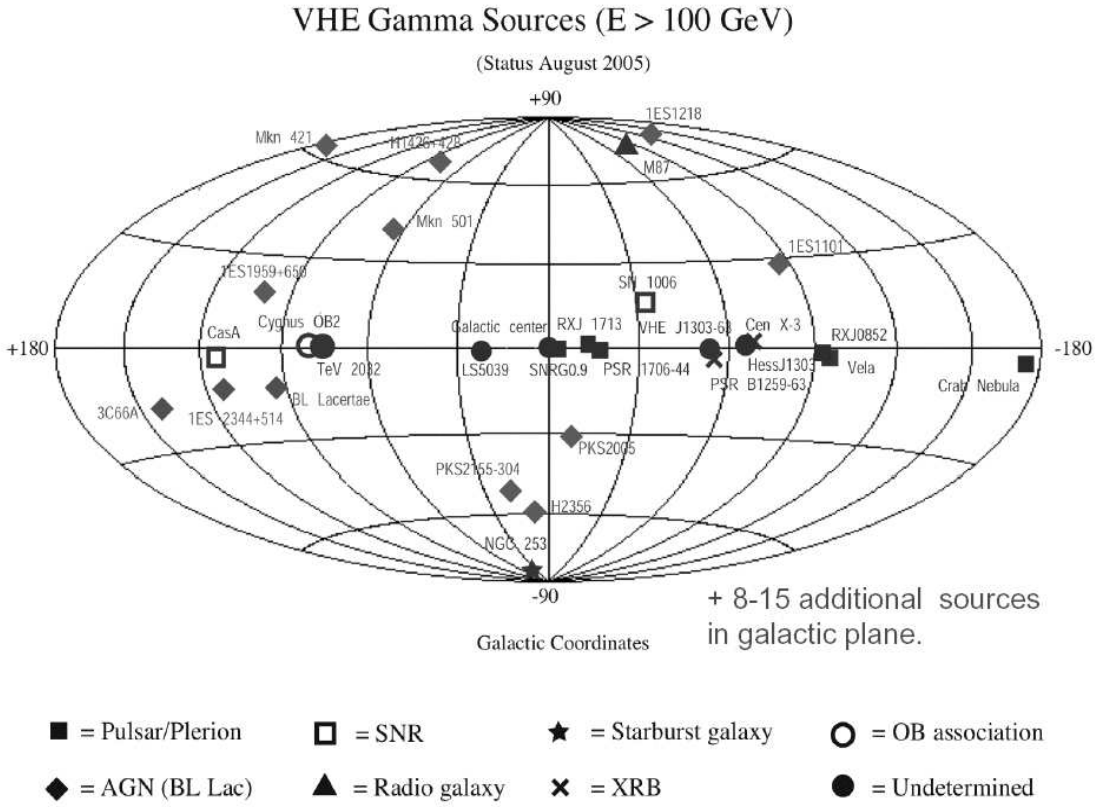

Figure 2.2: The state of the very high-energy γ-ray sky at the year 2005. We note that different types of sources, likely corresponding to very high-energy γ-ray populations, have been already detected, microquasars among them.

2.2 Microquasars as γ-ray sources

2.2.1 Microquasar picture

Before going further and for the sake of clarity concerning the next topics to comment, it might be worthy to give a more extended overview on the microquasar scenario than that given in the previous chapter. Nevertheless, we give just a brief summary, and we refer to the PhD thesis by Ribó (2002), as well as the one by Kaufman Bernadó (2004), for more detailed descriptions of a microquasar.

Although the microquasar definition is somewhat loose, we will adhere here to that stating that these objects are a binary system formed by a companion star and a compact object. Regarding the stellar companion, it can be either a low mass star already off the main sequence, with a strong mass loss rate due to expansion of the external layers of its envelope, or a high mass star with a strong mass loss rate in form of stellar wind (either isotropic or anisotropic). If of low mass, the companion star transfers the expelled matter to the compact object overflowing the Roche lobe; in the case of a high mass star, although Roche lobe overflow could happen, the transferring is in many cases dominated by the stellar wind. Both mechanisms of mass transfer lead to the so called Roche lobe overflow and wind fed accretion, respectively. The emission at intermediate energies (from infrared to ultraviolet) is dominated either by the companion in high-mass microquasars or by the accreted matter in low-mass ones.

As far as the lost stellar matter reaches the surroundings of the compact object, it tends to accumulate towards the plane perpendicular to its angular momentum direction due to angular momentum conservation, leading to the formation of a disk. The microphysics underlying accretion disks is not completely well known at the moment, although the observed emission inferred to be from the accretion disk can be pretty well explained by some models which require some phenomenological parameters (Shakura & Sunyaev 1973, Esin et al. 1997). Until now, what has been said of a microquasar can be also said of an X-ray binary, being the former a subclass of the latter, and what indeed allows to distinguish one from the other is the presence of a relativistic jet. In Chapter 5, the accretion process is treated but roughly, and no detailed accretion model is developed there. Nevertheless, we will provide of first order estimates on the accretion rate that can be derived from the Bondi-Hoyle

model (Bondi 1952). This model is more extensively discussed in Chapter 3.

Disk matter gets closer to the compact object dissipating energy and angular momentum via, e.g., heating and radiation. In the inner regions of the accretion disk, matter has reached X-ray emitting temperatures and, for certain accretion rates, the plasma properties are thought to be such that, through special magnetic field configurations, efficient transfer of accretion energy and angular momentum takes place to power the formation of outflows (see, e.g., Meier 2003, Hujeirat 2004; see Fig. 2.3 for the classical picture of a microquasar). In Chapter 5, from energetic considerations, we discuss jet formation and make rough estimates of the energy and matter rate balances between accreted and ejected matter without treating the launching mechanism itself. The corresponding formulae are presented in Chapter 3. We note that it will be assumed that ejection energy is extracted from the accretion disk. Nevertheless, it could be also the case, at least in some jet sources (Semenov et al. 2004), that jet power were extracted from the compact object rotational energy via a similar mechanism to that studied by Blandford & Znajek (1977)[2]. Despite the characteristics of the processes that lead to plasma ejections are still unclear, there is observational evidence of extended radio and X-ray jets (see below). Nevertheless, it is worthy to comment on the differences presented by such ejections, whether appearing as discrete or continuous. Thus, we should explore the phenomenology associated with each type of flow (see e.g. Fender et al. 2004).

2.2.2 X-ray binary states and jets

The typical X-ray spectrum produced by an X-ray binary presents two characteristic components, one is modeled by a multicolor black body and the other one is modeled by a power-law plus in some cases an exponential cutoff. Traditionally, it has been thought that the former component of radiation is generated in a thin Shakura-Sunyaev-like disk, and the latter component is originated in a hotter thicker flow surrounding the compact object whose geometry is not well determined (see, e.g., Narayan & Yi 1995, Zdziarski et al. 1998,). Different physical models have been proposed for this hot flow (corona, ADAF, CENBOL, etc), although the main properties are a high temperature geometrically thick and optically thin plasma,

[2]Some observational evidences that are commented below point to microquasar jets as accretion powered, although it might well happen that also a mechanism similar to the one studied by Blandford & Znajek (1977) contributed at some extent.

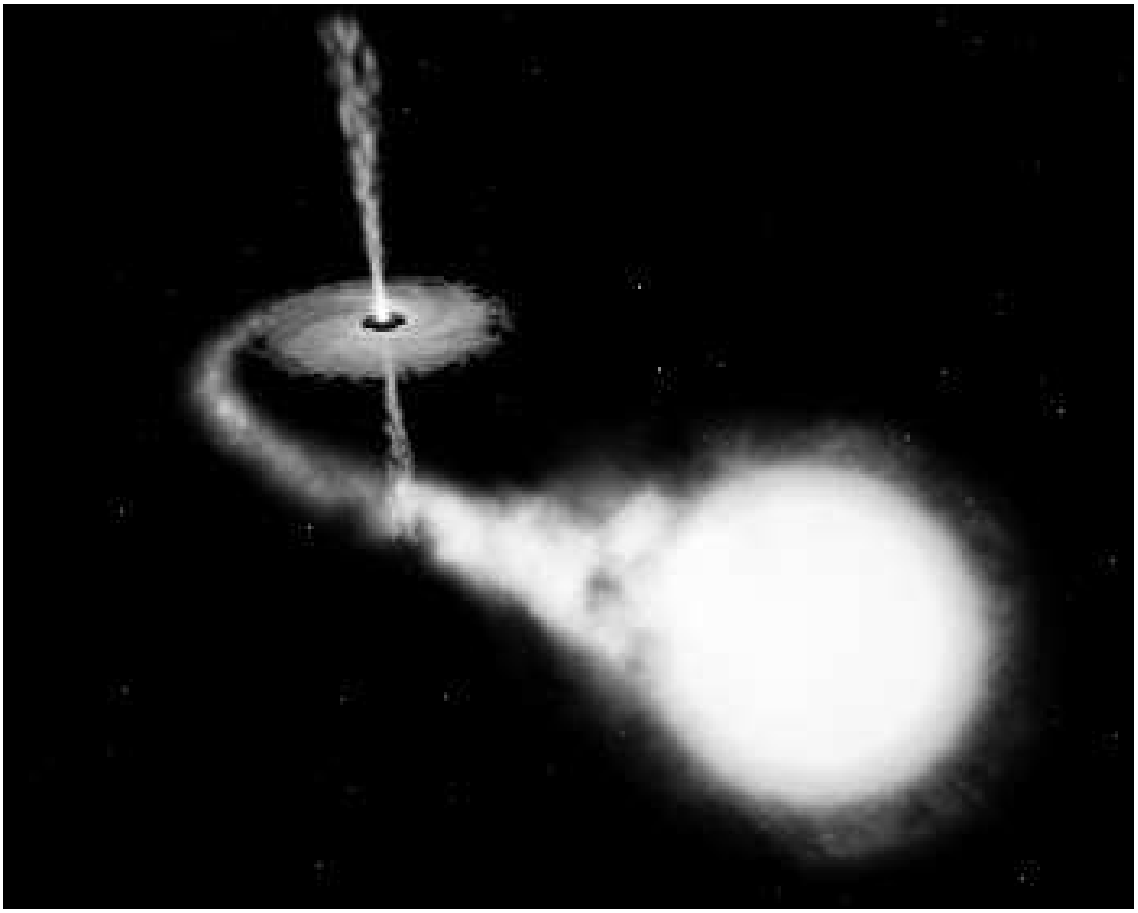

Figure 2.3: Artistic representation of a microquasar, not to scale (http://hubblesite.org/newscenter/newsdesk/archive/releases/2002/30/).

where a thermal population of quasi-relativistic electrons scatter seed photons up to hard X-rays. Depending on which component dominates the X-ray spectrum, and to what extent, the name of the X-ray state is different. In the classical view, when the spectrum peaks at $\sim$1 keV and is dominated by the disk component it is called high-soft state, since the luminosity is high at this energy band and the slope of the power-law component is steep, i.e. soft. Otherwise, when the spectral energy distribution peaks at $\sim$100 keV and is dominated by the power-law component it is called low-hard state, since the 1 keV luminosity is lower, and the spectrum is flatter, i.e. hard. It suffices for our purposes, although there are more states, all of them likely associated with the accretion rate (Esin et al. 1997).

Nowadays, the main trend is to consider the low-hard state as suitable for the formation of persistent mildly relativistic jets (Fender et al. 2003). This is founded on observational grounds, like the detection of persistent flat-to-inverted non-thermal radio emission during such state (Fender 2001), being in some cases resolved as a milli-arcsecond scale jet, as well as on theoretical ones, since some models of jet ejection rely on the existence of an inner disk region close to the compact object (Hujeirat 2004) very similar to what is thought to be present in the low-hard state. The radio emission presents quasi-linear correlation with the X-rays that is clearly observed in some objects and could be universal (see, e.g., Hannikainen et al. 1998, Gallo et al. 2003 and Falcke et al. 2004). The origin of such correlation is still not known, since neither the physics behind accretion processes nearby the compact object is properly understood, nor observations can still tell us properly whether low-hard state jets emit undoubtedly at X-rays (see Chapter 5). As mentioned above, it was supposed that hard X-rays came from the inner region of the disk (Zdziarski et al. 1998). Recently, observations have shown that jets could emit at very high energies (Paredes et al. 2000, Aharonian et al. 2005a), and indirectly it renders the X-ray origin uncertain. Theory points also to the fact that jets could contribute significantly at this energy band (see Chapters 4 and 5 for deeper discussion; for previous works on jet X-ray emission in the low-hard state, see, e.g., Markoff et al. 2001, Georganopoulos et al. 2002, and Chapters 4 and 5), and there is strong debate in the field (recent studies in this subject among a vast literature are for instance by Heinz & Sunyaev 2003, Heinz 2004, Yuan & Cui 2005, etc).

When transiting from the low-hard to the high-soft state , at higher accretion rates, sudden and violent ejections occur from time to time in some of the known microquasars, no matter whether persistent or transient activity objects. In this

intermediate state (accretion rate above the low-hard state, and below the high soft, see e.g. Esin et al. 1997, Fender et al. 2004), both the accretion rate and the soft X-ray flux increase, keeping otherwise the hard power-law component still significant. Moreover, the disk component peak shifts towards higher energies, which is interpreted as the inner radius of the thin disk moving inwards. Meanwhile, the inner thick, say, corona-like region is still radiatively significant and suitable for jet powering. Eventually, as far as accretion grows up, a sudden release of energy is triggered by some sort of instability (see Fender et al. 2004; for a schematic of the phenomenological model, see Fig. 2.4) and *travels* through the jet. It is not well known whether, either this extra release of energy is in the form of a fast blob, shocked material by faster ejected matter, or magnetically dominated plasma waves, heating the background jet matter. Traditionally, the first option was considered to be the case, modeled by a van der Laan model (van der Laan 1966). Nevertheless, going deeper in the study of jet emission, particle acceleration via jet internal instabilities, e.g. shocks, has arisen as a likely possibility, and the model proposed by Rees (1978) for explaining the extended optical emission coming from the jet of M 87 has been applied later in a more developed form to extragalactic as well as galactic jets (internal shocks are also present in low-hard state jet modeling, see Chapter 5). In the context of the microquasar discrete ejections, several authors have followed different approaches to model the emission at different wavelengths (Martí et al. 1992, Atoyan & Aharonian 1999, Kaiser et al. 2000).

After the sudden energetic ejection event, the permanent radio jet is not there anymore, at least at detectable levels. The discrete ejection or shocked background jet material becomes detached from the compact object, and its emission at radio frequencies is optically thin, fading as far as electrons lose their energy. The system remains in the high-soft state, with a dominant multi-color black body spectrum peaking at few keV and a very soft power-law spectrum at higher energies. When radio emission becomes too faint for detection, the microquasar becomes radio quite, i.e. without jet, no radio emission nor microquasar. Nevertheless, the presence of a soft γ-ray tail up to few MeV in some sources at the high-soft state has led to some authors to consider a jet origin for it, although it is under debate and other options like accelerated particles by magnetic reconnection above the disk have been proposed (for a review, see e.g. Barret 2004). It is worth mentioning that, besides the questions of the particular origin of the X-rays in the low-hard state and the ejection mechanism, there is a clear relationship between the jet radio emission, the accretion rate and the disk soft X-rays. Thus, it seems likely that the jet is accretion

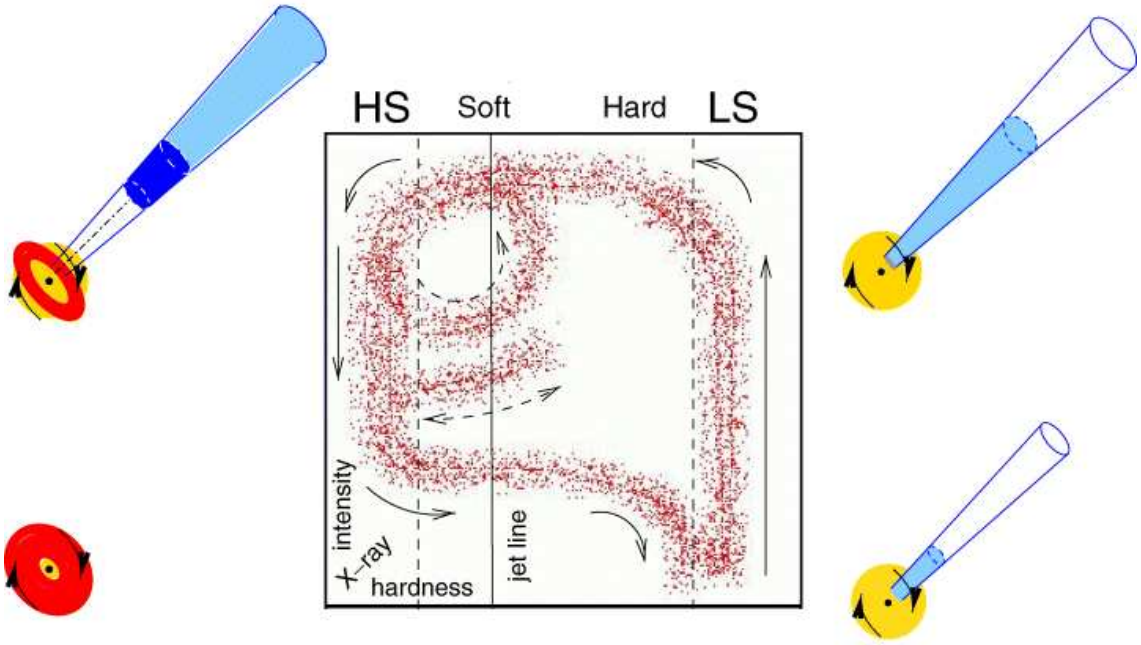

Figure 2.4: A sketch adapted from Fender et al. (2004) for the path covered by a microquasar depending on its flux and hardness state, modeled by the same authors. HS corresponds to the high-soft state and LS to the low-hard state. X-ray hardness increases to the right and hard X-ray flux/intensity upwards. At the jet line, the jet appears or disappears. At the highest fluxes, the jet disappears right when a sudden increase in ejection takes place, getting detached from the compact object. It is visible in the picture the geometry of the outer/inner disk depending on the X-ray state.

powered in X-ray binaries.

2.2.3 γ-rays and lower energy radiation

The discovery of the microquasar LS 5039 and its association with the high-energy γ-ray source 3EG J1824−1514 (Paredes et al. 2000) further demonstrates that a population of sources such as LS 5039 may be a substantial source of high energy particles and photons produced within our galaxy. The detection of the microquasar LS 5039 by Aharonian et al. (2005a) with the ground based Cherenkov telescope HESS has confirmed the prior EGRET source association proposed by Paredes et al. (2000). This finding is of great importance, since clearly states that microquasars are γ-ray emitters. The next question to answer is whether γ-rays are generated inside the jet, inside the binary system but outside the jet, or further away in the regions nearby the microquasar. Moreover, the γ-rays could be produced by hadronic or leptonic processes. We are not going to treat here in detail these issues, since Chapters 4, 5 and 6 are devoted to them. Nevertheless, a brief sketch on the γ-ray production scenario will be given, explaining also the related low energy emission scenario. We note that our goal is not to provide an exhaustive list of consequences, but a general and approximated view on the issue. A deeper description of the particular multiwavelength outcomes will be presented in the next chapters (for the observed broadband spectral energy distribution of a microquasar see Fig. 2.5).

As it is well known, microquasar and quasar jets contain high energy particles that, via thermal or non thermal mechanisms, can radiate at different frequency bands. If non thermal, particle energy is to be increased above the thermal tail at high energies. The mechanism that accelerates particles in jets is not known though Fermi acceleration, in its first or second order type (i.e. via either one shock acceleration or stochastic scattering acceleration, see Bell (1978) and Scott & Chevalier (1975) respectively), is a good candidate to play that role. There are other types of particle acceleration processes that could be relevant. Some are related to some kind of shock or velocity gradient, like the converter mechanism or the shear acceleration (see e.g. Derishev et al. (2003) and Rieger & Duffy (2004) respectively), and others are associated with magnetic field instabilities like magnetic reconnection (Larrabee et al. 2003). Although the acceleration efficiency can not be still derived from theoretical grounds due to our poor knowledge on the jet properties, the detection of LS 5039 at very high-energy γ-rays (Aharonian et al.

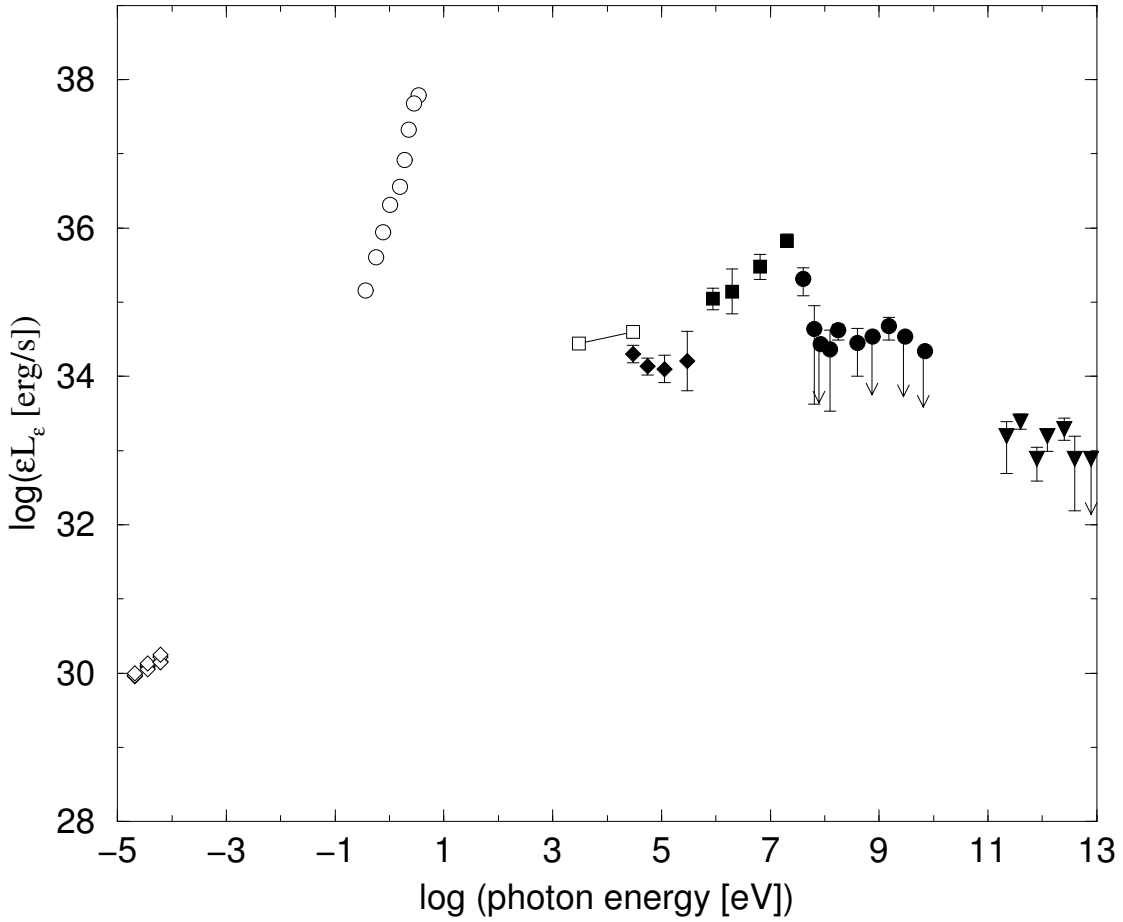

Figure 2.5: Spectral energy distribution of LS 5039, adapted from Paredes et al. (2006). The points observed are from Martí et al. (1998) (VLA, diamonds), Clark et al. (2001) and Drilling (1991) (optical, circles, corrected of absorption), Bosch-Ramon et al. (2005) (RXTE, squares), Harmon et al. (2004) (BATSE, filled diamonds), Collmar (2003) (COMPTEL, filled squares), Hartman et al. (1999) (EGRET, filled circles) and Aharonian et al. (2005a) (HESS, filled down triangles). The arrows in the EGRET and HESS data represent upper limits (3σ).

2005a) points to microquasar jets as highly efficient accelerators, no matter the origin of the detected radiation, whether leptonic or hadronic. Now, let us take a further step and explore how such emission has been produced.

Several scenarios can be considered. First, very high-energy γ-rays could be radiated in the jet inner regions via IC scattering of target photons, external or internal photons in relation to the jet, by relativistic leptons (see Atoyan & Aharonian 1999, Kaufman Bernadó et al. 2002 and Chapters 4 and 5). Second, this emission could also be generated in the inner jet regions by the jet relativistic protons through photo-meson (with disk/corona photons, see e.g. Aharonian et al. 2005b) and/or proton-proton interactions (with stellar wind ions, see e.g. Romero et al. 2003, Romero et al. 2005, Christiansen et al. 2006). These last two previously mentioned situations might not be common. In the former case, quite high photon densities and proton energies are required and, in the latter, usually a high mass stellar companion is required and the γ-ray absorption by the stellar photon field can be huge (see, e.g. Böttcher & Dermer 2005; Dubus 2006; and also Chapter 5). Moreover, particularly for leptons, energy losses in the inner jet could be very large, preventing efficient acceleration. At middle jet scales (i.e. milli-arcsecond scales -10^{14} cm-), a hadronic origin appears to be prevented by the lack of proton and photon targets. This is not the case for leptons, which might be accelerated to very high energies due to smaller losses and still radiate through stellar IC a significant part of their energy (see Chapters 5 and 6). This possibility appears more likely, since energy losses and absorption problems are much less serious, although the way how (and where) particles are accelerated is not clear yet (see Chapter 5). Finally, large scale jets are known particle accelerators (inferred from extended X-ray emission, see e.g. Corbel et al. 2002). At the moment, although requiring additional observational data, possible very high-energy γ-ray variability in LS 5039 (Casares et al. 2005) seems to preclude its large scale jet origin. Nevertheless, some radiation could be produced there and, although photon fields could be too faint for IC to be significant, accelerated hadrons could interact with high density interstellar medium nearby regions producing detectable amounts of very high energy photons (see Chapter 6).

The broadband spectrum consequences of hadronic and leptonic models are different. If radiation is mainly produced by hadronic interactions, the emission from the jet at lower energies will be given as a by-product. The main part of the relativistic particle energy, contained in hadrons, will be emitted as γ-rays whereas lower energies will be dominated by secondaries with a minor fraction of this energy

(an example on this is presented in Chapter 6). Otherwise, if the radiation origin is leptonic, fluxes at soft γ-rays or lower energies will be larger since, due to the presence of magnetic and photon fields, the radiative processes are more efficient than beyond 1 GeV (see Chapter 5). A mixed scenario could be possible, where primary leptons would dominate below 1 GeV, and hadrons above it. Nevertheless, the nowadays knowledge on the jet acceleration efficiencies for electrons and hadrons does not allow to give more weight to one or another option (this is discussed again in Chapter 5).

2.3 Hot topics and prospects

2.3.1 Multiwavelength studies on microquasars

Although X-ray binaries are indeed bright sources at X-rays, already in the 70s the complex spectral nature of these sources arose when radio emission of synchrotron origin was observed. The detection of strong radio outbursts from Cygnus X-3 (Gregory et al. 1972) and the extended radio jets of SS 433 (Spencer 1979) are clear examples of that, and though the use of the term microquasar spread after the detection of the jets of 1E 1740.7−2942 by Mirabel et al. (1992), during the previous decade the nature of these objects was intriguing for the community (some early attempts to explain the radio and sometimes the X-ray emission from X-ray binaries are by Band & Grindlay (1986), Hjellming & Johnston (1988), Martí et al. (1992), Peracaula (1997), etcetera). Therefore, it seems evident that broadband spectrum studies are required to discover more objects and better understand their properties. Following this line of work, identification studies at large scale were carried out by Paredes et al. (2002) (see also Ribó 2002) in order to enlarge the list of known microquasars. Several objects were proposed as candidates, but there was a source of undeniable microquasar nature, LS 5039, which has turned out to be among the most interesting sources in our Galaxy. As mentioned above, this has been the first microquasar proposed to be a high-energy γ-ray source[3] and detected at TeV energies. Therefore, multiwavelength studies have brought a source with

[3]LS I +61 303 was proposed as a high-energy γ-ray source (Gregory & Taylor 1978) before LS 5039. Nevertheless, the microquasar nature of the former was established after the discovery of the latter (Massi et al. 2001, 2004), delaying its recognition as γ-ray emitting microquasar.

challenging behavior (see Ribó (2002) and also Chapter 5), for which the origin and nature of some observed phenomena are to be unveiled yet.

2.3.2 New spectral windows and the multi-particle approach

The mentioned widening of the detected electromagnetic spectrum of microquasars, and further theoretical studies on other types of non electromagnetic radiation coming from them, have led to a new approach that is also valid and applicable in other astrophysical fields. As already mentioned in Sect. 2.2.3, TeV emission from microquasars had been predicted in the past by several authors. With a detection at these energies, virtually confirming the association with the EGRET and subsequently the COMPTEL and BATSE sources, microquasars are right now primary targets for all types of electromagnetic radiation instruments. However, the possible presence of relativistic hadrons has motivated the research of neutrino emission from microquasars. Photo-meson as well as proton-proton interactions possibly occurring in these objects lead to the production of neutrinos (see, e.g. Distefano et al. 2002, Bednarek 2005, Aharonian et al. 2005b, Christiansen et al. 2006). Actually, even if microquasars were relatively faint at TeV, it does not preclude neutrino production from being significant, since very high-energy γ-ray fluxes might be prevented by photon-photon absorption. The main factors to consider for neutrino production in microquasar jets are the maximum proton energy, the target photon energy, the photon or proton target densities and the kinetic energy carried by the relativistic particles. Finally, the presence of a significant amount of relativistic protons, by itself, can have unexpected observable consequences, sometimes in form of indirectly related radiation coming from nearby regions, or also a contribution to the galactic cosmic ray spectrum (see, e.g., Heinz & Sunyaev 2002 and Chapter 6).

From previous considerations, taking into account the new generation of detectors of different types of particles, it appears that the field of microquasars is a hot topic by itself. Indeed, there are several important queries to be answered, and the new findings are increasing fast the number of such questions. There are several questions that are not properly understood: the mechanism behind accretion and subsequent ejection (or other types of jet powering), available photon fields (inner disk region radiation), particle content, jet particle acceleration, jet Lorentz factor, overall jet power, relativistic particle power, energy transport, jet magnetic field and jet-environment interaction. All these questions and others equally important have

to be answered yet, and during next years such answers probably will come.

Bibliography

Aharonian F.A., Akhperjanian A.G., Aye K.M., et al., Jul. 2005a, Science, 309, 746 15, 18, 19

Aharonian F.A., Anchordoqui L.A., Khangulyan D., Montaruli T., 2005b, astro-ph/0508658 20, 22

Atoyan A.M., Aharonian F.A., Jan. 1999, MNRAS, 302, 253 16, 20

Band D.L., Grindlay J.E., Dec. 1986, ApJ, 311, 595 21

Barret D., Apr. 2004, In: AIP Conf. Proc. 703: Plasmas in the Laboratory and in the Universe: New Insights and New Challenges, 238–249 16

Bednarek W., Sep. 2005, ApJ, 631, 466 22

Bell A.R., Jan. 1978, MNRAS, 182, 147 18

Blandford R.D., Znajek R.L., May 1977, MNRAS, 179, 433 13

Bondi H., 1952, MNRAS, 112, 195 13

Bosch-Ramon V., Paredes J.M., Ribó M., et al., Jul. 2005, ApJ, 628, 388 19

Böttcher M., Dermer C.D., Nov. 2005, ApJ Letter, 634, L81 20

Casares J., Ribó M., Ribas I., et al., Dec. 2005, MNRAS, 364, 899 20

Christiansen H.R., Orellana M., Romero G.E., Mar. 2006, PhRvD, 73, 063012 20, 22

Clark J.S., Reig P., Goodwin S.P., et al., Sep. 2001, A&A, 376, 476 19

Collmar W., 2003, In: Proc. 4th Agile Science Workshop, p.177 19

Corbel S., Fender R.P., Tzioumis A.K., et al., Oct. 2002, Science, 298, 196 20

Derishev E.V., Aharonian F.A., Kocharovsky V.V., Kocharovsky V.V., Aug. 2003, PhRvD, 68, 043003 18

Distefano C., Guetta D., Waxman E., Levinson A., Aug. 2002, ApJ, 575, 378 22

Drilling J.S., Jul. 1991, ApJSS, 76, 1033 19

Dubus G., May 2006, A&A, 451, 9 20

Esin A.A., McClintock J.E., Narayan R., Nov. 1997, ApJ, 489, 865 12, 15, 16

Falcke H., Körding E., Markoff S., Feb. 2004, A&A, 414, 895 15

Fender R.P., Mar. 2001, MNRAS, 322, 31 15

Fender R.P., Gallo E., Jonker P.G., Aug. 2003, MNRAS, 343, L99 15

Fender R.P., Belloni T.M., Gallo E., Dec. 2004, MNRAS, 355, 1105 13, 16, 17

Gallo E., Fender R.P., Pooley G.G., Sep. 2003, MNRAS, 344, 60 15

Georganopoulos M., Aharonian F.A., Kirk J.G., Jun. 2002, A&A, 388, L25 15

Gregory P.C., Taylor A.R., Apr. 1978, Nature, 272, 704 21

Gregory P.C., Kronberg P.P., Seaquist E.R., et al., 1972, Nature, 239, 440 21

Hannikainen D.C., Hunstead R.W., Campbell-Wilson D., Sood R.K., Sep. 1998, A&A, 337, 460 15

Harmon B.A., Wilson C.A., Fishman G.J., et al., Oct. 2004, ApJSS, 154, 585 19

Hartman R.C., Bertsch D.L., Bloom S.D., et al., Jul. 1999, ApJSS, 123, 79 7, 9, 19

Heinz S., Dec. 2004, MNRAS, 355, 835 15

Heinz S., Sunyaev R., Aug. 2002, A&A, 390, 751 22

Heinz S., Sunyaev R.A., Aug. 2003, MNRAS, 343, L59 15

Hjellming R.M., Johnston K.J., May 1988, ApJ, 328, 600 21

Hujeirat A., Mar. 2004, A&A, 416, 423 13, 15

Kaiser C.R., Sunyaev R., Spruit H.C., Apr. 2000, A&A, 356, 975 16

Kaufman Bernadó M.M., Dec. 2004, Ph.D. Thesis, Universidad de Buenoas Aires, astro-ph/0504498 12

Kaufman Bernadó M.M., Romero G.E., Mirabel I.F., Apr. 2002, A&A, 385, L10 20

Larrabee D.A., Lovelace R.V.E., Romanova M.M., Mar. 2003, ApJ, 586, 72 18

Markoff S., Falcke H., Fender R., Jun. 2001, A&A, 372, L25 15

Martí J., Paredes J.M., Estalella R., May 1992, A&A, 258, 309 16, 21

Martí J., Paredes J.M., Ribó M., Oct. 1998, A&A, 338, L71 19

Massi M., Ribó M., Paredes J.M., Peracaula M., Estalella R., Sep. 2001, A&A, 376, 217 21

Massi M., Ribó M., Paredes J.M., et al., Jan. 2004, A&A, 414, L1 21

Meier D.L., Oct. 2003, New Astronomy Review, 47, 667 13

Mirabel I.F., Rodriguez L.F., Sep. 1994, Nature, 371, 46 8

Mirabel I.F., Rodriguez L.F., Cordier B., Paul J., Lebrun F., Jul. 1992, Nature, 358, 215 8, 21

Narayan R., Yi I., Oct. 1995, ApJ, 452, 710 13

Nolan P.L., Tompkins W.F., Grenier I.A., Michelson P.F., Nov. 2003, ApJ, 597, 615 9

Paredes J.M., Martí J., Ribó M., Massi M., Jun. 2000, Science, 288, 2340 7, 15, 18

Paredes J.M., Ribó M., Martí J., Oct. 2002, A&A, 394, 193 21

Paredes J.M., Bosch-Ramon V., Romero G.E., May 2006, A&A, 451, 259 19

Peracaula M., Jul. 1997, Ph.D. Thesis, Universitat de Barcelona 21

Rees M.J., Sep. 1978, MNRAS, 184, 61P 16

Ribó M., Nov. 2002, Ph.D. Thesis, Univesitat de Barcelona 10, 12, 21, 22

Rieger F.M., Duffy P., Dec. 2004, ApJ, 617, 155 18

Romero G.E., Benaglia P., Torres D.F., Aug. 1999, A&A, 348, 868 9

Romero G.E., Torres D.F., Kaufman Bernadó M.M., Mirabel I.F., Oct. 2003, A&A, 410, L1 20

Romero G.E., Grenier I.A., Kaufman Bernado M.M., Mirabel I.F., Torres D.F., Oct. 2004, In: ESA SP-552: 5th INTEGRAL Workshop on the INTEGRAL Universe, 703 9

Romero G.E., Christiansen H.R., Orellana M., Oct. 2005, ApJ, 632, 1093 20

Scott J.S., Chevalier R.A., Apr. 1975, ApJ Letter, 197, L5 18

Semenov V., Dyadechkin S., Punsly B., Aug. 2004, Science, 305, 978 13

Shakura N.I., Sunyaev R.A., 1973, A&A, 24, 337 12

Spencer R.E., Nov. 1979, Nature, 282, 483 21

van der Laan H., 1966, Nature, 211, 1131 16

Yuan F., Cui W., Aug. 2005, ApJ, 629, 408 15

Zdziarski A.A., Poutanen J., Mikolajewska J., et al., Dec. 1998, MNRAS, 301, 435 13, 15

Chapter 3

High energy processes in microquasars

In this chapter, we present different physical theories that play some role in our modeling of microquasars. Radiative processes, particle acceleration, accretion, creation and annihilation of pairs, special relativity, particle transport, all of them are the background upon which the different models are built. We intend to avoid overflow of formulae in the chapters devoted to the different works developed for this thesis. Thus, we show here in the context of their theory all those basic expressions used later in different modeling contexts, intending to give both a brief description of their basis and their meaning. We also describe here the basic properties of the cold matter dominated jet model used extensively in this thesis. It is worth noting that this is not an exhaustive review on the different processes that are thought to take place in microquasars, but just of those considered to explore observational features of microquasars. Just a few formulae are going to be presented in their corresponding context in next chapters. These are equations very related to the particular topic treated therein, like for instance the electron energy distribution or the spectral energy distribution in a given case.

3.1 Special relativity

When reference frames with relative velocities close to the speed of light are involved in emission processes (e.g. inverse Compton interactions between relativistic

jet electrons and external photon fields) and the emitter-observer relationship (e.g. Doppler boosted radiation), it is required to take into account special relativity effects. These effects are present in emitting processes whose characteristics use to be well known in a particular reference frame (e.g. the electron rest reference frame for the inverse Compton interaction, or the rest reference frame of the proton target in a proton-proton collision), requiring further transformation to the proper reference frame (e.g. the relativistic leptonic reference frame in the inverse Compton scattering, or the observer reference frame for jet emission). We give here few basic formulae that relate photon energy densities, spectral energy distributions, photon energies, lengths and volumes in different reference frames. For a more detailed explanation concerning special relativity and its role in the interaction processes themselves, we refer to the literature (see e.g. Blumenthal & Gould 1970, Pacholczyk 1970, Schutz 1985, Dermer & Schlickeiser 2002).

3.1.1 Reference frame transformations

Because of speed of light invariance, lengths and time intervals are different when measured in different reference frames relatively moving at velocities close to the speed of light. The tensor representing the transformation of these quantities can be found in any undergraduate course textbook, and we will just give a brief description of the effects on the quantities relevant for this work.

For transforming photon energies, it is needed the angle (θ) formed by the photon direction in the observer reference frame (i.e. the reference frame where the measure of the property is done) with the motion direction of the moving reference frame (i.e. the reference frame where the studied process takes place) in relation to the observer frame, and their relative velocity. This angle is required since the speed of light is finite, and light retarding effects affecting the observer view occur and depend on the mentionde angle. An electromagnetic wave/photon is a phenomenon extended in space and time, and its properties in respect to the observer will depend on the former angular dependence and the relative velocity, i.e. they will depend on the reference frame. The next formulae are used for energy transformation from the moving to the observer reference frame:

$$\epsilon' = \delta\epsilon \qquad \delta = \frac{1}{\Gamma(1-\beta\cos\theta')}, \tag{3.1}$$

β is the relative velocity in speed of light units (if the system is receding, $\beta\cos\theta' < 0$,

for the same θ'), i.e. $\beta = V/c$, $\Gamma = (1-\beta^2)^{-1/2}$ is the corresponding Lorentz factor, θ' is the angle in the observer reference frame, ϵ is the energy in the moving reference frame, and ϵ' is the energy in the observer reference frame (in this section, primes indicate observer reference frame).

Besides the light speed, another invariant is the number of particles per phase space volume unit, in space dx and momenta $d\mathbf{p}$ (for a photon gas, $\epsilon = |\mathbf{p}|c$), when there is no pair creation and/or annihilation. This implies that the energy density of photons per energy and solid angle units in the observer reference frame is:

$$U'(\epsilon', \Omega') = \delta^3 U(\epsilon, \Omega), \tag{3.2}$$

where Ω corresponds to the direction of the photons. If the coordinate choice is suitable, i.e. one where the angle θ is taken as the zenith one, the azimuthal angle does not change, and θ fulfills (as a visual example, see Fig. 3.1):

$$\cos\theta' = \frac{\cos\theta + \beta}{1 + \beta\cos\theta}. \tag{3.3}$$

$U'(\epsilon', \Omega')$ is used in the reference frame of the the jet (the jet would be the *observer*), for instance, to calculate the external photon energy density (note that in such a case the signs change). For illustrative purposes, see Fig. 3.2. To find the emissivity in the observer reference frame, there is the expression:

$$j'(\epsilon', \Omega') = \delta^2 j(\epsilon, \Omega), \tag{3.4}$$

from which it is possible to derive the luminosity per solid angle unit $L'(\epsilon', \Omega')$ integrating $j'(\epsilon', \Omega')$ over the emitting volume that, in the observer reference frame, is $V' = \delta V$. This comes from the apparent elongation/contraction, depending on the β and θ' values, of the length along the motion direction, $X' = \delta X$, where δ comes from taking into account retarding light effects and the length contraction in the observer reference frame. As an example, the spectral energy distribution in the optically thin case (inferred isotropic luminosity) from the viewpoint of an observer at Ω'_0, $\epsilon L'(\epsilon')_{\Omega'_0}$ can be derived from:

$$\epsilon' L'(\epsilon')_{\Omega'_0} = 4\pi\epsilon'\delta(\Omega'_0)^3 \int_V j(\mathbf{x}, \epsilon'/\delta, \Omega(\Omega'_0))dv. \tag{3.5}$$

in the more general case, when $j(\mathbf{x}, \epsilon'/\delta, \Omega(\Omega'_0))$ is not spatially homogeneous. When $j(\epsilon'/\delta, \Omega(\Omega'_0))$ is spatially homogeneous, isotropic and $\propto \epsilon'^{-\alpha}$ (where α is the spectral index), a classical expression is recovered:

$$\epsilon' L'(\epsilon')_{\Omega'_0} = \epsilon'\delta(\Omega'_0)^{3+\alpha} L(\epsilon'). \tag{3.6}$$

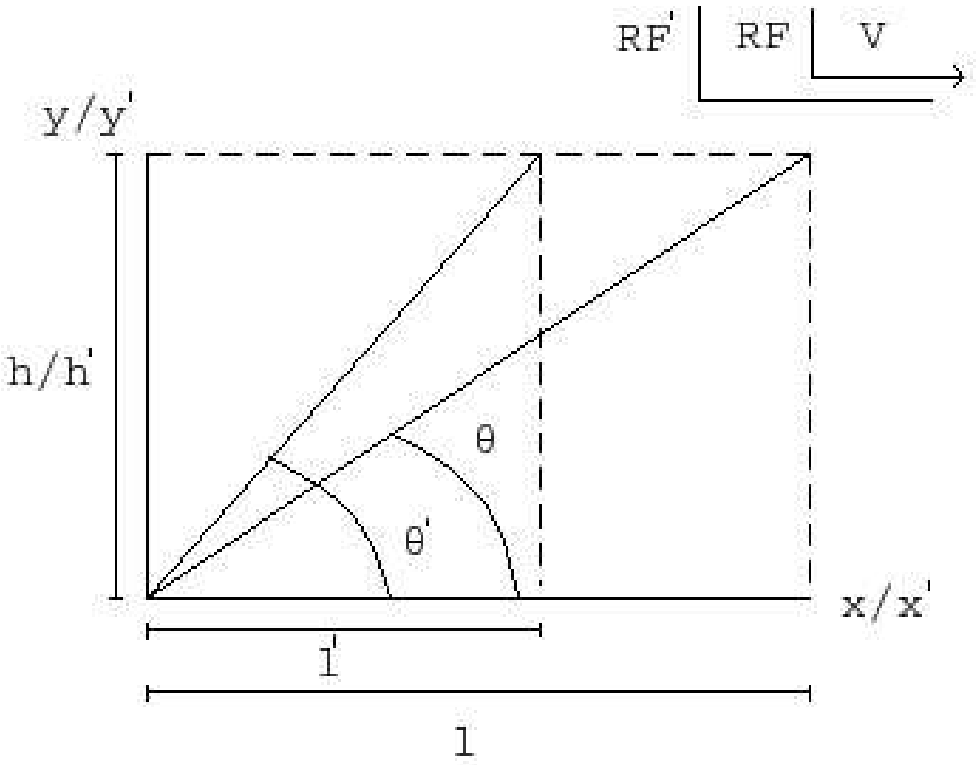

Figure 3.1: θ' in relation to θ due to length contraction when measuring in the observer reference frame (RF'). V is the velocity of motion of the moving reference frame (RF) in relation to the RF'.

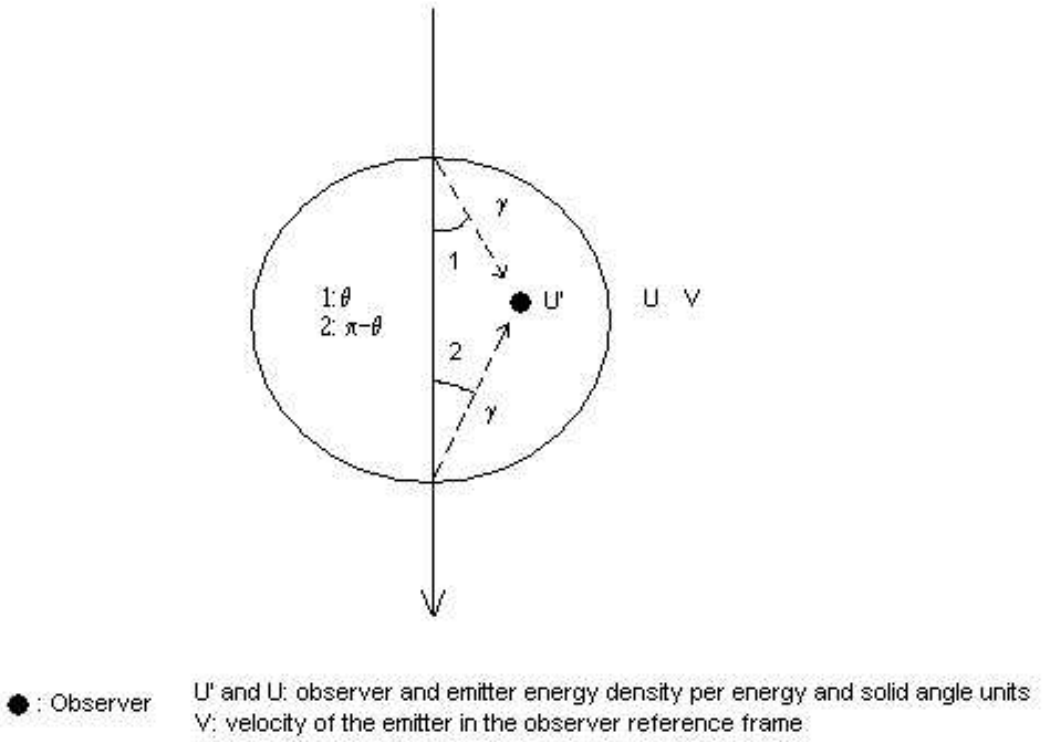

Figure 3.2: This picture intends to show the relationship between $U'(\epsilon', \Omega')$, $U(\epsilon, \Omega)$, angles and relative motion direction in the observer and emitter reference frames.

3.2 Radiative processes

To explore the possibility of detection of a microquasar in a certain energy range, or just to explain what has been observed, we have to assume a particular mechanism or mechanisms of radiation production. Concerning microquasar jets, due to our ignorance about their matter and energy content, it is necessary to guess what jet conditions appear reasonable from the point of view of general astrophysical knowledge to explain the broadband spectrum obtained from microquasars. It is clear that radiation at radio frequencies is produced by synchrotron emission, so relativistic leptons are present. Besides the previous fact, nothing else can be stated certainly in general for microquasar jets. As it is explained in further chapters, X-rays could be produced in the jet, but this could not be case. γ-rays could be originated by leptonic or hadronic processes in the jet, but again this could not be the case (perhaps further up[1], in the interstellar medium?). Moreover, even radio emitting electrons could be primary or secondary particles (i.e. originated by pair creation), depending on the leading relativistic leptonic population radiating at those energies. There are some facts of dubious interpretation that could be hints of relativistic hadrons in the jet, but the same could be said concerning leptons, on different grounds. In short, several equally possible scenarios can be put forward and they are to be discussed and explored in more detail, although only future observational data will be able to falsify some of them. In this section, two classes of processes producing electromagnetic radiation are presented, depending on the nature of the involved particles: leptons or hadrons. Different mechanisms of both types are explained, put briefly in context, and some useful expressions are given. We provide with formulae used by us in our calculations but, for full derivations, references are given in the text. We note that, if not explicitly stated, the units are in the cgs system.

[1]By 'futher up' we mean, in the jet, at larger distance from the compact object.

3.2.1 Leptonic processes

Synchrotron emission

Synchrotron radiation is produced when a charge suffers centripetal acceleration due to the presence of magnetic field lines. The particle moves along the field line direction, but it spirals around it due to the Lorentz force created by the magnetic field, the force being parallel to the plane perpendicular to the field lines. There is a radius and a frequency associated with such spiral motion. We will focus on the case of electron velocities close to c, when relativistic effects arise and the emission frequency is not the spiraling frequency. Nevertheless, emission is concentrated around the so called characteristic frequency, with the electron also emitting at lower and higher frequencies when observed in the observer reference frame. This characteristic frequency $\nu_{\rm c}$ can be expressed as in Pacholczyk (1970):

$$\nu_{\rm c}(\gamma, B_{||}) = 4.22 \times 10^6 B_{||} \gamma^2, \tag{3.7}$$

where $B_{||}$ is the magnetic field parallel to the particle motion (B, from now on), and γ is the electron Lorentz factor.

The electron is radiating following a power function that peaks at $0.29\nu_{\rm c}$. Although Bessel functions of second kind are involved for calculating the power of one electron, we use an approximation (Melrose 1980) that is valid up to $\sim 10\nu_{\rm c}$ with few per cent of error, good enough for the thesis purposes:

$$P(\gamma, \nu, B) = 4.39 \times 10^{-22} B \left(\frac{\nu}{\nu_{\rm c}}\right)^{1/3} \exp(-\nu/\nu_{\rm c}), \tag{3.8}$$

$P(\gamma, \nu, B)$, through B, could have spatial dependence, although it is not made explicit. From now on, we will work with the photon energy in $m_{\rm e}c^2$ units, ϵ, instead of ν, where $\epsilon = 8.07 \times 20^{-21}\nu$. Knowing the power radiated by an electron of Lorentz factor γ per frequency unit and the electron energy distribution density per solid angle unit $n(\mathbf{x}, \gamma, \Omega)$ [2], one can compute the emissivity $j(\mathbf{x}, \epsilon, \Omega)$ (from which luminosity can be obtained, see above), the absorption coefficient $k(\mathbf{x}, \epsilon, \Omega_{\rm obs})$ (for a certain observer direction), the energy distribution density per solid angle unit $U(\mathbf{x}, \epsilon, \Omega)$, and the intensity $I(\mathbf{x}, \epsilon, \Omega)$. The mentioned expressions have the form

[2] Besides the spatial dependence, there may be also a temporal dependence. It has not been included in this chapter for clarity.

(adapted from Pacholczyk 1970):

$$j(\mathbf{x},\epsilon,\Omega)=\int_{\gamma_{\rm min}}^{\gamma_{\rm max}} n(\mathbf{x},\gamma,\Omega)P(\gamma,\nu,B)d\gamma, \tag{3.9}$$

$$k(\mathbf{x},\epsilon,\Omega_{\rm obs})=-\frac{c^2h_{\rm Planck}^2}{2(m_{\rm e}c^2)^3\epsilon^2}\int_{\gamma_{\rm min}}^{\gamma_{\rm max}}\frac{d}{d\gamma}\left(\frac{n(\mathbf{x},\gamma,\Omega_{\rm obs})}{\gamma^2}\right)\gamma^2P(\gamma,\nu,B)d\gamma, \tag{3.10}$$

and (in the local approximation, see e.g. Ghisellini et al. 1985)

$$U(\mathbf{x},\epsilon,\Omega)=\frac{R_{\rm c}}{c}j(\mathbf{x},\epsilon,\Omega), \tag{3.11}$$

where $\gamma_{\rm min}$ and $\gamma_{\rm max}$ could have spatial or time dependence[3]. $R_{\rm c}$ is the characteristic size of the emitting region. For the intensity function, $I(\mathbf{x},\epsilon,\Omega)$, we have adopted the spatially homogeneous, one dimension (x), and isotropic case (then: $j(\epsilon,\Omega)=j(\epsilon)/4\pi$, $k(\epsilon,\Omega)=k(\epsilon)$, $U(\epsilon,\Omega)=U(\epsilon)/4\pi$ and $I(x,\epsilon,\Omega)=I(x,\epsilon)/4\pi$) of the differential equation for the radiative transport, enough for our purposes:

$$\frac{dI(x,\epsilon)}{dx}=j(\epsilon)-k(\epsilon)I(x,\epsilon), \tag{3.12}$$

with solution:

$$I(R_{\rm c},\epsilon)=\frac{j(\epsilon)}{k(\epsilon)}(1-\exp[-\tau(\epsilon)]), \tag{3.13}$$

where $\tau(\epsilon)=R_{\rm c}k(\epsilon)$ for the spatially homogeneous case. It is worth noting that more complex equations could be used concerning radiative transport. Nevertheless, when computing this quantities for a homogeneous region, or even in the case of a jet that is inhomogeneous in a particular direction, i.e. along the jet axis, the approach can be simplified and the given expressions are good enough for our level of approximation. There is one particular case in Chapter 6, when radiative transport equation has to be solved for the inhomogeneous spherically symmetric isotropic case:

$$\frac{dr^2I(r,\epsilon)}{r^2dr}=j(r,\epsilon)-k(r,\epsilon)I(r,\epsilon), \tag{3.14}$$

with solution:

$$I(r,\epsilon)=\frac{1}{4\pi r^2}\int_0^{\rm r}4\pi r_1^2j(r_1,\epsilon)\exp\left(-\int_{\rm r_1}^{r}k(r_2,\epsilon)dr_2\right)dr_1, \tag{3.15}$$

where r is the radius of the spherical source. It is worthy showing the optically thin case solution:

$$I(r,\epsilon)=\frac{1}{4\pi r^2}\int_0^{\rm r}4\pi r_1^2j(r_1,\epsilon)dr_1. \tag{3.16}$$

[3]In case of optically thick emission, $R_{\rm c}$ would turn to the mean length covered by the synchrotron photons before being absorbed.

Exchanging r by x, and $4\pi r^2$ by the typical emitting region surface, we get the solution for the one dimension problem.

So far an electron is radiating, it losses energy and the Lorentz factor decreases. When synchrotron absorption is not considered, it can be expressed as (Pacholczyk 1970):

$$\dot{\gamma} = -1.94 \times 10^{-9} B^2 \gamma^2. \tag{3.17}$$

We recall that, if not explicitly stated, units are cgs. Losses have a feedback effect on the electron energy distribution, and the computation of the spectral energy distribution needs to consider the geometry of the problem and relativistic effects. In next chapters we will give expressions concerning previous issues, taking into account particular characteristics of the problems to solve like spatial and temporal dependences of physical quantities, geometry (jet-like, spherical, etc) and Doppler boosting. It also applies to the other radiative processes treated here.

Inverse Compton

Electrodynamic interactions between electrons and photons with relative motion leads to the transfer of energy and momentum in an elastic form. Depending on the reference frame, the process is called normal or inverse Compton scattering, depending on who is gaining energy and momentum, the electron for the former and the photon for the latter (the process considered here). When the energy transferred from the electron to the photon is much smaller than the incoming electron energy, the problem can be treated very easily, since the cross section is roughly constant, and the interaction is called to occur in the Thomson or classical regime. However, when the outgoing photon to incoming electron energy ratio reaches a significant fraction of 1, quantum field effects must be taken into account, and the cross section becomes smaller than that in the Thomson regime at lower energies. This quantum regime of interaction is called Klein-Nishina, and the transition photon and electron energies fulfill $\epsilon_0 \gamma \sim 1$, where ϵ_0 and γ are the incoming photon and electron energies in $m_{\rm e}c^2$ respectively.

A useful expression for the cross section where the angular dependence is averaged, very used in this thesis and valid for both the Thomson and the Klein-Nishina

regime, has been obtained from Blumenthal & Gould (1970):

$$\frac{d\sigma(x_{\rm ic},\epsilon_0,\gamma)}{d\epsilon} = \frac{3\sigma_{\rm T}}{4\epsilon_0\gamma^2}\ f(x_{\rm ic}), \tag{3.18}$$

where

$$\begin{aligned} f(x_{\rm ic}) &= \left[2x_{\rm ic}\ln x_{\rm ic} + x_{\rm ic} + 1 - 2x_{\rm ic}^2 + \frac{(4\epsilon_0\gamma x_{\rm ic})^2}{2(1+4\epsilon_0\gamma x_{\rm ic})}(1-x_{\rm ic})\right] \\ &\quad \times P(1/4\gamma^2,\ 1,\ x_{\rm ic}). \end{aligned} \tag{3.19}$$

Here, $x_{\rm ic} = \epsilon/[4\epsilon_0\gamma^2(1-\epsilon/\gamma)]$, where ϵ_0 and ϵ are the energies of the incoming and the outgoing photons respectively; $\sigma_{\rm T} = 6.65\times10^{-25}$ cm^2 is the Thomson cross section, and $P(1/4\gamma^2,\ 1,\ x_{\rm ic}) = 1$ when $1/4\gamma^2 \leq x_{\rm ic} \leq 1$, and 0 otherwise.

Unlike synchrotron radiation, inverse Compton emission is optically thin for the cases studied in this work. To compute the emissivity, the next expression can be used:

$$j(\mathbf{x},\epsilon,\Omega) = m_{\rm e}c^2\int_{\gamma_{\rm min}}^{\gamma_{\rm max}}\int_{1/4\gamma^2<x_{\rm ic}<1} \epsilon n_{\rm phot}(\mathbf{x},\epsilon)cn(\mathbf{x},\gamma,\Omega)\frac{d\sigma(x_{\rm ic},\epsilon_0,\gamma)}{d\epsilon}d\gamma d\epsilon_0, \tag{3.20}$$

We note that, $n_{\rm phot}(\mathbf{x},\epsilon)$ could have a solid angle dependence though it is generally taken as isotropic. Nevertheless, when treating monodirectional photon fields like star and accretion disk ones when their sources are far enough, an additional term is introduced in the emissivity already in the observer reference frame $(1-\cos\theta'_{\rm f})^{(\alpha+1)/2}$, where θ is the angle between the electron and the photon directions (Dermer et al. 1992). It is only valid in the Thomson approximation, since the angular dependence becomes less important in the Klein-Nishina regime, but it is going to be enough at our level of approach. As it has been shown for synchrotron radiation, from the emissivity one can derive the inverse Compton $U(\mathbf{x},\epsilon,\Omega)$ and $I(\mathbf{x},\epsilon,\Omega)$ (knowing $R_{\rm c}$, it is trivial in the optically thin case). Concerning the spectral energy distribution, where volume, geometry and other aspects of each particular problem matter, its derivation is left for next chapters.

Regarding energy losses, there are two expressions that can be used, or combined, depending whether we are dealing either with the Thomson, a transitional or the Klein-Nishina regime. For the Thomson regime, energy losses are well described by (see e.g. Blumenthal & Gould 1970):

$$\dot{\gamma} = -3.20\times10^{-8}U_{\rm total}(\mathbf{x})\gamma^2, \tag{3.21}$$

and for the Klein-Nishina regime (see e.g. Aharonian 2004):

$$\dot{\gamma} = -8.90 \times 10^{-9} U_{\rm total}(\mathbf{x}) \frac{\ln[4\epsilon_0\gamma] - 11/6}{\epsilon_0^2}. \tag{3.22}$$

Here, $U_{\rm total}$ is the energy density of the photon field. This is a simplified version for the Klein-Nishina case, when the radiation field can be considered monoenergetic with photon energy ϵ_0.

Relativistic Bremsstrahlung

As noted above, when a charge is accelerated, it radiates. In the case of electrons, when they are moving freely through an ionic or atomic field, the electrostatic fields generated by the atoms/ions deviate the electrons accelerating them. When considering relativistic electrons under the effect of non relativistic ions (e.g. leptonic cosmic rays moving though interstellar medium), to compute emission coming from those electrons, we can use the next cross section (see e.g. Lang 1980):

$$\frac{d\sigma(\gamma,\epsilon)}{d\epsilon} = \frac{4\alpha Z^2 q_{\rm e}^4}{\epsilon (m_{\rm e}c^2)^2}\phi(\gamma,\epsilon), \tag{3.23}$$

where

$$\phi(\gamma,\epsilon) = \left[1 + \left(1 - \frac{\epsilon}{\gamma}\right)^2 - \frac{2}{3}\left(1 - \frac{\epsilon}{\gamma}\right)\right]\left[\ln\left(\frac{2\gamma(\gamma-\epsilon)}{\epsilon}\right) - \frac{1}{2}\right] \tag{3.24}$$

for the case of a bare nucleus, while for a fully screened nucleus:

$$\phi(\gamma,\epsilon) = \left[1 + \left(1 - \frac{\epsilon}{\gamma}\right)^2 - \frac{2}{3}\left(1 - \frac{\epsilon}{\gamma}\right)\right] \times \ln\left(\frac{191}{Z^{1/3}}\right) + \frac{1}{9}\left(1 - \frac{\epsilon}{\gamma}\right). \tag{3.25}$$

Here, $\alpha = 1/137.04$ is the fine structure constant, Z is the atomic number and $q_{\rm e}$ is the electron charge. The emissivity for Bremsstrahlung emission can now be derived:

$$j(\mathbf{x},\epsilon,\Omega) = m_{\rm e}c^2 \int_{\gamma_{\rm min}}^{\gamma_{\rm max}} \epsilon n_{\rm p}(\mathbf{x}) c n(\mathbf{x},\gamma,\Omega) \frac{d\sigma(\gamma,\epsilon)}{d\epsilon} d\gamma, \tag{3.26}$$

where $n_{\rm p}(\mathbf{x})$ is the density of targets. We note that the cross section is known in the reference frame where the target is at rest (e.g. at rest in the jet reference frame, when computing the relativistic Bremsstrahlung produced by interaction between the jet relativistic electrons and jet cold protons; at rest in the compact object reference frame when computing the same but for stellar wind ions). As explained

above, from $j(\mathbf{x}, \epsilon, \Omega)$ the other physical quantities concerning radiation ($U(\mathbf{x}, \epsilon, \Omega)$, $I(\mathbf{x}, \epsilon, \Omega)$) can be derived, as well as the spectral energy distribution taking into account the particular scenario to study.

For computing the effect of radiation on $n(\mathbf{x}, \gamma, \Omega)$, we need the expression for the energy losses. Next we present the formulae for the bare nucleus and the full screened nucleus case respectively (Longair 1994):

$$\dot{\gamma} = -6.9 \times 10^{-17} n_{\rm p}(\mathbf{x}) Z^2 (\ln \gamma + 0.36)\gamma, \tag{3.27}$$

$$\dot{\gamma} = -6.9 \times 10^{-17} n_{\rm p}(\mathbf{x}) Z^2 \left(\ln(183 Z^{-1/3}) - \frac{1}{18}\right)\gamma. \tag{3.28}$$

3.2.2 Hadronic processes

Hadrons, e.g. protons, can carry information and/or produce emission, telling us about the conditions in the regions either crossed by them or where they were accelerated. For instance, ultra high-energy neutrons can cover kpc distances before beta-decaying due to relativistic effects, providing data about the place they were released; protons radiate all along their way through the interstellar medium, tracing matter densities as well as informing about diffusion coefficients; hadronic radiation can be detected from point-like sources, being an indicator of the extreme conditions therein. Other products of hadronic interactions like neutrinos and pairs can be important when investigating the nature of the mechanisms involved in the emission. In case of relativistic jets, no matter whether galactic or extragalactic, the detection of neutrinos would be an evidence of the presence of relativistic hadrons. Moreover, radiation produced by secondary particles could imply the existence of a counterpart at lower energies detectable and relatively fainter than the hadronic emission itself. In this thesis the different hadronic mechanisms are not treated in detail, but only proton-proton interaction and its secondary pairs produced by the interaction of a relativistic jet with its environment (see Chapter 6). Concerning the different possibilities that could be given in many astrophysical scenarios, we refer elsewhere (see e.g. Cheng & Romero 2004 and Aharonian 2004).

Proton-proton collisions

Relativistic protons and nuclei interact with ambient gas producing secondary pions (π), kaons and hyperons. These baryons decay producing γ-rays and other secondary products like electron-positron pairs. Neutral pions are the main channel of conversion of proton kinetic energy to γ-rays, although there is also production of pairs through charged pion decay to muons, which finally decay to pairs and neutrinos. These secondary pairs contribute to the spectrum at high and low energies through synchrotron, relativistic Bremsstrahlung and inverse Compton effect. The channels of proton-proton interaction that yield either π^0, π^- or π^+ are roughly equiprobable at high energies, and the functions that represent the photon, the electron and the positron energy distributions resulting from the pion decay can be taken to be similar. Concerning the ratio between the energy that goes to γ-rays through neutral pion decay and the one that goes to pairs through charged pion/muon decay, it is about one half for proton energy distribution of power-law index ~ 2 (for a more detailed treatment on this, see e.g. Drury et al. 1994). In Chapter 6, a treatment on the emission from a particular proton spectrum is presented. Here, we give the expressions necessary for calculating the emissivity of the photons produced by π^0-decay (j_γ) for any proton energy distribution density ($n_{\rm p}(t,\mathbf{x},\gamma,\Omega)$). The time dependence is included, and ϵ is in $m_{\rm p}c^2$ units. The emissivity is (Aharonian & Atoyan 2000):

$$j_\gamma(t,\mathbf{x},\epsilon,\Omega) = 2\eta_{\rm A} m_{\rm p} c^2 \epsilon \int_{\gamma_{\pi\rm min}}^{\gamma_{\pi\rm max}} \frac{q_\pi(t,\mathbf{x},\gamma_\pi,\Omega)}{\sqrt{\gamma_\pi^2-1}} d\gamma_\pi, \tag{3.29}$$

where $\eta_{\rm A} \sim 1$ takes into account the effect of the nuclei, in both the relativistic and the target particles (Aharonian & Atoyan 1996), ϵ and γ_π are the energy of the emitted photon and the decaying pion respectively, $\gamma_{\pi\rm min} = \epsilon + m_\pi^2 c^4/4(\epsilon m_{\rm p}^2 c^4)$, and m_π is the pion mass. q_π, the pion number emissivity (of units: $\gamma_\pi^{-1}{\rm cm}^{-3}{\rm s}^{-1}{\rm srad}^{-1}$), can be computed from:

$$\begin{aligned} q_\pi(t,\mathbf{x},\gamma_\pi,\Omega) &= c n_{\rm H} \int_{\gamma_{\rm min}}^{\gamma_{\rm max}} \delta(\gamma_\pi - k_\pi E_{\rm kin}) \sigma_{\rm pp}(\gamma) n_{\rm p}(t,\mathbf{x},\gamma,\Omega) d\gamma \\ &= \frac{c n_{\rm H}}{k_\pi} \sigma_{\rm pp}(1+\gamma_\pi m_\pi/k_\pi m_{\rm p}) n_{\rm p}(t,\mathbf{x},1+\gamma_\pi m_\pi/k_\pi m_{\rm p},\Omega), \end{aligned} \tag{3.30}$$

where k_π is the mean fraction of the kinetic energy ($E_{\rm kin} = \gamma - 1$) of the proton transferred to the secondary leading pion per collision, $n_{\rm H}$ is the density of target nuclei (in some cases $n_{\rm H}(\mathbf{x})$), and $\sigma_{\rm pp}(\gamma) = 3\times10^{-26}[0.95+0.06\ln(\gamma/1.1)]$ cm^2 is the cross section of the pp interaction. We note that, as in relativistic Bremsstrahlung,

the cross section is known in the target nuclei reference frame. This approach of emissivity calculation of π^0-decay γ-rays gives quite good accuracy down to energies $\sim$1 GeV (Aharonian & Atoyan 2000). It is worth noting that we follow the approach when the spectrum at high energies is dominated by the isobar channel, even when energetically the interaction is dominated by the fireball channel (Pfrommer & Enßlin 2003).

Although in most of cases the proton-proton energy losses are negligible, the expression for the energy loss rate can be derived from the cross section given above:

$$\dot{\gamma} = -4.5 \times 10^{-16} n_{\rm H} \left[0.95 + 0.06 \ln\left(\frac{\gamma}{1.1}\right)\right] \gamma, \tag{3.31}$$

were the inelasticity coefficient has been taken into account (Aharonian & Atoyan 1996).

3.3 Particle acceleration

Very hot matter radiating thermally can be found for instance in the inner regions of black hole accretion disks, either stellar or super-massive ones, or inside the stars. Nevertheless, the typical energy of the radiation produced in such environments hardly will be above that of X-rays. As an example, the thermal distribution of electrons thought to be present close to the X-ray binary compact object, with temperatures of 10^9 K, radiates peaking around 100 keV. It is by far too small for explaining emission beyond 1 MeV, indeed observed in these sources. Moreover, such γ-ray emission does not follow the spectral shape of the emission from thermal matter, but it is usually a power-law-like spectrum, clearly generated by a non thermal population of particles, of any type whatsoever, either hadrons or leptons. It is worth mentioning that nuclear transitions produce γ-ray lines, but cannot explain the most of the γ-ray detections.

Acceleration beyond the thermal tail is an old problem in astronomy. In fact, the idea that the γ-ray sky is actually plenty of sources arose not many years ago (see Chapter 2). The detection of more and more sources emitting above X-rays is evidence of the importance of the role played by particle acceleration. Particle acceleration by either first or second order Fermi mechanism, or some sort of magnetic instability, is inferred to explain the observed high energy emission from different types of source. Moreover, low energy radiation can be also produced, via e.g.

synchrotron or curvature emission, and some sources present a broadband spectrum that could be completely nonthermal (e.g. some microquasars, see Chapter 5). Here it is not intended to give a review on particle acceleration, but just to briefly sketch the treatment performed in this work to explain the existence of very high energy emitting particles in microquasars. For more details, many works can be found in the literature (see e.g. Scott & Chevalier 1975, Bell 1978a, Drury 1983, Jones & Ellison 1991, Derishev et al. 2003, Rieger & Duffy 2004).

3.3.1 The Fermi process of particle acceleration

It is well known nowadays that transport of energy is required for powering large scale emission in/around microquasars. Observations have shown that emission can suddenly rise, for instance at X-rays, after a quiet period of silent advance of a blob through the interstellar medium (Corbel et al. 2002). Moreover, heated radio emitting interstellar medium has been observed surrounding galactic objects (Gallo et al. 2005). Nevertheless, it was established much earlier that extragalactic jets had large radio lobes that were powered by a radiatively inefficient flow (e.g. Neff & Brown 1984), and it seems very likely that all these phenomena are associated with the heating of particles beyond a thermal distribution, up to synchrotron radio emitting energies or beyond.

In the leptonic scenario of microquasars, if no particle acceleration takes place, the conditions of the jet inner region do not allow electrons to reach the regions where they emit at radio frequencies with enough energy to do so with the observed spectrum. Particles will radiate all their energy in the very inner part of the jet (see Chapter 4) due to the likely presence of strong radiation and magnetic fields. It seems, as it will be explained in Chapter 5, that an acceleration mechanism is operating there. We have adopted a simple power-law distribution for the injected particles, assuming for simplicity that the acceleration mechanism, some kind of shock moving through the background jet medium, keeps the electron energy distribution with an injection-like energy distribution even when radiative losses occur. It is a rough oversimplification, since it will happen only if the mechanism prevents particle accumulation at lower energies due to inefficient losses.

The main idea is that the shock moves through the upstream medium (i.e. unshocked region), which would be the relatively cold matter background of the jet,

and some particles, those with enough energy to diffuse through the shock, cross it entering into the downstream medium (i.e. the shocked region). These particles, which do not follow initially an isotropic distribution of velocities in the downstream, isotropize and, eventually, a fraction of them emerges again to the upstream region but with larger energy, extracted from the shock. The process takes place several times, and finally particles either stop accelerating due to radiation energy losses or simply leave the acceleration/shock region due to its diffusion length is larger than the size of the accelerator. This description corresponds to the so called first order Fermi acceleration mechanism. When particles interact with several scattering centers in a background medium acquiring some of their energy and momentum, it is called second order Fermi acceleration mechanism.

As mentioned above, particles diffusing through the shock must be energetic enough (Bell 1978b). One way to understand this problem is thinking on the diffusion length of the particles to be accelerated in comparison with the width of the shock, which in a magnetized plasma can be taken similar to the gyroradius ($r_{\rm g}$) of the particles that form the shock itself:

$$r_{\rm g} = \frac{Vmc}{q_{\rm e}B}, \tag{3.32}$$

for a non relativistic plasma and

$$r_{\rm g} = \frac{\gamma mc^2}{q_{\rm e}B}. \tag{3.33}$$

for a relativistic one. If particles to be accelerated cannot diffuse through the shock to reach the downstream region and isotropize, the acceleration mechanism will not be efficient. It means that particles with energies larger than the shock particle energy can be effectively accelerated, providing with a rough estimate of the minimum Lorentz factor ($\gamma_{\rm min}$) of accelerated particles. It is a weak condition for protons in general, but not for electrons, which need to be already relativistic if the plasma is energetically dominated by protons, even by non relativistic ones. This problem is the well known injection problem in particle acceleration. Here, we will assume that an unspecified mechanism is injecting electrons. It is not a serious problem after all, since the significant source of energy that feeds particles comes from the shock mechanism, and not from the unspecified one (Mastichiadis & Kirk 1995).

The acceleration rate is modeled here in a very simple way. We have parametrized the maximum acceleration rate allowed by classical electrodynamics:

$$\dot{\gamma} = \eta q_{\rm e} Bc/mc^2. \tag{3.34}$$

η is the parameter which plays the role of a function in Fermi acceleration theory that depends on the diffusion coefficients in the shock downstream and the shock speed in the upstream (unshocked medium) $V_{\rm S}$. Depending on the angle formed by the magnetic field line direction with the shock surface perpendicular direction, the diffusion coefficient ($C_{\rm B}$ times Bohm diffusion) will render a different dependence on $C_{\rm B}$:

$$\eta = \frac{3C_{\rm B}}{8}\left(\frac{V_{\rm S}}{c}\right)^2 \tag{3.35}$$

when such angle is of $\pi/2$, and

$$\eta = \frac{3}{20C_{\rm B}}\left(\frac{V_{\rm S}}{c}\right)^2 \tag{3.36}$$

when it is 0° (Protheroe 1999). The Bohm diffusion regime is that corresponding to the case when typical diffusion length of the particle is equal to its gyroradius, taking B as the magnetic field in the upstream. This is valid for the non relativistic case. Relativistic shocks might take place in microquasars, although it seems that at least in some cases they are not very relativistic, since jet and counter jet are both observable in radio implying no strong beaming (e.g. for LS 5039, see Paredes et al. 2000, and for LS I +61 303, see Massi et al. 2004). Therefore, a non relativistic approach has been used as a first order approximation to constrain η values. This subject is discussed also in Chapter 5.

3.4 Accretion and jet ejection

The potential well of the compact object in a microquasar traps the matter expelled from the companion due to either a strong wind or Roche lobe overflow. To roughly know whether matter will be kept by the compact object gravity, one can compare the kinetic and the potential energy of matter around the accreting object. In case the latter overcomes the former, the matter infall takes place. Nevertheless, there is an excess of accreted matter angular momentum in relation to the compact object, implying that the infall will not be radial, but some motion on the plane perpendicular to the angular momentum direction will occur. In such a case a disk is formed, consisting on rings of matter following almost Keplerian orbits around the compact object. Energy is dissipated in the disk and angular momentum is transported, allowing matter to get closer and closer to the gravity source and

suffering a large increase of its density and temperature. The structure of matter, the accretion mode, is to change so far conditions become more extreme. In the standard scenario, the macroscopic configuration of the magnetic field lines in the inner regions of the accretion disk can affect the accreted plasma by magneto-centrifugal forces driving it upwards, away from the disk plane, transporting also energy and angular momentum. Matter will follow open field lines and take energy from them until being eventually ejected out of the potential well. The source of energy for ejection could be accretion itself, although the rotational energy of the compact object is also a possibility (Blandford & Znajek 1977). Although in some cases, however, the latter mechanism might be dominant, accretion is perhaps more likely as an energy provider for jet launching in microquasars during the low-hard state (see discussion in Semenov et al. 2004), when jets are thought to be a common feature of these objects (Fender et al. 2003).

From previous considerations, it seems natural to treat somehow accretion and ejection processes at least in a rough way, when studying jet emission in microquasars where disk-jet coupling has to be taken into account (such coupling was proposed for instance by Falcke & Biermann 1995). The Bondi-Hoyle model for accretion in a homogeneous medium (Bondi 1952) has been used to estimate, when necessary (see Chapter 5), the accretion rate for certain orbital parameters and companion lost matter density. This approximation is rough though enough in a first order approach. Concerning jet launching and ejection energetic balance, this has been investigated accounting for the energy incomes and outcomes (i.e. accretion luminosity, disk and corona emission, advected energy and jet kinetic energy), considering the inner parts of the accretion disk, i.e. the launching region itself, as a black box.

3.4.1 The Bondi-Hoyle model

Here, the compact object is considered to move through the expelled matter from the companion. If the density does not change within the length scale of the compact object, this medium can be treated as homogeneous. The characteristic length scale ($r_{\rm Gr}$) adopted here is the distance at which medium matter has a potential energy larger than its kinetic energy, in relation with the compact object. It is:

$$r_{\rm Gr} = \frac{2GM_{\rm x}}{V_{\rm rel}^2}, \tag{3.37}$$

where $G = 6.7 \times 10^{-8}$ (in cgs units) is the gravitational constant, and $V_{\rm rel}$ is the velocity of the medium relative to the compact object of mass $M_{\rm x}$. To know the rate of matter accreted, one just needs to multiply the cross section obtained from $r_{\rm Gr}$ by the density of the medium ($\rho_{\rm w}$) and $V_{\rm rel}$:

$$\dot{m}_{\rm acc}(\mathbf{x}) = \frac{4\pi(GM_{\rm x})^2\rho_{\rm w}(\mathbf{x})}{V_{\rm rel}^3}, \tag{3.38}$$

The form of $\rho_{\rm w}$, which has in general spatial dependence, will depend on the case (i.e. a fast and spherical wind, an asymmetric one, a slow one, etc). Nevertheless, the spatial dependence will be basically a function of the orbital distance and phase angle ($R_{\rm orb}$ and ϕ). $R_{\rm orb}$ as a function of ϕ is computed from:

$$R_{\rm orb} = \frac{a(1-e^2)}{(1-e\cos\phi)}, \tag{3.39}$$

where a is the orbital semi-major axis, ϕ=0° corresponds to apastron passage and ϕ=180° to periastron passage, and e is the eccentricity of the system. In an purely elliptic orbit, $V_{\rm rel}$ can be calculated from:

$$V_{\rm rel} = \sqrt{(V_{\rm w1}+V_\phi)^2 + (V_{\rm w2}+V_{\rm r})^2}, \tag{3.40}$$

where V_ϕ is the azimuthal velocity of the compact object in relation to the companion reference frame, and $V_{\rm r}$ its radial one:

$$V_\phi = R_{\rm orb}(1-e\cos\phi)^2\sqrt{\frac{G(M_{\rm x}+M_\star)}{(a(1-e^2))^3}}, \tag{3.41}$$

$$V_{\rm r} = R_{\rm orb}e\sin(\phi)(1-e\cos\phi)\sqrt{\frac{G(M_{\rm x}+M_\star)}{(a(1-e^2))^3}}. \tag{3.42}$$

$V_{\rm w1}$ is the azimuthal velocity of the expelled matter itself, that due to angular momentum conservation can be significant, and $V_{\rm w2}$ is its radial velocity. These two quantities depend on the particular situation. The luminosity in the infinity associated with accretion at a given distance (r) to the compact object is:

$$L_{\rm acc}(r) = \frac{GM_{\rm x}\dot{m}_{\rm acc}}{r}. \tag{3.43}$$

3.4.2 Energetic balance in jet ejection

The energetic balance of the accretion/ejection processes can be estimated assuming that no other sources of energy are significant but accretion. Accreted matter is

divided in two parts, one which goes to the jet, and another one which reaches the compact object:

$$\dot{m}_{\rm acc} = 2\dot{m}_{\rm jet} + \dot{m}_{\rm adv}. \tag{3.44}$$

The factor 2 is due to the existence of a jet and its counter jet. The region where ejection itself takes place is characterized by the parameter $r_{\rm l}$, or launching radius. This quantity refers to a radius where energy is transfered to jet matter and this is ejected. Nevertheless, it could be taken as a characteristic distance of the process though being spatially extended in fact. This is the only parameter that refers to the ejection properties where the jet matter is launched, which are not considered here and taken for granted. We introduce the parameter κ through the relationship: $\dot{m}_{\rm jet} = \kappa\dot{m}_{\rm acc}$. To assign a certain amount of extra kinetic luminosity to the ejected matter, we have taken into account the energy dissipated in the disk and the corona in form of radiation, as well as the energy borne by the advected matter after transferring part of its kinetic energy to the jet. This remaining advected kinetic luminosity has been assumed to be associated with the Keplerian velocity at the launching radius, which comes out to be:

$$L_{\rm k\ adv}(r_{\rm l}) \sim \frac{R_{\rm Sch}}{4r_{\rm l}}\dot{m}_{\rm adv}c^2. \tag{3.45}$$

A Newtonian approximation was used for treating the gravitational fields, enough at our level of approach. Previous considerations give a first order estimate of the injection jet velocity. The equation we obtain is:

$$L_{\rm acc}(r_{\rm l}) = L_{\rm k\ jet} + L_{\rm k\ adv} + L_{\rm disk} + L_{\rm cor}. \tag{3.46}$$

$L_{\rm k\ jet}$ is the jet kinetic luminosity at the jet launching radius and magnetic field and relativistic particle kinetic luminosities are also included. This accounts for the kinetic luminosity required to carry the jet matter outside the potential well plus the kinetic luminosity out of the ejection region, corresponding to a jet Lorentz factor $\Gamma_{\rm jet}$:

$$L_{\rm k\ jet}(r_{\rm l}) = \frac{GM_{\rm x}2\dot{m}_{\rm jet}}{r_{\rm l}} + (\Gamma_{\rm jet} - 1)(2\dot{m}_{\rm jet})c^2. \tag{3.47}$$

$L_{\rm disk}$ is the disk radiated luminosity, and $L_{\rm cor}$ is the corona radiated luminosity. We show now the final expression for $\Gamma_{\rm jet}$:

$$\Gamma_{\rm jet}(r_{\rm l}) = 1 + \frac{1}{2\dot{m}_{\rm jet}}\left(\frac{R_{\rm Sch}}{4r_{\rm l}}\dot{m}_{\rm adv} - \frac{L_{\rm disk} + L_{\rm cor}}{c^2}\right). \tag{3.48}$$

3.5 Creation and annihilation of pairs

One of the most complicated issues concerning high energy astrophysics is the proper treatment of electromagnetic cascades (see, e.g. Akharonian et al. 1985). The concept is somehow simple and can be described as the result of the interaction between relativistic electron-positron pairs and a photon field, when pair Compton scattered radiation generate more pairs when colliding with ambient photons since their energies are above the pair creation threshold (Gould & Schréder 1967):

$$x_{\gamma\gamma} > 1, \qquad x_{\gamma\gamma} = \epsilon_1 \epsilon_2, \tag{3.49}$$

where ϵ_1 and ϵ_2 are the two colliding photon energies in $m_{\rm e}c^2$ units. For instance, a relativistic electron goes through a photon field, scattering photons. Let us assume that the scattered photons have obtained enough energy to create pairs in interaction with the ambient photons. These new pairs could scatter more photons, which might have energy enough to again create more pairs. The energy degrades and at the very end the last generation of pairs and scattered photons cannot keep the process working. Nevertheless, if there is a continuous injection of relativistic electrons and/or energetic enough photons, the corresponding photon and electron energy distributions are related by the cascade process, and must be computed altogether to know their characteristics. The introduction of a magnetic field, however, can simplify the scenario because, if energy losses are dominated by the synchrotron channel, the amount of energy that goes to scattered photons the above threshold is a minor one, and the next generation pairs might be even negligible (i.e. the cascade is suppressed).

We provide with some useful expressions that can be used for computing the pair creation and annihilation rates (Coppi & Blandford 1990). They are approximations valid within an error of several %, enough for our purposes.

$$R(x_{\gamma\gamma}) = c\sigma_{\rm T} \frac{(x_{\gamma\gamma}-1)^{3/2}}{x_{\gamma\gamma}^{5/2}} \left[\frac{1}{2} x_{\gamma\gamma}^{-1/2} + \frac{3}{4}\ln(x_{\gamma\gamma})\right] H(x_{\gamma\gamma}-1) \tag{3.50}$$

for the creation rate, where $H(x_{\gamma\gamma}-1)$ is the Heaviside function, and

$$R(x_{\gamma\gamma}) = \frac{3c\sigma_{\rm T}}{8x_{\gamma\gamma}}[x_{\gamma\gamma}^{-1/2} + \ln(x_{\gamma\gamma})] \tag{3.51}$$

for the annihilation rate. Assuming that the photon and the pair energy distributions are known, one can derive the amount of pairs that will be created. It can be enough

for simple estimations of the number of second generation pairs, for instance, or for computing the photon-photon absorption. For useful formulae concerning the pair production spectrum, see e.g. Böttcher & Schlickeiser (1997) and references therein.

3.6 Particle transport

Observations at low and high energies show that microquasars are accelerators of particles. On the one hand, leptons emit at radio frequencies, and leptons and/or protons could produce γ-rays. Actually, the detection of very high-energy γ-rays from these objects clearly indicates that they can accelerate particles up to ~ 10 TeV. In the case of microquasars, the acceleration site could be the inner jet region and/or the larger scale jets. Because of a lack of knowledge of the jet conditions, at the moment it is not known what distance from the compact object is the most suitable for very high energy particle acceleration, although it seems probable that strong magnetic fields and strong photon fields from the star or the accretion disk/corona will prevent electrons to reach such high energies. It would imply that middle or large scale jets are better accelerators (see Chapter 5).

Whatever the site where particles are accelerated, they can leave the acceleration region if confinement is not enough. Then, these particles diffuse either within the binary system or farther up. Depending on the propagating region, they will lose energy as well as they drift influenced by the ambient magnetic field, and an energy dependent diffusion coefficient can render a very particular profile of density for the diffusing particles. In general, the local energy distribution for leptons will be much more affected by losses than in the case of protons.

To determine the energy distribution of protons and electrons with distance and time we have used the solution of the diffusion equation (Ginzburg & Syrovatskii 1964) in the spherically symmetric case, with spatially homogeneous diffusion, taking into account different radiative homogeneous losses (depending on the particle nature: either protons or electrons), and adding energy independent escape losses of timescale T:

$$\frac{\partial f_{\rm p/e}}{\partial t} = \frac{D}{r^2}\frac{\partial}{\partial r}\left[r^2\frac{\partial f_{\rm p/e}}{\partial r}\right] + \frac{\partial}{\partial \gamma}(Pf) - f_{\rm p/e}/T + Q. \qquad (3.52)$$

$f_{\rm p/e}(\gamma, r, t)$ is the function that describes the density of particles per energy unit at distance r and time $t - t_0$ from the injection place moment, with source function in

the origin $Q(\gamma,t) = f_{\rm p/e0}(\gamma)\delta(t-t_0),\ \gamma_{0\ \rm min} < \gamma_0 < \gamma_{0\ \rm max}$, for the case of a sudden injection of particles. D is the diffusion coefficient, assumed to be $D(\gamma) \propto \gamma^{\chi}$, and P is the continuous energy loss rate, $P = -d\gamma/dt$.

The Green function for Eq. 3.52, i.e., its solution for a source δ-function, has the following form (Atoyan et al. 1995):

$$G(\gamma,\gamma_0,r,t,t_0) = \frac{exp\left[-\tau/T - r^2/4\lambda\right]\delta(t-t_0-\tau)}{P(4\pi\lambda)^{3/2}}, \tag{3.53}$$

where the functions λ and τ are defined as:

$$\lambda(\gamma,\gamma_0) = \int_{\gamma_0}^{\gamma} \frac{D(\gamma'')}{P}{\rm d}\gamma'', \tag{3.54}$$

and

$$\tau(\gamma,\gamma_0) = \int_{\gamma_0}^{\gamma} \frac{d\gamma''}{P}. \tag{3.55}$$

The corresponding diffusion radius is defined as $2\sqrt{\lambda}$.

The solution of Eq. (3.52) can be written as:

$$f_{\rm p/e}(\gamma,r,t) = \int_{-\infty}^{\rm t} dt'' \int_{\gamma 0\ \rm min}^{\gamma 0\ \rm max} d\gamma'' Q(\gamma'',t'') G(\gamma,\gamma'',r,t,t''), \tag{3.56}$$

where $\gamma_{\rm max}(t-t'')$ comes from solving the differential equation with the significant energy losses. If we want to find the continuous injection solution $F_{\rm p/e}(\gamma,r,t)$, then we must take into account that the injection function turns to a rate $\rm s^{-1}$, is extended in time, and could be time dependent:

$$F_{\rm p/e}(\gamma,r,t) = \int_{\rm t_0}^{\rm t} f_{\rm p/e}(\gamma,r,t-t'')dt''. \tag{3.57}$$

3.7 Cold-matter jet properties

Along the development of this work, the study of the emission from low-hard state microquasar jets has been carried out in different ways. In Chapter 4, when computing their emission, the jet properties are not considered but very roughly. The

geometry and the emitting particle content are taken for granted. In Chapter 5, the approach changes. There, we have studied jets in relation to their matter content, confinement, magnetic field, relativistic population, etc., finally adopting a reasonable model for the jet from the point of view of present knowledge on microquasars. Such a model is based on a cold matter dominated jet, although other possibilities cannot be discarded. We do not study in detail the evolution of the jet plasma in interaction with the magnetic field, but it is assumed that the magnetic field is proportional to the equipartition value with jet matter in the jet reference frame. The main idea is that there are some observational hints that point to jets moving at mildly relativistic speeds ($\Gamma_{\rm jet} < 2$; see, e.g., for LS 5039, Paredes et al. 2002; for LS I +61 303, Massi et al. 2004; and for SS 433, Hjellming & Johnston 1981). This fact, combined with a probable lack of effective external collimation, leads to the requirement that the particle mean velocity ($\sim V_{\rm exp}$, the expansion velocity) in the moving (jet) reference frame must be low enough for avoiding to violate the collimation constraints imposed from observations, which are usually of few degrees of jet half-opening angle (e.g. for LS 5039, see Paredes et al. 2002; for SS 433, see Marshall et al. 2002). Other observational evidences of cold matter content come from the detection of X-ray thermal continuum (Brinkmann et al. 1991) and spectroscopic lines in SS 433 (Kotani et al. 1996, Marshall et al. 2002) and surrounding media heated environment (Martí et al. 2005, Gallo et al. 2005).

The explanation for the cold matter dominance in the jet could be related to the fact that particles coming from accretion disk or corona regions are thought to be non relativistic. If the jet matter comes from accretion, one can assume that, in principle, there is a large amount of relatively cold protons dominating jet pressure. If cold accretion matter is ejected and afterward some part is accelerated by some plasma instabilities like e.g. shocks, the efficiency dissipating energy of the acceleration mechanism is constrained by the energy reservoir, and this energy reservoir is ultimately the jet kinetic energy. Therefore, if kinetic energy dissipation takes place along the jet, the relativistic particle energy density will grow consequently along the jet, being radiated away or lost adiabatically. Since dissipation efficiency will hardly be of a 100% (it is more reasonable 1-10%, see Chapter 5), and losses are efficiently removing relativistic particle energy, it seems natural that the mean energy per particle will be such that will fulfill the half-opening angle constraints all along the jet. Actually, another model available that could be energetically reasonable is a pair flux with magnetic confinement and reacceleration due to magnetic energy dissipation, but it is unclear yet whether it can explain the confinement all the way

up to the largest jet scales, the level of polarization of the emission, or the fluxes of synchrotron radiation.

A consequence of all this discussion is roughly that cold particles, in general cold protons, have more energy density than relativistic ones:

$$e_{\rm cold} = n_{\rm cold}\frac{1}{2}m_{\rm p} < V_{\rm p}^2 > \geq n_{\rm hot}m_{\rm hot}c^2 < \gamma_{\rm hot} >= e_{\rm hot}, \tag{3.58}$$

where $n_{\rm cold}$ and $n_{\rm hot}$ are the densities for the cold and hot particles respectively, and all the quantities are in the jet reference frame. Concerning magnetic field, also in the jet reference frame, its value can be estimated from:

$$B = \sqrt{8\pi\varrho e_{\rm cold}}, \tag{3.59}$$

where ϱ is the fraction of the equipartition value with jet matter. It is worth mentioning that the magnetic field cannot be very low compared with its equipartition value, since strong magnetic fields close to the compact object are likely involved in the jet formation process.

Concerning the constraints of matter energy dissipation efficiency, they can be obtained from comparison between the jet dissipation and loss luminosities per length unit for different distances from the compact object:

$$\frac{dL_{\rm dis}(z)}{dz} \geq \frac{dL_{\rm loss}(z)}{dz}, \tag{3.60}$$

where $dL_{\rm loss}(z)/dz$ has the form:

$$\frac{dL_{\rm loss}(z)}{dz} = \int_{\gamma_{\rm min}}^{\gamma_{\rm max}(z)} \pi R_{\rm jet}^2 n(z,\gamma)\dot{\gamma}_{\rm loss}d\gamma. \tag{3.61}$$

Here, $n(z,\gamma)$ is the electron energy distribution density. Unlike $n(\mathbf{x},\gamma,\Omega)$, there is no angular dependence, and the spatial one reduces to z. $\dot{\gamma}_{\rm loss}$ must take into account radiative losses, given in Sect. 3.2, as well as adiabatic ones, which for a conical jet are:

$$\dot{\gamma}_{\rm ad} = \frac{2V_{\rm exp}}{3R_{\rm jet}}\gamma, \tag{3.62}$$

where $V_{\rm exp}$ is the jet lateral expansion velocity, assumed to be constant, and $R_{\rm jet}$ is the jet radius, which will in general present some dependence with z. The jet radius at the base of the jet, assuming that it is formed close to the compact object (in the corona-like region), should be several $R_{\rm Sch}$, but not more, since otherwise it would

be even larger than the corona itself. Provided that all the quantities are already in the compact object reference frame, $dL_{\rm dis}$ can be written as:

$$\frac{dL_{\rm dis}(z)}{dz} \sim C_{\rm dis} f_{\rm dis}(z), \tag{3.63}$$

where $f_{\rm dis}$ is a function representing the efficiency of energy dissipation at different z, which has been parametrized at this stage as $1/z$. The normalization constant $C_{\rm dis}$ can be obtained by integrating the total amount of shock energy available per length unit along the jet, from z_0 to $z_{\rm max}$, and equating it to a suitable fraction (ξ) of the jet kinetic luminosity:

$$C_{\rm dis} = \frac{\xi L_{\rm k\ esc}}{\ln(z_{\rm max}/z_0)}. \tag{3.64}$$

The value of $z_{\rm max}$, the maximum jet length, will depend on the situation.

It is worth mentioning that, by definition, the cold matter particles are confined within the jet. It does not need to be so in case of relativistic particles which do not dominate the dynamical properties of the jet. Since there is a fraction of accelerated particles, protons and/or electrons, they could escape if their gyroradius is larger than the width of the jet $R_{\rm jet}$. In our computations, we account only for those particles which are confined in the jet, with energy distributions with a cutoff at the escape energy. Nevertheless, some fraction of the jet kinetic energy could be released in form of particles escaping from the jet (Aharonian et al. 2005). We neglect this at this stage.

Bibliography

Aharonian F.A., 2004, Very High Energy Cosmic Gamma Radiation : a crucial window on the extreme Universe, River Edge, NJ: World Scientific Publishing, 2004 39, 40

Aharonian F.A., Atoyan A.M., May 1996, A&A, 309, 917 41, 42

Aharonian F.A., Atoyan A.M., Oct. 2000, A&A, 362, 937 41, 42

Aharonian F.A., Anchordoqui L.A., Khangulyan D., Montaruli T., 2005, astro-ph/0508658 54

Akharonian F.A., Kririllov-Ugriumov V.G., Vardanian V.V., Oct. 1985, Ap&SS, 115, 201 49

Atoyan A.M., Aharonian F.A., Völk H.J., Sep. 1995, PhRvD, 52, 3265 51

Bell A.R., Jan. 1978a, MNRAS, 182, 147 43

Bell A.R., Feb. 1978b, MNRAS, 182, 443 44

Blandford R.D., Znajek R.L., May 1977, MNRAS, 179, 433 46

Blumenthal G.R., Gould R.J., 1970, Reviews of Modern Physics, 42, 237 30, 38

Bondi H., 1952, MNRAS, 112, 195 46

Böttcher M., Schlickeiser R., Sep. 1997, A&A, 325, 866 50

Brinkmann W., Kawai N., Matsuoka M., Fink H.H., Jan. 1991, A&A, 241, 112 52

Cheng K.S., Romero G.E. (eds.), Oct. 2004, Cosmic Gamma-Ray Sources 40

Coppi P.S., Blandford R.D., Aug. 1990, MNRAS, 245, 453 49

Corbel S., Fender R.P., Tzioumis A.K., et al., Oct. 2002, Science, 298, 196 43

Derishev E.V., Aharonian F.A., Kocharovsky V.V., Kocharovsky V.V., Aug. 2003, PhRvD, 68, 043003 43

Dermer C.D., Schlickeiser R., Aug. 2002, ApJ, 575, 667 30

Dermer C.D., Schlickeiser R., Mastichiadis A., Mar. 1992, A&A, 256, L27 38

Drury L., Sep. 1983, Space Science Reviews, 36, 57 43

Drury L.O., Aharonian F.A., Voelk H.J., Jul. 1994, A&A, 287, 959 41

Falcke H., Biermann P.L., Jan. 1995, A&A, 293, 665 46

Fender R.P., Gallo E., Jonker P.G., Aug. 2003, MNRAS, 343, L99 46

Gallo E., Fender R., Kaiser C., et al., Aug. 2005, Nature, 436, 819 43, 52

Ghisellini G., Maraschi L., Treves A., May 1985, A&A, 146, 204 36

Ginzburg V.L., Syrovatskii S.I., 1964, The Origin of Cosmic Rays, New York: Macmillan, 1964 50

Gould R.J., Schréder G.P., Mar. 1967, Physical Review, 155, 1404 49

Hjellming R.M., Johnston K.J., Jun. 1981, ApJ Letter, 246, L141 52

Jones F.C., Ellison D.C., 1991, Space Science Reviews, 58, 259 43

Kotani T., Kawai N., Matsuoka M., Brinkmann W., Aug. 1996, PASJ, 48, 619 52

Lang K.R., 1980, Astrophysical Formulae, A Compendium for the Physicist and Astrophysicist, XXIX, 783 pp. 46 figs., 69 tabs.. Springer-Verlag Berlin Heidelberg New York. Also Springer Study Edition 39

Longair M.S., 1994, High Energy Astrophysics. Vol.2: Stars, the galaxy and the interstellar medium, Cambridge: Cambridge University Press, —c1994, 2nd ed. 40

Marshall H.L., Canizares C.R., Schulz N.S., Jan. 2002, ApJ, 564, 941 52

Martí J., Pérez-Ramírez D., Garrido J.L., Luque-Escamilla P., Paredes J.M., Aug. 2005, A&A, 439, 279 52

Massi M., Ribó M., Paredes J.M., et al., Jan. 2004, A&A, 414, L1 45, 52

Mastichiadis A., Kirk J.G., Mar. 1995, A&A, 295, 613 44

Melrose D.B., 1980, Plasma Astrohysics. Nonthermal processes in diffuse magnetized plasmas - Vol.1: The emission, absorption and transfer of waves in plasmas; Vol.2: Astrophysical applications, New York: Gordon and Breach, 1980 35

Neff S.G., Brown R.L., Feb. 1984, AJ, 89, 195 43

Pacholczyk A.G., 1970, Radio Astrophysics. Nonthermal processes in galactic and extragalactic sources, Series of Books in Astronomy and Astrophysics, San Francisco: Freeman, 1970 30, 35, 36, 37

Paredes J.M., Martí J., Ribó M., Massi M., Jun. 2000, Science, 288, 2340 45

Paredes J.M., Ribó M., Ros E., Martí J., Massi M., Oct. 2002, A&A, 393, L99 52

Pfrommer C., Enßlin T.A., Aug. 2003, A&A, 407, L73 42

Protheroe R.J., 1999, In: Topics in Cosmic-Ray Astrophysics, 247 45

Rieger F.M., Duffy P., Dec. 2004, ApJ, 617, 155 43

Schutz B.F., Feb. 1985, A First Course in General Relativity, A First Course in General Relativity, by Bernard F. Schutz, pp. 392. ISBN 0521277035. Cambridge, UK: Cambridge University Press, February 1985. 30

Scott J.S., Chevalier R.A., Apr. 1975, ApJ Letter, 197, L5 43

Semenov V., Dyadechkin S., Punsly B., Aug. 2004, Science, 305, 978 46

Chapter 4

High-energy γ-ray emission from microquasars

From the observational point of view, two microquasars had been proposed to be associated with two EGRET sources before the begining of this thesis work, LS 5039/3EG J1824−1514 (Paredes et al. 2000) and LS I +61 303/3EG J0241+6103 (Kniffen et al. 1997), the latter source being associated with a COS-B source already in the 70s by Gregory & Taylor (1978) though its microquasar nature was established later than for LS 5039 (Massi et al. 2001, 2004). The proposed association of two microquasars as EGRET sources led naturally to the idea that these objects could be counterparts of a fraction of the unidentified γ-ray sources in our Galaxy, concretely the variable ones (e.g. Kaufman Bernadó et al. 2002). The jets of microquasars had been considered sources of high energy emission from the theoretical point of view (Atoyan & Aharonian 1999, Markoff et al. 2001, Georganopoulos et al. 2002), although the capability of these objects to accelerate particles was well established observationally at that time only up to energies to emit at synchrotron infrared emission (see, e.g., Mirabel et al. 1998). In this chapter, we present our first approach to model the high energy emission from microquasar jets, investigating the emission from a jet filled with relativistic particles, first in the high-energy γ-ray range and, later on, from radio to γ-rays. Thus, we have developed two models. The first one intends to reproduce the evolution and emission above 100 MeV of a distribution of electrons in a cylindrical jet under the effects of radiation and magnetic fields and it is applied to the mentioned EGRET microquasars (Bosch-Ramon & Paredes 2004a,b). The second one is based on a conical jet, filled with relativistic

electrons evolving adiabatically and emitting in the whole energy range, accounting for the present radiation and magnetic fields. This model is applied to microquasars in general as well as to unidentified γ-ray sources in the galactic plane, to which a statistical analysis is also performed to study in a different way the possible link between microquasars and γ-ray sources (Bosch-Ramon et al. 2005b, Bosch-Ramon et al. 2006).

4.1 A leptonic model for the γ-ray emission in microquasars

As a first step we were interested in investigating whether microquasars were able to generate the high-energy γ-ray emission detected by EGRET, using a numerical model based on inverse Compton (IC) scattering, taking into account energy losses, external Compton (EC) and synchrotron self-Compton (SSC) interactions.

The scenario of our model consists on an X-ray binary (XRB) system where close to the compact object a matter outflow is ejected, not necessarily perpendicular to the orbital plane. We assume that the leptons dominate the radiative processes that generate γ-rays. Relativistic electrons, already accelerated and flowing away into a cylindrical jet, are exposed to photons from the star, assumed to be an isotropic photon field, as well as to photons from the synchrotron emission of the same population of electrons, since we suppose the presence of a magnetic field. This cylindrical jet region, that might radiate γ-rays, is called the γ-jet. This γ-jet is assumed to be short enough to allow the magnetic field to be considered constant, and it is also assumed to be much closer to the compact object than the observed radio jets. The energy losses of the leptonic plasma in the γ-jet are due to its own synchrotron emission, the SSC scattering and the EC scattering of the stellar photons by the relativistic electrons. Because of the strong losses, the electron energy distribution density along the γ-jet varies significantly, and in this sense the γ-jet is inhomogeneous. The magnetic field in the γ-jet is tangled in such a way that the resulted synchrotron emission is isotropic in the jet reference frame (RF). The γ-jet is studied by splitting it into cylindrical transverse cuts or slices at different z from the jet origin. The size of the slices has to be suitable to get almost homogeneous physical conditions within them: constant energy densities of the radiation and the electrons, and constant maximum energy for the electrons.

Although some features like disk-jet interaction, reacceleration of the particles in the jet, corona-jet interaction and pair creation-annihilation phenomena could be significant at some level, their study is not considered here but treated in Chapter 5. The parameters of the model that cannot be constrained from observations are the magnetic field (B), the maximum electron Lorentz factor at the base of the jet ($\gamma_{\rm max}(z_0)$), and the leptonic kinetic luminosity ($L_{\rm k}$, i.e. the power of the relativistic leptons injected in the jet).

The synchrotron and both the EC and SSC emissivities have been computed using the formulae provided in Chapter 3. Also, the electron energy distribution density, $n(z,\gamma)$, along the jet is to be obtained. The relevance of the SSC process for certain values of the magnetic field introduces a non-linearity to the problem of solving the differential equation for electron energy losses in this scenario, since to know $\gamma_{\rm max}(z)$ we need to know the synchrotron photon energy density $U_{\rm sync}(z)$, which also depends on $\gamma_{\rm max}(z)$. This non-linearity also affects obtaining $n(z,\gamma)$ in each slice or z (where $n(z,\gamma) = 4\pi n(\mathbf{x},\gamma,\Omega)$ is isotropic in the momentum space and homogeneous in the directions perpendicular to the jet axis). To overcome this, we have computed the first slice value of $U_{\rm sync}$ from the electron energy distribution density injected in the first slice ($n(z_0,\gamma)$) and introduced such $U_{\rm sync}(z_0)$ in the differential equation of the electron energy losses to solve it and find the $\gamma_{\rm max}$ for the next slice (i.e. at $z_0+\Delta z$). This process has been repeated for each slice, solving Eq. (4.1) for each slice with the previous slice $U_{\rm sync}$ value. The differential equation that describes the electron energy evolution is:

$$\dot{\gamma} = -1.94\times10^{-9}B\gamma^2 - 3.20\times10^{-8}U_{\rm total}(z)\gamma^2, \tag{4.1}$$

where $U_{\rm total}(z) = U_{\rm star}(z)+U_{\rm sync}(z)$, and $U_{\rm star}(z) \sim \Gamma_{\rm jet}^2 L_{\rm star}/4\pi d_*^2 c$ in the jet RF (for the isotropic field approximation), with d_* being the distance from a certain slice to the star in the compact object RF and $L_{\rm star}$ being the star bolometric luminosity. The IC losses in Eq. (4.1) are taken to be in the Thomson regime, valid enough for the involved electron and target photon energies at this level of approximation. Solving this equation for the given conditions, after some algebra we get the electron Lorentz factor evolution expression:

$$\gamma(z) = \frac{\gamma(z_0)}{1+\gamma(z_0)m_{\rm e}c^2\left[\frac{C_{\rm s}(z-z_0)}{V_{\rm jet}} + \frac{C_{\rm c}}{V_{\rm jet}R_{\rm orb}\sin\varpi}(\arctan\frac{z-R_{\rm orb}\cos\varpi}{R_{\rm orb}\sin(\varpi)} - \arctan\frac{z_0-R_{\rm orb}\cos\varpi}{R_{\rm orb}\sin(\varpi)})\right]}. \tag{4.2}$$

Electrons are injected at a distance z_0 from the compact object and their evolution continues along the jet axis to farther z. $V_{\rm jet}$ is the jet bulk velocity, ϖ is the angle

between the jet and the orbital plane, $C_{\rm s} = (a_{\rm s} B_\gamma^2 + a_{\rm c} U_{\rm syn})$, and $C_{\rm c} = a_{\rm c} \Gamma_{\rm jet}^2 L_{\rm star}/4\pi c$. $n(z_0, \gamma_0)$ follows a power-law:

$$n(z_0, \gamma_0) = Q \gamma_0^{-p}, \qquad \gamma_{\rm min}(z_0) \leq \gamma_0 \leq \gamma_{\rm max}(z_0), \tag{4.3}$$

where Q is the normalization constant of the electrons, related to the leptonic kinetic luminosity as:

$$L_{\rm k} = \pi R_{\rm jet}^2 V_{\rm jet} m_{\rm e} c^2 \Gamma_{\rm jet}^2 Q \frac{\gamma_{\rm max}(z_0)^{2-p} - \gamma_{\rm min}(z_0)^{2-p}}{2-p}. \tag{4.4}$$

Taking into account the conservation of the number of particles along a cylindrical jet, $n(z, \gamma) d\gamma = n(z_0, \gamma_0) d\gamma_0$, the evolution of Eq. (4.3) along the jet is found:

$$\begin{aligned} n(z, \gamma) &= Q \gamma^{-p} \left[1 - \gamma m_{\rm e} c^2 \left(C_{\rm s} \frac{z - z_0}{V_{\rm jet}} + \frac{C_{\rm c}}{V_{\rm jet} R_{\rm orb} \sin(\varpi)} F(z, \varpi) \right) \right]^{p-2}, \\ F(z, \varpi) &= \arctan \frac{z - R_{\rm orb} \cos \varpi}{R_{\rm orb} \sin(\varpi)} - \arctan \frac{z_0 - R_{\rm orb} \cos \varpi}{R_{\rm orb} \sin(\varpi)}. \end{aligned} \tag{4.5}$$

We need to compute the synchrotron photon density per energy unit, $n_{\rm sync\ phot}(z, \epsilon_0)$, and $U_{\rm sync}(z)$, which both can be easily obtained from Eq. (3.11). For the stellar photon field, $n_{\rm star\ phot}(z, \epsilon_0) = U_{\rm star\ phot}(z, \epsilon_0)/\epsilon_0$ and $U_{\rm star}(z)$ can be derived from the gray body specific energy density $U_{\rm gb}(d_*, \epsilon_0)$, that must be scaled to the star luminosity taking into account the distance at which the star is located:

$$U_{\rm gb}(d_*, \epsilon_0) \propto \frac{1}{d_*^2} \frac{\epsilon_0^3}{\exp(m_{\rm e} c^2 \epsilon_0 / k_{\rm b} T) - 1}, \; L_{\rm star}/4\pi d_*^2 c = \int_{\epsilon_{0\ \rm min}}^{\epsilon_{0\ \rm max}} U_{\rm gb}(d_*, \epsilon_0) d\epsilon_0. \tag{4.6}$$

The seed photon fields must be employed in the suitable RF (see Chapter 3 and Dermer & Schlickeiser 2002). Using the formulae provided in Chapter 3 and in this chapter, we can now give the expression for computing the SED in the direction to the observer (Ω_0'), which is the one corresponding to IC emission in the optically thin case:

$$\epsilon' L'(\epsilon')_{\Omega_0'} = \epsilon' \delta (\Omega_0')^3 \int_{z_{\rm min}}^{z_{\rm max}} \pi R_{\rm jet}^2 j(z, \epsilon'/\delta) dz. \tag{4.7}$$

where $j(z, \epsilon'/\delta) = 4\pi j(z, \epsilon'/\delta, \Omega)$ for an inferred isotropic luminosity, $R_{\rm jet}$ is the γ-jet radius, $z_{\rm min}$ is arbitrary but must fulfill $z_{\rm min} \ll R_{\rm orb}$, and $z_{\rm max}$ is the distance at which electrons still emit photons of energy ϵ. Ω_0' is directly related to the angle θ', which is the angle between the observer line of sight and the jet axis in the observer RF (see Fig. 3.2), i.e. the viewing angle.

Next, we apply this model to LS 5039 and LS I +61 303. We obtain the different SEDs beyond 100 MeV computed for different free parameter values, discussing the implications of the results in terms of the maximum particle energy and the magnetic field. The leptonic kinetic luminosity is adopted such that the EGRET luminosities are reproduced, and the electron power-law index p is inferred from radio observations ($p = 2\alpha + 1$ where the flux density $F(\nu) \propto \nu^{-\alpha}$, see below). We note that at this stage we do not intend to give predictions at energies below high-energy γ-rays, since a different and more complex scenario should be considered (see below and Chapter 5).

4.1.1 Application to LS 5039

Before going into the modeling of the high-energy γ-ray emission, let us discuss briefly the most remarkable characteristics of LS 5039. This high-mass XRB (HMXB) was discovered by Motch et al. (1997) in ROSAT data, presenting moderately low fluxes (see also Bosch-Ramon et al. 2005a for the latest results at the X-ray band). The optical counterpart of LS 5039 is a bright (V $\sim$ 11) star of ON6.5 V((f)) spectral type, the compact object is likely a black hole, and the system is located at an estimated distance of 2.5 kpc (Casares et al. 2005b). The system, with galactic coordinates $l = 16.9$ and $b = -1.3$, presents a pretty high proper motion moving outwards from the galactic plane (Ribó et al. 2002). The two components of the binary are relatively close (semi-major axis of 2.2×10^{12} cm), the accretion process is thought to be of the wind-fed type, and the system seems to be close to the Roche lobe overflow during the periastron passage, and has an orbital period 3.9060 days (Casares et al. 2005b). Non-thermal optically thin radio emission ($\alpha \sim 0.5$) was discovered by Martí et al. (1998) increasing the appeal of the source in the multiwavelength domain and, later, the discovery of the radio jets, presented in the work of Paredes et al. (2000) (where the association with 3EG J1824−1514 was also proposed), stated without doubt the microquasar nature of this object. For an extensive and detailed discussion about the properties of LS 5039, we refer to Ribó (2002). Finally, it is worth mentioning the detection by HESS of LS 5039 as a very high-energy γ-ray emitter (Aharonian et al. 2005), which renders the association proposed by Paredes et al. (2000) with the EGRET source certain.

Concerning the modeling as such, we use the orbital and other physical parameters of the system obtained by Casares et al. (2005b), the radio spectrum parameter

Table 4.1: Fixed parameters

symbol	parameter	value
a	Orbital semi-major axis	2.2×10^{12} cm
$L_{\rm star}$	Star total luminosity	8×10^{38} erg s^{-1}
e	System eccentricity	0.35
θ	Viewing angle	25°
ϖ	Angle between the jet and the orbital plane	90°
$\Gamma_{\rm jet}$	Jet Lorentz factor	1.02
η	Spectral energy index within 100–1000 MeV	0.2
p	Electron power-law index	2
$R_{\rm jet}$	γ-jet radius	10^7 cm
$L_{>100\ \rm MeV}$	Luminosity at the EGRET band	2×10^{35} erg s^{-1}
$\eta_{\rm i}$	Spectral energy index at the band 100–1000 MeV	0.2

values found by Martí et al. (1998), and the EGRET spectral information presented in Hartman et al. (1999). Other parameters, e.g. the jet radius, have been taken similar to those adopted by other authors (see, e.g., Kaufman Bernadó et al. 2002), which is large enough for preventing electrons in the jet to escape. The angle ϖ has been taken for simplicity to be 90°. All the fixed parameter values, altogether with their description, are listed in Table 4.1, and the luminosity and spectral energy index ($\eta_{\rm i}$, where $\nu F_\nu \propto \nu^{-\eta_{\rm i}}$) observed by EGRET are given in the same table at the bottom, both being employed to test different free parameter values.

Results

We explore the range of the free parameters of the model taking into account the observational constraints to see whether we can reproduce the observational data. To determine its behavior with different magnetic field strengths, we have run our model for several values of the magnetic field strength and a fixed value of $\gamma_{\rm max}(z_0) = 5 \times 10^4$. We show at the top of Fig. 4.1 the computed IC SED (ϵL_ϵ) for three representative cases (1, 10 and 100 G). The spectral slopes in the energy range 100–1000 MeV, where EGRET detected the source, are similar. Since our model generates similar spectra for a wide range of magnetic field values, we have to focus

our attention on the distances reached by the γ-jet, which is strongly dependent on B. Then, high magnetic fields (tens of G or higher) would imply a γ-jet evolving very fast up (under strong energy losses) to $\sim 10^9 - 10^{10}$ cm, whereas low magnetic fields (few G or lower) would imply a γ-jet evolving smoothly up to $\sim 10^{11} - 10^{12}$ cm (see Figs. 4.3 and 4.4). Moreover, regarding values well below 1 G, we notice that upper limits of 0.2 G have been estimated from radio observations (Paredes et al. 2002) for the magnetic field in the radio jet. Therefore, B of about several tenths of G could be taken as a lower limit in the γ-jet. To explore the dependence of the IC SED on $\gamma_{\rm max}(z_0)$, three $\gamma_{\rm max}(z_0)$ (10^4, 5×10^4 and 10^5) have been used, fixing $B = 10$ G. The results are shown at the bottom of Fig. 4.1. For $\gamma_{\rm max}(z_0) = 10^4$, the computed η, about 0.7, is 2.5 σ softer than that given by EGRET observations. Therefore, $\gamma_{\rm max}(z_0) > 10^4$ is needed. An upper limit cannot be clearly fixed yet, since we do not know properly the spectral energy cutoff[1].

The computed IC SEDs for two different values of the magnetic field are shown in Fig. 4.2. We also show the EGRET data points of 3EG J1824−1514 (Hartman et al. 1999). The kinetic luminosity has been adopted such that the level of the observed flux at 100 MeV can be reproduced. The parameter values used in both cases are summarized in Table 4.2. Since we are dealing with an eccentric system, the star radiation density in the jet is affected by the orbital distance variation. We have explored the importance of this effect by computing the IC SED at periastron and apastron passage as well as for $R_{\rm orb} = a$. In the case $B = 10$ G, since SSC is strongly dominant, the effect of the orbital eccentricity on the computed IC luminosity is not significant. However, for a $B = 1$ G, the EC scattering is dominant and the orbital distance variation between apastron and periastron passages produces a change of about 50 per cent in the computed IC luminosity. At the top of Fig. 4.2, we have plotted our results obtained at three orbital distances: 1.4×10^{12} cm for periastron, 2.2×10^{12} cm for the semi-major axis of the orbit and 3.0×10^{12} cm for apastron. Since the viewing periods of EGRET are longer than the orbital period of the system, we cannot relate the variability predictions of our model to the variability detected by EGRET. As can be seen in Fig. 4.2, our model reproduces properly the EGRET data below about 1 GeV. Beyond this energy, the computed spectrum becomes significantly softer, but it is not in disagreement with the upper limits given by EGRET in this energy range.

[1]HESS detection of LS 5039 shows that the electron Lorentz factor could reach values well above those treated here, although it is not clear in which region of the jet acceleration process can be so efficient. This is treated in Chapter 5.

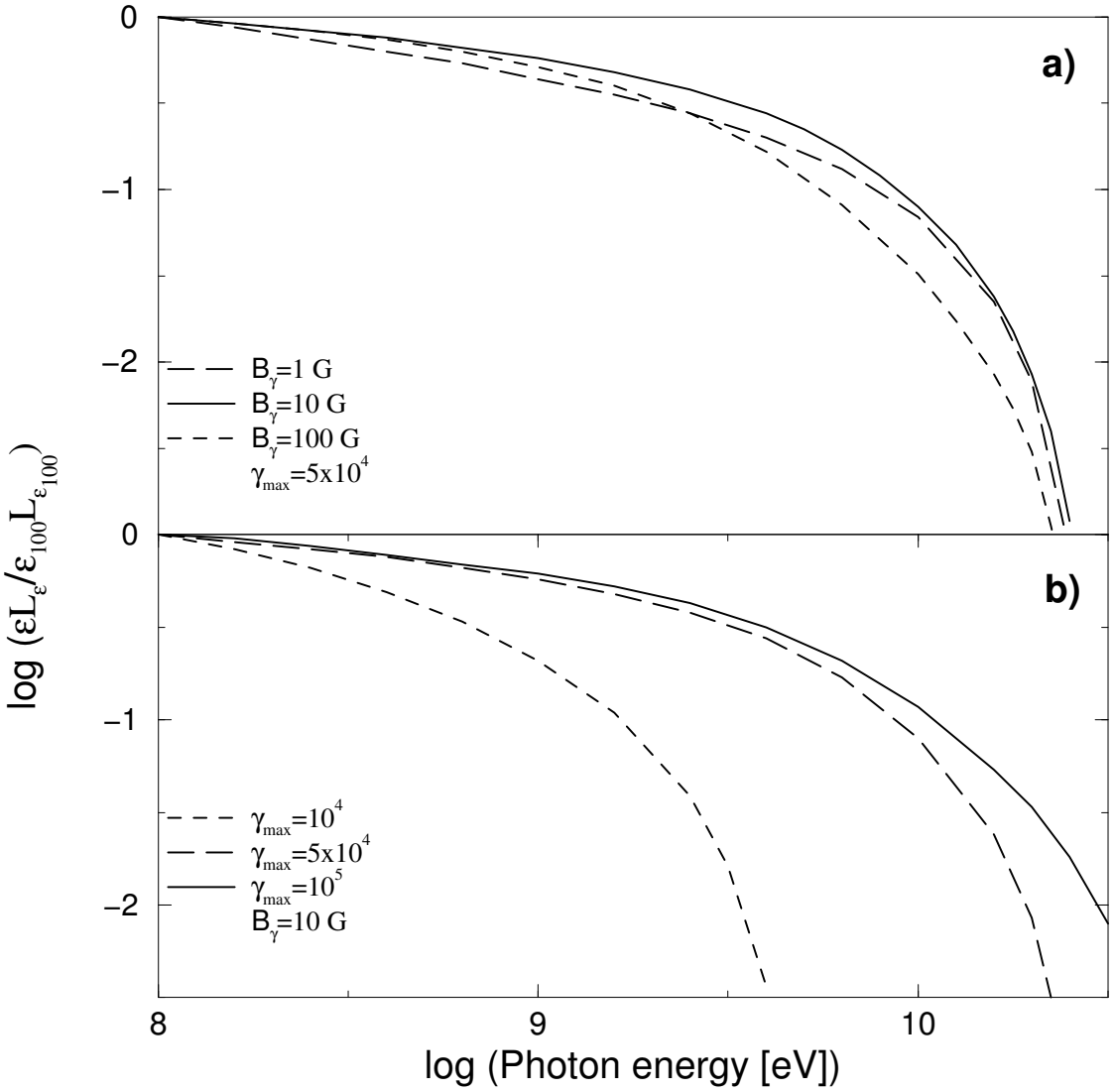

Figure 4.1: Computed IC SEDs normalized to their value at 100 MeV for different values of the magnetic field strength and the maximum electron Lorentz factor. **a)** For values of the magnetic field of 1, 10 and 100 G and fixing the maximum Lorentz factor at 5×10^4. **b)** For values of the maximum Lorentz factor of the electrons of 1×10^4, 5×10^4 and 1×10^5 and fixing the magnetic field to 10 G.

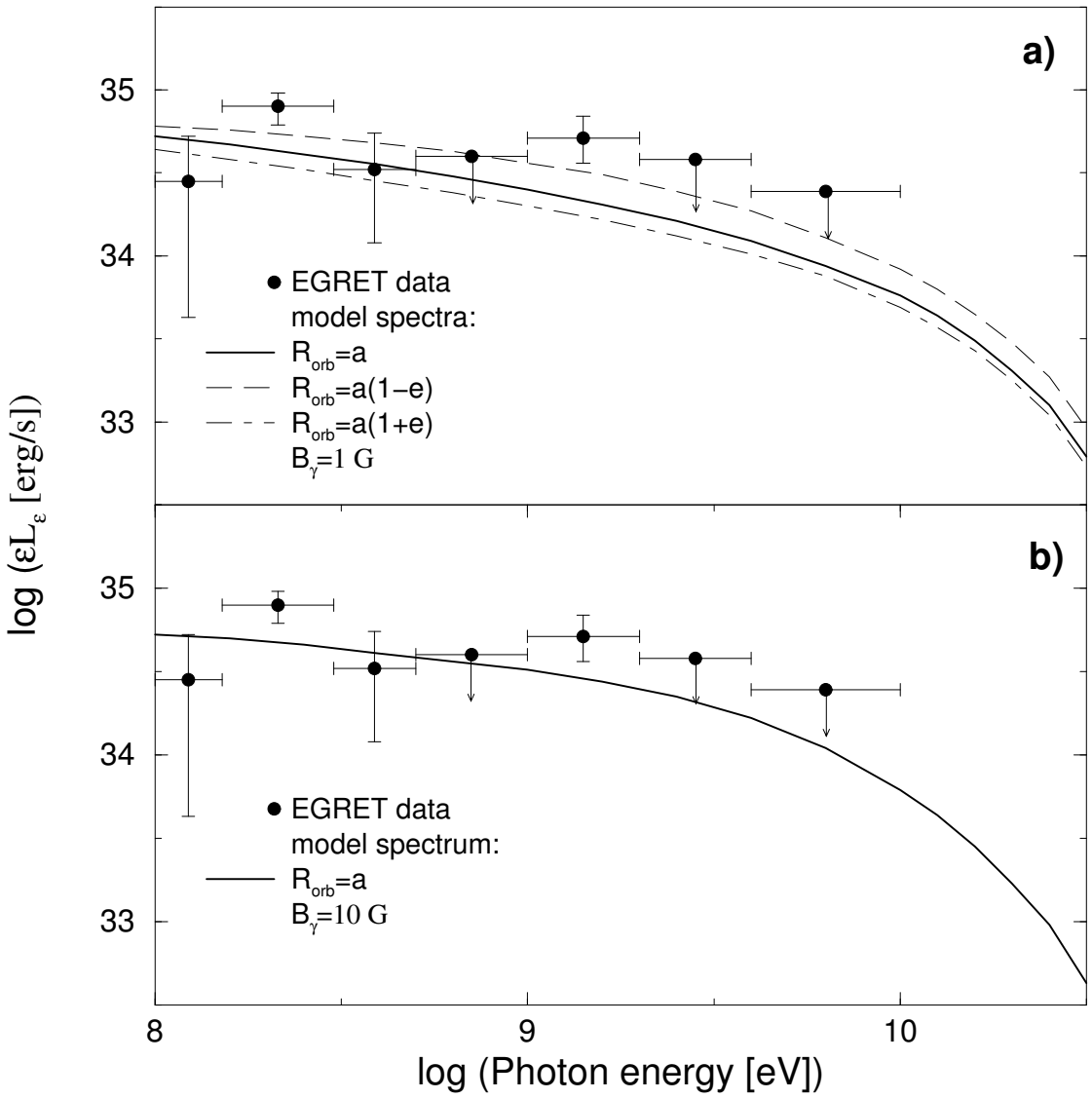

Figure 4.2: Two IC SEDs computed with the present model using the free parameter values of Table 4.2. The EGRET data points are also shown. The upper limits on undetected EGRET points are plotted with arrows. **a)** A magnetic field of 1 G has been assumed. Also, the IC SED for both the apastron and the periastron passage are shown. **b)** A magnetic field of 10 G has been assumed.

Table 4.2: Parameter values used in the model for Fig. 4.2

Parameter	dominant EC	dominant SSC
B	1 G	10 G
$L_{\rm k}$	10^{36} erg s^{-1}	3×10^{36} erg s^{-1}
$\gamma_{\rm max}(z_0)$	10^5	10^5

Additional comments have to be made about the magnetic field in the γ-jet. We have plotted the temporal evolution of the synchrotron and companion star radiation energy densities for both a B of 1 G and a B of 10 G within a given slice moving along the jet (Figs. 4.3 and 4.4). It is shown that a variation of one order of magnitude in B implies a variation of more than two orders of magnitude in the synchrotron radiation energy density. Therefore, in the context of our model, magnetic fields between 1 and 10 G or higher could be tightly related to the high-energy γ-ray emission in LS 5039, as the SSC loss process is important and even dominant. Finally, we have explored the infrared synchrotron emission from the γ-jet. Taking a $B = 10$ G, we have obtained a luminosity in the range 10^{12}–10^{14} Hz of about 10^{32} erg s^{-1} for LS 5039. If we compare this value to the luminosity of the companion star in this frequency band, we find that the infrared jet luminosity is two orders of magnitude lower.

Discussion

As we have shown, our model is able to reproduce the high-energy γ-ray emission of the EGRET source 3EG J1824−1514 by assuming its origin in the microquasar LS 5039. Since there are no special constraints associated with a particular source in our model, it could be applied to other unidentified EGRET sources that might be also associated with microquasars. A maximum electron Lorentz factor higher than 10^4 is a good parameter range to obtain the observed spectral slope. An upper limit on $\gamma_{\rm max}(z_0)$ has not been determined yet due to the lack of knowledge about the high energy cutoff. Further observations by the next, more sensitive, hard γ-ray instruments are needed to determine this cutoff (e.g. HESS detection has shown that $\gamma_{\rm max} >> 10^5$, but its value remains unclear). To reproduce the observed luminosities, $L_{\rm k} \sim 10^{36}$ erg s^{-1} is needed for a magnetic field of 1 G, and $L_{\rm k} \sim 3 \times 10^{36}$ erg s^{-1} is needed for a magnetic field of 10 G. We must note that this factor of 3 is not physical

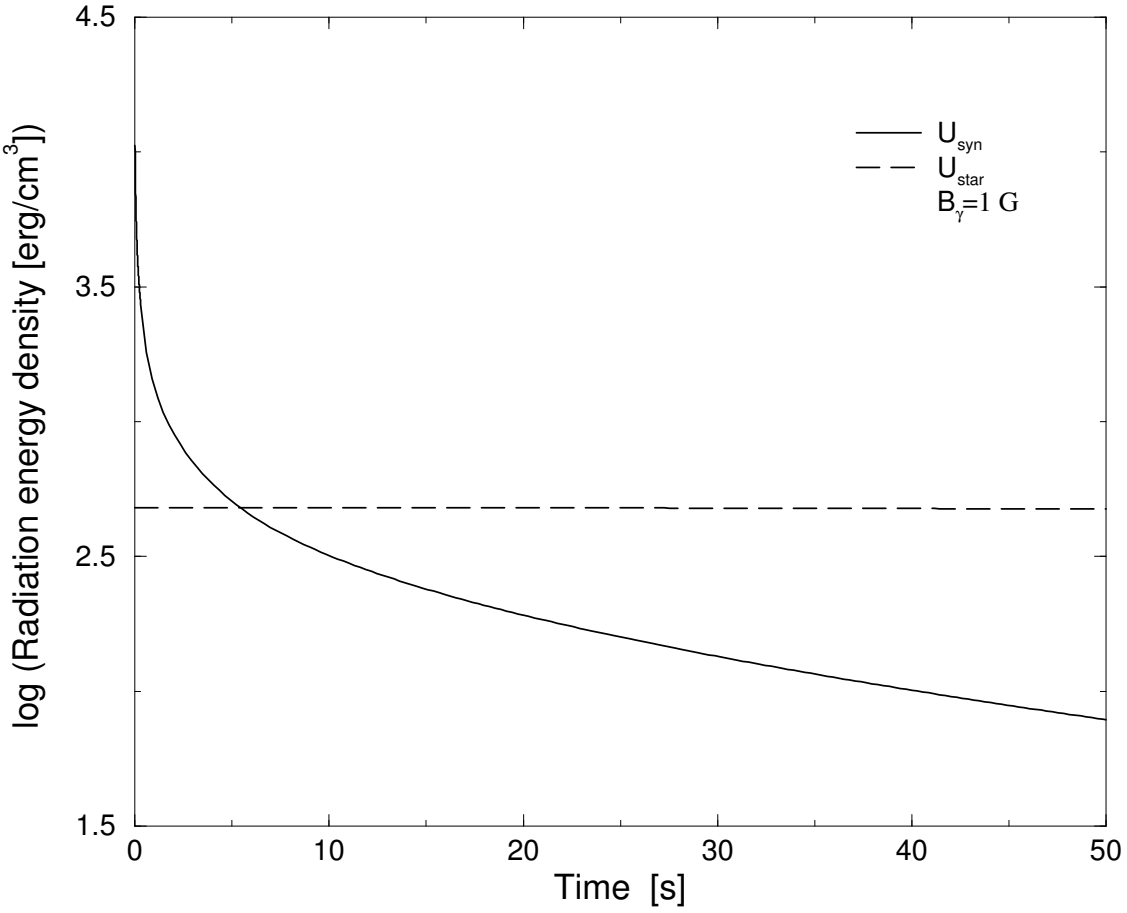

Figure 4.3: The evolution of the synchrotron and companion star radiation energy densities within a given slice. The value of the magnetic field is $B = 1$ G and the maximum Lorentz factor of the electrons is 5×10^4. The time axis finishes when a given slice moving along the jet stops emitting due to losses through the IC effect at 100 MeV. 50 s imply a distance of $3{\times}10^{11}$ cm.

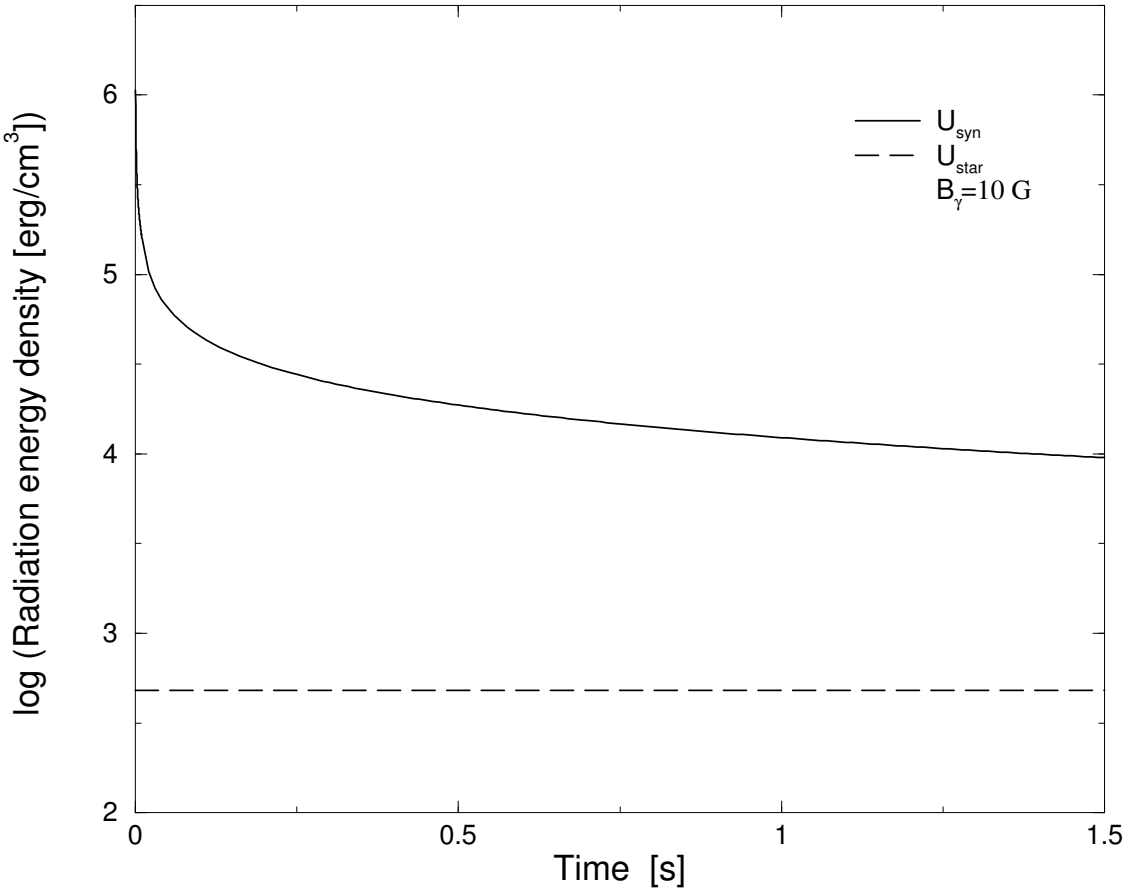

Figure 4.4: Same as Fig. 4.3 but for $B = 10$ G. 1.5 s imply a distance of 9×10^9 cm.

and is due to the fact that, when in the SSC dominance regime ($B = 10$ G), emission above 100 MeV is mainly due to IC interactions with synchrotron photons above ultraviolet frequencies. This interactions will be close to or within the Klein-Nishina regime, and using Thomson losses for IC interaction we overestimate such losses. In any case, the kinetic luminosity required to power the γ-ray emission is slightly high. It is due to the γ-ray radiative efficiency of a jet as the one modeled here is not high, since the most part of the energy is released at lower energies, unlike other models which accounted for information at other wavelengths as well and a different geometry and jet physics (see below and Chapter 5).

For LS 5039, regarding the intensity of the magnetic field, the SSC effect would be dominant for values of about 10 G or higher, and at least non-negligible for values of about 1 G. In the second case, due to the importance of the star seed photons, variations in the orbital distance have a significant effect on the IC flux on the scale of the orbital period of the system. In the case of high B (above 10 G), due to the strong energy losses, the electrons might need to be reaccelerated after leaving the γ-jet to reach the observed radio jet. For $B = 1$–10 G, reacceleration might not be necessary in regions closer to the compact object than the radio jet. This issue will be treated in the next chapter.

4.1.2 Application to LS I +61 303

LS I +61 303 is a HMXB system whose optical counterpart is a bright (V$\sim$10.8) star of B0 V spectral type (Paredes & Figueras 1986) with a decretion disk (Be), located at 2 kpc (Frail & Hjellming 1991). The microquasar nature of this source arose when relativistic jets where observed, with velocities of about $0.6c$, and strong hints pointing to fast jet precession were found (Massi et al. 2001, 2004). It is still unclear whether the compact object is a neutron star or a black hole (Casares et al. 2005a) though the orbit can be characterized by a period $P = 26.4960$ days (Gregory 2002), an eccentricity $e = 0.72$ (Casares et al. 2005a), and an orbital semi-major axis $a = 5 \times 10^{12}$ cm (Taylor & Gregory 1982).

LS I +61 303 was proposed by Gregory & Taylor (1978) as the possible counterpart of the high-energy γ-ray source 2CG 135+01 (Hermsen et al. 1977), which was also detected by EGRET (3EG J0241+6103; Kniffen et al. 1997). The proposed association between LS I +61 303 and the high-energy γ-ray source is still unclear due

to the large EGRET source error boxes. Nevertheless, no radio loud active galactic nucleus or strong radio pulsar is known within the error box of 3EG J0241+6103, which includes LS I +61 303 (Kniffen et al. 1997). Variability studies can help us to reinforce the association between LS I +61 303 and 3EG J0241+6103. Tavani et al. (1998) found that the γ-ray flux varied by a factor of 3. Also, Wallace et al. (2000) showed that in the EGRET viewing period 211.0 (1993 February 25–March 9) there was a γ-ray flare at an orbital phase around 0.5. Moreover, Massi (2004) presented a variability analysis of the EGRET data, obtaining a γ-ray period of 27.4±7.2 days, in agreement with the orbital one. The results of that work also seem to suggest the presence of two peaks in the γ-ray flux: the first one would be in a phase around 0.2 (periastron passage, Casares et al. 2005a), which was not covered in the data studied by Wallace et al. (2000), and the second one would be in a phase around 0.5, like in Wallace et al. (2000). It is worth mentioning that X-ray observations performed by ROSAT just six months before the EGRET viewing period 211.0 (1992 August–September) showed also an X-ray peak at an orbital phase around 0.5 (Peracaula 1997, Taylor et al. 1996). All these results strengthen the 3EG J0241+6103/LS I +61 303 association. At very high-energy γ-rays, Hall et al. (2003) gave upper limits for the emission associated with this source from observations performed with the Cherenkov telescope Whipple. Observations with the Cherenkov telescope MAGIC are being carried out, and their results will be reported soon elsewhere. We note that, for this source, predictions of possible detection at very high energies have been made by Romero et al. (2005).

To model the source, we have adopted the orbital and other physical parameter values provided by Casares et al. (2005a) and the radio spectral information from Ray et al. (1997) to roughly constrain p, and the γ-ray spectrum and photon flux given by Hartman et al. (1999). The procedure employed here is basically the same as when studying the γ-ray emission from LS 5039, adopting the same free parameters: B, $\gamma_{\rm max}(z_0)$, and $L_{\rm k}$, the last one being fixed comparing with γ-ray fluxes. As previously, the jet radius has been taken large enough for preventing electrons in the jet to escape, and $\varpi = 90°$. The fixed parameter values, altogether with their description, are listed in Table 4.3, and the photon flux and photon index observed by EGRET are given in the same table at the bottom, both being employed to test different free parameter values.

Table 4.3: Fixed parameters

symbol	parameter	value
a	Orbital semi-major axis	5×10^{12} cm
$L_{\rm star}$	Star total luminosity	2×10^{38} erg s^{-1}
e	System eccentricity	0.7
θ	Viewing angle	30°
ϖ	Angle between the jet and the orbital plane	90°
$\Gamma_{\rm jet}$	Jet Lorentz factor	1.25
p	Electron power-law index	1.7
$R_{\rm jet}$	γ-jet radius	10^7 cm
$I_{>100\ \rm MeV}$	Photon flux at the EGRET band	8×10^{-7} photon cm^{-2} s^{-1}
Γ	Photon index at the EGRET band	2.2

Results

We have computed the normalized SEDs for two different values of B and $\gamma_{\rm max}(z_0)$ (see Fig. 4.5). For $\gamma_{\rm max}(z_0) = 10^4$ and B=100 G, the computed spectral photon index above 100 MeV is 2.4, which is steeper than the observed one (2.2±0.1). In case that the magnetic field strength is lower, the spectrum will get softer, because the computed maximum electron energy cut-off is at relatively low energies. For $\gamma_{\rm max}(z_0) = 10^5$ and B=100 G, the spectrum becomes more similar to the one observed in the EGRET energy range. Now, in case that the magnetic field strength is lower the spectrum will get harder, since interaction becomes further in the Klein-Nishina regime when stellar field dominates (it is also present in LS 5039 spectra, but less clearly). Because of the lack of data (just upper limits) beyond 10 GeV, we cannot still restrict $\gamma_{\rm max}(z_0)$.

The values of the model parameters that reproduce properly the observations are shown in Table 4.4. We have taken separately the case in which the dominant source of seed photons is the companion star (i.e. B=1 G, see Figs. 4.6 and 4.7) and the case in which the dominant source of seed photons is the synchrotron process within the jet (i.e. B=10 G, see Fig. 4.8). Also, in order to study the implications on variability of the orbital eccentricity at the EGRET energy range, we have calculated

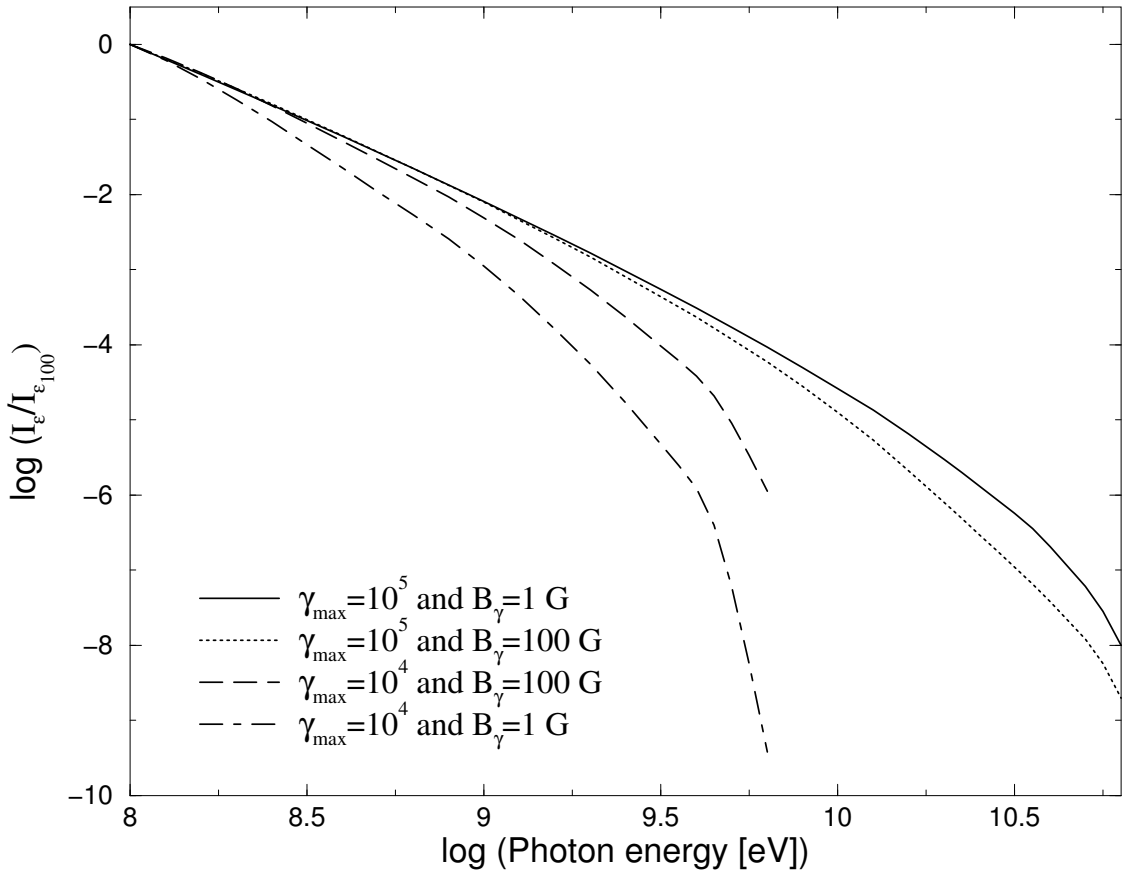

Figure 4.5: Computed spectral photon distributions normalized to the photon flux value at 100 MeV for different values of the magnetic field and the maximum electron Lorentz factor. The solid and dotted lines represent the spectral photon distribution for two different B: 1 and 100 G, respectively, and a $\gamma_{\max}(z_0)$ of 10^5. The dot-dashed and dashed lines represent the spectral photon distribution for two different B: 1 and 100 G, respectively, and a $\gamma_{\max}(z_0)$ of 10^4.

Table 4.4: Two sets of free parameters used to reproduce the observations

Parameter	dominant EC	dominant SSC
B	1 G	10 G
$L_{\rm k}$	10^{35} erg s^{-1}	3×10^{35} erg s^{-1}
$\gamma_{\rm max}(z_0)$	10^5	10^5

the spectral photon distribution at an orbital distance equal to the orbital semi-major axis, at the periastron passage and at the apastron passage. However, in a first and simpler situation (Fig. 4.6), only the variations in the stellar photon density have been taken into account. In the other two cases (Figs. 4.7 and 4.8), accretion variation has been added. Following the Bondi-Hoyle accretion model (Bondi 1952), the accretion rate/ejection rate has been taken to be proportional to the density of the medium surrounding the compact object and further dependences have been neglected here. We have assumed also that the ambient density decreases like $1/R^2_{\rm orb}$ (no Be disk considered).

It is worth noting that, although for the two magnetic field strengths quoted before the spectral photon distribution is quite similar, the physical origin of the seed photons and the length of the γ-jet are different. When B=1 G, the length reached by the jet electrons emitting at 100 MeV by IC process (the γ-jet length) is of about one astronomical unit whereas, for B=10 G, the length of such a jet is roughly one hundred times smaller.

Discussion

Our model is able to explain the observed data, supposing that the emission detected by EGRET comes from a compact cylindrical jet close to the compact object. In order to reach the observed levels of emission, a $L_{\rm k}$ of 10^{35} erg s^{-1} for B=1 G, or of 3×10^{35} erg s^{-1} for B=10 G, is necessary. These values for the relativistic leptonic jet power are similar to the value inferred for the γ-ray total luminosity, and this implies that the energetic requirements are less important than in LS 5039. It is explained partially because p is harder, the distance to the observer is shorter and the Doppler boosting larger than in the case of LS 5039. Regarding $\gamma_{\rm e0}^{\rm max}$, for a value of 10^5, the model reproduces properly the observations. Otherwise, future

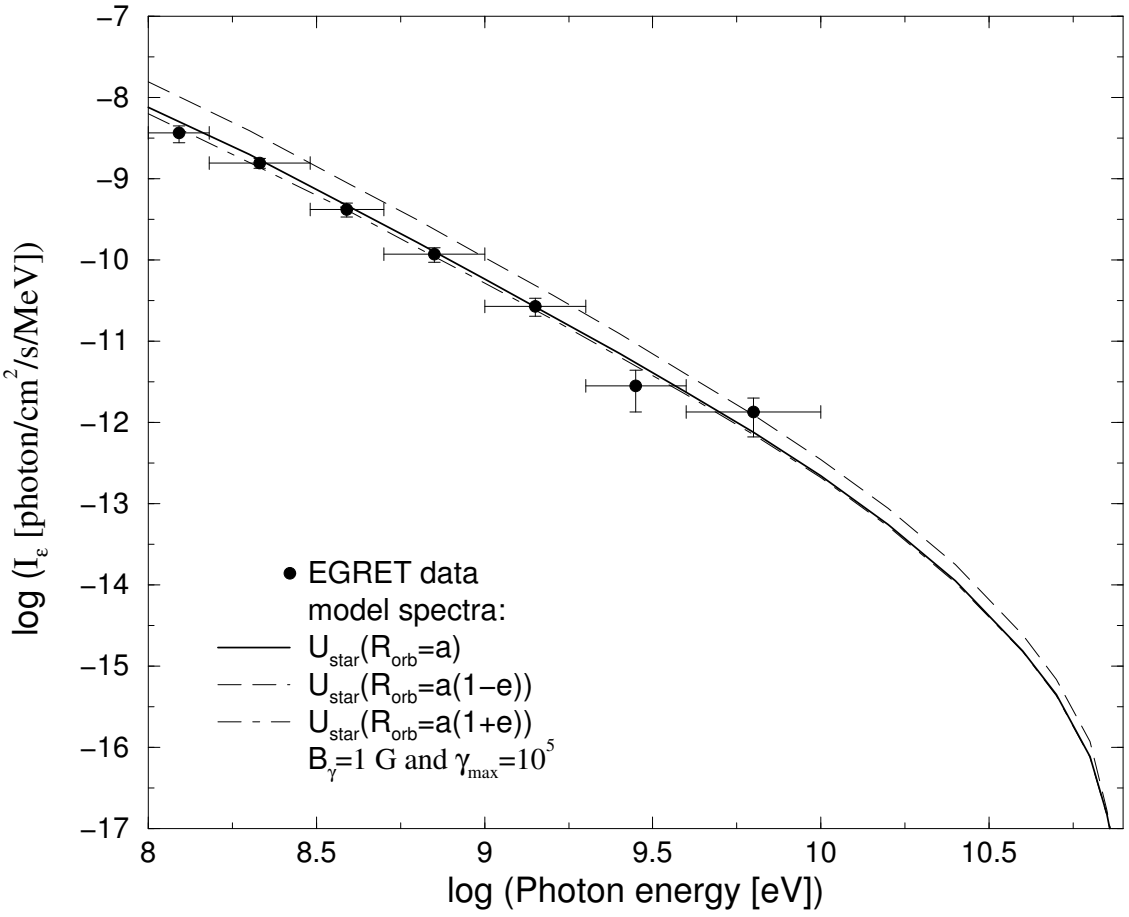

Figure 4.6: Computed spectral photon distributions above 100 MeV plotted with the EGRET data points. Only changes in the stellar photon density have been taken into account and, due to the low magnetic field, EC dominates. $\gamma_{\max}(z_0) = 10^5$, and B=1 G. We have plotted the spectral photon distribution for different orbital radii: the semi-major axis a (solid line), the distance at the periastron passage ($a(1-e)$, dashed line), and the distance at the apastron passage ($a(1+e)$, dotted line).

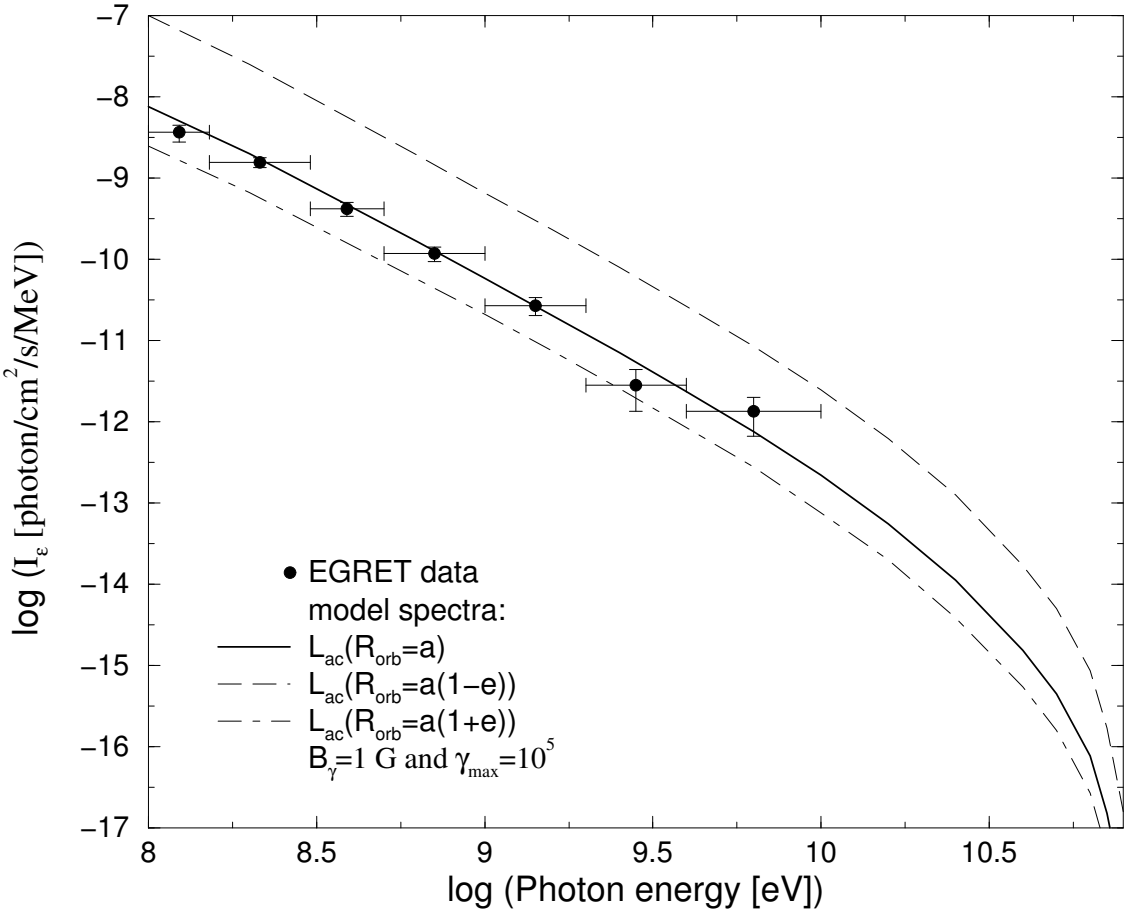

Figure 4.7: Same as in Fig. 4.6 but now changes in both the stellar photon density and the accretion rate have been taken into account.

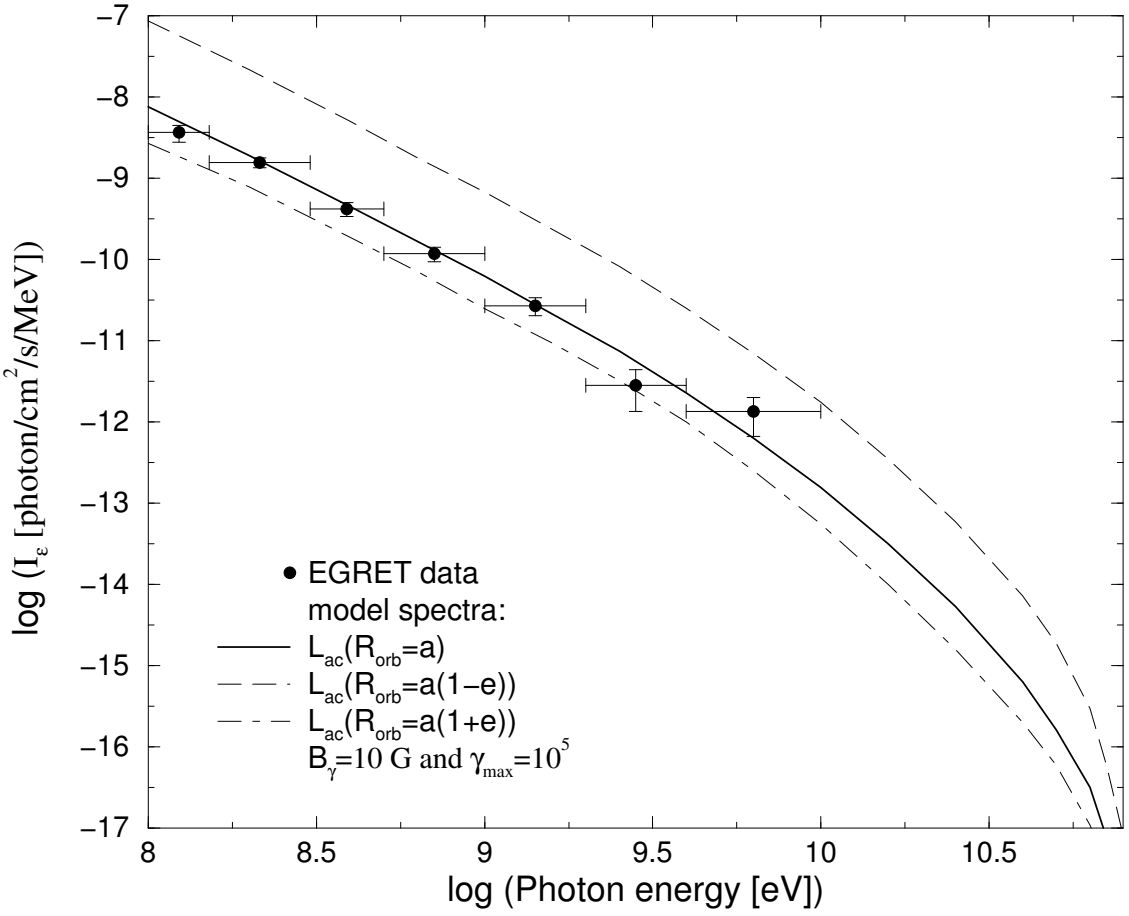

Figure 4.8: Same as in Fig. 4.7 but with B=10 G.

instruments covering EGRET and higher energy ranges (AGILE, GLAST, MAGIC) will allow to get a better constraint on $\gamma_{\max}(z_0)$, as well as will permit to check whether the predicted spectral shape follows the real source spectrum. Our model also predicts that, during a flare, variations in both the intensity and the slope of the spectrum at higher energies should be detected in correlation with the ones observed at radio frequencies, since we assume that the emitting electron population is the same. This is not necessarily in contradiction with the observed shift in time of the emission peaks at different energy bands, which have been linked to changes in the environment and within the jet itself (Martí & Paredes 1995, Strickman et al. 1998, Gregory et al. 1999) and whose study is beyond the scope of this work. Otherwise, good timing and spectral resolution observations at high-energy γ-rays and coordinated observations at different energy bands are needed in order to find out whether both the low- and the high-energy emission have the same origin. We will not go, for the moment, into the study of the emission at frequencies below the high-energy γ-rays, being necessary to extend the modelisation of the jet up to bigger scales. A further comment can be done, regarding the role of the magnetic field in our model: unlike in some other models developed before, B could play an important role in the generation of seed photons in the high energy IC emission. It is worth also mentioning that the upper limits of emission at hundreds of GeV (Hall et al. 2003) would be in agreement with the softening of the computed spectral photon distribution above $\sim$10 GeV. This softening above $\sim$10 GeV would make the source pretty faint at hundreds of GeV and above. The previous point and a spectrum at X-rays harder than at EGRET energies, likely due to the electron energy losses, seem to point to a dominant leptonic radiative mechanism in the jet (IC) instead of a hadronic one.

Regarding variability, our model predicts that important variations of the flux might occur along the eccentric orbit. For the sake of simplicity, we have contemplated two cases. The first one accounts for the variation of the EC photon flux along the orbit due only to the changes in the stellar photon density because of the eccentricity (see Fig. 4.6). This is only relevant if the SSC effect is not significant. The second one takes into account the variation of the IC photon fluxes due to the changes in both the stellar photon density and the accretion rate because of the orbital eccentricity (see Figs. 4.7 and 4.8). The high-energy γ-ray emission variability is clearly dominated by the accretion rate variations along the orbit. As mentioned above, the high-energy γ-ray emission of 3EG J0241+6103 varies a factor of 3. Also, all of the computed spectral photon distributions present fluxes

that vary within a range of 2–30 times. Because of the EGRET timing sensitivity, the periodic outburst at γ-rays associated with the periastron passage could not be sampled properly though the detected *averaged* emission could explain the observed variability of 3EG J0241+6103, being also related to the strong radio outbursts. Such a γ-ray outburst would be detected smoother and earlier in orbital phase than the radio one. If this is true, more sensitive timing observations at high-energy γ-rays along the orbit will find larger variability than the one previously found. It is interesting to note that our model predicts a γ-ray peak at periastron, at orbital phase 0.2 (as it was found by Massi 2004), when the accretion rate is expected to be higher. The previously mentioned second peak at phase 0.5 can be explained in the context of an eccentric orbit where the interaction between the compact object and the wind of the stellar companion produces an increase in the accretion rate under certain conditions (Martí & Paredes 1995). This would produce also a variability effect on the γ-ray flux like the one shown in Figs. 4.7 and 4.8.

Short timescale variability could be produced by precession (see, e.g., Kaufman Bernadó et al. 2002). In Massi et al. (2004), the authors found evidence of precession of the jets in LS I +61 303 on timescales of a few days, similar to the shorter variability timescales found at high-energy γ-rays by Tavani et al. (1998) for 2CG 135+01/3EG J0241+6103. We have computed the fluxes for different values of the angle θ, from 0 to $\pi/2$, obtaining variations in the intensity of the IC emission of almost two orders of magnitude. This gives us just an upper limit for the intensity changes of the γ-ray emission due to precession, in agreement with observed variability at these energy ranges.

Regarding the effect of the magnetic field on the length-scale of the γ-jet, for B above 10 G and due to the strong energy losses induced by the SSC effect, the electrons might need to be reaccelerated significantly after leaving the γ-jet to reach the distance of the observed radio jet. However, for B lower than 10 G, reacceleration might not be necessary in regions closer to the compact object than the radio jet. As for LS 5039, there is a factor of three of difference between $L_{\rm k}$ in both cases, 1 G and 10 G. Recall it is not physical, but both $L_{\rm k}$ should be basically the same.

4.2 A semi-analytical model for jet broadband emission

The model presented in the previous section could be considered as the starting point in the process of understanding γ-ray generation in jets that are thought to be present during the low-hard state, when radio emission is detected, as explained in Chapter 2. However, a cylindrical jet beyond the smallest scales is probably not a good approximation. Therefore, when exploring γ-ray emission from jets in a more realistic way, it is necessary to include other energy bands and emission mechanisms to obtain consistent results concerning the SED of the broadband radiation. The next step has been therefore to develop a model which is based on a free expanding jet, of conical shape, whose particles lose energy adiabatically. Although it might be considered a too naive approach, it is reasonable even for quite small scales in jets if magnetic and photon fields are not very strong. Nevertheless, we indeed consider different radiation mechanisms, the synchrotron and IC processes with the disk, corona, star and synchrotron photons themselves, to compute the SED in a wide spectral energy range. It is worth noting that later on in this thesis we explore also the case in which the magnetic field is strong enough to overcome other loss mechanisms. This could be well founded physically, but the present study is worthy because it explores a significant range in the parameter space, allowing to know better the different possibilities that could be at work.

To show that, as a first approach, the modeling of the particle evolution in a jet can be done taking into account just adiabatic losses, see in Table 4.5 the different energy densities to be accounted for losses in the case of a microquasar that could be an unidentified EGRET source. For an electron with $\gamma \sim 10^3$, the loss timescale for the most important process is similar to that of adiabatic losses, the former growing much faster with z than the latter. The star photon field corresponds to a bolometric luminosity of 10^{39} erg s^{-1} for a source at a distance of 1 AU from the inner regions of the jet. The disk and corona luminosities, considered now, are faint, due to the X-ray spectra of EGRET microquasars LS 5039 and LS I +61 303 appear to be free of disk and corona features (see Bosch-Ramon et al. 2005a and Leahy et al. 1997 respectively), showing a pure power-law spectrum up to γ-ray energies. A comparison between radiative and adiabatic losses in the jet is shown in Fig. 4.9, from which it is seen that the adiabatic loss channel dominates almost everywhere all along the jet for electrons with energies ~ 10 GeV.

Table 4.5: Energy densities (U) at the base of the jet in units of erg cm^{-3}, luminosities (L) in erg s^{-1}, and magnetic field in G.

Model	$L_{\rm star}$	$L_{\rm disk/cor}$	B	$U_{\rm sync}$	$U_{\rm star}$	$U_{\rm disk}$	$U_{\rm cor}$
'Realistic'	5×10^{38}	3×10^{32}	200	6.6×10^{6}	15.4	351.0	2.2×10^{5}

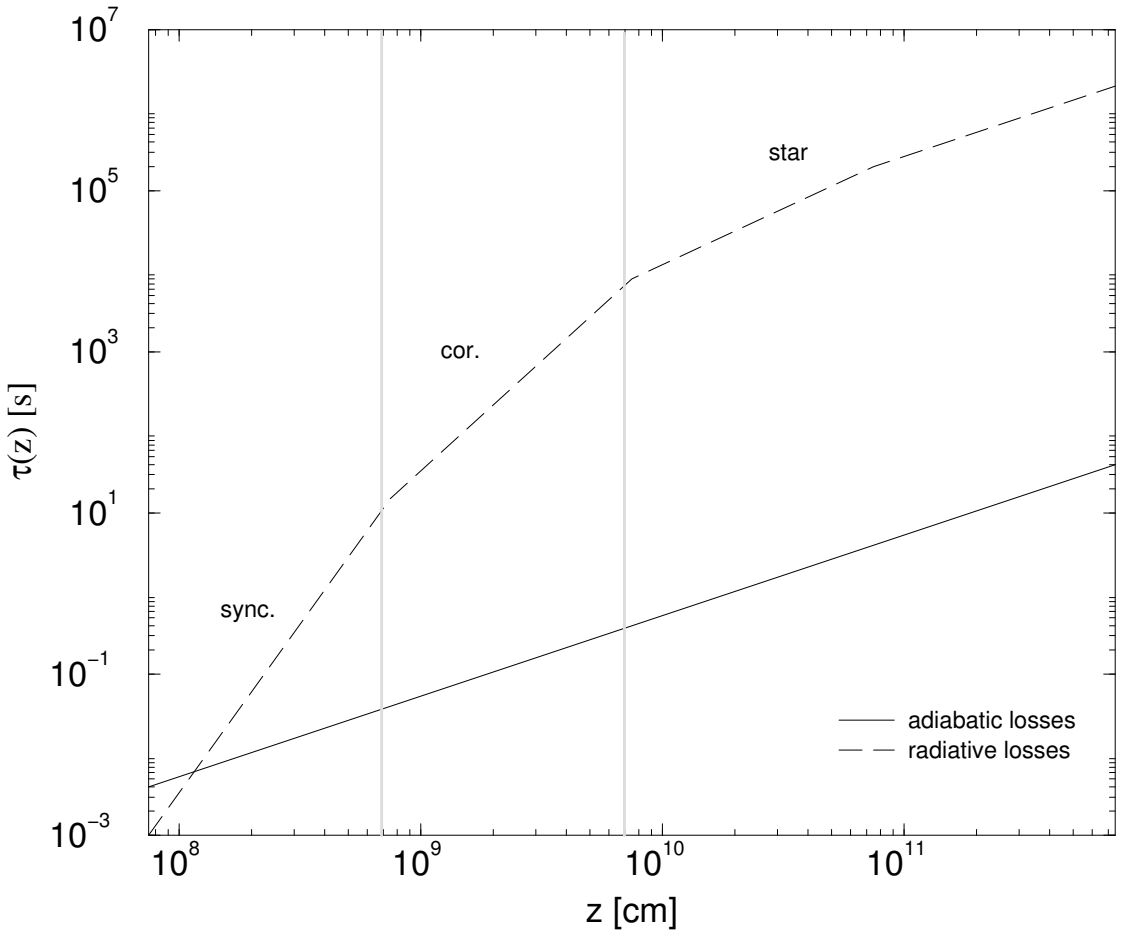

Figure 4.9: Cooling time evolution with z for adiabatic (solid line) and radiative (long-dashed line) losses in a microquasar that might appear as an unidentified γ-ray source. Three regions in the plot have been established depending on the dominant source of radiative losses, which happen to be the synchrotron losses in the base of the jet, corona IC losses further up, and the star IC losses in the farthest shown away (at higher distances, adiabatic losses would dominate again).

We present now the expression for the particle energy distribution density $n(z,\gamma)$, the maximum particle Lorentz factor, and the magnetic field along the jet in its RF (for a similar approach, see Ghisellini et al. 1985):

$$n(z,\gamma) = Q(z)\gamma^{-p}, \qquad \gamma_{\rm min} < \gamma < \gamma_{\rm max}(z) \tag{4.8}$$

$$Q(z) = Q(z_0)\left(\frac{R_0}{R}\right)^2 = Q(z_0)\left(\frac{z_0}{z}\right)^{2\varepsilon}, \tag{4.9}$$

$$\gamma_{\rm max}(z) = \gamma_{\rm max}(z_0)\left(\frac{z_0}{z}\right)^{e\varepsilon}, \tag{4.10}$$

$$B(z) = B(z_0)\left(\frac{R_0}{R}\right) = B(z_0)\left(\frac{z_0}{z}\right)^{\varepsilon}. \tag{4.11}$$

ε and e allow to parametrize the opening angle of the jet along z and the effect of losses on the particle energy, respectively. $\varepsilon = 1$ corresponds to a conical jet and $e = 1$ corresponds to the case of a blob. For a jet, e would be 2/3, but we strength the energy decay to $e = 1$, as it would be the case for blobs, *to account* for the extra losses due to radiation. We note that $R_{\rm jet}$ is now simply R, which changes as $R = R_0(z/z_0)^{\varepsilon}$. From Eq. (4.8), we can calculate the IC SED from Eq. (3.20) and Eq. (4.7), taking into account this new behavior of the jet radius. For the synchrotron emission, it can be computed from Eq. (3.13), where one can find the expression $I(R,\epsilon)$, the intensity function multiplied by 4π of a jet section at z (to compute the isotropic luminosity):

$$\epsilon' L'(\epsilon')_{\Omega'_0} = \epsilon'\delta(\Omega'_0)^3 \int_{\rm z_{min}}^{\rm z_{max}} 2\pi R I(R, \epsilon'/\delta) dz. \tag{4.12}$$

Regarding the IC seed photon fields, we use Eq. (4.6) for the star and the disk photon fields, where the distance to the disk is taken to be z. Moreover, concerning the disk IC interactions, we have adopted the approach of Dermer et al. (1992), where the seed photon energy density is reduced by a factor $(1-\cos\theta')^{(p+1)/2}$ (we recall that θ' is the viewing angle in the observer RF), since it is considered here that disk photons come from *behind* the jet. For the corona photon fields, we adopt a power-law plus an exponential cutoff, at the corona peak energy $E_{\rm cor\ max}$, normalized to the total corona luminosity:

$$\propto E^{-p_{\rm cor}} \exp(E/E_{\rm cor\ max}). \tag{4.13}$$

Synchrotron energy density can be computed from Eq. (4.8) and Eq. (3.11). We recall that the seed photon fields are to be transformed accordingly with the RF where the interaction is considered (Dermer & Schlickeiser 2002). Next, we apply

this model, altogether with some statistical considerations, to explore whether high-mass microquasars can be behind some of the unidentified variable γ-ray sources in the galactic plane.

4.2.1 High-mass microquasars as variable EGRET sources in the galactic plane

Among the unidentified γ-ray sources in the galactic plane, most of them detected by EGRET, there is a subgroup that displays significant variability on timescales of weeks to months (Torres et al. 2001, Nolan et al. 2003). Recently, Kaufman Bernadó et al. 2002 and Romero et al. (2004) have suggested that this subgroup of low-latitude unidentified γ-ray sources might consist of high-mass microquasars (i.e. microquasars formed by a compact object and an early-type stellar companion), where the γ-ray emission arises from interactions between relativistic particles in the jet and external photon fields, most notably the stellar UV emission (Paredes et al. 2000). We note that we will assume in the following that the very majority of the low-latitude sources are of galactic nature. Population studies by several authors (Grimm et al. 2002; Miyagi & Bhattacharya 2004, private communication) suggest that HMXBs are distributed in the Galaxy following the spiral structure, presenting a steeper $\log N - \log S$ distribution than low-mass XRBs (LMXB), which means that LMXB are more uniformly distributed in the Galaxy than HMXB. Since high-mass microquasars form a subset of the whole set of HMXB, they are also expected to be distributed along the spiral arms, as seems to be the case of low-latitude unidentified γ-ray sources (Bhattacharya et al. 2003). In this work we explore in more detail this hypothesis, using a $\log N - \log S$ analysis for studying the low-latitude unidentified EGRET source population, and a more detailed model for the γ-ray emission than the one presented above. In particular, we include the interaction of the microquasar jet with the X-ray fields produced by the accretion disk and the hot corona that is thought to surround the compact object, altogether with the stellar UV field. We also include synchrotron self-Compton emission, Klein-Nishina effects, and a simplified back-reaction of the different losses in the particle energy distribution of the jet. We calculate the broadband SED for a characteristic set of the parameter values that characterize a γ-ray emitter high-mass microquasar without clear counterpart at lower energies.

Results I: statistical study

Unidentified γ-ray sources concentrated in the galactic plane present a good spatial correlation with young stellar objects (Romero et al. 1999). The variability analysis of these sources (Torres et al. 2001) clearly shows evidence for the existence of a subgroup with variable emission on timescales from weeks to months. This is corroborated by the recent results presented by Nolan et al. (2003), which are based on a maximum likelihood re-analysis of the EGRET data. These authors identify 17 variable sources within $\mid 6^\circ \mid$ from the galactic plane. These sources are clumped within $\mid 55^\circ \mid$ of the galactic center.

A $\log N - \log S$ analysis for all low-latitude unidentified γ-ray sources yields a distribution that is consistent with a power-law with index $\beta \sim 3.1$ (Bhattacharya et al. 2003). This is far steeper than what is expected for a population uniformly distributed along the galactic disk. For instance, for pulsars detected at 400 MHz the slope is $\beta \sim 1.05$. The unidentified γ-ray sources, on the contrary, seem to be concentrated mainly in the inner spiral arms. To find possible further evidence for different populations among low-latitude unidentified γ-ray sources, we have implemented a $\log N - \log S$ analysis of both variable and non-variable low-latitude sources.

First we have considered the 17 variable sources listed by Nolan et al. (2003). To take into account systematic effects introduced by different exposure and background resulting in non-uniform detectability, we have adopted the procedure described by Reimer (2001). The obtained $\log N - \log S$ plot is shown in Fig. 4.10, lower panel. The normalized distribution can be fitted by a power-law $N(S) \propto S^{-\beta}$, with $\beta = 1.66 \pm 0.31$, significantly harder than for the entire sample. If we now consider those sources that classify as non-variable or dubious cases, we get the $\log N - \log S$ plot shown also in Fig. 4.10, upper panel. In this case the distribution can be fitted by a power-law with index $\beta = 2.92 \pm 0.36$. The average spectral index is also different for both samples: in the case of the variable sources we have $\langle \Gamma \rangle = 2.04$, whereas for the remaining sources $\langle \Gamma \rangle = 2.16$. All this suggests that there are two different groups of sources, one formed by steady sources concentrated towards the inner spiral arms, and a second group with variable sources and a wider distribution along the galactic plane, although not as wide as that of radio pulsars (Bhattacharya et al. 2003).

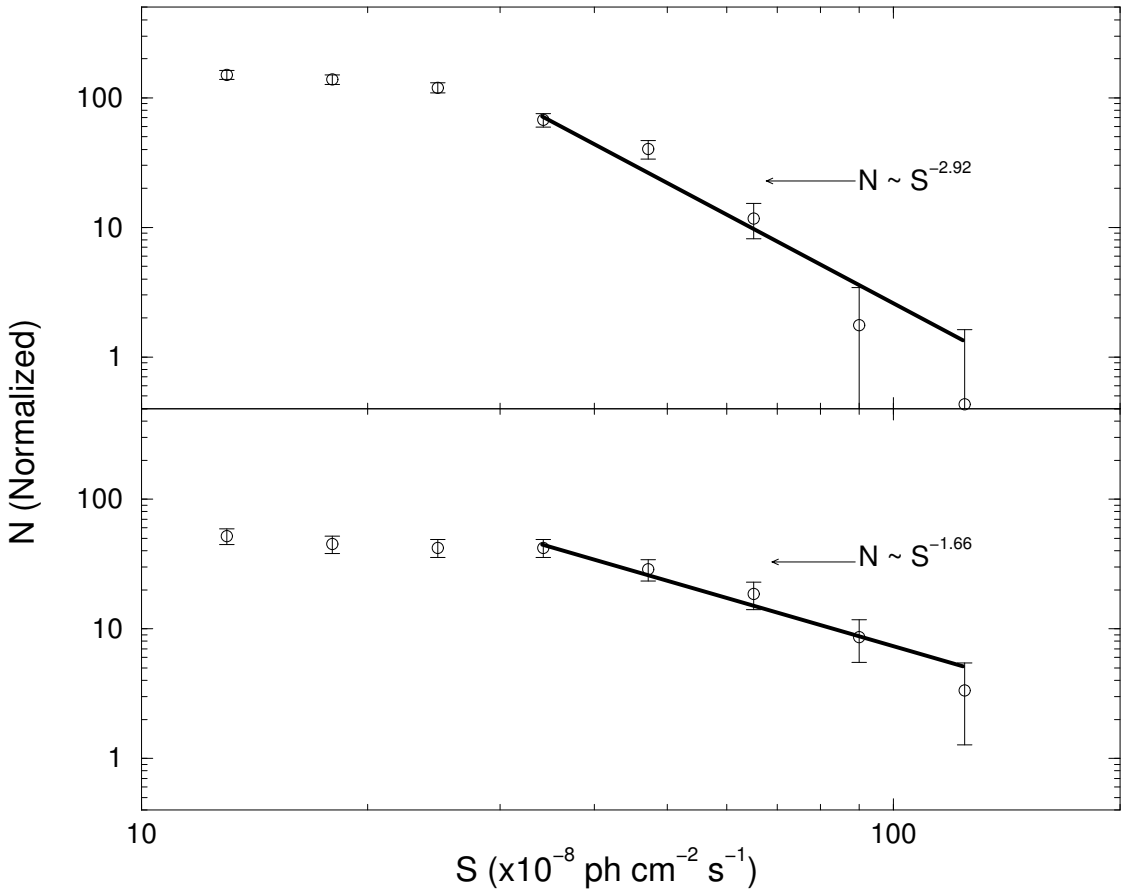

Figure 4.10: Log $N - \log S$ plot for unidentified γ-ray sources within $|b| < 6^{\circ}$. Upper panel: For non variable γ-ray sources. Lower panel: For variable γ-ray sources.

Microquasars appear to be good candidates for compact and variable γ-ray sources in the galactic plane. Since they can have very large proper motions (Ribó et al. 2002, Mirabel et al. 2004), their distribution along the plane should be broader than that presented by supernova remnants and molecular clouds, which can be traced by star-forming regions and OB associations. Their spread, however, is limited by the lifespan of the companion massive star, and hence it is not as extended as that of radio pulsars. It is worth noting that Miyagi & Bhattacharya (private communication) obtained for HMXBs a β of about 1.9.

Results II: a high-mass microquasar model for an unidentified variable γ-ray source

The two microquasars proposed to be counterparts of EGRET sources, LS 5039[2] (Paredes et al. 2000) and LS I +61 303 (Kniffen et al. 1997, Massi et al. 2001), present also persistent radio jets (Paredes et al. 2002, Massi et al. 2004), likely powering the γ-ray emission (Paredes et al. 2000, Bosch-Ramon & Paredes 2004a,b), and moderate radio and X-ray emission (Martí et al. 1998 and Bosch-Ramon et al. 2005a for LS 5039; Ray et al. 1997 and Paredes et al. 1997 for LS I +61 303). Although both systems have different eccentricities and orbital periods, and LS 5039 star is brighter, the SED for both microquasars is roughly similar, peaking at γ-rays (putting aside the star component), and presenting just different variability patterns. To show that our model can reproduce the spectra of these objects, accounting also for EGRET data, we plot in Fig. 4.11 the SED obtained by a source model with the parameter values presented in Table 4.6. We refer to Fig. 2.5 to note that the LS 5039 luminosities from radio to γ-rays shown there and in Fig. 4.11 are similar, although we remark that a broadband spectrum accurate reproduction was not intended (see otherwise Chapter 5). The parameter values adopted here are similar to those presented above for the known γ-ray microquasars. Even when dealing with the free parameters, their values are also similar but the relativistic leptonic jet power, that is smaller, provided that radiation in this model is generated mainly in the γ-rays due to the introduction of adiabatic losses and magnetic field evolution with z. Since no clear disk/corona features are present in the X-ray spectrum of LS 5039 (Martocchia et al. 2005, Bosch-Ramon et al. 2005a) and LS I +61 303 (Leahy et al. 1997), we have fixed their luminosities to low values. Nevertheless,

[2]Actually, HESS detection confirms the EGRET source association for LS 5039 (Aharonian et al. 2005).

although minor, the IC contribution from these sources might be significant and even dominant in some cases (low-mass and/or low jet magnetic field systems).

It is worth mentioning that radio emission has been computed modifying the electron Lorentz factor evolution once electrons have suffered strong losses and are already in the radio emitting synchrotron regime. In that region ($100z_0$), high energy emission is not significant, and the ε is set to values $\sim$0.1, allowing to reach detectable radio fluxes. Nevertheless, it is just a phenomenological parameter and can only be understood as pointing to the need to introduce some sort of acceleration mechanism, provided that evolution driven by (conical jet) adiabatic and radiative losses do not allow otherwise the formation of detectable fluxes of extended radio emission.

The emission from the high mass star could be easily detectable at galactic distances if no strong absorption takes place. Nevertheless, as discussed in Bosch-Ramon et al. (2005, in press) and references therein, microquasars located in the galactic plane can present significant enshrouding (reprocessed and/or scattered radiation by dust and gas), masking the optical counterpart and making it hardly noticeable. Even when no strong absorption takes place, the relatively recent association of the optical emission coming from the bright stars in LS 5039 and LS I +61 303 with their counterparts at other wavelengths shows that a significant fraction of the variable unidentified γ-ray sources in the galactic plane might be indeed microquasars. These sources could have unnoticed but detectable faint radio and X-ray emission, and a moderately bright optical counterpart.

Discussion

We have shown that the variable γ-ray sources found on the galactic plane have some common features that make it reasonable to consider them as a distinctive group among the low-latitude unidentified γ-ray sources. We have suggested that these sources might be microquasars with high-mass stellar companions and we have developed a broadband model to explain the γ-ray production in this type of objects. Microquasars are not, of course, the only kind of galactic object that might display variable γ-ray emission. Other alternatives include early-type binaries (Benaglia & Romero 2003), accreting neutron stars (Romero et al. 2001), pulsar wind nebulae (Roberts et al. 2002) and exotic objects (Punsly et al. 2000). However, microquasars

Table 4.6: Parameter values in the models

symbol	Parameter	Value
$M_{\rm x}$	Black hole mass	$5M_{\odot}$
$R_{\rm Sch}$	Schwarzschild radius	1.5×10^6 cm
$L_{\rm star}$	Stellar bolometric luminosity	$5{\times}10^{38}$ erg s^{-1}
θ	Viewing angle to the jet axis	10°
z_0	Distance from jet apex to the compact object	50 $R_{\rm Sch}$
R_0	Initial jet radius	5 $R_{\rm Sch}$
$R_{\rm orb}$	Orbital radius	$\sim$1 AU
$kT_{\rm disk}$	Peak energy of the disk	1 keV
$E_{\rm cor\ max}$	Peak energy of the corona	150 keV
$kT_{\rm star}$	Peak energy of the star	10 eV
$\gamma_{\rm min}$	Min. electron Lorentz factor (jet frame)	~ 1
p	Electron energy distribution power-law index	2
$\Gamma_{\rm cor}$	Photon index for the corona	1.6
$L_{\rm disk/cor}$	Disk/Corona luminosity	$3{\times}10^{32}$ erg s^{-1}
$\Gamma_{\rm jet}$	Jet bulk Lorentz factor	1.1
$B(z_0)$	Magnetic field	200 G
$\gamma_{\rm max}(z_0)$	Maximum electron Lorentz factor	10^4
$L_{\rm k}$	Relativistic leptonic jet power	3×10^{35} erg s^{-1}

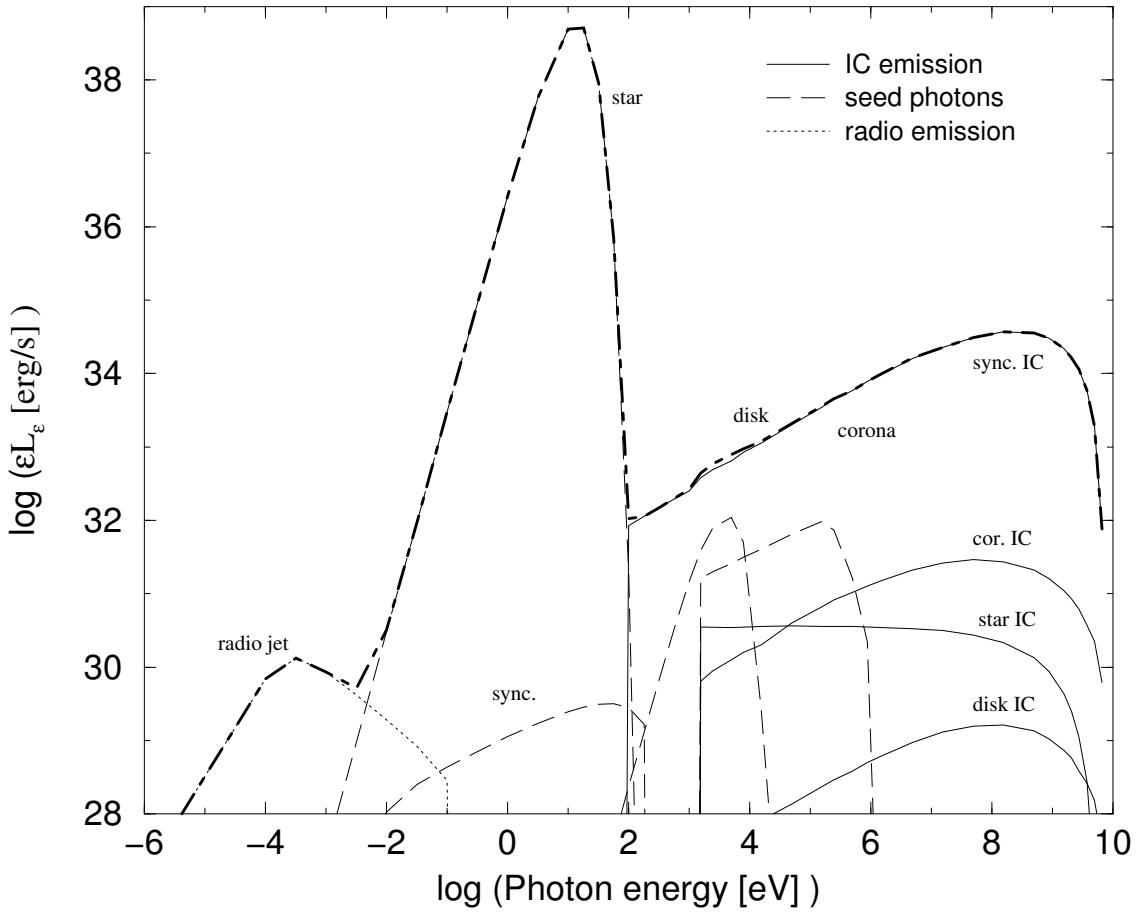

Figure 4.11: SED for a high mass microquasar that, if suffering absorption in the optical and ultraviolet bands in the galactic plane, could appear as an unidentified γ-ray source, since this energy band would be the most prominent.

are perhaps the most attractive candidates, because of the presence of relativistic jets in these objects, as well as the external photon fields provided by the companion star and the accreting matter. The presence of a massive star could not imply an easy identification due to the strong absorption present towards the galactic plane. It seems clear that the microquasar phenomenon can be naturally extended up to the highest energies, being the dominant energy range for jet emission, and that we can expect these objects to manifest themselves as a distinctive group of γ-ray sources that might be detectable with satellite-borne instruments like those to be carried by AGILE, GLAST, and even by ground-based Cherenkov telescopes like HESS and MAGIC, as it has been the case for LS 5039 (Aharonian et al. 2005).

4.2.2 Application to three unidentified γ-ray sources

We apply the model presented in this section to three low-latitude unidentified γ-ray sources, two of them detected by EGRET, 3EG J1735−1500 and 3EG J1828+0142 (Hartman et al. 1999), and another one by COMPTEL, GRO J1411−64 (Zhang et al. 2002). These three sources were chosen due to its high variability (Torres et al. 2001, Zhang et al. 2002; concerning 3EG J1735−1500, in Nolan et al. 2003 it still appears as a variable source but with a minor assigned variability degree). Our goal is to explore whether, taking into account γ-ray data and constraints on the fluxes at lower energies, imposed by the radio and X-ray sources observed in the γ-ray error boxes, a microquasar model can be applied to these three sources.

Results

We reproduce the SED of the three unidentified γ-ray sources without violating the observational constraints, which are imposed by the fluxes of the detected sources at radio and X-ray energies in the fields of the γ-ray error boxes. Because of the X-ray constraints, and because the reduction of disk scattered radiation due to interaction geometrical effects (Dermer et al. 1992), we have neglected the disk and the disk IC contribution, keeping only the corona one, which is dominant over the disk in the context of this jet model for microquasars in the low-hard state. In Table 4.7, we show the adopted values of the parameters of the model. At the top of the table, the common parameter values are given and, at the bottom, those specific to each source are also provided (descriptions are not shown here, being the same

Table 4.7: Common and specific values for the parameters

symbol	Parameter	values
$M_{\rm x}$	Black hole mass	3 $M_\odot$
$R_{\rm Sch}$	Schwarzschild radius	10^6 cm
$L_{\rm star}$	Stellar bolometric luminosity	10^{38} erg s^{-1}
$kT_{\rm star}$	Peak energy of the star	10 eV
z_0	Distance from the apex of the jet to the compact object	50 $R_{\rm Sch}$
R_0	Initial jet radius	5 $R_{\rm Sch}$
$\gamma_{\rm min}$	Minimum Lorentz factor for electrons in the jet (jet frame)	~ 1
$\Gamma_{\rm cor}$	Photon index for the corona	1.6
$E_{\rm cor\ max}$	Peak energy of the corona	150 keV
$R_{\rm orb}$	Orbital radius	3×10^{12} cm
θ	Viewing angle to the axis of the jet	45°
$\Gamma_{\rm jet}$	Jet Lorentz factor	1.2

	3EG J1735−1500	3EG J1828+0142	GRO J1411−64
$L_{\rm k}$ [erg s^{-1}]	5×10^{34}	10^{35}	3×10^{35}
$\gamma_{\rm max}(z_0)$	$3{\times}10^3$	$4{\times}10^3$	$5{\times}10^2$
$B(z_0)$ [G]	10000	5000	8000
p	2	2	1.5
$L_{\rm disk/cor}$ [erg s^{-1}]	$3{\times}10^{34}$	3×10^{33}	3×10^{33}

as in Table 4.6). Those parameters that cannot be constrained by observations are set up to fiducial standards for microquasars (similar to those presented also in Table 4.6) or fixed to reproduce observations/avoid constraint violations. Because of our previous consideration concerning the possible location of a population of γ-ray emitting microquasars, the inner spiral arms, we have fixed a distance to the γ-ray emitters of 4 kpc. The SEDs for the three γ-ray sources are presented in Figs. 4.12, 4.13 and 4.14, and the mean and maximum γ-ray luminosities are shown there. As in the case studied above and plotted in Fig. 4.11, here radio emission is computed changing ε from 1 to 0.1. Next, we provide a description of the γ-ray emitters altogether with considerations about the possible lower energy counterparts within the γ-ray error boxes.

3EG J1735−1500

3EG J1735−1500 was considered in the work of Torres et al. (2001) as the most variable EGRET source, and in Nolan et al. (2003) it was also among the group of likely variable EGRET sources (probability $\sim 60\%$). The EGRET spectrum shows a photon index $\Gamma \sim 3.2 \pm 0.5$ and an average flux $\sim 3 \times 10^{-11}$ erg s^{-1} cm^{-2}. The error box of 3EG J1735−1500 was explored by Combi et al. (2003), who proposed two potential counterparts: a radio galaxy (J1737−15) and a compact radio source (PMN J1738−1502, a blazar candidate), that presents a flat radio spectrum and flux densities of about 0.3 Jy. However, since at the present stage it is still hard to explain both whether a radio galaxy can present the variability of 3EG J1735−1500 and the absence of X-ray counterpart for the compact radio source, we have not considered them as definitive solutions of the identification problem. To model the SED of a microquasar that could be the origin of the EGRET emission, we take into account the known observational data and constraints at different wavelengths. At the adopted distance, the typical luminosities of the radio sources in the EGRET error box would be of about $2{\times}10^{30}$ erg s^{-1}, the X-ray luminosities would be $\sim 10^{34}$ erg s^{-1}, and at COMPTEL energies the upper limits would be $\sim 10^{36}$ erg s^{-1} (Zhang et al. 2004). The used parameter values are presented in Table 4.7. The computed SED for both the average and the maximum luminosity levels of the γ-ray source are shown in Fig 4.12. It appears that 3EG J1735−1500, even if detectable at X-rays during its maximum luminosity level, would be faint at radio wavelengths. At optical wavelengths, we have computed the visual extinction of 1.4 magnitudes from the relationship by Predehl & Schmitt (1995) and tha Galactic hydrogen column density Dickey & Lockman (1990). It seems from Fig. 4.12 that additional intrinsic absorption would be necessary to obscure the source in the optical band to prevent an easy identification, since it still has an absolute brightness of 13.4 magnitudes. To reproduce the observed γ-ray variability through the jet precession, with the adopted mildly relativistic velocity of the jet, the variation in the angle should be large and reaching almost 0°. However, an orbital eccentricity of 0.5 or less could be enough to change the relativistic leptonic jet power, producing the observed ratio of maximum to average luminosity (see, e.g., Bosch-Ramon et al. 2005a).

3EG J1828+0142

3EG J1828+0142 is the second most variable low galactic latitude non-transient γ-ray source in the list of variable EGRET sources of Torres et al. (2001), considered

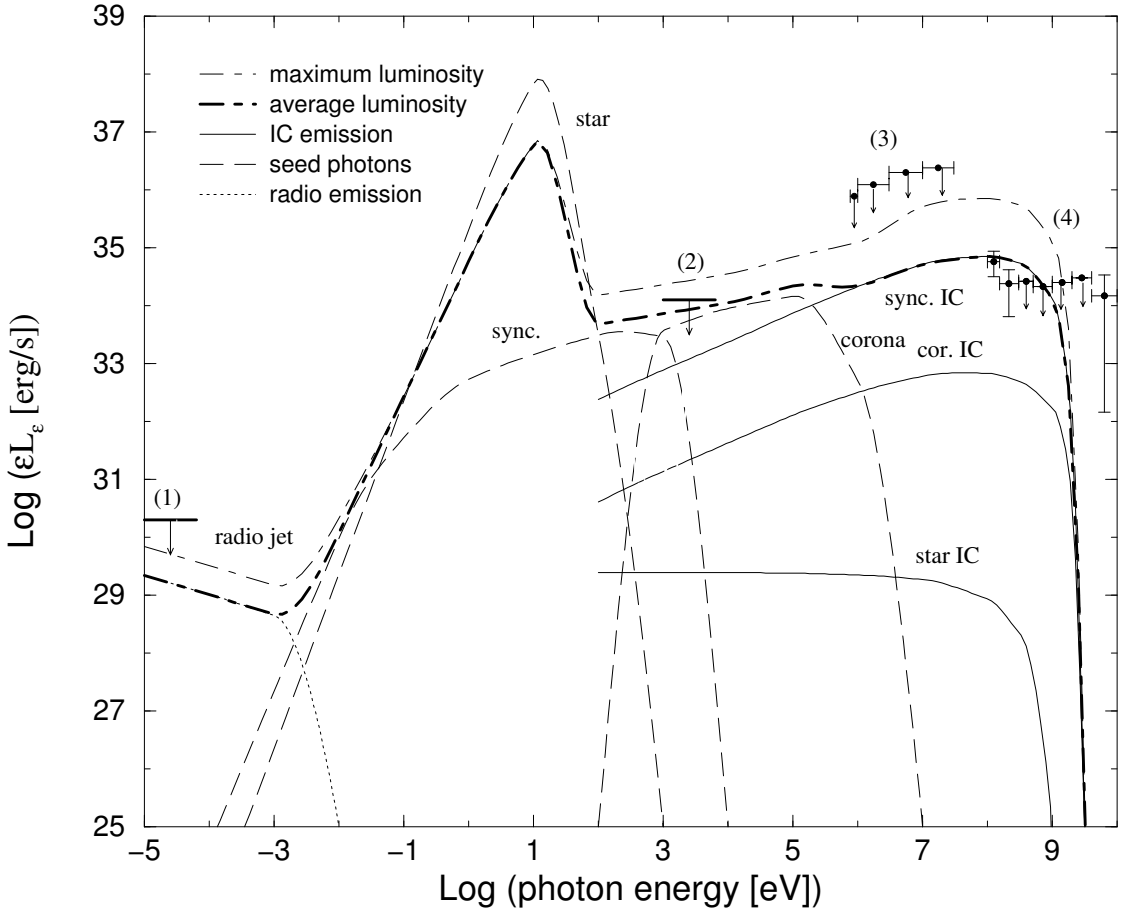

Figure 4.12: SED for a broadband microquasar model of the source 3EG J1735−1500. The SED of the average as well as the maximum luminosity level of the source are shown. The adopted values for the different parameters are shown in Table 4.7. Upper limits at radio (1), X-ray (2) and COMPTEL (3) energies, as well as the average EGRET spectrum (4), are presented. To compute the total emission, the star component has been reduced a certain factor, in accordance to the maximum visual extinction found in the direction of the EGRET source. For the UV, we have followed roughly the relationship between different wavelengths provided by Valencic et al. (2004).

also very variable by Nolan et al. (2003). The EGRET photon index is $\Gamma \sim 2.7 \pm 0.4$, with an average flux $\sim 4 \times 10^{-11}$ erg s^{-1} cm^{-2}. Within the error box of this EGRET source, there are several faint non-thermal radio sources with luminosities around 5×10^{30} erg s^{-1} (Punsly et al. 2000), and X-ray sources (observed by the ROSAT All Sky Survey) with typical luminosities of about 10^{33} erg s^{-1}. COMPTEL upper limits are also known (Zhang et al. 2004), corresponding to luminosities of about 10^{36} erg s^{-1}; the assumed distance still being the same. A supernova remnant (SNR), located at $\sim$1 kpc, has been proposed by Punsly et al. (2000) to be associated with the object emitting at γ-rays. This SNR, yet not part of the Green's Catalog, was not a member of the sample in the systematic study of molecular material by Torres et al. (2003), although the source variability argues against a physical association with the SNR shock. Association with the SNR would imply a lower energy requirement to explain the observed EGRET flux, although with such a distance the source would not be associated with the Carina arm, as most of the EGRET sources in the galactic plane seem to be (Bhattacharya et al. 2003). Also, there is a strong flat spectrum radio source within the error box of 3EG J1828+0142 which has been proposed to be a blazar (Halpern et al. 2003; Sowards-Emmerd et al. 2003 assigned to the blazar J1826+0149 an association probability of 60–80%). Further observational data is needed for a firm association of the source with any particular counterpart. The values used for the different parameters are presented in Table 4.7 and the computed SED for both the average and the maximum luminosity level of the γ-ray source are shown in Fig 4.13. It appears that the X-ray emission of 3EG J1828+0142 could be at the level of the detected source fluxes, and it might be one of the radio sources in the EGRET error box during its most active state. For an absorption of 2.6 magnitudes in the optical band as done in the previous case, the optical counterpart would be of a magnitude of about 15, which makes this source largely irrelevant from the optical point of view among other sources in 1°-field. This will be more so in the ultraviolet, preventing a clear identification. Regarding the variability, the same remarks made for the previous source are applicable to this case, although the ratio of the maximum to average luminosity is slightly smaller and lower eccentricity and/or precession could explain this finding.

GRO J1411−64

The detection by COMPTEL of a variable unidentified γ-ray source in the galactic plane, GRO J1411−64, was reported by Zhang et al. (2002). This source has a photon index $\Gamma \sim 2.5 \pm 0.2$ and a flux of about 5×10^{-10} erg s^{-1} cm^{-2} at 10 MeV.

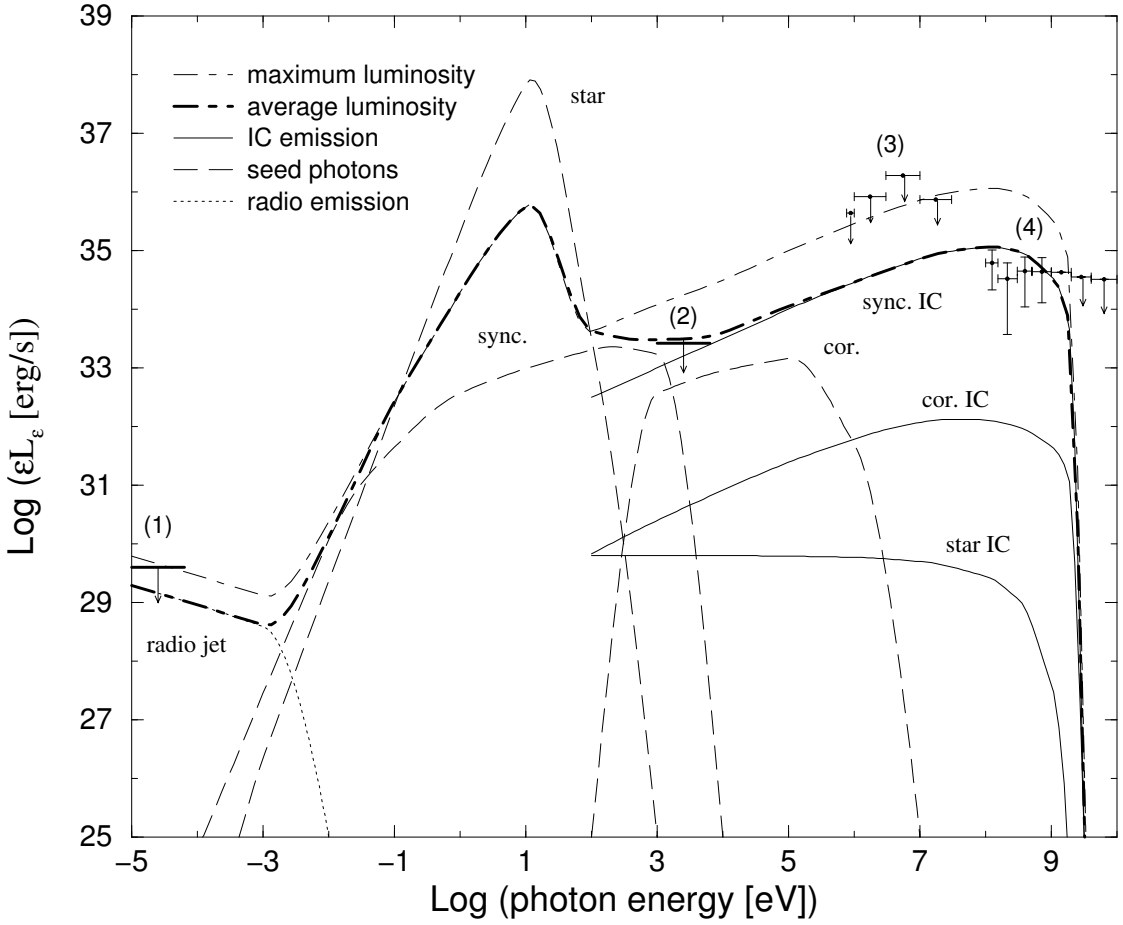

Figure 4.13: Same as in Fig. 4.12 but for 3EG J1828+0142.

The error box of COMPTEL is large, with a radius of about 2 degrees. Several models have been proposed by Zhang et al. (2002) to explain the γ-ray emission from this source as a Be/XRB (Romero et al. 2001), a weak galactic microblazar (Kaufman Bernadó et al. 2002) or an isolated black hole (Punsly et al. 2000). Inside the COMPTEL error box, there are only two identified X-ray sources: 2S 1417−624, a transient Be/XRB pulsar (see Orellana & Romero 2005), and GS 1354−645, a transient black-hole low-mass XRB. The remaining detected X-ray sources have no counterparts at other wavelengths. These two XRBs lie just inside the 4σ region, and a physical association does not seem likely if the center of gravity of the source location is correct. The Circinus Galaxy is inside the error box though, if there are not ultraluminous γ-ray objects in this galaxy, this type of source is unlikely to be the counterpart of GRO J1411−64. In the radio band, the typical flux of the sources found by the PMN survey (Parkes-MIT-NRAO) is taken as the upper limit at these wavelengths: a few 10 mJy, or about 10^{30} erg s^{-1}. For the constraints on the X-ray flux we will take a luminosity similar to most of the sources detected by ROSAT, i.e. about 10^{34} erg s^{-1}. The distance was assumed to be 4 kpc. At high-energy γ-rays, we will consider the sensitivity limit of EGRET in the region of GRO J1411−64 as the upper limit. For this case, the average flux and the maximum flux observed by COMPTEL are very similar (Zhang et al. 2002). The values used to compute the SED for the different parameters are presented in Table 4.7 and the SED is shown in Fig 4.14. As can be seen, the counterpart might be one of the X-ray sources detected in the COMPTEL error box but its radio emission is too faint for detection. The visual extinction within the COMPTEL error box can reach 7 magnitudes. This could imply that an additional intrinsic absorption is not required to preclude the detection of the optical and ultraviolet counterpart.

Discussion

Our general conclusions are that, to reproduce the observed soft spectra at γ-rays, a leptonic radiative process and a low maximum energy for the particles seem to be required. Generally, if the mechanism of emission were hadronic, the spectra would be harder. Moreover, the electron maximum energies for the two microquasars likely to be γ-ray sources, LS 5039 and LS I +61 303 (Bosch-Ramon & Paredes 2004a,b, Aharonian et al. 2005) seem to be significantly higher than for the sources treated here, likely pointing to a more efficient acceleration mechanism. In addition, if the sources were microquasars, the dominant emitting process at high energies

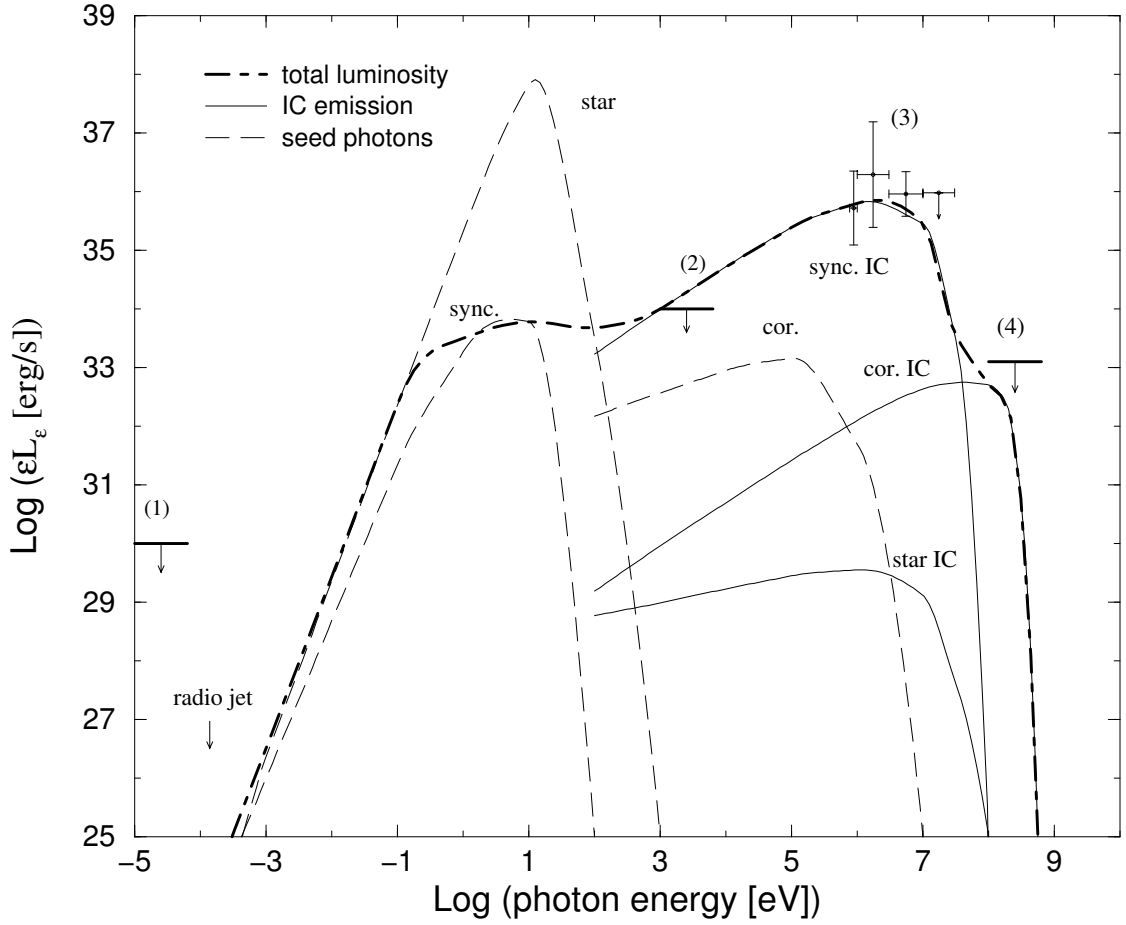

Figure 4.14: SED for a broadband microquasar model of GRO J1411−64. The total COMPTEL spectrum (3), the same for the average and the maximum level of emission, as well as the upper limits at radio (1), X-ray (2) and EGRET energies (4). The adopted values for the different parameters are shown in Table 4.7. The total emission has been reduced in the optical and ultraviolet bands according to the visual extinction in the COMPTEL source direction.

likely would be SSC. The dominance of SSC scattering implies that the magnetic field is strong enough to obtain γ-ray fluxes in agreement with observations and preventing to increase the leptonic jet power to untenable values. This would be the case if the magnetic field were too low and/or the corona scattered photons the dominant ones. Within the context of the model, the values for the magnetic field, the jet power and the maximum electron energy distribution can be restricted roughly to 10000 G, 10^{35} erg s^{-1} and 1 GeV respectively. Concretely, the COMPTEL source would present slightly higher relativistic leptonic power and lower maximum electron energy than the two EGRET sources. Otherwise the observed spectrum at γ-rays could not be reproduced taking into account the observational constraints and the previous theoretical considerations. It is worth noting that these values are coarse estimates of the source properties under a microquasar assumption, not being possible to achieve a better precision because of the lack of knowledge of the counterpart fluxes at low energies. Concerning losses, a $B = 10^4$ G implies dominant SSC losses in the very base of the jet, being overcome by adiabatic ones at slightly larger z due to the strong synchrotron energy density decrease. Below 100 keV, the spectra must be hard enough to agree with observations. This means that, while for 3EG J1735−1500 and 3EG J1828+0142 an electron power-law index of 2 is hard enough, an index of 1.5 is required for GRO J1411−64 to keep the X-ray fluxes to those presented by the sources in the γ-ray error box. This could be related to a more relativistic shock acceleration in the particle injection of GRO J1411−64, and the lower maximum energy could be associated with stronger losses. We also note that the magnetic field values are 100 times smaller than those of equipartition with relativistic electrons[3], which is about 10^6 G for a leptonic jet power of 10^{35} erg s^{-1}. Finally, as noted above, due to the stringent constraints in X-rays, the corona should be faint, which is in agreement with the moderate X-ray emission as well as the lack of clear disk and corona features (like a hard X-ray cutoff due to Comptonization) in the X-ray data of the two likely EGRET microquasars LS 5039 (Bosch-Ramon et al. 2005a) and LS I +61 303 (Leahy et al. 1997).

The radio jets associated with 3EG J1735−1500 and 3EG J1828+0142 could only be detected if the electron energy losses are very low and/or there is re-acceleration, perhaps due to shocks with the interstellar medium at large scales or to internal shocks caused by different flow velocities (Marscher & Gear 1985). In such a case,

[3]Usually, it is considered to be around equipartition in the inner disk regions. However, this magnetic field is not known at the base of the jet (at $\sim 10^8$ cm from the compact object). Here it has been treated as a free parameter.

in the context of our model, there would be emission at low frequencies (below 1 GHz) up to large distances (about 1 pc). To detect it would require an instrument with low angular resolution (about 1 arcmin) and high sensitivity (about 0.1 mJy). For GRO J1411−64, it seems that radio emission would not be detectable due to the low maximum electron energies and the strong losses in the inner jet. Therefore, these microquasars, in contrast to what is usually expected, would not present clear radio jets. Instead, they would present at most diffuse and faint radio lobes.

The two mechanisms of variability that we have studied are leptonic jet power changes, associated with accretion rate changes (e.g. for LS 5039, see Bosch-Ramon et al. 2005a), and precession (e.g. for LS I +61 303, see Massi et al. 2004; for a general case, see Kaufman Bernadó et al. 2002). We note that the plotted maximum luminosity SEDs for 3EG J1735−1500 and 3EG J1828+0142 below γ-rays correspond to those produced by the variation in the leptonic jet power. However, precession cannot be discounted. 3EG J1735−1500 and 3EG J1828+0142 present average luminosities at γ-rays that are close to those of their minima (Hartman et al. 1999), which could mean that the peaks are short duration events (e.g. periastron passage of an eccentric orbit or a minimum θ during the precession of the jet) on the timescales of the EGRET viewing periods (of about two weeks). Instead, GRO J1411−64 shows a long duration burst (Zhang et al. 2002), that could be more associated with a high accretion rate phase than to a persistent jet affected by regular changes of its characteristics. The fact that this source appears to be the brightest, assuming the same distance as for the rest, would give weight to this option.

In the radio band, a low resolution and high sensitivity instrument would be required to detect 3EG J1735−1500 and 3EG J1828+0142, expecting a very soft spectrum, whereas GRO J1411−64 would not be detectable. If this source is strongly absorbed in the optical and the UV band, it could be still detectable in the infrared band, with higher emission at longer than at shorter wavelengths. However, to test such statement, the location accuracy of the sources should be improved, due to the large number of infrared sources within the γ-ray error boxes. At X-rays, 3EG J1828+0142 could be detected with reasonable exposure times (e.g. with XMM), whereas 3EG J1735−1500 and GRO J1411−64 would be easily detected due to their higher emission levels at this energy band. For the three sources, the X-ray spectra would present photon indices of 1.5 or less. We note that XMM and INTEGRAL observations of GRO J1411−64 are underway, and we will report on them

elsewhere. Observations with the next generation γ-ray instruments are fundamental to properly associate the γ-ray sources with their counterparts at lower energies. In the COMPTEL energy range, 3EG J1735−1500 and 3EG J1828+0142 might be detected, at the adopted distance of 4 kpc, with an instrument 1–2 orders of magnitude more sensitive than COMPTEL. In the EGRET energy range, GRO J1411−64 might be detected by GLAST with reasonable exposure times, if observed during an activity period similar to that presented during COMPTEL observations. Because of the very steep cut-offs at energies beyond 1 GeV for 3EG J1735−1500 and 3EG J1828+0142, and beyond 100 MeV for GRO J1411−64, these sources would not be detected by the new Cherenkov telescopes, although it does not prevent the detection of other microquasars with higher maximum electron energies and/or more beaming. Finally, there are different observational features depending on the dominant variability mechanism. A precessing jet would likely show a periodic variation of both the photon index and the maximum detectable energy at γ-rays. Moreover, the corona would not suffer variations, whereas γ-rays (SSC) and radio (synchrotron) emission would vary in the same manner (Dermer 1995). If accretion is the origin of variability, SSC emission mechanism will imply a different response to accretion changes than that presented at X-rays when dominated by the corona. In both cases, however, if our microquasar hypothesis is true, 3EG J1735−1500 and 3EG J1828+0142 variability should be periodic.

Bibliography

Aharonian F.A., Akhperjanian A.G., Aye K.M., et al., Jul. 2005, Science, 309, 746 63, 87, 91, 97

Atoyan A.M., Aharonian F.A., Jan. 1999, MNRAS, 302, 253 59

Benaglia P., Romero G.E., Mar. 2003, A&A, 399, 1121 88

Bhattacharya D., Akyüz A., Miyagi T., Samimi J., Zych A., Jun. 2003, A&A, 404, 163 84, 85, 95

Bondi H., 1952, MNRAS, 112, 195 75

Bosch-Ramon V., Paredes J.M., Apr. 2004a, A&A, 417, 1075 59, 87, 97

Bosch-Ramon V., Paredes J.M., Oct. 2004b, A&A, 425, 1069 59, 87, 97

Bosch-Ramon V., Paredes J.M., Ribó M., et al., Jul. 2005a, ApJ, 628, 388 63, 81, 87, 93, 99, 100

Bosch-Ramon V., Romero G.E., Paredes J.M., Jan. 2005b, A&A, 429, 267 60

Bosch-Ramon V., Paredes J.M., Romero G.E., Torres D.F., Feb. 2006, A&A, 446, 1081 60

Casares J., Ribas I., Paredes J.M., Martí J., Allende Prieto C., Jul. 2005a, MNRAS, 360, 1105 71, 72

Casares J., Ribó M., Ribas I., et al., Dec. 2005b, MNRAS, 364, 899 63

Combi J.A., Romero G.E., Paredes J.M., Torres D.F., Ribó M., May 2003, ApJ, 588, 731 93

Dermer C.D., Jun. 1995, ApJ Letter, 446, L63 101

Dermer C.D., Schlickeiser R., Aug. 2002, ApJ, 575, 667 62, 83

Dermer C.D., Schlickeiser R., Mastichiadis A., Mar. 1992, A&A, 256, L27 83, 91

Dickey J.M., Lockman F.J., 1990, ARA&A, 28, 215 93

Frail D.A., Hjellming R.M., Jun. 1991, AJ, 101, 2126 71

Georganopoulos M., Aharonian F.A., Kirk J.G., Jun. 2002, A&A, 388, L25 59

Ghisellini G., Maraschi L., Treves A., May 1985, A&A, 146, 204 83

Gregory P.C., Aug. 2002, ApJ, 575, 427 71

Gregory P.C., Taylor A.R., Apr. 1978, Nature, 272, 704 59, 71

Gregory P.C., Peracaula M., Taylor A.R., Jul. 1999, ApJ, 520, 376 79

Grimm H.J., Gilfanov M., Sunyaev R., Sep. 2002, A&A, 391, 923 84

Hall T.A., Bond I.H., Bradbury S.M., et al., Feb. 2003, ApJ, 583, 853 72, 79

Halpern J.P., Eracleous M., Mattox J.R., Feb. 2003, AJ, 125, 572 95

Hartman R.C., Bertsch D.L., Bloom S.D., et al., Jul. 1999, ApJSS, 123, 79 64, 65, 72, 91, 100

Hermsen W., Swanenburg B.N., Bignami G.F., et al., Oct. 1977, Nature, 269, 494 71

Kaufman Bernadó M.M., Romero G.E., Mirabel I.F., Apr. 2002, A&A, 385, L10 59, 64, 80, 84, 97, 100

Kniffen D.A., Alberts W.C.K., Bertsch D.L., et al., Sep. 1997, ApJ, 486, 126 59, 71, 72, 87

Leahy D.A., Harrison F.A., Yoshida A., Feb. 1997, ApJ, 475, 823 81, 87, 99

Markoff S., Falcke H., Fender R., Jun. 2001, A&A, 372, L25 59

Marscher A.P., Gear W.K., Nov. 1985, ApJ, 298, 114 99

Martí J., Paredes J.M., Jun. 1995, A&A, 298, 151 79, 80

Martí J., Paredes J.M., Ribó M., Oct. 1998, A&A, 338, L71 63, 64, 87

Martocchia A., Motch C., Negueruela I., Jan. 2005, A&A, 430, 245 87

Massi M., Jul. 2004, A&A, 422, 267 72, 80

Massi M., Ribó M., Paredes J.M., Peracaula M., Estalella R., Sep. 2001, A&A, 376, 217 59, 71, 87

Massi M., Ribó M., Paredes J.M., et al., Jan. 2004, A&A, 414, L1 59, 71, 80, 87, 100

Mirabel I.F., Dhawan V., Chaty S., et al., Feb. 1998, A&A, 330, L9 59

Mirabel I.F., Rodrigues I., Liu Q.Z., Jul. 2004, A&A, 422, L29 87

Motch C., Haberl F., Dennerl K., Pakull M., Janot-Pacheco E., Jul. 1997, A&A, 323, 853 63

Nolan P.L., Tompkins W.F., Grenier I.A., Michelson P.F., Nov. 2003, ApJ, 597, 615 84, 85, 91, 93, 95

Orellana M., Romero G.E., Jun. 2005, Ap&SS, 297, 167 97

Paredes J.M., Figueras F., Jan. 1986, A&A, 154, L30 71

Paredes J.M., Marti J., Peracaula M., Ribó M., Apr. 1997, A&A, 320, L25 87

Paredes J.M., Martí J., Ribó M., Massi M., Jun. 2000, Science, 288, 2340 59, 63, 84, 87

Paredes J.M., Ribó M., Ros E., Martí J., Massi M., Oct. 2002, A&A, 393, L99 65, 87

Peracaula M., Jul. 1997, Ph.D. Thesis, Universitat de Barcelona 72

Predehl P., Schmitt J.H.M.M., Jan. 1995, A&A, 293, 889 93

Punsly B., Romero G.E., Torres D.F., Combi J.A., Dec. 2000, A&A, 364, 552 88, 95, 97

Ray P.S., Foster R.S., Waltman E.B., Tavani M., Ghigo F.D., Dec. 1997, ApJ, 491, 381 72, 87

Reimer O., 2001, In: ASSL Vol. 267: The Nature of Unidentified Galactic High-Energy Gamma-Ray Sources, 17–34 85

Ribó M., Nov. 2002, Ph.D. Thesis, Univesitat de Barcelona 63

Ribó M., Paredes J.M., Romero G.E., et al., Mar. 2002, A&A, 384, 954 63, 87

Roberts M.S.E., Gaensler B.M., Romani R.W., 2002, In: ASP Conf. Ser. 271: Neutron Stars in Supernova Remnants, 213 88

Romero G.E., Benaglia P., Torres D.F., Aug. 1999, A&A, 348, 868 85

Romero G.E., Kaufman Bernadó M.M., Combi J.A., Torres D.F., Sep. 2001, A&A, 376, 599 88, 97

Romero G.E., Grenier I.A., Kaufman Bernado M.M., Mirabel I.F., Torres D.F., Oct. 2004, In: ESA SP-552: 5th INTEGRAL Workshop on the INTEGRAL Universe, 703 84

Romero G.E., Christiansen H.R., Orellana M., Oct. 2005, ApJ, 632, 1093 72

Sowards-Emmerd D., Romani R.W., Michelson P.F., Jun. 2003, ApJ, 590, 109 95

Strickman M.S., Tavani M., Coe M.J., et al., Apr. 1998, ApJ, 497, 419 79

Tavani M., Kniffen D., Mattox J.R., Paredes J.M., Foster R., Apr. 1998, ApJ Letter, 497, L89 72, 80

Taylor A.R., Gregory P.C., Apr. 1982, ApJ, 255, 210 71

Taylor A.R., Young G., Peracaula M., Kenny H.T., Gregory P.C., Jan. 1996, A&A, 305, 817 72

Torres D.F., Romero G.E., Combi J.A., et al., May 2001, A&A, 370, 468 84, 85, 91, 93

Torres D.F., Romero G.E., Dame T.M., Combi J.A., Butt Y.M., Aug. 2003, Phys. Rep., 382, 303 95

Valencic L.A., Clayton G.C., Gordon K.D., Dec. 2004, ApJ, 616, 912 94

Wallace P.M., Griffis N.J., Bertsch D.L., et al., Sep. 2000, ApJ, 540, 184 72

Zhang S., Collmar W., Schönfelder V., Dec. 2002, A&A, 396, 923 91, 95, 97, 100

Zhang S., Collmar W., Hermsen W., Schönfelder V., Jul. 2004, A&A, 421, 983 93, 95

Chapter 5

Spectral and variability properties of emission from microquasars

In Chapter 4 we have shown that, from the point of view of theory, γ-ray emission from microquasars can be easily explained as IC interaction between relativistic jet electrons and ambient photon fields, from the star, the accreted matter, and/or the synchrotron emission itself. These relativistic electrons would be the same as those radiating in the radio band by synchrotron process. In Chapter 2, we have discussed about different possibilities concerning the origin of γ-rays in microquasars, among them hadronic mechanisms. Although IC scattering appears quite effective if enough power is injected in relativistic leptons, relativistic hadrons could be also present, producing a perhaps non negligible amount of γ-rays (see, e.g., Romero et al. 2003, 2005, and Chapter 6). Nevertheless, in this chapter we focus in the case when leptons are radiatively dominant. We are not going to argue about which mechanism could be the most likely. On the one hand, the acceleration efficiency for both types of particles, hadrons and leptons, is not known in microquasar jets[1]. On the other hand, the total amount of power going to one or another type of these particles is unknown either. In what follows, however, making some assumptions that seem to be reasonable, we plan to explore deeper the leptonic case in the context of a jet containing both types of particles, studying the spectral and temporal properties of the radiation altogether with the likely underlying physical processes. What is presented in this chapter can be found in Bosch-Ramon et al. (2006a), Paredes et al.

[1]It must not follow necessarily the proton to lepton ratio of 100 (Longair 1992), as for the galactic cosmic rays.

(2006) and Bosch-Ramon et al. (2006b).

5.1 A cold matter jet model for microquasar broad-band emission

Observational and theoretical studies point to microquasars as possible counterparts of a significant fraction of the unidentified γ-ray sources detected so far. At present, a proper scenario to explain the emission beyond soft X-rays from these objects is not known, nor what the precise connection is between the radio and the high energy radiation. It is known, in some sources, that radio emission comes from a jet, since it has been resolved. In other cases, non-thermal radio emission has been detected, but no jets have been observed likely due to lack of sensitivity and/or angular resolution limitations. Nevertheless, it has been proposed that when radio emission is observed, the jet is there, and when it is quenched, the jet (almost?) disappears. As mentioned above, the low-hard state of the X-ray emission is associated with radio emission (or its higher accretion rate version, the intermediate state, see for instance Fender et al. 2004).

We develop a new model for a jet produced during microquasar low-hard state. The jet is assumed to be dynamically dominated by cold protons and radiatively dominated by relativistic leptons. Because of lack of effective external confinement, the jet follows free (conical) expansion, with a collimation related to the speed of the sound of the jet plasma and the jet bulk velocity. The matter content and the power of the jet are both related to the accretion process. The magnetic field is assumed to be close to equipartition, although it is attached to and dominated by the jet matter in the jet RF. For the relativistic particles in the jet, their maximum energy depends on both the acceleration efficiency and the energy losses. The model takes into account the interaction of the relativistic jet particles with the magnetic field and all the photon and matter fields. Such interaction produces significant amounts of radiation from radio to very high energies through synchrotron, relativistic Bremsstrahlung, and IC processes. Adiabatic losses are also taken into account. Variability of the emission produced by changes in the accretion rate (e.g. via orbital eccentricity) is also expected. The effects of the γ-ray absorption by the external photon fields on the γ-ray spectrum have been taken into account, revealing clear spectral features that might be observed. This model is consistent to

the accretion scenario, energy conservation laws, and current observational knowledge, and can provide deeper physical information of the source when tested against multiwavelength data.

5.1.1 Insights in jet physics

In Chapter 3, the general features of the model for cold matter dominated jets, altogether with the employed formulae, are provided. Next, we give a brief description of the different elements that play some role in our modeling.

Accretion

As explained in Chapter 2, accretion in microquasars can occur either through Roche lobe overflow, when the external layers of the companion reach the inner Lagrangian point, or through the stellar wind, when some fraction of it is bounded to the compact object through its gravitational potential. LMXB are fed by Roche lobe overflow and use to present circularized orbits. HMXB can be fed by both mechanisms, and in case of wind fed accretion systems the eccentricity can be high.

It is worth mentioning that winds in O type stars are fast, about 2×10^8 cm s^{-1}. It has been discussed (this Chapter, Casares et al. 2005) that the microquasar LS 5039 might require a slower/additional equatorial wind in order to explain the observed emission at γ-rays, in case it comes from a jet (for other O type stars with slow winds, see Ribó et al. 2006). The key point is that accretion rates of a few per cent of the Eddington luminosity (Esin et al. 1997), or several 10^{37} erg s^{-1}, cannot be reached with typical orbital and wind parameters of wind-fed systems. And these luminosities are required under reasonable assumptions about the γ-ray production energetics in the jet (i.e. 10% of accretion luminosity goes to power the jet, and a 10% of the jet power goes to power γ-rays). It is discussed afterward.

Jet ejection

We adopt the prescription presented in Chapter 3 to treat the accretion process. Following such reasoning line, if the total jet mass outflow carries a 10% of the

accreted matter (5% going to each jet), it implies that the Lorentz factor of the jet will range 1.04–2.5 for a launching radius ranging 1.5–50$R_{\rm Sch}$ (it is a very rough estimate for $r_{\rm l} \sim R_{\rm Sch}$ since general relativity effects should be taken into account). This shows that the jet velocity is limited to mildly relativistic values, as it seems to be the case (see Chapter 2).

A relatively high jet to accretion ratio like $\kappa = 0.1$ can be justified in another way. If the jet is dynamically dominated by cold matter but radiatively efficient, the density of the jet cannot be low, since otherwise the cold matter energy density would not be enough to confine the relativistic radiative component. Therefore, we note that, for a cold matter dominated jet with efficient emissivity, the bulk of the cold matter must be heavier than the one of the relativistic component, as well as moderately slow, since the energy budget is limited by accretion.

Magnetic field

B is taken as dominated by cold matter in the jet RF, as explained in Chapter 3. B is indeed unknown at jet scales smaller than the radio emitting ones and, even there, its determination depends on the knowledge about the source size. Nevertheless, in case it would be, say, in equipartition with the bulk kinetic energy density in the compact object RF, it would reach so large values that almost all the energy could be radiated in the base of the jet. Moreover, the geometry of the magnetic field would be a very particular one, and its energy density in the jet RF, dominant in there, would probably lead to special polarization patterns which are not found (e.g. a high degree of polarization). Instead, we assume a quite turbulent magnetic field tangled with and dominated by cold matter in the jet RF, such that the random component would dominate the ordered component. In case of a free expanding jet, when external confinement lacks, it will expand conically, and the magnetic field will decrease like $1/z$. In any case, further work is to be done to constrain the magnetic field strength in jets, and sensitive polarization measures should be performed in microquasar jets to better establish the magnetic field configuration, as well as properties of the plasma, like the ratio of cold to hot leptons.

Particle acceleration

It seems reasonable that matter can be ejected at different velocities, generating plasma instabilities like shocks of different strength all along the jet. These shocks could accelerate particles beyond the original energy distribution, which might be thermal. Since it is not possible at the moment to infer from data the values of basic physical parameters of the shocks in the plasma, we adopt the simple approach described in Chapter 3, where an acceleration mechanism of Fermi is assumed, adopting different acceleration efficiencies η.

The conditions imposed on the acceleration process, concerning the amount of energy that can go to relativistic particles, have been given also in Chapter 3 as limits in the maximum fraction of the jet kinetic energy that can be dissipated (ξ). Moreover, the pressure balance between cold and hot particles also imposes an additional constraint on the ratio of hot to cold particles ζ, (fixed to about 0.001 for protons, but for electrons it could be up to $\sim$0.1), affecting the maximum number of relativistic particles. As mentioned above, we will focus on the leptonic emission processes, and therefore the maximum number of relativistic leptons can be higher than for protons. It is worth noting, however, that in this particular scenario leptons will be radiatively dominant over protons due to the larger radiative efficiency of the former. Because of the pressure constraint on the number of relativistic particles, the fraction of dissipated jet kinetic energy can be smaller than ξ (see Eqs. 3.63 and 3.64).

Emitting particle energy distribution

The emitting particle energy distribution is assumed to be a power-law all along the jet whose normalization is mainly modified by the shock dissipation efficiency and its maximum energy depends on the shock acceleration efficiency. Actually, from now on we refer to electrons only, since protons do not suffer strong losses, are radiatively little efficient, and their normalization constant is controlled only by the cold matter pressure dominance conditions (neglecting particle escape). For the power-law index, we will adopt in general $p = 2.2$, a typical value in particle acceleration theory (Jones & Ellison 1991), since the particular conditions of the shock that would allow to know p are not quantitatively constrained (like the compression ratio of the shock, see Protheroe 1999). We have therefore adopted an expression for the particle energy

distribution very similar to that shown in Eq. (4.8). We note just that now the normalization function Q must be derived from Eq. (3.61). The minimum electron Lorentz factor is taken to be the one corresponding to the gyro-radius of the cold protons that form the shock. With typical expansion velocities of few % the speed of light, the corresponding proton temperatures are of about few hundreds of keV. For electrons of smaller energies the diffusion length is too short to allow them to suffer effective shock scattering.

The fact that the electron power-law index is kept as the injection one all along the jet can be understood as an average. Regarding how to treat the cooled component of the particle energy distribution, we assume that, since acceleration takes place everywhere in the jet, it is going to be always the injection spectrum. It would be true only in case the acceleration process reallocated cooled particles to the their (initial) injection energy. Also, η, fixed here to be the same value all along the jet, is likely changing with z, since the properties of shocks, or whatever the acceleration mechanism at work, vary with z and time (matter ejection rate and velocity, matter density, magnetic field, etc). We adopt this approach for simplicity, leaving for further and more detailed works a deeper treatment of this issue.

Emission and absorption

We model the emission processes in the context described above: particle energy distribution, particle energy powering, tangled magnetic field, conical jet, and present photon and matter fields. We can gather now the ingredients to compute the spectral energy distributions (Eq. 4.7 for IC and relativistic Bremsstrahlung and Eq. 4.12 for synchrotron). It is done using the expressions for the emissivity coefficients, the shock acceleration and energy dissipation rates provided in Chapter 3, and the electron power-law energy distribution described above.

Relativistic Bremsstrahlung emission deserves further comments. The density of the target nucleus $n_{\rm p}(\mathbf{x})$ (see Eq. 3.26) must be estimated for the stellar wind as well as the jet itself. Although it is dubious that all the stellar wind protons directed towards the jet will penetrate the it, a fraction could enter after being affected by the external jet layers, diffusing through them. For this particles, the target density and the associated Bremsstrahlung emissivity are taken as an upper limit, where in

the jet RF:

$$n_{\mathrm{p}*}(\mathbf{x}) =\sim \frac{\rho_{\mathrm{w}}(\mathbf{x})}{m_{\mathrm{p}}c^2}. \tag{5.1}$$

For the cold protons, the density will be related to the jet matter injection rate:

$$n_{\mathrm{pjet}}(\mathbf{x}) = \frac{\dot{m}_{\mathrm{jet}}}{\pi R^2 V_{\mathrm{jet}}}. \tag{5.2}$$

Since we take into account, besides the internal fields, the radiation fields of the star, the disk and the corona fields (see Chapter 4), proper RF transformations must be performed to compute the IC scattering. Moreover, we have introduced the angular dependence of the IC interaction in relation with the observer: $(1-\cos\theta'_{\mathrm{f}})^{(p+1)/2}$. θ'_{f} is the angle between the incoming photon and the observer. It is because the scattered photon is going to follow roughly the direction of the electron[2], and the interaction is less efficient when this angle goes to zero. This approach is adopted for the star (θ'_{f} depends on the orbital phase) and the disk photons ($\theta'_{\mathrm{f}} \sim \theta'$). For the corona, since it could extent up to the inner regions of the jet, where corona IC would be important, we have adopted the isotropic field approximation, as in Chapter 4.

We investigate the effects of pair creation and annihilation phenomena on the jet emission by calculating the γ-ray opacities ($\tau_{\gamma\gamma\epsilon'}$) for jet photons of different ϵ' and produced at different z'. To calculate opacities as well as the number of created and annihilated pairs, we have used the pair creation and annihilation rates given in Eqs. 3.50 and 3.51. The effects of the photon-photon absorption by the external fields in the production spectrum can be significant, as well as the emission of the secondaries. We estimate roughly the absorption and secondary emission effects on the observed spectrum, computing for the latter the IC emission of the secondaries under the star photons. Such a rough approach provides results in agreement with more detailed models (Khangulyan & Aharonian 2006). Below, examples of the photon-photon absorption are provided.

The γ-ray opacity by pair creation inside the jet, due to internal fields, can be very high at $z' \sim z'_0$, being sensitive to the jet width that is uncertain. Because of this uncertainty, the pair creation due to jet internal fields is not treated here, remaining for future work. It is worth mentioning that the slopes at very high energies could be affected by these extra particles. Concerning annihilation rates inside a cold matter dominated jet, the luminosity that could be emitted in form

[2]As noted in Chapter 3, it is valid in the Thomson regime, although it is enough at this stage.

of an annihilation line is too low to be distinguished from the continuum emission. Other models, like the one by Punsly et al. (2000), where a pure pair plasma is assumed, could produce detectable annihilation lines.

5.1.2 Application to a general case

We explore four different cases. First, a high-mass and a low-mass XRB presenting a jet with a high particle acceleration efficiency are studied in case **A** and **B**, respectively. For these two particular scenarios, the accretion disk and the corona have been taken to be faint. Here, the effect of the presence of a strong star photon field on the predicted spectra is investigated. In case **C**, the model is applied to a high-mass system considering luminous accretion disk and corona with a low particle acceleration efficiency. For these three cases the velocity is fixed to a mildly relativistic value, where the jet Lorentz factor, $\Gamma_{\rm jet}$, is 1.5. This provides restrictions to the fraction of accreted matter that is ejected, since the energy budget is limited and some part is radiated during the accretion process. Also, the different acceleration efficiency has a strong effect on the spectrum at the higher energies. In case **D**, a light jet pointing towards the observer without a speed restriction ($\Gamma_{\rm jet} = 3.8$) and with a faint disk and corona is investigated. A high particle acceleration efficiency has also been considered for this particular scenario, which shows that the jet could be a very strong emitter of X-rays and γ-rays under suitable conditions, appearing almost as an ultra luminous X-ray source (ULXs) if located at large distances. We recall that it is supposed that all these systems are in a low-hard-like state, when compact jets are thought to be present with rather stable characteristics (Gallo et al. 2003). In Table 5.1, we present the parameter values, altogether with their symbols, used in this model to produce the different SEDs presented below. At the top of Table 5.1, the common parameter values are shown and, at the bottom of Table 5.1, the parameter values for each particular model can be found. All of them have been fixed to typical values for microquasars or within their ranges (see Chapter 4, and the considerations above about this model). It is worth mentioning that the radiative efficiency of the jets for our particular parameter choice (for ϱ, ξ and η) is of about 1–10%, not far from estimates obtained by different approaches (see, e.g., Fender 2001, Yuan & Cui 2005). The effects of losses in the jet speed are shown in Fig. 5.1, since the energy powering relativistic electrons comes from the kinetic energy of the bulk. With such initial Lorentz factors, the jet kinetic luminosities (one jet) are 8.7×10^{36} erg s^{-1}, 8.7×10^{36} erg s^{-1}, 3.5×10^{36} erg s^{-1} and 4.9×10^{37} erg s^{-1}

for **A**, **B**, **C** and **D**, respectively.

Results

The different radiation components produced in the jet and the predicted SEDs have been computed for the four specific scenarios considered here. The effects of pair creation phenomena due to the external photon fields interacting with the produced γ-ray photons are taken into account, and the secondary radiation produced by the created pairs is estimated. The calculations are performed at the periastron passage, when the compact object is in opposition to the observer and the interaction angle between star photons and jet leptons implies more luminosity for the star IC component, showing the importance of such an effect. However, such an angle dependence depends on the electron energy due to the peculiarities of the IC interaction in the Klein-Nishina regime, which should be taken into account in more detailed models (e.g., Dermer & Böttcher 2006, Khangulyan & Aharonian 2006). The periastron passage is not associated in our model to the highest accretion phase, since the adopted wind speeds are not high, implying shifts in the accretion peak by wind and compact object velocity composition. The SED for the cases **A**, **B C** and **D** are represented in Figs. 5.2, 5.3, 5.4 and 5.5, respectively. We comment the main spectral features next.

At γ-rays the main component is different in each explored scenario, although the star can play a very relevant role. For the case **A**, the star Comptonized photons are dominant, reaching 10^{34} erg s^{-1} at 100 MeV, with a photon index of about 2, and 5×10^{32} erg s^{-1} at 100 GeV. At very high-energy γ-rays (VHE), due to the gamma-gamma absorption, the model predicts a soft photon index that hardens at higher energies. There could be additional spectral features related to the secondaries created in the corona, the disk and the star photon field. These features would appear as bumps at energies of a few GeV for disk pairs and a few tens of GeV for star photons (negligible in the case **A**). Even for negligible disk and corona sources, a decrease in the predicted flux beyond 50 GeV is unavoidable if we deal with a relatively close and massive binary system. In the case **B**, the dominant components are the corona IC and the SSC ones, with luminosities of about 10^{33} erg s^{-1} at 100 MeV with a photon index of 2 (beyond the synchrotron component, see Fig. 5.3), and few 10^{32} erg s^{-1} at 100 GeV. In this case, the low mass star photon field does not significantly affect the VHE spectrum, and only a small bump due to the secondaries

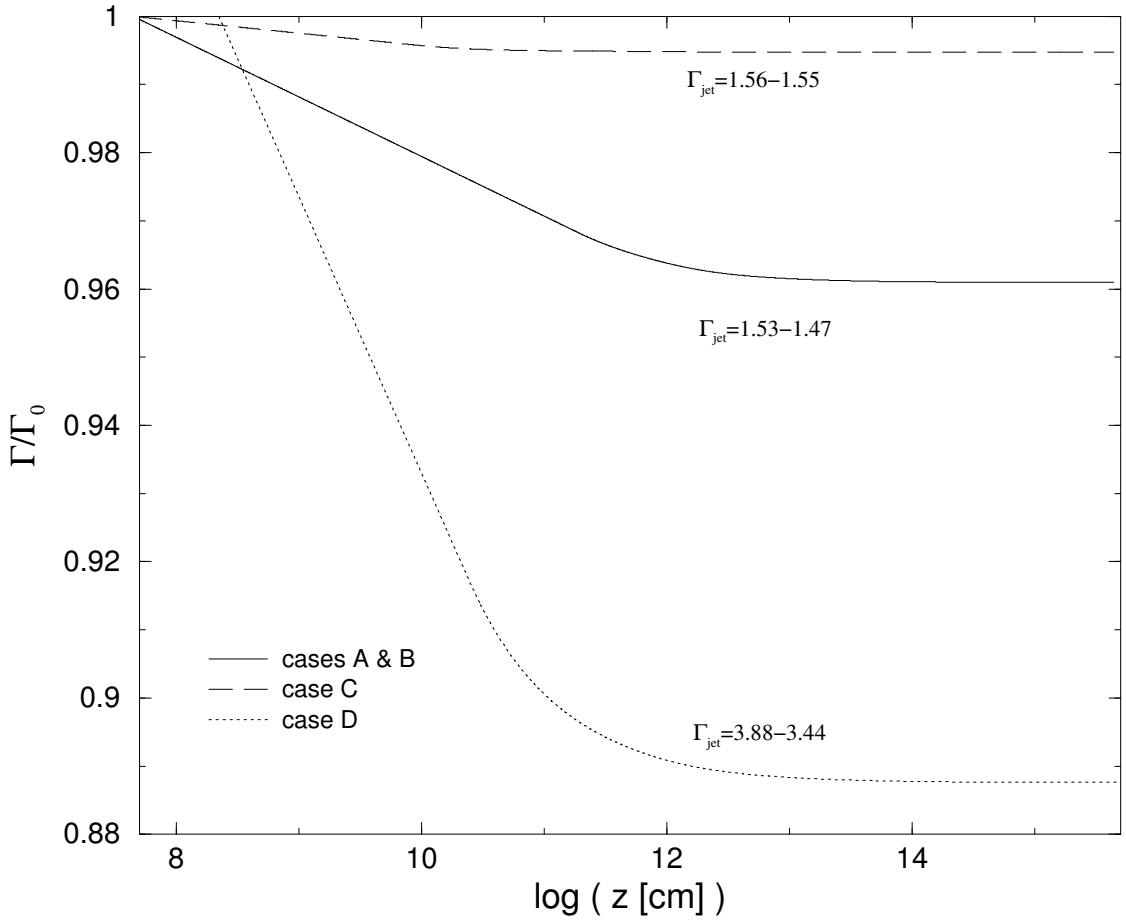

Figure 5.1: The evolution of $\Gamma_{\rm jet}$ along the jet for $\mathbf{A}$, $\mathbf{B}$, $\mathbf{C}$ and $\mathbf{D}$, normalized to its initial value. The initial and the final values of $\Gamma_{\rm jet}$ are shown for each case. The free parameter values adopted for these cases are shown in Table 5.1.

Table 5.1: Model parameters

symbol	parameter	value
e	Eccentricity	0.3
a	Orbital semi-major axis [$R_\odot$]	45
$\dot{m}_{\rm w}$	Stellar mass loss rate [$M_\odot$ yr^{-1}]	10^{-6}
$kT_{\rm disk}$	Disk inner part temperature [keV]	0.1
$p_{\rm cor}$	Corona photon index	1.6
$R_{\rm disk}$	Disk inner radius [$R_{\rm Sch}$]	50
$r_{\rm l}$	Launching radius [$R_{\rm Sch}$]	4
z_0	Jet initial point in the compact object RF [$R_{\rm Sch}$]	50
χ	Jet semi-opening angle tangent	0.1
ϱ	Equipartition parameter	0.1
ζ	Max. ratio hot to cold lepton number	0.001
$q_{\rm acc}$	Fraction of the Eddington accretion rate	0.05
p	Electron power-law index	2.2

	A	**B**	**C**	**D**
$M_{\rm x}$: Compact object mass [$M_\odot$]	3	3	3	15
$R_\star$: Stellar radius [$R_\odot$]	15	1	10	10
$M_\star$: Stellar mass [$M_\odot$]	30	1	20	20
$L_\star$: Stellar bolometric luminosity [erg s^{-1}]	10^{39}	10^{33}	10^{38}	10^{38}
$T_\star$: Stellar surface temperature [K]	4×10^4	6×10^3	3×10^4	3×10^4
κ: Jet-accretion rate parameter	0.05	0.05	0.02	0.01
ξ: Shock energy dissipation efficiency	0.25	0.25	0.05	0.5
θ: Jet viewing angle [°]	45	45	45	1
η: Acceleration efficiency	0.1	0.1	0.0001	0.1
$\alpha_{\rm disk}$: Disk radiative efficiency	0.025	0.025	0.25	0.025
$\alpha_{\rm cor}$: Corona radiative efficiency	0.005	0.005	0.05	0.005
$\Gamma_{\rm jet}$: Jet Lorentz factor	1.56	1.56	1.53	3.88

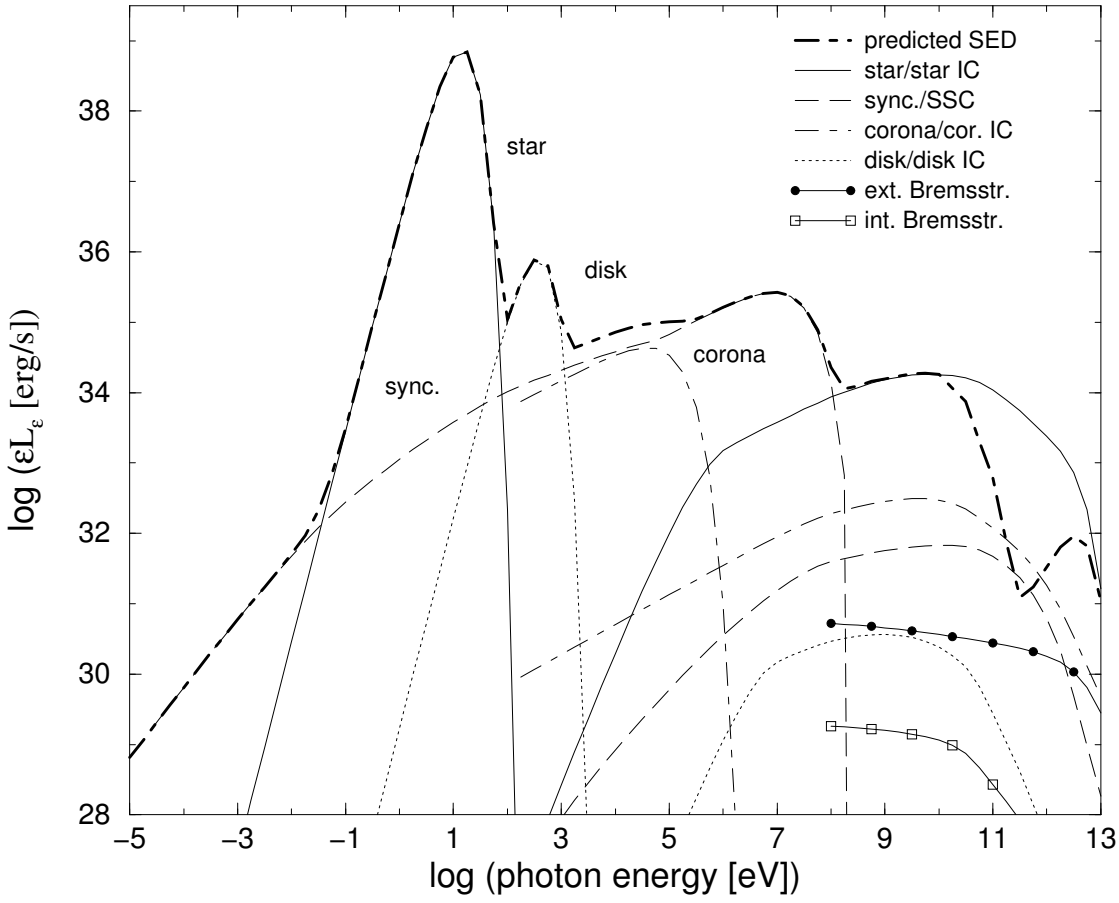

Figure 5.2: Case **A** computed SED for the entire spectrum as it would be observed. Attenuation of the jet photons due to absorption in the external photon fields is taken into account, as well as the IC emission of the first generation of pairs created within them. Isotropic luminosity is assumed. The different IC, relativistic Bremsstrahlung, synchrotron and other seed photon fields are shown. For the several components, the production SED is shown.

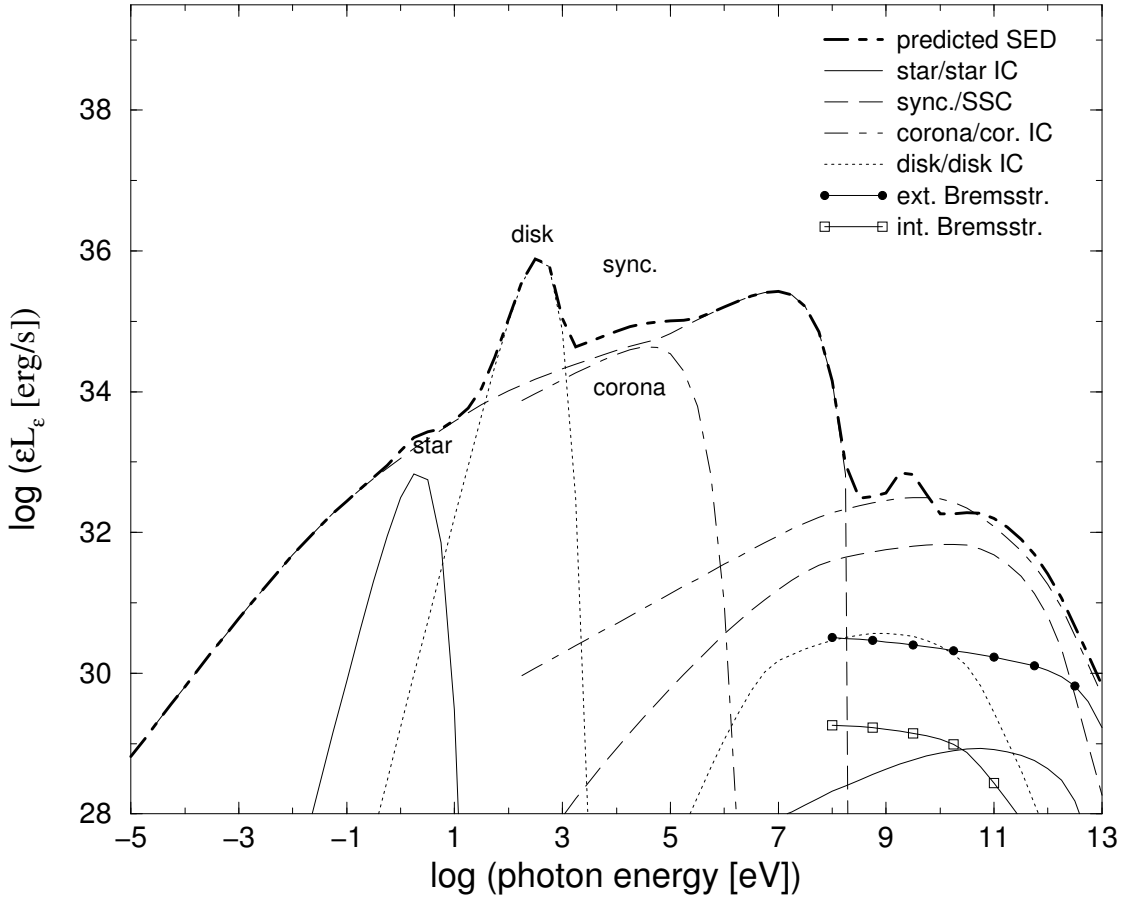

Figure 5.3: The same as in Fig. 5.2 but for the case **B**. The small bumps present from beyond 100 MeV come from the IC radiation emitted by those leptons generated by pair creation in the disk and the stellar photon field. These pair components are not made explicit in the plot for clarity.

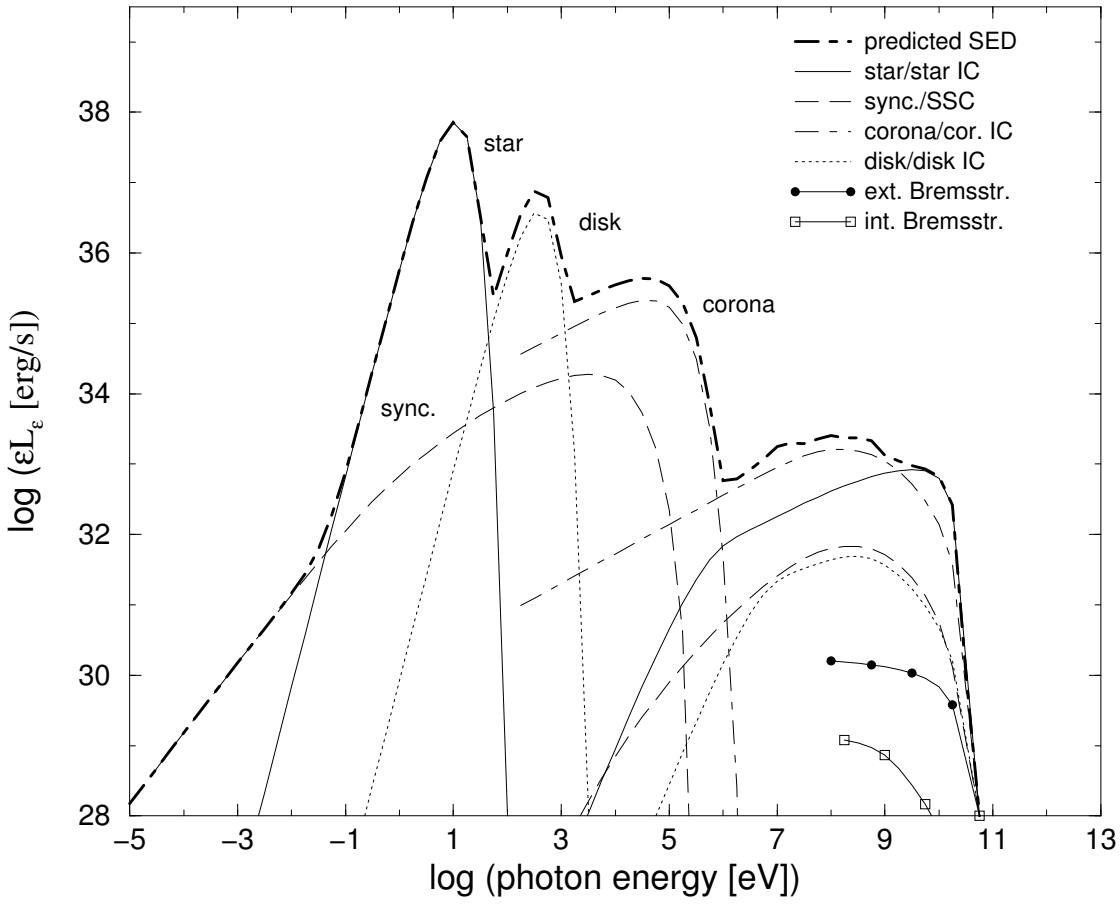

Figure 5.4: The same as in Fig. 5.2 but for the case **C** with a jet with low acceleration efficiency. For this particular situation it is possible to see the small bump at 10 MeV produced through IC scattering by the pairs created in the corona photon field.

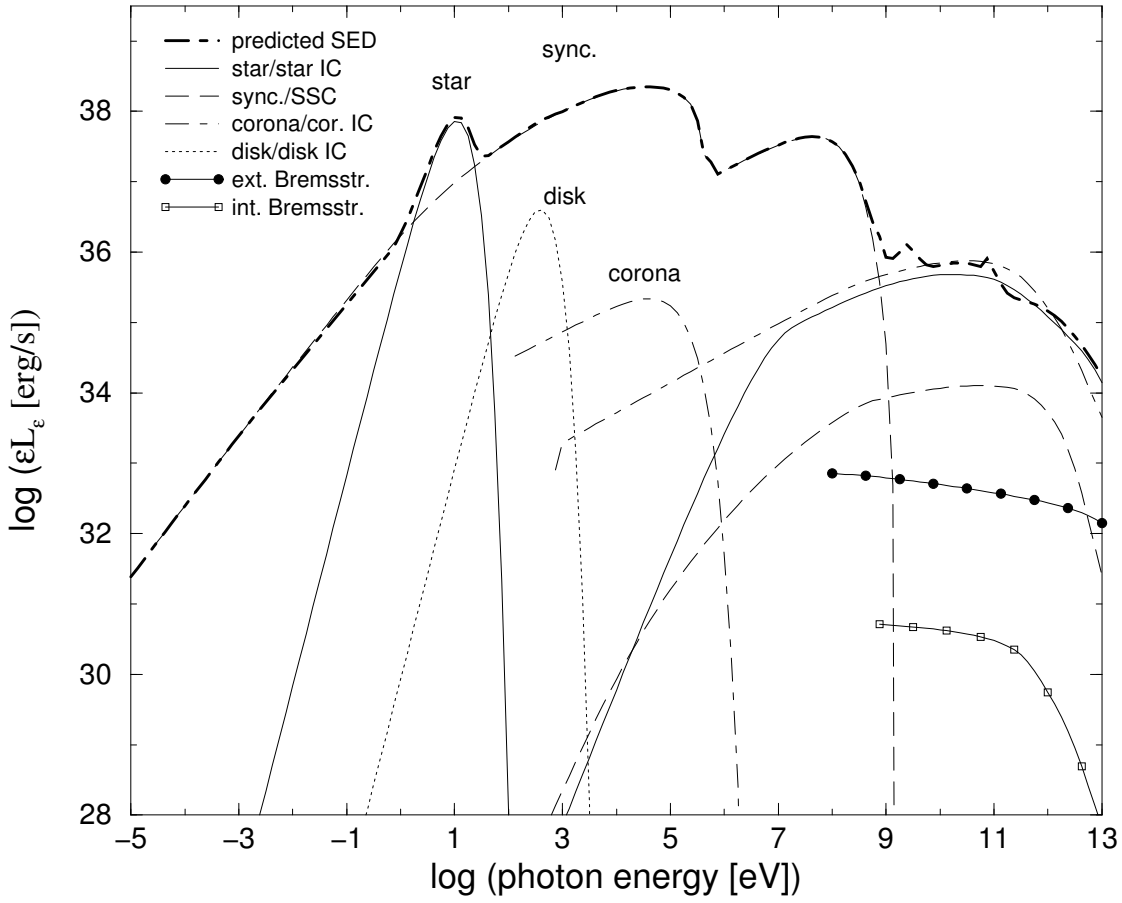

Figure 5.5: The same as in Fig. 5.2 but for the case **D**.

created within the disk photon field is visible in the SED. Therefore, the photon index beyond 10 GeV gets softer because of the Klein-Nishina effect, although it is a smoother steepening than in the case **A** that is due to absorption. Concerning the case **C**, the luminosity dominated by the corona IC emission at 100 MeV is about 10^{33} erg s^{-1} and the photon index is similar to the one predicted in the previous cases. Otherwise, only disk and corona gamma-gamma absorption effects are significant, visible in the plots at about 1 GeV and 10 MeV respectively (see Fig. 5.4). The star IC component turns to dominate beyond a few GeV. For the case **D**, the Doppler boosting affects synchrotron radiation, which reaches 100 MeV with luminosities higher than 10^{37} erg s^{-1}. However, the SSC component is not dominant at all because it is very sensitive to the jet density, and the jet is now the least dense among the four studied cases. Therefore, beyond 1 GeV the source is dominated by the corona and star IC components, with a photon index softer than 2 and some absorption produced by the star photon field. Small peaks of the IC emission of the secondaries are also present produced within the star and the disk photon fields.

At X-rays, the emission is synchrotron dominated in most cases (except in the case **C**). This is because the magnetic field is below but not far from equipartition. The matter energy density at the jet base is so high that the magnetic field reaches values around 10^5 G, allowing synchrotron radiation to dominate up to soft γ-ray energies. Similar results have been obtained by Markoff et al. (2001) for the case of shock acceleration limited mainly by synchrotron losses. In our model particle acceleration is limited by shock energy dissipation efficiency, jet size, adiabatic and all the radiative losses (including Klein-Nishina regime for IC losses). Because of the evolution of $\gamma_{\rm max}$, which rises when z is larger (for reasonable parameter values), the synchrotron spectrum changes smoothly at energies around 100 keV. Nevertheless, the disk and corona are not negligible in general, and in the case **C**, disk and corona overcome the jet radiation up to 1 MeV. The case **D** as an X-ray source is extremely bright. This result shows that a light and fast jet observed from very small viewing angles might turn out to be an ULX. Because of the low probability of being observed, it is more likely to detect them in other galaxies (for previous works on microquasars as ULXs, see, e.g., Georganopoulos et al. 2002, Körding et al. 2002).

Below the energies of the stellar photons, synchrotron radiation dominates again. If stellar emission were reprocessed by absorption and shifted to lower energies, it is likely that the far infrared would still be dominated by the enshrouded stellar

component. At radio frequencies, there is significant radio emission, with isotropic luminosities of about 10^{29} erg s^{-1} at 5 GHz (few mJy at 3 kpc). Our model predicts core-dominated emission, strongly self-absorbed due to the high efficiency of the inner jet to radiate through synchrotron process. The SED in the radio band corresponds to a spectral index equal to zero (or $\epsilon L_\epsilon \propto \epsilon^{+1}$), as it would be expected from a conical jet. The case **C** presents the weakest radio emitting jet, weaker than in cases **A** and **B**, and the case **D** is the strongest radio source due to the Doppler boosting.

Discussion

We conclude that persistent jets in microquasars in the low-hard state, despite accreting at relatively low rate, and under reasonable conditions for the jet matter, energy and magnetic field, can radiate with significant luminosities from radio to γ-rays. The model provides predictions about the shape of the SEDs and points to microquasars as VHE sources, as has been recently confirmed by Aharonian et al. (2005b) in the case of LS 5039. The importance of the synchrotron cooling channel for relativistic particles in the jet is high. This points to the fact that, for certain objects, the jet could overcome at all wavelengths any other emitting region of the microquasar, except the star itself for high mass systems. We note that for a relatively weak disk and corona (10^{34} erg s^{-1}), and even with $\varrho \sim$0.01 (one tenth of the one adopted here), the spectrum would be jet dominated and well described by a power-law at X-ray wavelengths (see below). An observational feature that could determine whether X-rays come from a jet is the dependence of the X-ray fluxes on the accretion rate, if the latter can be estimated. In the scenario presented here, X-rays vary with $\dot{m}_{\rm acc}$, but it is also indirectly connected to B and $\gamma_{\rm max}$, the latter also being sensitive to the overall jet conditions and size, and both quantities depend on the accretion rate as well. Long exposure multiwavelength observations will be required if a relationship between radiation components of different origin is to be found with high accuracy, particularly considering the moderate X-ray fluxes of permanent jet sources like LS 5039, which do not appear to follow the *typical* behavior of X-ray binaries in the low-hard state (Bosch-Ramon et al. 2005). An additional observational feature that would favor the jet as the origin of the X-rays would be the detection of some amount of polarization in this radiation.

At γ-rays, our jet model, more detailed and in accordance to the current knowl-

edge of microquasars than our previous works, still shows that microquasars could be behind some EGRET sources, and also predicts features like radiation bumps and dips in the spectra due to gamma-gamma absorption with external photon fields, and a non trivial relationship between pair creation and particle injection within the jet itself. GLAST and AGILE, with a sensitivity at least several times better than that of EGRET, should be able to detect microquasars even when they were low mass systems (case **B**) and/or they had weaker jets (case **C**). The detection of the microquasar LS 5039 by HESS shows that the efficiency of the particle acceleration processes should be high. Because of the strong photon absorption beyond ~ 100 GeV, it might be that the bulk of the TeV emission came from regions where the stellar photon density is not significant.

Although we are using accretion rates which are a small fraction of the Eddington luminosity, the wind velocity is required to be low to power accretion and the jet itself. This points to the fact that O stars with spherical fast winds would not be able in general to power some of the compact jets observed in the galaxy, implying that some special wind density profile should be given, likely produced by the presence of the compact object plus other factors like companion star rotation, etc (see below). For the launching radius, we have taken 4 $R_{\rm Sch}$ to reach mildly jet Lorentz factors. Although our approach to estimate the energy balance between the jet and accretion is rough, this value for $r_{\rm l}$ is between the last stable orbit and the limits of the corona-like region, consistent with the present state of knowledge on this issue.

Predictions on variability as well as a deeper insight on radio emission can be done in the context of this model. We discuss these topics below when applying the model to LS 5039, since information concerning the orbital parameters, the wind, and accretion rate changes along the orbit is available, allowing for testing the model as well as suggesting observational features to observe.

5.1.3 Application to LS 5039

We apply the model described above to LS 5039. The characteristics of this microquasar have been already discussed in previous chapters, so we do not discuss here again its peculiarities more than briefly. Basically, this is a persistent radio jet microquasar (Paredes et al. 2000, 2002) emitting also γ-ray emission up to several TeV (Paredes et al. 2000, Aharonian et al. 2005b). The emission at X-rays is

non-thermal, faint, with a permanent low-hard-like state without disk traces (see Bosch-Ramon et al. 2005 and references there in). It is an eccentric close binary system, whose compact object is likely a black hole and the stellar companion is an ON6.5((f)) type star (Casares et al. 2005). In Table 5.2, the primary parameter values adopted here are presented. For those that are inferred from observations on this or similar sources, we give the references. Other parameters are set to values typical for microquasars, as it has been done in previous works. In Table 5.3, we show the values of those parameters that have been fitted to reproduce the spectral and temporal behavior of LS 5039 broadband emission. We note that wind parameters are taken such that X-ray variability is roughly reproduced, parameters related to the magnetic field and the particle acceleration are fixed to reproduce the maximum detected energy of photons as well as the levels of emission at radio frequencies, X-rays and soft γ-rays; finally, the jet matter rate and launching radius have been normalized to have enough kinetic energy in matter to power the jet radiation, dominated by the γ-rays. With the adopted parameter values, a 15% of the bulk kinetic luminosity ($\sim 2 \times 10^{36}$ erg s^{-1}) is dissipated via radiation.

To reproduce approximately the variations in the X-rays, we have assumed the existence of a slow equatorial wind (outflowing velocity $\sim 6 \times 10^7$ cm s^{-1}) that would increase the accretion rate up to the (moderate) levels required by the observed emission in the context of our model, and would produce a peak after periastron. Only a small fraction of the wind being slower at the equator is enough to increase significantly the accretion rate along the orbit if one assumes pseudo-synchronization. In this case, the orbital plane and the plane perpendicular to the companion star rotation axis will be likely the same (Casares et al. 2005), allowing for the compact object to accrete from this slow equatorial wind all along the orbit. To explain the second peak we have introduced a stream, with a velocity of 5×10^6 cm s^{-1} and an additional mass loss rate of $\sim 1\%$ of the normal wind, that is formed near periastron passage when the attraction force between the two components of the system is at its maximum. This slower matter stream would produce a very delayed peak at phase 0.7. The formation of a matter stream, due to gravitational stress at the smallest orbital distances, is not unusual in close binary systems like LS 5039. We have used the approach followed by Leahy (2002) to explain the X-ray lightcurve of GX 302$-$1, also with a peak before periastron passage. Although there is still a shift of 0.1 in phase between the model peaks and the observed ones, it is important to note that there is likely an accretion disk, and the matter that reaches the disk spends some time in it until part of this matter is ejected as a jet (a lower-limit for the accre-

Table 5.2: Primary parameter values

symbol	Parameter	value
e	Eccentricity	0.35^a
a	Orbital semi-major axis [cm]	2.2×10^{12} ^{a}
θ	Jet viewing angle [°]	24.9^a
$\dot{m}_{\rm w}$	Stellar mass loss rate [$M_\odot$ yr^{-1}]	7×10^{-7} ^{a}
$M_{\rm x}$	Compact object mass [$M_\odot$]	3.7^a
$R_\star$	Stellar radius [$R_\odot$]	9.3^a
$M_\star$	Stellar mass [$M_\odot$]	22.9^a
$L_\star$	Stellar bolometric luminosity [erg s^{-1}]	8×10^{38} ^{a}
$T_\star$	Stellar surface temperature [K]	3.9×10^4 ^{a}
p	Electron power-law index	2.2^b
$\Gamma_{\rm jet}$	Jet injection Lorentz factor	1.1^c
χ	Jet semi-opening angle tangent	0.1^c
$kT_{\rm disk}$	Disk inner part temperature [keV]	0.1
$p_{\rm cor}$	Corona photon index	1.6
z_0	Jet initial point [$R_{\rm Sch}$]	50
κ	Jet-accretion rate parameter	0.1^d

^{a}(Casares et al. 2005), ^{b}(Bosch-Ramon et al. 2005), ^{c}(Paredes et al. 2002), ^{d}(Fender 2001), (Hujeirat 2004).

Table 5.3: Secondary parameter values

symbol	Parameter	value
ξ	Shock energy dissipation efficiency	0.5
f_B	B energy dens./cold matter energy dens.	0.01
η	Acceleration efficiency	0.1
$V_{\rm w}$	Equatorial wind velocity [cm s^{-1}]	6×10^7
$\dot{m}_{\rm jet}$	Jet injection rate [$M_\odot$ yr^{-1}]	3×10^{-10}
ζ	Max. ratio hot to cold leptons	0.1
$r_{\rm l}$	Launching radius [$R_{\rm Sch}$]	9
$V_{\rm stream}$	Periastron stream velocity [cm s^{-1}]	5×10^6

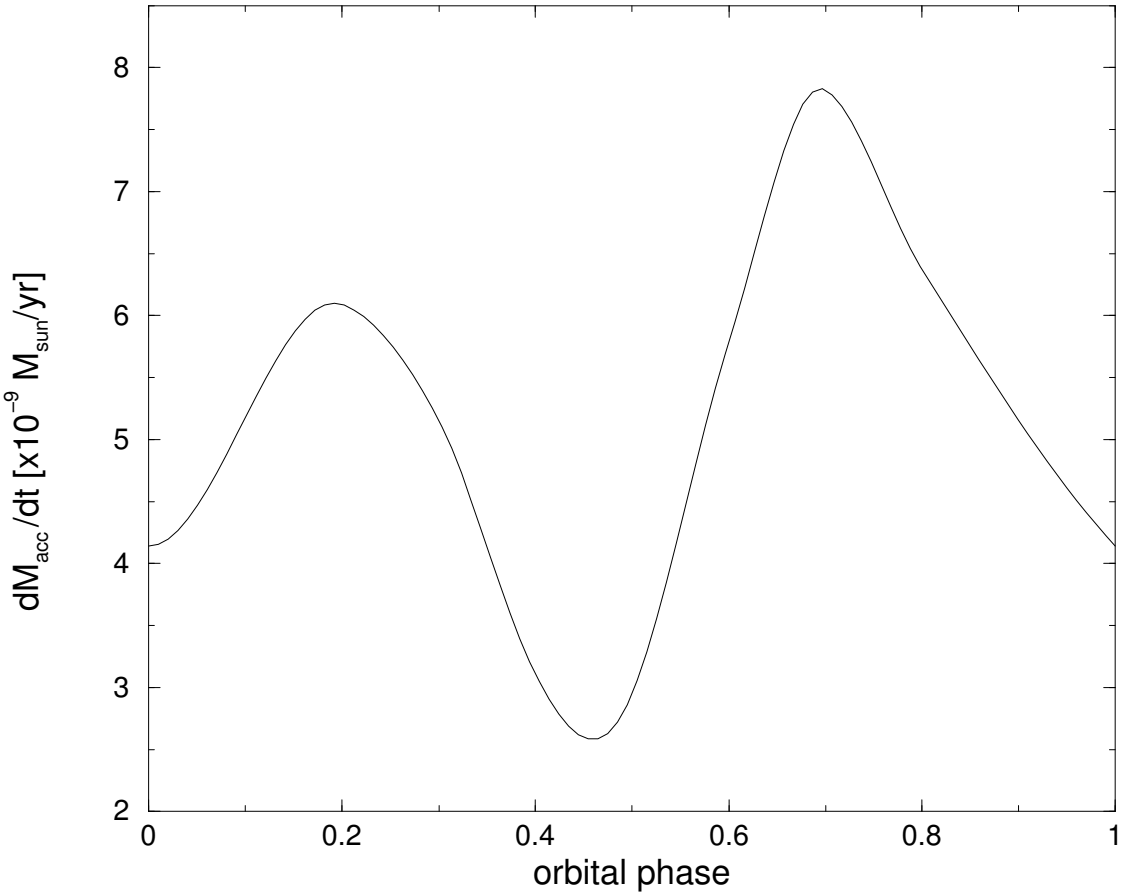

Figure 5.6: Accretion curve along an orbital period inferred from the observed X-ray lightcurve, adopting the accretion model developed for this work.

tion time is the free fall time, implying a shift of $\sim$0.06 in phase, when falling from 10^{12} cm). The accretion rate evolution obtained from the model described here is shown in Fig. 5.6.

Before presenting the results, we show in Fig. 5.7 the photon absorption coefficient for different energies within and outside the binary system, at both periastron and apastron passages. Although it is approximated, it illustrates the large opacity of the binary system in its inner regions.

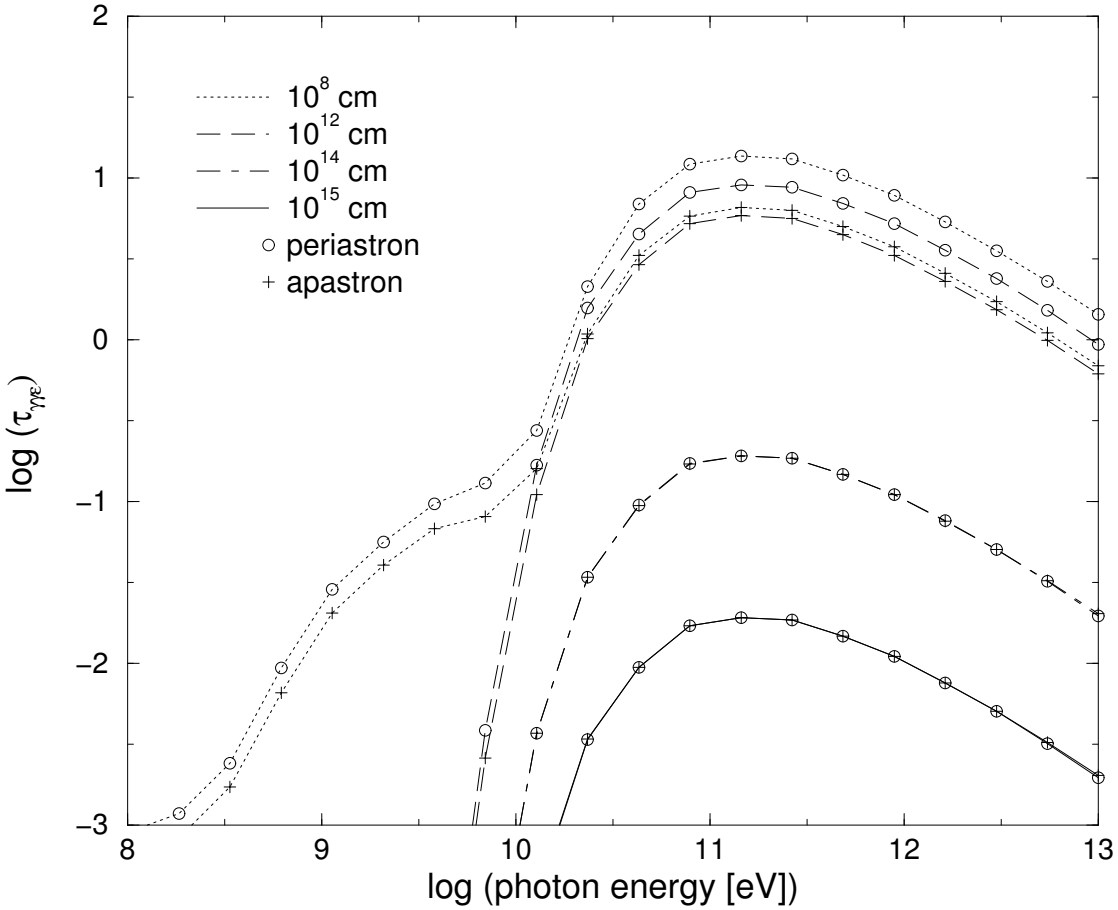

Figure 5.7: The photon absorption coefficient as a function of the energy for photons emitted in the jet at different distances from the compact object, at periastron and apastron passages.

Results

Figure 5.8 shows the computed SED (continuous thick line) of LS 5039 at the periastron passage (phase 0.0) using the physical parameters listed in Table 5.2 and 5.3. We have plotted also the contributions from the star, disk, corona and synchrotron radiation as well as the inverse Compton emission and relativistic Bremsstrahlung[3]. In the same figure we plot also the observational data. There is a general agreement between the model and the observed data, although there are some discrepancies that require some explanation. First at all, we note that the multiwavelength data were not taken simultaneously, and this can be an important source of discrepancy for any time-dependent model.

At the radio band, the computed spectrum is affected enough by the optically thick synchrotron emitting region of the jet to present an spectrum harder than the observed one. It is steeper than a flat to inverted spectrum, although the spectral index is 0.3, instead of the observed 0.5 (Martí et al. 1998). It seems that an additional process, not contemplated in our scenario, rises up the number of electrons emitting optically thin radio emission (e.g., interactions with the wind or the environment). Concerning the spatial distribution of radio emission, our computed fluxes at 5 GHz are about 10, 6 and 0.1 mJy for the inner part of the jet (< 1 AU), at middle distances from the origin (1–1000 AU) and beyond ($>$ 1000 AU), respectively. This roughly reproduces the extended emission of the radio source observed using VLBI techniques (Paredes et al. 2002).

At the X-ray band, most of the emission is synchrotron radiation coming from the relativistic electrons of the jet and only a marginal contribution comes from the disk and almost a null contribution from the corona components (see also, e.g., Markoff et al. 2001). Such small radiation from the disk represents less than 1% of the accretion energy (less than a 0.01% of the Eddington Luminosity), showing that the disk is very radiatively inefficient. The computed X-ray luminosities and photon indices are very close to those detected so far (Bosch-Ramon et al. 2005).

Gallo et al. (2003) have proposed that radio emitting X-ray binaries, when in the low-hard state, follow a particular correlation concerning radio and X-ray luminosi-

[3]We note that the total luminosity radiated by relativistic protons through proton-proton interaction should be close to that calculated for relativistic Bremsstrahlung due to similar cross-sections and target densities, assuming the same energy distribution for both relativistic protons and relativistic electrons.

ties. In the context of this correlation, LS 5039 is pretty under luminous at X-rays, presenting a permanent low-hard-like X-ray state. This could be explained by the fact that its radio emission is optically thin, coming mainly from regions outside the binary system, instead of being optically thick and completely core dominated (as in the case of models such as the one presented by Markoff et al. 2001, see also Heinz & Sunyaev 2003). As noted above, it might be qualitatively explained by the increase in relativistic electrons predicted by our model, although the issue requires further investigation since our radio spectrum, although steeper than a flat to inverted one, is still too hard.

At BATSE and COMPTEL energies, the main contribution still comes from synchrotron emission of the jet. There is a small disagreement between the predicted luminosity and the one observed by BATSE. However, we note that these data are averaged along effective duration eppochs spanning several days (Harmon et al. 2004), whereas the plotted SED is computed at phase 0.0, when the accretion is significant though not the highest. Otherwise, at the COMPTEL energy range, the moderate disagreement between the computed and observed data is likely produced by the fact that the MeV radiation coming from the COMPTEL source GRO J1823−12, to which LS 5039 is associated, might be a superposition of the MeV emissions of the three different EGRET sources that are in the field of view (Collmar 2003). This means that the data from COMPTEL should be actually taken as an upper limit. In such a case, our computed values would be consistent with the data.

At high-energy γ-rays (0.1–10 GeV), the computed luminosities are similar to those observed by EGRET while the computed photon indices are slightly harder. This fact could be naturally associated with the low temporal resolution of EGRET, with the shortest viewing periods spanning for one week and providing time averaged spectra that could mask harder ones. Nevertheless, slopes, unlike fluxes, are not very reliable due to pair creation inside the jet. The dominant component at this band of the spectrum is star IC, whereas the synchrotron radiation is only important at the lower part of EGRET energies. The emission of secondary pairs created within the binary system is not significant.

At VHE γ-rays, star IC emission dominates. The spectrum reaches several TeV, and it is limited by the maximum particle energy, which can reach ~ 10 TeV. The contribution of the star IC scattering is favored during the periastron passage due to a higher photon density as well as a smaller interaction angle between the electrons

and the photons, which influences the IC scattering. During apastron, the SSC component is a minor but more significant fraction of the whole VHE radiation. The VHE spectrum is strongly affected by the $\gamma\gamma$ opacity due to pair creation within the binary system, being the absorption stronger at the periastron passage. It appears therefore unavoidable an important decrease of the emission as well as an additional source of variability at those energies. Also, a hardening of the emission, as seen in Fig. 5.8, could take place. Our model underestimates the TeV emission, although the difference is less than one order of magnitude. Possibly, some high energy processes involving particle acceleration and emission are taking place in the jet at middle scales, where the 100 GeV photon absorption is not important. This could also be related to the optically thin nature of the radio emission. This outer emission would not be as variable as the emission from the compact jet. In any case, a deeper treatment at this energy band concerning VHE emission and pair creation phenomena is required (Khangulyan & Aharonian 2006).

The results obtained by applying other leptonic models (e.g. Chapter 4, Dermer & Böttcher 2006) do not differ substantially from the comprehensive model presented here, which can explain the broad-band emission from LS 5039. Otherwise, hadronic models can reproduce the emission at VHE energies (Romero et al. 2003) though it is hard to explain how typical EGRET fluxes could be achieved (see the high-energy γ-ray fluxes for the case of LS I +61 303, adopting a reasonable energetic budget in relativistic particles, computed by Romero et al. 2005). Comparing both types of model, it seems that the leptonic ones can explain better than the hadronic ones the broadband spectrum at least up to ~ 1 GeV, being both suitable at higher energies since the energetic requirements are not as strong as those to explain the whole emission from the source.

The accretion model has been applied to reproduce roughly the X-ray lightcurve, exploring also what are the consequences in other bands of the spectrum. In Fig. 5.9 we show the flux variations along the orbit at four energy bands. At radio and X-ray energies, the predicted flux variations are well correlated to accretion, since they have similar shapes to the accretion orbital curve. The predicted amplitude variations are of about one order of magnitude in radio and a factor of three at X-rays, although we note that, if the radio emitting region is large enough, say 10^{15} cm, the variations at these wavelengths will be significantly smoothened by light crossing time limitations (as it seems to be the case, see Ribó 2002). Emission at EGRET energies deserves a special comment. The emission varies almost one order of magnitude (we note

that, for EGRET itself, orbital variability was not observable because its viewing periods lasted at least one week), although the shape of the lightcurve is different due to the higher rate of IC interaction due to angular effects. At VHE, however, the emission is strongly absorbed by the stellar field, producing a dip around periastron passage. At phases 0.6–0.9, there is a long standing peak that is related to the stream related peak at phase 0.7 (0.8) that is not close enough to the stellar companion for vanishing due to $\gamma\gamma$ absorption. A similar peak seems to be present in HESS data (Aharonian et al. 2005b) when folded in phase with the new ephemeris of Casares et al. (2005), although further observations should be carried out to confirm this. At phases 0.2–0.3, a smaller peak is seen, which might detected eventually in future VHE observations. We note that, as it is seen in Fig. 5.7, if TeV emission comes from distances typically larger than the semi-major orbital axis it would not be significantly attenuated by photon absorption. In such a case, variability would be limited by the size of the emitting region. Concerning the variations of the radio spectral indices along the orbit, due to the model limitations at radio and γ-rays mentioned above, it is not treated here. However, it is worth mentioning that at X-rays, the photon index shows a trend similar to that found by (Bosch-Ramon et al. 2005), i.e. higher fluxes when harder spectrum. Nevertheless the anticorrelation is not as strong as that observed.

Discussion

The computed SED from radio to VHE γ-rays has been compared with the available observational data from LS 5039, gathered at different bands of the electromagnetic spectrum, showing in general a good agreement. Although the model is limited by its phenomenological nature, we can extract some general conclusions that could be useful to understand the physics behind these objects as well as for going deeper in more basic theoretical aspects concerning the jet plasma characteristics, particle acceleration and jet formation phenomena. In particular, in the context of our model, we can state that the jets are radiatively efficient ($\sim$ 15%) and sites of particle acceleration up to multi-TeV energies.

The strong absorption of VHE γ-rays by the stellar photon field seems to make hard the detection of high fluxes of radiation if they are generated in the inner regions of the jet, closest to the compact object. Possibly, since the source is not very faint at these energies, some high energy processes involving particle acceleration

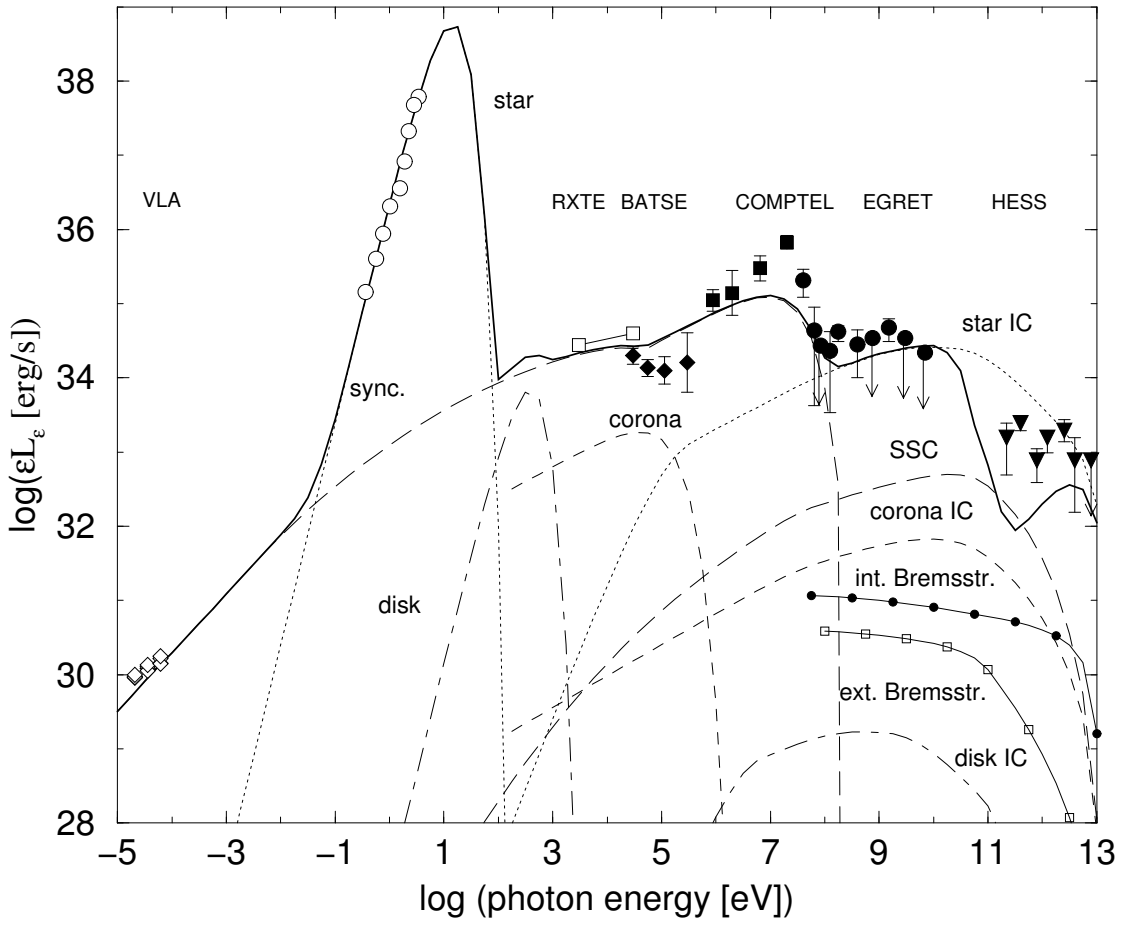

Figure 5.8: Comparison of the spectral energy distribution of LS 5039 computed from the present model, at the periastron passage and using the parameters of Tables 5.2 and 5.3, with the observed data. We show the different components of the emission as well as the sum of all of the them (solid line), which is attenuated due to $\gamma\gamma$ absorption. The points observed are from Martí et al. (1998) (VLA, diamonds), Clark et al. (2001) and Drilling (1991) (optical, circles, corrected of absorption), Bosch-Ramon et al. (2005) (RXTE, squares), Harmon et al. (2004) (BATSE, filled diamonds), Collmar (2003) (COMPTEL, filled squares), Hartman et al. (1999) (EGRET, filled circles) and Aharonian et al. (2005b) (HESS, filled down triangles). The arrows in the EGRET and HESS data represent upper limits (3σ).

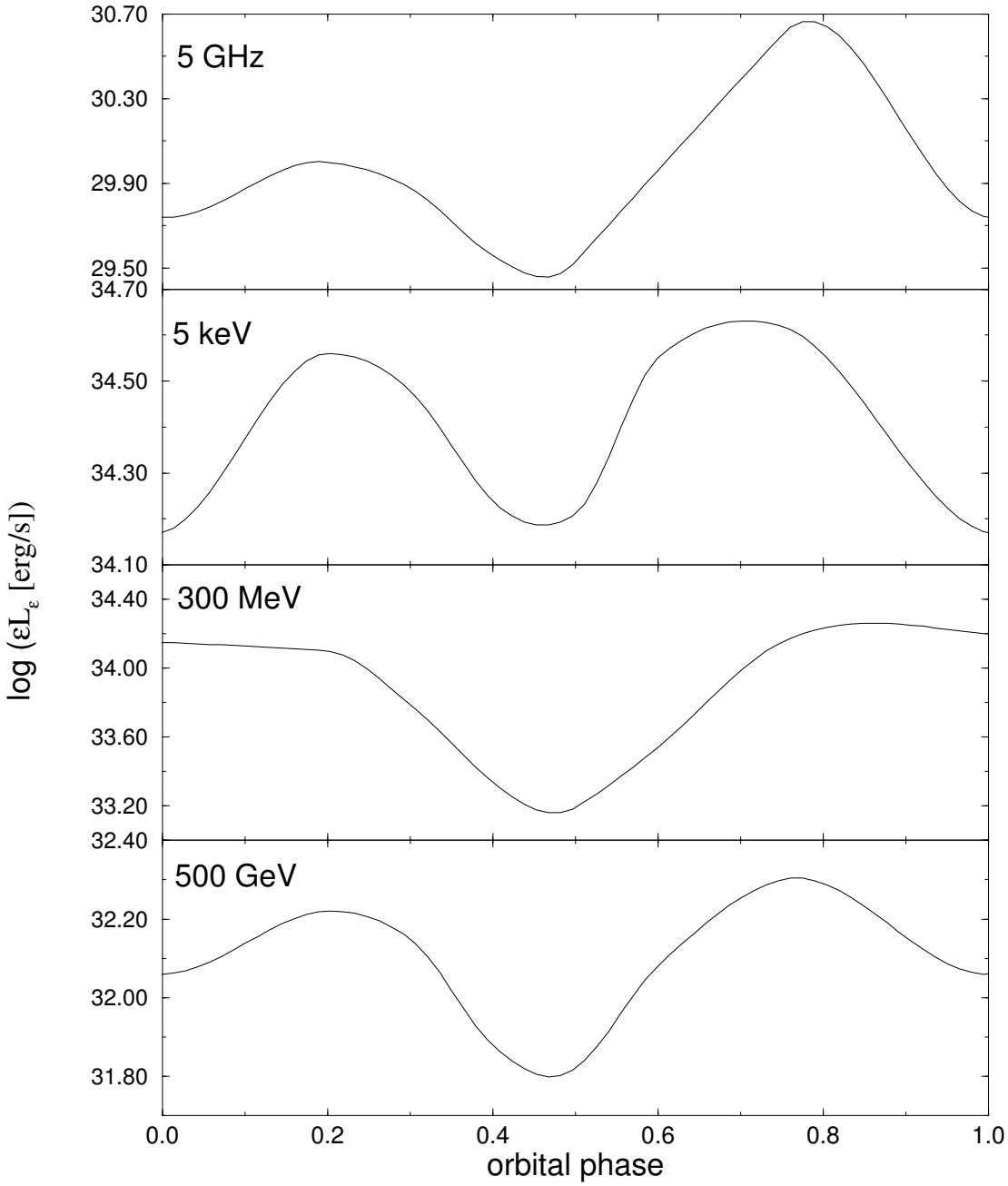

Figure 5.9: The panel shows the flux variations along the orbit for the four energy bands considered here. We note that emission at very high-energy γ-rays is strongly attenuated by the photon absorption in the star photon field.

and emission are taking place in the jet at middle scales, where the 100 GeV photon absorption is not important. This could also be related to the moderately high fluxes and the optically thin nature of the radio emission. Variability at these energy bands could provide information about the location of the particle acceleration processes and emitting regions.

Changes in the accretion rate due to the orbital eccentricity and a particular wind density profile can explain the variability properties observed at X-rays. It hints to a companion stellar wind that is not spherically symmetric nor fast in the equator, since otherwise the γ-ray radiation could not be powered.

We can conclude that, with reasonable values for the different parameters, our model seems to be good enough as to describe the general features of the spectrum of LS 5039 from radio to TeV γ-ray energies.

5.1.4 Application to 1E 1740.7−2942

1E 1740.7−2942, discovered by the Einstein satellite (Hertz & Grindlay 1984), is a very bright X-ray source located at less than one degree from the Galactic Center. The satellite GRANAT apparently detected a line-like feature around the electron-positron annihilation energy (Bouchet et al. 1991), although it has not been confirmed afterward (see, e.g., Jung et al. 1995, de Cesare et al. 2004). 1E 1740.7−2942 was considered the first microquasar when extended radio jets were observed (Mirabel et al. 1992), reaching large angular distances from the core ($\sim 1'$). There are hints of correlation between the X-ray and the radio emission (Mirabel et al. 1993), and X-ray state changes with timescales similar to those of other X-ray binaries have been observed (Del Santo et al. 2005 and references therein). Moreover, a 12.7-days periodical modulation of a 3–4% in the X-ray emission seems to be produced by the orbital motion of the system (Smith et al. 2002). This X-ray behavior suggests the galactic nature of the source. The modulation period and the upper limits in magnitude obtained in the infrared suggest that the stellar companion in 1E 1740.7−2942 might be a low-mass star (Martí et al. 2000), implying a Roche-lobe overflow accretion mechanism. Also, the strong X-ray radiation is a hint of powerful accretion, giving support to the Roche-lobe overflow. The behavior of the X-ray spectrum, very similar to other galactic black-hole candidates (Del Santo et al. 2005), points to the compact object as a black-hole. The small 3–4% modu-

lation of the X-rays might imply a quite circularized orbit, strengthening again the possibility of Roche-lobe overflow accretion. The fact that the companion has not been detected yet would be related to the very strong absorption from the infrared up to soft X-rays in the region, with a hydrogen column density of about 10^{23} cm^{-2}, found by Gallo & Fender (2002), who also detected a possible extended X-ray halo. This is even higher than the typical values in the direction of the Galactic Center ($\sim 10^{22}$ cm^{-2}; Dickey & Lockman 1990), and might imply that this object is embedded within a molecular cloud (Yan & Dalgarno 1997). This is likely related to the very extended structures detected at different wavelengths around this source, as was pointed out by Mirabel et al. (1992). Regarding the distance to 1E 1740.7−2942, we have adopted in this work a distance of 8 kpc, as it would be close to the Galactic Center.

Concerning the emission properties, the radio emission coming from the core is spectrally flat and faint with a flux density of less than 1 mJy (Fender 2001 and references therein; $\sim 10^{29}$ erg s^{-1} at 8 kpc), whereas the radio emission coming from the radio lobes is optically thin. At X-rays, the object radiates with fluxes of about 10^{-9} erg s^{-1} cm^{-2} ($\sim 10^{37}$ erg s^{-1} at 8 kpc) between 10 and 100 keV. This radiation has been modeled as thermal Comptonized photons (e.g. in a corona or similar hot inner region) coming from an underlying fainter disk, which also contributes at lower energies (Del Santo et al. 2005). Although the luminosity is dominated by the hard X-rays, extending up to about 300 keV, the disk contribution varies, reaching similar luminosities to those of the Comptonized radiation during the intermediate/soft state (Del Santo et al. 2005). Regarding other energy bands, little can be said. EGRET observed intensively the Galactic Center region, and there are upper limits for the region because the source is not detected. At the Galactic Center distance the luminosity upper limits are around several times 10^{32} erg s^{-1} (Hartman et al. 1999). In addition, the flux of the nearby 3EG J1744−3011 can be taken as an absolute upper limit for the region because a source is not *clearly* detected in the position of 1E 1740.7−2942[4], being about 10^{36} erg s^{-1} at the mentioned distance. The strong absorption prevents to constrain properly the source emission from IR to soft X-rays.

We want to explain the emission of this object in the context of microquasars, considering the radiation produced in a compact jet thought to be present during

[4]The EGRET sensitivity in that region is confuse, as it is seen in Fig. 3 of Hartman et al. (1999), and the angular resolution is poor all along the Galactic plane.

the low-hard state (Fender et al. 2003) and taking also into account the radiation from accretion processes. Data in the radio band and X-rays/soft γ-rays (RXTE and INTEGRAL, being the latter re-analyzed here because available new software and more data)[5], and upper limits at high-energy γ-rays (EGRET), have been considered. We have applied a detailed jet model to explain the data and to make predictions at high energies, as well as to give some constraints about the physics of the processes involved in the broadband emission.

From the considerations already made, we assume that the source is likely to be a low mass system with bright disk/corona emission (Del Santo et al. 2005). Therefore, the high-energy electrons in the jet will interact basically with the disk/corona photons at the base of the jet, and with the magnetic field in the same region and further from the compact object. Depending on the magnetic field and particle acceleration properties of the jet, the main part of the emission can be radiated either at higher (γ-rays) or at lower energies (X-rays or below). To restrict the number of parameters to explore, we have fixed some of them to values adopted in previous works on microquasars (see above and Chapter 4). The magnetic field energy density is taken to be one tenth of the one corresponding to a magnetic field in equipartition to the cold matter of the jet, which dominates pressure. The density of relativistic leptons is kept low to avoid their pressure dominance, fixing a relativistic lepton to cold proton number ratio of 1/10. Relativistic protons are not treated here, although some amount could be present in the jet, constrained by the cold matter pressure dominance (concerning their radiative properties, see, e.g., Romero et al. 2005). We have fixed the jet Lorentz factor to 1.25, since it is known that microquasar jets during the low-hard state seem to be mildly relativistic. All this makes the Doppler effect not very significant, so we have adopted a jet viewing angle of 45°. Concerning the orbital parameters, we will adopt an orbital period of 12.7 d, a black-hole mass of 5 $M_\odot$, and a low mass stellar companion of 2 $M_\odot$. This renders a semi-major orbital axis of 3×10^{12} cm. A luminosity of 10^{36} erg s^{-1} and a surface temperature of 10^4 K have been adopted for the star. All these parameters are summarized in Table 5.4 along with the parameters for the jet geometry, which are fixed to typical values from the literature. The electron power-law index has been taken to be 2.2, except when it is stated otherwise.

[5]CHANDRA data from the observations performed by Gallo & Fender (2002) is not considered here due to its non-simultaneity with the observations carried out by RXTE and INTEGRAL. We note however that at that time the flux at few keV was about one order of magnitude lower than the flux presented here for similar energy ranges.

Results

To find the different sets of parameter values that reproduce the observed SED, we have explored three parameters: the jet to accretion rate ratio (the fraction of accreted matter going to the two jets), the acceleration efficiency, and the shock energy dissipation efficiency. Several values of the jet to accretion rate ratio have been taken, ranging 0.004–0.1; smaller ratios do not yield enough radio emission, a bit larger values are still possible but unlikely, since too high ratios could not provide enough kinetic energy to reach relativistic jet speeds. When the mentioned ratio is 0.1, one can reproduce the observed radio emission in different ways. For the highest value of the acceleration efficiency, 0.1 ($\times q_{\rm e}Bc$), the corresponding shock energy dissipation efficiency is 0.01. In this case, radiation is produced up to TeV energies. For the smallest value of the acceleration efficiency, 10^{-5}, the corresponding shock energy dissipation efficiency is 0.001. Then, the spectrum reaches GeV energies. When the ratio of jet to accretion rate is 0.004, the acceleration efficiency is to be low, 10^{-5}, and the corresponding shock energy dissipation efficiency must be high, 0.1. In such a case, emission beyond 10 MeV is very faint. Mild jets (2% of accreted matter) can produce higher fluxes at hundreds of GeV than powerful jets (10%), since their energy dissipation efficiency can reach 0.1, emitting more radiation at very high-energy γ-rays without overcoming observed radio fluxes, for the same acceleration efficiency. The different explored parameter values are shown in Table 5.5. Next, we explore two cases. In the first case, corona dominates at X-rays, as proposed for this source (Del Santo et al. 2005) and, in the second case, jet dominates at X-rays, as proposed by some authors for other X-ray binaries (Markoff et al. 2001, Georganopoulos et al. 2002).

In Fig. 5.10, we show the SED for the first case, when corona dominates and the jet is mild, with high acceleration efficiency. We have neglected here those components that are not relevant for the modeling of the source SED. The accretion rate, 1.2×10^{-8} $M_\odot$ yr^{-1}, has been fixed assuming that the total X-ray luminosity (corona+disk) is $0.05\times c^2$ the total accretion rate. The corresponding Eddington accretion rate for a 5 $M_\odot$ black hole is 2×10^{-7} $M_\odot$ yr^{-1}. The magnetic field in the base of the jet[6] and the (one) jet total kinetic luminosity are about 8×10^4 G and 2×10^{36} erg s^{-1}, respectively. This source might be detectable by on-board satellite instruments and ground-based Cherenkov telescopes as GLAST or HESS[7]

[6]The magnetic field decreases as far as cold matter energy density goes down along the jet.

[7]Apparently there is no signal in the region of the source in the survey presented by Aharonian

with moderately long exposures. The source might have been detected by EGRET, since it is slightly over the lower EGRET limit. Otherwise, its contribution to the nearby source could not be significant.

In Fig. 5.11, we show the SED for the case of an X-ray dominant jet. In this case, to try to reproduce the broadband emission, we adopt more extreme parameter values than those explored above. The synchrotron modeling of the X-rays requires a jet with a jet to accretion rate ratio of 0.2, energy dissipation efficiency of a 60%, acceleration efficiency of 0.001 and an accretion rate taken to be a 10% of the Eddington accretion rate quoted above (i.e. $2{\times}10^{-8}$ $M_{\odot}$ yr^{-1}). The magnetic field and jet total kinetic luminosity are 3×10^5 G and 3×10^{37} erg s^{-1}. In such a case, radio fluxes are exceeded by one order of magnitude, and an electron power-law index of 1.7 is required, which might be difficult to obtain (see Protheroe 1999 and references there in). The parameter values adopted in the two presented particular cases are shown in Table 5.6.

The X-rays might be produced via IC processes. When attempting to reproduce the observed X-ray spectrum with an IC jet model with a weak corona, it is not possible to reach the X-ray fluxes through IC of stellar photons and/or SSC emission because the jet power requirements are too high, and it is not possible to keep the particle energy low enough as to make them radiate just up to a few hundreds of keV for any reasonable acceleration rate. In addition, for the SSC model, radio constraints are also violated. We conclude that the corona X-ray dominated emission reproduces better the observed broadband SED than the jet X-ray dominated emission in 1E 1740.7−2942.

Finally, we have explored qualitatively the production of very extended radio emitting jets under particular conditions of the environment like an enhanced magnetic field (1E 1740.7−2942 could be located within a molecular cloud, see Yan & Dalgarno 1997). After studying whether extended radio emission could be detectable up to 2–3 pc, the size of the radio lobes detected by Mirabel et al. (1992) at 8 kpc, we note that a magnetic field of 10^{-4} G all along that jet region and a jet carrying at least 1% of the accreted matter would be required. This magnetic field is similar to what is typically found in molecular clouds (Crutcher 1999) and higher

et al. (2006, 2005a), although it is probably premature to state that it could not be detected at very high energies with longer exposures. In fact, the microquasar LS 5039, proposed to be the counterpart of 3EG J1824−1514 (Paredes et al. 2000), has been recently detected by HESS (Aharonian et al. 2005b).

Table 5.4: Common parameter values

Parameter [units]	value
Orbital semi-major axis [$R_\odot$]	43
Disk inner part temperature [keV]	0.5
Disk luminosity [erg s^{-1}]	1.5×10^{36}
Corona photon index	1.6
Corona emission peak [keV]	300
Disk inner radius [$R_{\rm Sch}$]	50
Jet initial point in the compact object RF [$R_{\rm Sch}$]	50
Jet semi-opening angle tangent	0.1
Equipartition parameter	0.1
Max. ratio hot to cold lepton number	0.1
Compact object mass [$M_\odot$]	5
Stellar mass [$M_\odot$]	2
Stellar bolometric luminosity [erg s^{-1}]	10^{36}
Stellar surface temperature [K]	10^4
Jet Lorentz factor	1.25
Jet viewing angle [°]	45

than the equipartition value to matter jet in those regions.

Discussion

The observed SED and the radio structure of 1E 1740.7−2942 can be roughly explained by a model of a cold-matter dominated and magnetized jet whose radiation mechanisms are powered by internal shocks (large scale jets likely require enhanced magnetic field). In addition, in the context of our model, corona emission appears to explain better the observed emission at hard X-rays than jet emission. If the source were detected at 100 GeV energies, it would imply that the jet is not very heavy (moderate jet to accretion rate ratio), with high energy dissipation and particle acceleration efficiencies. If the source were detected only at high-energy γ-rays (e.g. by GLAST), it would imply that the jet power is likely high, with moderate energy dissipation and low acceleration efficiency. Since no high fluxes are pre-

Table 5.5: Parameter space exploration

jet/accr. ratio	accel. eff.	diss. eff.	prediction
0.1	0.1	0.01	up to TeV
0.1	10^{-5}	0.001	up to GeV
0.02	0.1	0.1	"bright" at 100 GeV
0.004	10^{-5}	0.1	up to MeV

Table 5.6: Specific parameter values for different models

Parameter [units]	corona-dominated	jet-dominated
Accretion rate $[M_\odot/\mathrm{yr}]$	1.2×10^{-8}	2×10^{-8}
Corona luminosity [erg s^{-1}]	3.5×10^{37}	10^{35}
Jet-accretion rate ratio	0.02	0.2
Shock dissipation efficiency	0.1	0.6
Acceleration efficiency	0.1	0.001
Electron power-law index	2.2	1.7

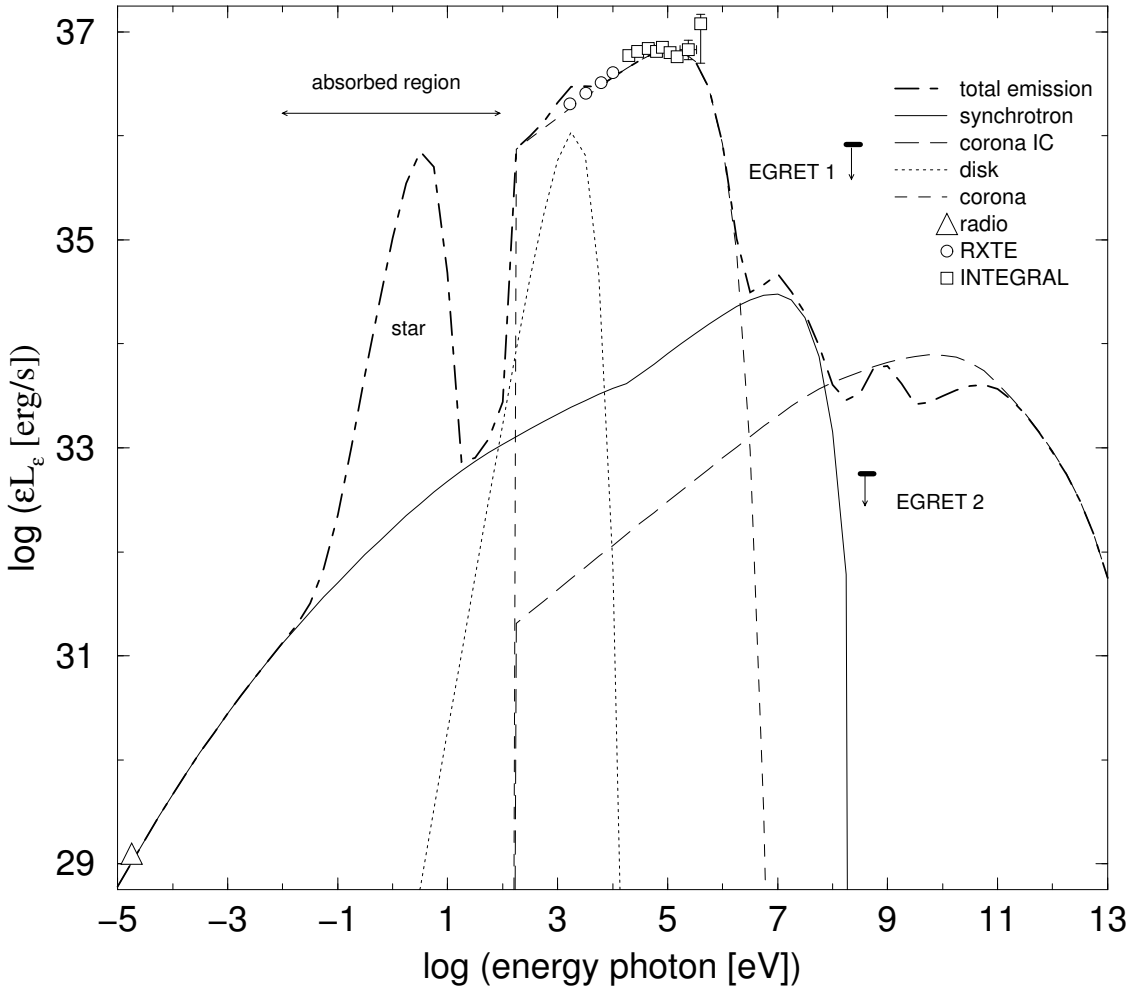

Figure 5.10: Computed broad-band SED for 1E 1740.7−2942, when the corona is dominant at X-rays, plotted along with the data points and observational upper limits (extended radio emission is not taken into account). The parameter values are those corresponding to the case when the source could be detected at even very high-energy γ-rays. At the radio band, a typical luminosity from the core at the adopted distance is shown. The slope at this range is similar to that observed, which is not shown explicitly (see Fender 2001 and references therein). At X-rays/soft γ-rays, RXTE and INTEGRAL data are plotted (they were already presented by Del Santo et al. 2005 and re-analyzed for the present work). At high-energy γ-rays, two upper limits are shown: one from the spectrum of EGRET source 3EG J1744−3011 (EGRET 1), as absolute upper limit (Hartman et al. 1999), and the other obtained from the sensitivity limits of EGRET (EGRET 2) in the region (Hartman et al. 1999). The error bars are shown when larger than the symbols.

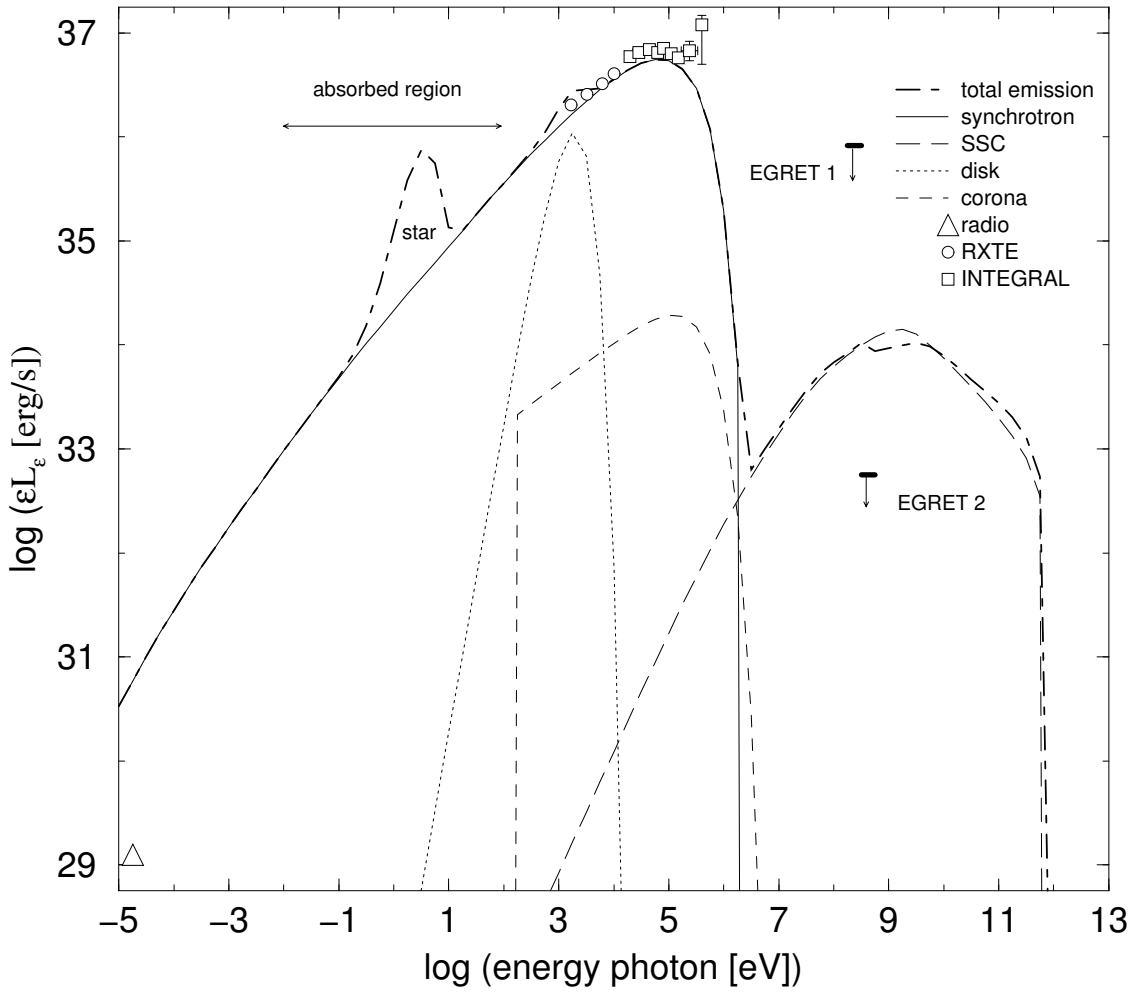

Figure 5.11: The same as in Fig. 5.10, but for the case when X-rays are dominated by synchrotron emission from the jet. Notice that the radio constraints are violated.

dicted, it seems unlikely that 1E 1740.7−2942 could be a significant contributor to the nearby EGRET source. Finally, if emission at higher energies than the coronal one is not detected, it will imply that the jet is light (low jet to accretion rate ratio), or radiatively inefficient regardless its total kinetic power.

Bibliography

Aharonian F., Akhperjanian A.G., Bazer-Bachi A.R., et al., Jan. 2006, ApJ, 636, 777 138

Aharonian F.A., Akhperjanian A.G., Aye K.M., et al., Mar. 2005a, Science, 307, 1938 139

Aharonian F.A., Akhperjanian A.G., Aye K.M., et al., Jul. 2005b, Science, 309, 746 123, 124, 132, 133, 139

Bosch-Ramon V., Paredes J.M., Ribó M., et al., Jul. 2005, ApJ, 628, 388 123, 125, 126, 129, 132, 133

Bosch-Ramon V., Romero G.E., Paredes J.M., Feb. 2006a, A&A, 447, 263 107

Bosch-Ramon V., Romero G.E., Paredes J.M., et al., 2006b, A&A, submitted 108

Bouchet L., Mandrou P., Roques J.P., et al., Dec. 1991, ApJ Letter, 383, L45 135

Casares J., Ribó M., Ribas I., et al., Dec. 2005, MNRAS, 364, 899 109, 125, 126, 132

Clark J.S., Reig P., Goodwin S.P., et al., Sep. 2001, A&A, 376, 476 133

Collmar W., 2003, In: Proc. 4th Agile Science Workshop, p.177 130, 133

Crutcher R.M., Aug. 1999, ApJ, 520, 706 139

de Cesare G., von Ballmoos P., et al., 2004, In: 35th COSPAR Scientific Assembly, 2863 135

Del Santo M., Bazzano A., Zdziarski A.A., et al., Apr. 2005, A&A, 433, 613 135, 136, 137, 138, 142

Dermer C.D., Böttcher M., Jun. 2006, ApJ, 643, 1081 115, 131

Dickey J.M., Lockman F.J., 1990, ARA&A, 28, 215 136

Drilling J.S., Jul. 1991, ApJSS, 76, 1033 133

Esin A.A., McClintock J.E., Narayan R., Nov. 1997, ApJ, 489, 865 109

Fender R.P., Mar. 2001, MNRAS, 322, 31 114, 126, 136, 142

Fender R.P., Gallo E., Jonker P.G., Aug. 2003, MNRAS, 343, L99 137

Fender R.P., Belloni T.M., Gallo E., Dec. 2004, MNRAS, 355, 1105 108

Gallo E., Fender R.P., Dec. 2002, MNRAS, 337, 869 136

Gallo E., Fender R.P., Pooley G.G., Sep. 2003, MNRAS, 344, 60 114, 129

Georganopoulos M., Aharonian F.A., Kirk J.G., Jun. 2002, A&A, 388, L25 122, 138

Harmon B.A., Wilson C.A., Fishman G.J., et al., Oct. 2004, ApJSS, 154, 585 130, 133

Hartman R.C., Bertsch D.L., Bloom S.D., et al., Jul. 1999, ApJSS, 123, 79 133, 136, 142

Heinz S., Sunyaev R.A., Aug. 2003, MNRAS, 343, L59 130

Hertz P., Grindlay J.E., Mar. 1984, ApJ, 278, 137 135

Hujeirat A., Mar. 2004, A&A, 416, 423 126

Jones F.C., Ellison D.C., 1991, Space Science Reviews, 58, 259 111

Jung G.V., Kurfess D.J., Johnson W.N., et al., Mar. 1995, A&A, 295, L23 135

Khangulyan D., Aharonian F.A., 2006, in preparation 113, 115, 131

Körding E., Falcke H., Markoff S., Jan. 2002, A&A, 382, L13 122

Leahy D.A., Aug. 2002, A&A, 391, 219 125

Longair M.S., Mar. 1992, High Energy Astrophysics. Vol.1: Particles, photons and their detection, Cambridge, UK: Cambridge University Press, March 1992. 107

Markoff S., Falcke H., Fender R., Jun. 2001, A&A, 372, L25 122, 129, 130, 138

Martí J., Paredes J.M., Ribó M., Oct. 1998, A&A, 338, L71 129, 133

Martí J., Mirabel I.F., Chaty S., Rodríguez L.F., Nov. 2000, A&A, 363, 184 135

Mirabel I.F., Rodriguez L.F., Cordier B., Paul J., Lebrun F., Jul. 1992, Nature, 358, 215 135, 136, 139

Mirabel I.F., Rodriguez L.F., Cordier B., Paul J., Lebrun F., Jan. 1993, A&ASS, 97, 193 135

Paredes J.M., Martí J., Ribó M., Massi M., Jun. 2000, Science, 288, 2340 124, 139

Paredes J.M., Ribó M., Ros E., Martí J., Massi M., Oct. 2002, A&A, 393, L99 124, 126, 129

Paredes J.M., Bosch-Ramon V., Romero G.E., May 2006, A&A, 451, 259 107

Protheroe R.J., 1999, In: Topics in Cosmic-Ray Astrophysics, 247 111, 139

Punsly B., Romero G.E., Torres D.F., Combi J.A., Dec. 2000, A&A, 364, 552 114

Ribó M., Nov. 2002, Ph.D. Thesis, Univesitat de Barcelona 131

Ribó M., Negueruela I., Blay P., Torrejón J.M., Reig P., Apr. 2006, A&A, 449, 687 109

Romero G.E., Torres D.F., Kaufman Bernadó M.M., Mirabel I.F., Oct. 2003, A&A, 410, L1 107, 131

Romero G.E., Christiansen H.R., Orellana M., Oct. 2005, ApJ, 632, 1093 107, 131, 137

Smith D.M., Heindl W.A., Swank J.H., Oct. 2002, ApJ Letter, 578, L129 135

Yan M., Dalgarno A., May 1997, ApJ, 481, 296 136, 139

Yuan F., Cui W., Aug. 2005, ApJ, 629, 408 114

Chapter 6

Microquasars as Cosmic Ray sources

The existence of relativistic particles in microquasar jets has been discussed extensively in previous chapters. Concerning the question whether these jets are leptonic or hadronic, the presence of the former type of matter is clear from the observed synchrotron emission and, in the case of the latter, the detection of lines in SS 433 (Kotani et al. 1996, Marshall et al. 2002) is evidence of the presence of cold hadronic matter. Moreover, some microquasars show extended structures at radio frequencies (e.g. 1E 1740.7−2942; Mirabel et al. 1992) or at X-rays (e.g. XTE J1550−564, Corbel et al. 2002) at scales of 0.1–1 pc, which could be related to acceleration of particles via jet interaction with the environment (e.g. Wang et al. 2003). In addition, the existence of a non observable matter content in the jets, likely cold protons, has been inferred from its effects in the surrounding regions of microquasars (Gallo et al. 2005, Heinz 2006, Martí et al. 2005). Provided that particle acceleration is apparently more efficient in case of hadrons than in case of leptons, at least in the context of classical shock acceleration mechanism (see, e.g., Bell 1978), and electron acceleration is known to occur (at least) in some jets, it seems reasonable that a fraction of jet protons will be relativistic. In this chapter we explore what could happen when relativistic particles, leptons and protons, accelerated in the jets of microquasars were released in the interstellar medium (ISM). The scenario considered here is consistent with that of the cold matter dominated jet, sketched in Chapter 3 and explored in Chapter 5.

Next, we assume that relativistic leptons and hadrons escape in the jet termination point diffusing through the ISM. Electrons interact with the environment magnetic and photon fields and protons with surrounding higher density regions of the ISM (e.g. clouds). A previous and somewhat seminal work on microquasars and cosmic rays was developed by Heinz & Sunyaev (2002). A treatment of the radiative outcomes of the microquasar/ISM interaction can also be found in Bosch-Ramon et al. (2006), leptons, and Bosch-Ramon et al. (2005), for protons.

6.1 Leptonic broadband emission from the jet termination region

The diffusion of relativistic particles in a magnetized medium is a common astrophysical phenomenon. This process can take place under different geometries and energy dependences, and further factors like particle energy losses and convection can be added (Ginzburg & Syrovatskii 1964). In case these particles are injected/accelerated in a region much smaller than the typical diffusion radius (see Chapter 3) for the timescales involved, the injection/acceleration process of relativistic particles can be supposed to be spatially point like. Several applications of models considering particle diffusion effects are found in the literature. For instance, the spatial distribution of the leptonic component in galactic cosmic rays can be described using such approach (Atoyan et al. 1995), and similar work has been done for protons (Aharonian & Atoyan 1996). Moreover, the radiation coming from such diffusing particles have been studied in different contexts, like in those mentioned before (Aharonian & Atoyan 2000), and also in other cases like microquasars (next section) and extreme regions of star formation (Torres 2004). Also, to properly estimate the background and foreground affecting EGRET source detection, complex models of particle diffusion and its emission in the Galaxy have been developed (Strong et al. 2000).

One particular scenario where transport and radiation processes can be explored is the microquasar jet termination region. As it has been treated in previous chapters, the jet itself radiates dissipating a minor but significant fraction of the energy that it carries. Moreover, the remaining kinetic energy can be released at some

point via heating of ISM if the interaction is via a shock[1], similar to that produced by γ-ray burst jets when braked by their environment matter, i.e. during afterglow phase (although in our case it is going to be more like a steady shock). The outcome of this process could be the formation of a new population of relativistic particles following a non-thermal distribution, containing a part of the overall initial jet kinetic energy. We treat here the behavior of the relativistic leptons once released in the environment of the termination shock. These particles diffuse away and radiate, being affected by both the magnetic field, probably enhanced by the jet-ISM interaction, and the photon field. We adopt a high-mass microquasar scenario, allowing for significant IC emission.

6.1.1 A model for diffusing electrons and their emission

We assume that the involved spatial scales for variations in magnetic field, cold matter and photon densities are bigger than the typical distances covered by the injected relativistic electrons during their radiative lifetime. It means that all these fields can be treated as homogeneous. The distances covered by the electrons depend on the energy losses and the diffusion coefficient, as well as on the age of the source. Such electrons are injected with a certain energy distribution, taken here to be a power-law, as usual in shock particle acceleration. The diffusion rate has been adopted as a power-law in energy, and proportional to Bohm diffusion. In addition, an energy independent escape/convective timescale is introduced. The terminal shock is assumed to be point like. It implies that the diffusion radius associated with the lifetime of particles must be larger than the size of that region. For the physical consistency of the performed treatment, SSC losses cannot be significant in the injection region nor synchrotron self-absorption can affect significantly the electron population, since otherwise the latter would be thermalized (Ghisellini et al. 1988). In Chapter 3, we give the expressions to use for solving the problem planned here. We note that the losses to take into account for electrons at the energies we are concerned with are in general synchrotron, Bremsstrahlung and IC in both the Thomson and the Klein-Nishina regimes (see also Chapter 3). Some sort of adiabatic losses in the shock region (Heinz & Sunyaev 2002) have been neglected. From the adopted injection electron energy distribution, diffusion rate and convective timescale, and knowing the dominant types of particle energy losses, the particle

[1]It may happen that the jet terminates smoothly in the ISM (see, e.g., Heinz & Sunyaev 2002).

energy distribution depending on time, position and energy can be derived, as well as its radiative outcome.

6.1.2 Synchrotron and IC emission from jet termination regions

The scenario we face here consists on a persistent jet terminating with a shock against the ISM, generating a continuous injection of relativistic electrons. The jet termination shock is a steady structure injecting relativistic particles in the surrounding medium with a constant rate, similar to the Crab nebula shock between the pulsar wind and the ISM. The distance to the compact object is taken to be $d_* = 10^{17}$ cm, which could be the characteristic length scale for the ISM magnetic and matter fields, as well as for the photon field. This is not the size of the shock itself, which could be, say, $\sim 10^{15}$ cm. This fulfills the "point like" condition stated above for diffusion radii being typically $\sim 10^{16-17}$ cm, as well as the condition of negligible SSC and synchrotron selfabsorption effects. These diffusion radii also allow to treat the present fields as roughly homogeneous for the treatment of particle energy losses.

The particle energy distribution injected in the jet termination region is taken to be a power-law of index p =2.2, normalized to some fraction of the total jet kinetic luminosity. The injection energy of the electrons ranges from 1 MeV to 10 TeV. For calculating the injection maximum energy, we have used $\gamma_{\rm max} = 0.1 q_{\rm e} B(10^{-2} d_*)$. We assume that this process has been active during $\tau_{\rm source} = 3 \times 10^4$ yr (close to a steady state solution). We have adopted a total jet kinetic luminosity similar to those appearing in previous chapters, i.e. $L_{\rm k\ jet} \sim 10^{36-37}$ erg s^{-1}, from which some fraction is transferred to the relativistic leptons in the jet termination point ($L_{\rm k} = 10^{35}$ erg s^{-1}). The diffusion radius is derived from a diffusion coefficient whose normalization is taken to be 1, 10 and 100 times the Bohm diffusion one ($D_{\rm Bohm} = c r_{\rm g}/3$). The magnetic field is fixed to $B = 10^{-4}$ G, slightly higher than the equipartition one with the environment matter, which is in fact compressed by the jet and the stellar wind. The radiation field energy density is $U_{\rm star} \sim 3 \times 10^{-7}$ erg cm^{-3}, assuming a 10^{39} erg s^{-1} star at $d_* = 10^{17}$ cm, whose spectrum peaks at ultraviolet energies. To account for Bremsstrahlung losses, we have adopted a hydrogen nuclei density of $n_{\rm p} = 10$ cm^{-3}, a value slightly higher than the typical ISM one ($\sim$ 0.1 cm^{-3}), which can be understood as related to ISM swept by the high mass star

wind. Bremsstrahlung turns out to be negligible, and its radiative outcome has not been taken into account and only the SEDs of synchrotron and IC emission have been computed. Formulae presented in Chapter 3 have been employed to compute the emissivities and SEDs. The Doppler boosting effect is not accounted due to the isotropization of the relativistic particle population in the observer reference frame by the shock.

We have explored three different cases corresponding to three different diffusive and convective timescales. In one case, the Bohm diffusion rate confines the relativistic electrons within the emitting region making them radiate almost all their energy. The escape or convective time, $\tau_{\rm esc}$, has been adopted larger than $\tau_{\rm source}$. In the other two studied situations, convection removes particles from the emitting region in an energy independent way; the corresponding $\tau_{\rm esc}$ has been fixed to 1 and 100 yr, and the diffusion coefficient to 10 and 100 $D_{\rm Bohm}$ respectively in each case.

Results

We have computed the SEDs corresponding to a termination jet region with the properties described above. In Table 6.1 the adopted parameter values are shown and, in Fig. 6.1, the SEDs from radio to VHE γ-rays, for the non-convective and the convective cases respectively, are shown. When no convective losses are considered, synchrotron emission ranges from radio to ultraviolet frequencies, reaching luminosities from $\sim 10^{31}$ erg s^{-1} in the radio band to several 10^{32} erg s^{-1} at ultraviolet frequencies. For the IC, luminosities of several 10^{33} erg s^{-1} are obtained from X-rays to γ-rays. The SED is steeper than flat at all energies but at optical and ultraviolet frequencies, when Klein-Nishina cooling dominates (see below). In case of mild convective losses, synchrotron radiation reaches luminosities of few 10^{29} erg s^{-1} at radio wavelengths, and $\sim 10^{32}$ erg s^{-1} at ultraviolet frequencies. At X-rays and γ-rays, by IC scattering, luminosities of $\sim 10^{30}$ erg s^{-1} and $\sim 10^{33}$ erg s^{-1} are generated, respectively. Finally, for strong convective losses, synchrotron radiation is emitted with luminosities of $\sim 10^{27}$ erg s^{-1} in the radio band and $\sim 10^{30} - 10^{31}$ erg s^{-1} at ultraviolet frequencies, and IC luminosities range from 10^{28} erg s^{-1} at X-rays to 10^{31} erg s^{-1} at γ-rays. In the scenarios with convection, the SEDs are hard but at VHE, due to the strong decrease in the Klein-Nishina IC cross section. For completeness, the overall electron energy distribution $\times\gamma^2$ for different energies is shown in Fig. 6.2. Next, we discuss different regimes of emission depending on the emitting

Table 6.1: Model parameters

symbol	parameter	value
$L_{\rm k}$	Relativistic leptonic luminosity [erg s^{-1}]	10^{35}
p	Electron power-law index	2.2
d_*	Distance to the star/compact object [cm]	10^{17}
$U_{\rm star}$	Stellar field energy density [erg cm^{-3}]	3×10^{-7}
B	Magnetic field [G]	10^{-5}
$n_{\rm p}$	ISM nuclei density [cm^{-3}]	10
$\tau_{\rm source}$	Source age [yr]	3×10^4
$E_{\rm min}$	Electron minimum energy [MeV]	1
$E_{\rm max}$	Electron maximum energy [TeV]	10

symbol	parameter	No conv.	Mild conv.	Strong conv.
D	Diffusion coeff. [$D_{\rm Bohm}$]	1	10	100
$\tau_{\rm esc}$	Escape time [yr]	$> 3 \times 10^4$	100	1

electron energy and the different factors that affect the spectral shapes.

Discussion

In Fig. 6.1 is seen that, in the radio band, synchrotron emission can be strongly suppressed when low energy particles are removed away by convection, being important however when they are confined within the emitting region. Therefore, a radio detection would probably imply inefficient convection and low diffusion rate. We note that very sensitive instruments, with moderate angular resolution (~ 0.1"), would be required to detect such radio emission, which would appear as a halo around the microquasar. At X-rays, for low diffusion rates and inefficient convection, IC emission could be detectable. This radiation would be detectable for CHANDRA if the source is located at galactic distances, appearing as extended. At energies of about 1−100 GeV, emission is not as much affected by convection as in the radio and X-ray bands. It could be detectable in two cases, the non convective and the mildly convective ones, with the new instruments operating at high-energy and VHE γ-rays (AGILE, GLAST, HESS, MAGIC). It is remarkable that, even without the presence of a bright star, the jet termination region might produce detectable

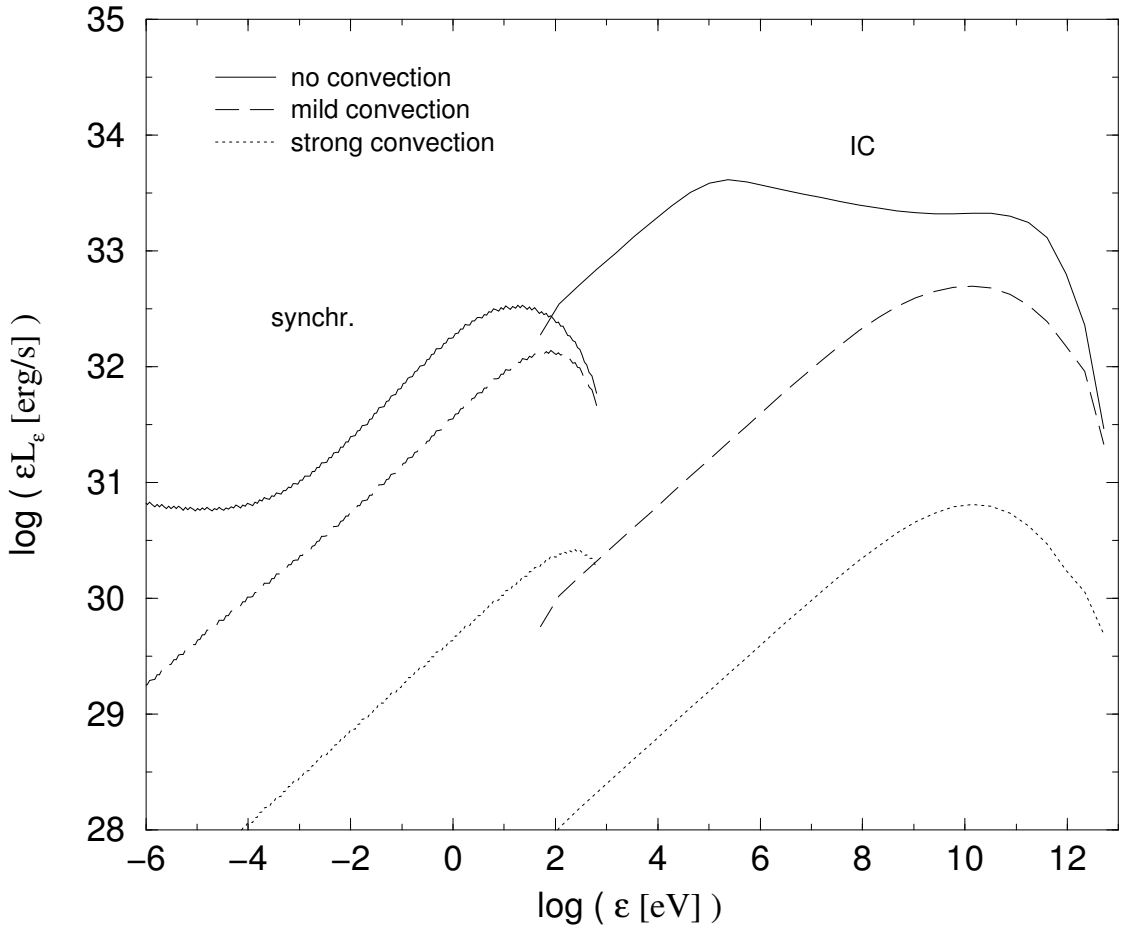

Figure 6.1: Spectral energy distribution from the relativistic electrons forming a halo around the microquasar. The non-convective (solid line), the mildly convective (long dashed line) and the strongly convective cases (dotted line) are shown.

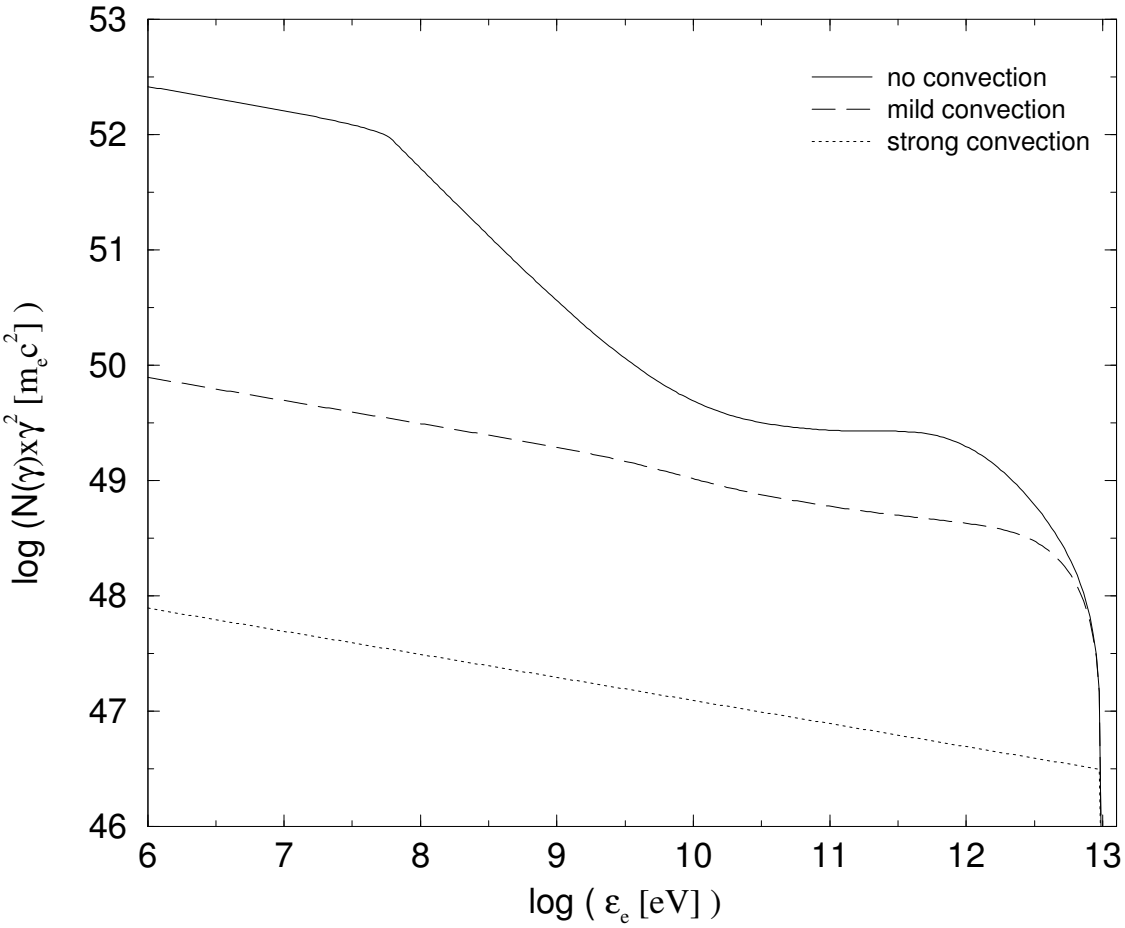

Figure 6.2: Electron energy distribution $N(\gamma) \times \gamma^2$ of the relativistic electrons. Electron energy ($\epsilon_{\rm e}$) units are eV. The non convective (solid line), the mildly convective (long dashed line) and the strongly convective cases (dotted line) are shown.

emission via synchrotron and, for a very dense medium, via Bremsstrahlung.

Regarding the spectral shape, convective and radiative losses are important in this scenario. The former keep the SED shape corresponding to the injected electron energy distribution below the energies at which electrons with lifetime longer than $\tau_{\rm esc}$ emit. Above photon energies emitted by electrons with lifetime $< \tau_{\rm esc}$, the SED is produced by the Thomson IC cooled part of the electron population. It stops at the energies of the Klein-Nishina cooling regime, when the SED hardens again. At higher energies, synchrotron emission can dominate Klein-Nishina cooling making the steepening in the Klein-Nishina IC spectrum more dramatic. This relationship between the particle and the spectral energy distribution is seen when comparing Figs. 6.1 and 6.2. It is worth noting the critical influence of convection and confinement when low energy electron radiation is concerned. In the non convective case, it is remarkable that the lowest energy part of the particle spectrum is uncooled, as is seen in Fig. 6.2. These particles emit via synchrotron far below radio wavelengths, but their IC emission is important at X-rays.

It is unclear where the detected VHE γ-rays are produced in microquasars. On the one hand, strong losses in the jet within the binary system will prevent electrons from reaching very high energies, and strong absorption can prevent the detection of VHE photons (see Chapter 5). On the other hand, at larger distances (i.e. outside the binary system), if the efficiency of internal shocks transferring energy to relativistic leptons in the jet is not high, convection due to jet bulk motion will drive these particles away from the still strong photon fields, either from the star, the accretion process or the synchrotron emission. Therefore, effective confinement around the termination jet region could yield the dominant source at VHE. It is interesting in this sense the hints of variability at timescales similar to the orbital period found by Casares et al. (2005) when folding in phase the HESS data of LS 5039 (Aharonian et al. 2005b). It would point to the small/middle scales as the stronger TeV emitting region in LS 5039.

The emitting size will be related to the diffusion radius of the particles at $\tau_{\rm source}$. In the Bohm diffusion limit and no escape of particles, the particles will fill the emitting region, leaving it after delivering almost all the energy they carried. When convection is significant, some fraction of this energy will be depleted. Actually, the lowest and highest energy particles will be present only in the inner regions of the source, because the low diffusion coefficient for the former, and because the short

lifetime for the latter. In case of effective (energy independent) convective/escape losses, the size of the emitting region at different energies will not only depend on the diffusion coefficient, but also on the convective mechanism. It is reasonable to guess that particles will be also roughly spread in the emitting region though highest energy particles might be also more concentrated towards the injection point for energy independent convection because of their short lifetimes.

From this study on the radiative properties of electrons diffusing from microquasar jet termination shocks, in the environments surrounding these objects, we conclude that it is still possible to have detectable amounts of emission in radio, X-rays and γ-rays, if the source is located at typical galactic distances (i.e. $\sim$ 3–4 kpc) and particle acceleration and confinement are effective.

6.2 Electromagnetic radiation triggered in microquasar bombarded clouds

In this section, we study the interaction between high energy protons released from microquasar jets and nearby molecular clouds. This could generate indirect and steady sources of γ-rays and lower frequency radiation. We develop a time-dependent model that calculates the broadband spectrum of the emission coming out from the proton-proton primary interactions as well as the emission produced by the secondary particles, electrons and positrons, created during the first process. This model takes into account the propagation effects due to both energy-dependent diffusion and the proton-proton interaction energy losses of protons during their travel from the accelerator to the cloud. From this point, when referring to an impulsive microquasar, we mean a transient jet of microquasar interacting with a cloud, and by a continuous microquasar, we mean the same but for a persistent jet. We do not focus here only on a microquasar when in the low-hard state, nor in the case when a high-mass stellar companion is present. This model is applicable to any accelerator, although we focus here on the energetics of microquasars and their two characteristic modes of ejection: persistent or transient.

6.2.1 Protons diffusing in the ISM and cloud interaction

Some microquasars present persistent jets that emit at different energy bands up to hundreds of AU with typical jet kinetic energy luminosities from 10^{37} to 10^{39} erg s^{-1} (e.g. LS 5039, previous chapter, Ribó 2002; SS 433, Marshall et al. 2002, Spencer 1984). Other members belonging to this type of galactic jet sources present very powerful transient ejections that can extend to larger distances and contain several orders of magnitude more jet kinetic energy than the persistent cases (e.g. GRS 1915+105, Mirabel & Rodriguez 1994; Cygnus X-3, Martí et al. 2000).

We assume that the jet has a significant population of protons. These protons can be cold, or cooled during their propagation through the jet due to, i.e., adiabatic losses. They can be cold in the reference frame of the jet, but in the frame of the ISM their energy could be as large as $\Gamma_{\rm jet} m_{\rm p} c^2$. However, they can also be accelerated in the terminal part of the jet owing to shocks between the matter of the jet and the ISM. Therefore, a population of non-thermal protons can extend up to very high energies, and these particles are released since the low magnetic field strength is not enough to keep them within the accelerator. Once the particles break free, they diffuse in the ISM with a diffusion speed depending on their energy and, close to or further from the releasing point, the protons interact with higher density regions like molecular clouds. The interaction between the high energy protons and the interstellar hydrogen nuclei will produce charged and neutral pions (π^-, π^+ and π^0); the first will decay to electrons and positrons and the second to photons. The primary radiation, π^0-decay photons, is in the γ-ray band, but the secondary particles can produce significant fluxes of synchrotron (from radio frequencies to X-rays) and Bremsstrahlung emission (from soft γ-rays to TeV range), and generally with less efficiency, IC emission through interaction with the ambient infrared (IR) photons.

6.2.2 Extended broadband radiation from microquasar nearby clouds

To calculate the emissivity of a source due to the different mechanisms at work, we need to know first what is the energy distribution of the high energy protons at different times and distances from the acceleration site. Therefore, we have assumed

that the injection energy distribution of the accelerated protons follows a power-law plus an exponential high-energy cutoff (or $\gamma_{\rm max}$):

$$f_{\rm p0}(\gamma) = K\gamma^{-p}\exp(-\gamma/\gamma_{\rm max}), \tag{6.1}$$

where p is fixed to 2.2, and K is the normalization constant of the function. For a continuous source, K is obtained assuming a jet of total kinetic luminosity $\sim 10^{37}$ erg s^{-1}, from which a 10% goes to power the relativistic protons in the termination point of the jet, i.e. $L_{\rm k} = 10^{36}$ erg s^{-1}. For an impulsive microquasar, K is derived from the total kinetic energy $E_{\rm k}$=10^{48} erg, released in relativistic particles during a certain period of time, which is to be shorter than the time for those particles to diffuse up to the cloud (a 10^{39} erg s^{-1} relativistic particle source active during $\sim$ 30 yr). $\gamma_{\rm max}$ is determined by the efficiency of the accelerator and is fixed to[2] 10^5, and $\gamma_{\rm min}$ to 1. The energy distribution function with time for both cases, the continuous and the impulsive one can be derived from Eqs. 3.56 and 3.57 presented in Chapter 3 (see also Aharonian & Atoyan 1996). To do so, the properties of the ISM medium around the microquasar are to be given: the density, fixed to $n = 10$ cm^{-3}, and the diffusion coefficient, characterized as a power-law in energy $D = D_0\gamma^{\xi}$ of normalization constant $D_0 = 3\times10^{26}$ and index $\xi = 0.5$. For computing the hadronic emissivity in the cloud, the properties of the interaction region are needed. We assume the presence of a spherical cloud at a distance of 10 pc from the microquasar with 3 pc of radius and target density of $n_{\rm H} = 10^4$ cm^{-3}, magnetic field of $B = 5\times10^{-4}$ G, and photon field energy density $U_{\rm IR\ photons} = 1.6\times10^{-11}$ erg cm^{-3} (10 eV) peaking at infrared energies. With the particle energy distribution computed above and the cloud properties given here, the emission formulae in Chapter 3 are used to compute the SED. Again, no Doppler boosting effect is taken into account, since the proton bulk is not moving relativistically when interacting with the cloud. As explained in Chapter 3, secondary electrons and positrons are produced with rates of about one half those of the γ-rays. This implies that the injection kinetic luminosity of the pairs is about one half of that going to γ-rays, with maximum energies of about $0.1\gamma_{\rm max}m_{\rm p}c^2$ and similar energy distribution than that of photons. From the injection energy distribution of pairs, altogether with the radiative losses affecting secondaries and the evolution of their energy with time, the total energy distribution can be computed. It is worth noting that secondary pairs radiate their energy within the cloud, whereas the protons leave the cloud without suffering sig-

[2]With no significant radiative losses, for an acceleration region size of $\sim 10^{15}$ cm, acceleration efficiency of 0.1 and magnetic field of 10^{-3} G, then $\gamma_{\rm max} \sim 10^5$.

Table 6.2: Model parameters

symbol	parameter	value
D_0	Diffusion coefficient normalization constant [cm^2 s^{-1}]	3×10^{26}
ξ	Diffusion power-law index	0.5
n	ISM medium density [cm^{-3}]	10
$n_{\rm H}$	Cloud density [cm^{-3}]	10^4
M	Mass of the cloud [$M_\odot$]	3×10^4
B	Cloud Magnetic field [G]	5×10^{-4}
$U_{\rm IR\ photons}$	Cloud infrared radiation energy density [erg cm^{-3}]	$1.6{\times}10^{-11}$
p	Power-law index of the high energy protons	2.2
$\gamma_{\rm min}$	Low energy cut-off	1
$\gamma_{\rm max}$	High energy cut-off	10^5
$L_{\rm k}$	Kinetic luminosity for the continuous case [erg s^{-1}]	10^{36}
$E_{\rm k}$	Kinetic energy for the impulsive case [erg]	10^{48}

nificant losses, due to the radiative and diffusion timescales involved. The whole set of model parameters is presented in Table 6.2.

Results

In Figs. 6.3 and 6.4, we show the relevance of the microquasar cosmic rays comparing with the local ones when the parent microquasar is located at 10 pc from the detectors. It shows that for such distances, the effect on the cosmic ray spectrum is very prominent, being the cosmic ray fluxes up to two orders of magnitude above the local value in the impulsive case and at energies >1 TeV. It is worth noting that the same impulsive source at 100 pc would contribute about a 10% of the local cosmic ray spectrum. In Figs. 6.5 and 6.6 we show the SEDs corresponding to the continuous and the impulsive case respectively, computing the former in the steady regime and the latter for different source ages (time after injection): 10^2 yr, 10^4 yr and 10^6 yr. The synchrotron, Bremsstrahlung and neutral pion decay components are shown, and IC is neglected due to the low effectiveness of such mechanism under the considered conditions. As seen from the plots, in both cases synchrotron emission is significant at radio and even X-rays. Also, at γ-rays, neutral pion decay photons

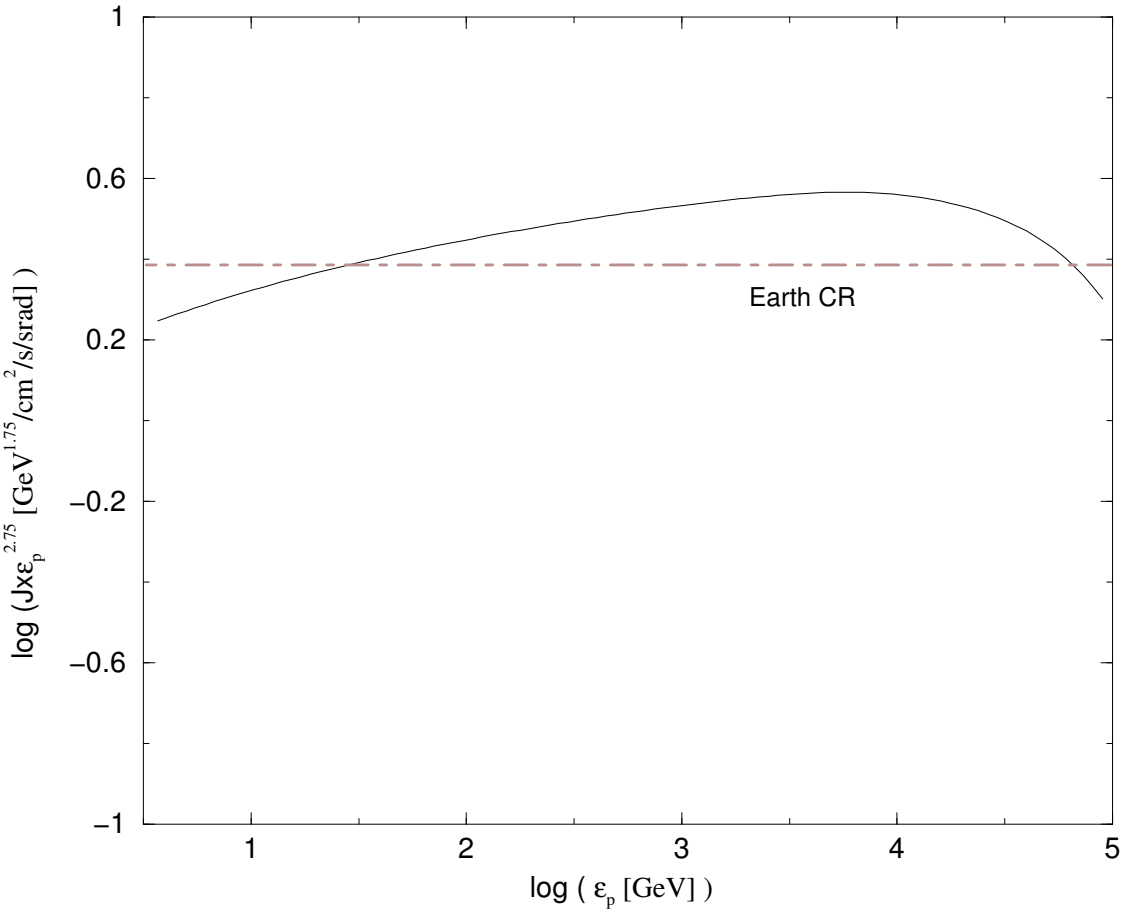

Figure 6.3: Computed cosmic ray energy specific flux ($J(\mathbf{x},\gamma,\Omega)\times\gamma^{1.75} = cn(\mathbf{x},\gamma,\Omega)\times\gamma^{2.75}$) for a continuous source compared with the energy distribution density of the local galactic cosmic rays (thick dot-dashed line). The proton energy ($\epsilon_{\rm p}$) units are GeV.

dominate, but below GeV energies where Bremsstrahlung is significant. The radiative relevance of the different components and their spectral shape depend on the source type and its age when impulsive. Next, we discuss the different observational outcomes depending on the case.

Discussion

If a continuous microquasar releases in the environment some fraction of its energy in form of cosmic rays, and the source is located in cloud crowded regions like the inner spiral arms, as seems to be the case for high-mass microquasars (see Chapter 4), it is likely that high density regions of the ISM will play the role of smoking guns

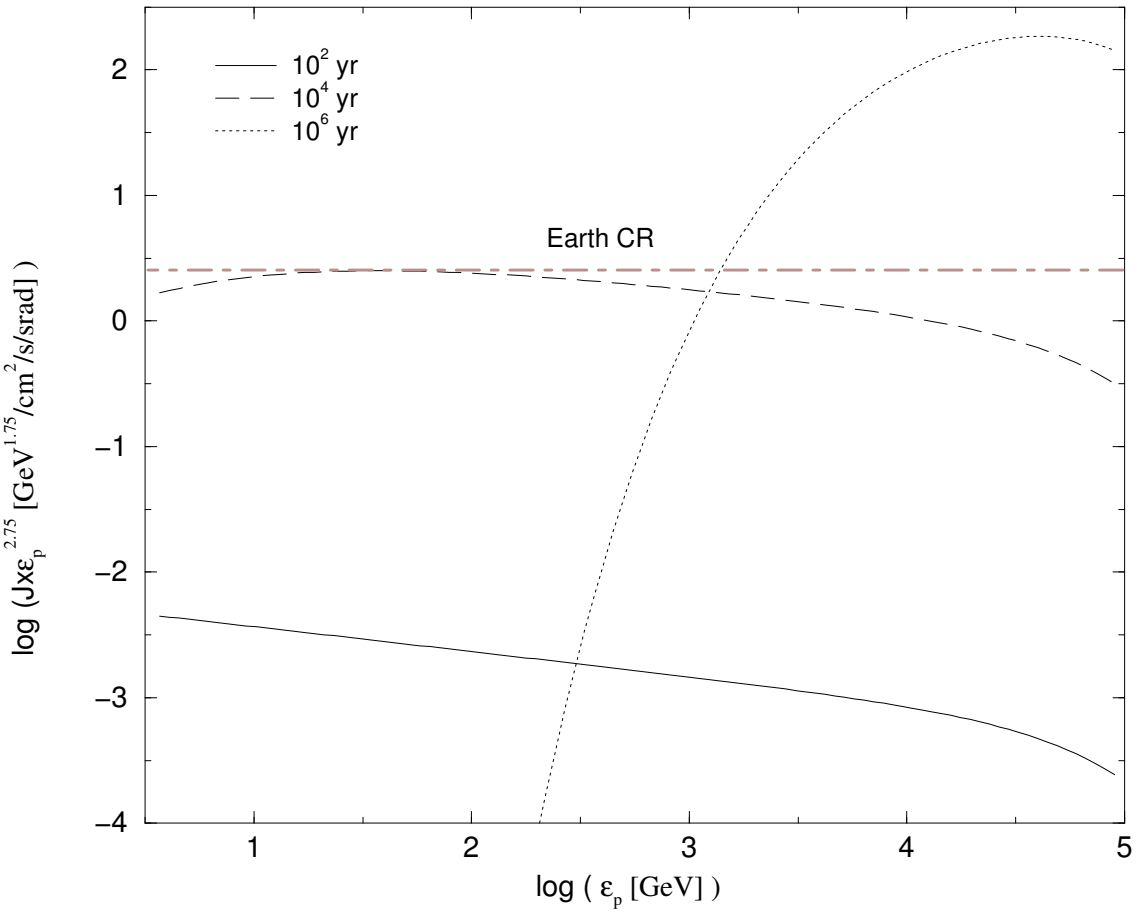

Figure 6.4: The same as in Fig. 6.3 (note that the vertical scales are different) but for an impulsive source and source ages: 100 yr (solid line), 10000 yr (long dashed line) and 100000 yr (dotted line).

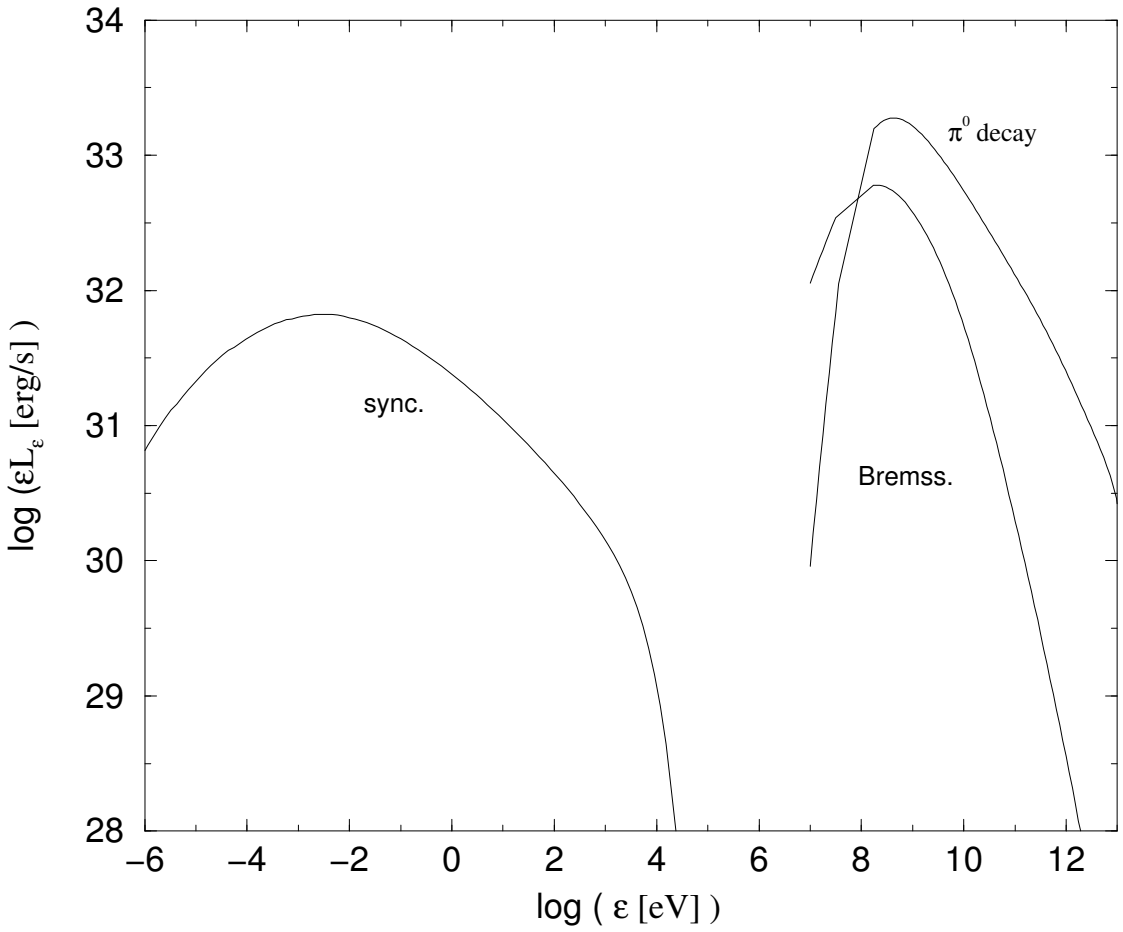

Figure 6.5: Computed spectral energy distribution from radio to TeV energies for a continuous source in the steady regime.

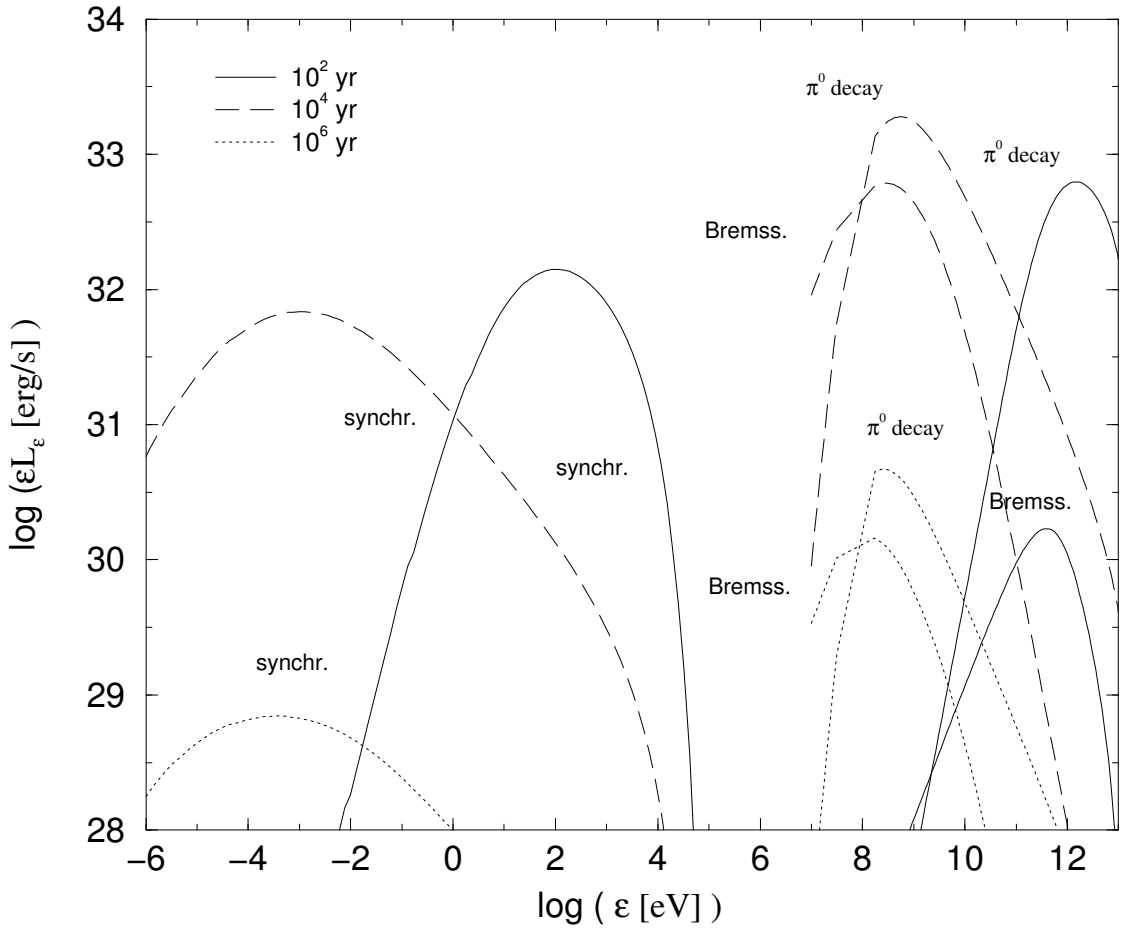

Figure 6.6: The same as in Fig. 6.5, but for the impulsive case and source ages: 100 yr (solid line), 10000 yr (long dashed line) and 100000 yr (dotted line).

of the (present or previous) activity of microquasar jets, as well as there will be a significant bump at the dominant particle energy in the cosmic ray spectrum. The most significant contribution would come from an impulsive source at the higher energies ($\geq$TeV).

If the source is permanent, like microquasar jets during low-hard state, if reaching the steady regime, nearby clouds could be detectable in radio due to synchrotron emission. As in the case of the regions around the jet termination point, instruments should be highly sensitive and too high resolution would not be recommendable in radio ($\geq$ 0.1"). At γ-rays, GLAST could detect emission from the cloud and, with moderately long exposures, ground based Cherenkov telescopes (e.g. HESS, MAGIC) might detect the radiation at $\sim$ 100 GeV. Actually, some of the unidentified EGRET sources in the galactic plane of low or non variability could be microquasar bombarded clouds (Bosch-Ramon et al. 2005).

If the microquasar jet is a transient phenomena but with high activity periods from time to time, the energy of the dominant emission will depend on the age of the source due to energy dependence of the diffusion coefficient. *Young* sources would present mainly VHE emission via neutral pion decay as well as synchrotron X-rays, which might be detectable for long enough exposures. *Old* sources would be more easily detected at radio and GeV energies, with radiation fading as far as the source becomes older.

Consequences of the microquasar/cloud scenario could be the detection at radio wavelengths and perhaps X-rays from two sources, one being faint and quite extended, the bombarded cloud, the other being brighter and more compact (though perhaps extended as well), the microquasar itself. Something similar might occur at X-rays, and even at γ-rays, if the microquasar is powerful and can power emission from a cloud separated enough to be distinguished by the instruments observing at GeV and $\sim$ 100 GeV (few arcminutes for instruments like GLAST, HESS or MAGIC). Relevant information could be extracted from observing a source as those modeled here, like the kinetic energy released in the ISM, the cloud magnetic field and the target density. In case there were two or more sources of emission powered by a nearby microquasar, the diffusion coefficient of the ISM in the region could be inferred (Bosch-Ramon et al. 2005).

We conclude that, besides being possible sources of galactic cosmic rays, microquasars could be powering extended and yr-timescale steady sources emitting from

radio to TeV energies in the galactic plane. In case some studies pointing to microquasars as non negligible producers of cosmic rays (Heinz & Sunyaev 2002, Fender et al. 2005) would be right, a significant number of unidentified and extended GeV and/or TeV sources in the galactic plane (Aharonian et al. 2005a) could be powered by microquasars.

Bibliography

Aharonian F.A., Atoyan A.M., May 1996, A&A, 309, 917 150, 160

Aharonian F.A., Atoyan A.M., Oct. 2000, A&A, 362, 937 150

Aharonian F.A., Akhperjanian A.G., Aye K.M., et al., Mar. 2005a, Science, 307, 1938 167

Aharonian F.A., Akhperjanian A.G., Aye K.M., et al., Jul. 2005b, Science, 309, 746 157

Atoyan A.M., Aharonian F.A., Völk H.J., Sep. 1995, PhRvD, 52, 3265 150

Bell A.R., Feb. 1978, MNRAS, 182, 443 149

Bosch-Ramon V., Aharonian F.A., Paredes J.M., Mar. 2005, A&A, 432, 609 150, 166

Bosch-Ramon V., Khangulyan D., Aharonian F., Paredes J.M., 2006, in preparation 150

Casares J., Ribó M., Ribas I., et al., Dec. 2005, MNRAS, 364, 899 157

Corbel S., Fender R.P., Tzioumis A.K., et al., Oct. 2002, Science, 298, 196 149

Fender R.P., Maccarone T.J., van Kesteren Z., Jul. 2005, MNRAS, 360, 1085 167

Gallo E., Fender R., Kaiser C., et al., Aug. 2005, Nature, 436, 819 149

Ghisellini G., Guilbert P.W., Svensson R., Nov. 1988, ApJ Letter, 334, L5 151

Ginzburg V.L., Syrovatskii S.I., 1964, The Origin of Cosmic Rays, New York: Macmillan, 1964 150

Heinz S., Jan. 2006, ApJ, 636, 316 149

Heinz S., Sunyaev R., Aug. 2002, A&A, 390, 751 150, 151, 167

Kotani T., Kawai N., Matsuoka M., Brinkmann W., Aug. 1996, PASJ, 48, 619 149

Marshall H.L., Canizares C.R., Schulz N.S., Jan. 2002, ApJ, 564, 941 149, 159

Martí J., Paredes J.M., Peracaula M., Dec. 2000, ApJ, 545, 939 159

Martí J., Pérez-Ramírez D., Garrido J.L., Luque-Escamilla P., Paredes J.M., Aug. 2005, A&A, 439, 279 149

Mirabel I.F., Rodriguez L.F., Sep. 1994, Nature, 371, 46 159

Mirabel I.F., Rodriguez L.F., Cordier B., Paul J., Lebrun F., Jul. 1992, Nature, 358, 215 149

Ribó M., Nov. 2002, Ph.D. Thesis, Univesitat de Barcelona 159

Spencer R.E., Aug. 1984, MNRAS, 209, 869 159

Strong A.W., Moskalenko I.V., Reimer O., Jul. 2000, ApJ, 537, 763 150

Torres D.F., Dec. 2004, ApJ, 617, 966 150

Wang X.Y., Dai Z.G., Lu T., Jul. 2003, ApJ, 592, 347 149

Chapter 7

Discussion and conclusions

7.1 Discussion

Microquasar jets can be studied, theoretically and observationally, following a comprehensive approach accounting for their intrinsic emission, like the jet broadband radiation and its variability properties, and for the extended broadband emission of the escaping electrons and protons accelerated in the jets. We note that the results obtained from applying the cold matter dominated jet model, although not founded on first principles, are pretty accurate at the present stage of our observational knowledge. Moreover, the cold matter dominated jet model, although used here to describe the low-hard state jet, can be modified to embrace other variants of outflows. For instance, hotter and faster outflows modeling the ejections during the transition to the high-soft state could also contain both a radiatively inefficient cold population and a radiatively efficient relativistic population heated by e.g. shocks with former/latter ejections or external matter. In such cases, modifying the jet radius dependence with z, it would be possible to include phenomenologically some sort of external medium interaction and collimation. Moreover, extra particle heating could be introduced.

In the explored scenario, the jet is studied in two parts, one part where jet matter is evolving without suffering external influences, radiating some part of its internal kinetic energy *by internal causes*; another part where the jet terminates interacting with the ISM, releasing its energy via a shock heating matter and producing a non thermal distribution of electrons and protons. This picture could be too simple, as

shown by the complex extragalactic jet morphologies at different scales. Nevertheless, it is useful at the present state of observational knowledge for deriving testable detailed predictions in the presented scenario. We comment these predictions below ordering them in different energy bands, discussing also briefly the impact of a possible numerous γ-ray microquasar population in the Galaxy. It is implicit that the predictions refer to what could be observed by the instruments already at work or forthcoming at different wavelengths, from radio to TeV, including also cosmic rays and neutrinos.

Although radio observations showed the microquasar jets for the first time, in fact radiation at this energy band might not be detected coming from the jet well within the binary system due to synchrotron self-absorption. In that region, for systems with dense photon and/or matter fields, radio emission would be produced by secondary pairs generated by photon-photon absorption and proton-proton collisions, presenting a halo shape. The spectral properties of such emission would depend on, besides the energy losses, the diffusion and convection properties in there. Potentially, variability could be fast, with timescales of about or less than minutes. Outside the binary system, at $\sim$ 1 AU, radio emission could be significant and optically thin. In such region, still within the core of the sources detected with present radio interferometers, the spectral index would hint whether particle acceleration is taking place. In the simple scenario considered here, particles keep their injection spectrum all along the jet, although it is likely not the case. Since observations of LS 5039 and LS I +61 303 (when not in outburst) show that radio emission corresponds to an uncooled electron distribution, the uncooled emission must come from a region which is left by radiating electrons before they cool. The lack of angular resolution precludes right now to know what jet part is dominant emitting this radiation. The variability timescales not far from the binary system could be of several minutes to one hour. The considerations made for parts of the jet at distances similar or a bit larger than the size of the binary system are also applicable for scales $\sim 10^{15}$ cm, but variability will be of timescales one or two orders of magnitude longer. Therefore, precision interferometry can tell us where particle acceleration is taking place and, otherwise, variability can hint it, i.e. large variability and strong emission peaks and dips will come from the inner parts, little variability and flux smoothing will be originated in the outer parts. Actually, LS 5039 radio variability seems to point to the second possibility. At the largest scales, where ISM interaction might be important, radio emission from the jet and the interaction region is to be disentangled. To separate both radio components, deep observations

with a low frequency sensitive radio interferometer are required, although with moderate angular resolution. Emission should be steady, with different spectral indices, likely harder around the interaction point than in the surroundings.

Hard X-rays can be produced by the accretion processes although the jet could also contribute or even dominate. Regarding a massive binary system, the detection of correlated spectral and flux behavior at hard X-rays and TeV energies would show that the former is coming from the jet. It would be explained by the same population of electrons emitting synchrotron and scattering stellar photons. This is so because of the highest energy particle would not be found at the base of the jet, where magnetic field is likely to dominate losses, but at distances $\sim 10^{11}$–10^{12} cm. At such distances, synchrotron emission would reach the highest energies, and stellar IC interaction would be also dominant in its energy range. The hard X-ray/TeV correlation would be likely smoothed at some extent by the photon-photon absorption within the binary system. Also, contribution in the TeV due to SSC and accretion photon IC might also affect the correlation though it would be much more photon-photon absorbed than the star IC component. In any case, even for a weak stellar photon field, the other IC components and synchrotron radiation would also appear correlated at the energies at which synchrotron emission from the base of the jet is mainly radiated, significantly lower than the synchrotron high energy cutoff. We note that because of particle maximum energy is not likely the same situation in the base of the jet and further up, emission in one or other region will present some observable spectral differences, as seen in Chapter 5. The extension of the X-ray spectrum up to larger energies, at least several MeV γ-rays, would also be a strong hint that X-rays come from a non thermal jet instead of the accretion process. Because of the probable decrease of the magnetic field with distance, jet synchrotron emission (from the microquasar itself) is likely to be significant only within the binary system. Extended X-rays could be observed but only at the largest scales and by external interaction, where jet core emission would not overcome them (i.e. where it could be resolved).

γ-rays can be originated at the base of the jet but limited by the energy losses. Therefore, the SSC mechanism will be constrained by these strong energy losses since it occurs basically in the base of the jet, and a high mass system appears more likely to be detected at VHE due to the presence of the stellar strong photon field. Otherwise, emission in the GeV could be observed from both a high mass and a low mass system, due to disk/corona photon IC, star IC or SSC for the former, and

disk/corona photon IC and SSC for the latter. Variability imposes upper limits to the size of the emitting region. Extremely fast variability ($\sim$ 1 s or less) would imply an origin close to the base of the jet, pointing to SSC or IC with disk/corona photons. However, the required temporal resolution is far shorter than that of the present or next instruments working at GeV and TeV energies. If the lightcurve were properly sampled, smoothed variations in the flux would point to star IC radiation origin at the jet intermediate scales, out of the photon-photon opaque region within the binary system. This could also be linked to the generation of significant optically thin uncooled radio emission. The fact that the TeV emission observed by HESS seems to be more variable than radio emission could be explained by the much longer lifetime of the radio emitting electrons.

In the scenario treated here relativistic protons could produce also VHE emission via proton-proton interactions, although we have not given quantitative predictions for this case, for which we have referred to the literature. Nevertheless, the Bremsstrahlung fluxes presented in Chapter 5 give an idea of what the proton-proton emission component[1] would be in our model if the kinetic energy in relativistic protons were similar to that in relativistic electrons. In any case, it is a very crude estimate, and does not prevent that in some cases hadronic emission above 1 GeV could be dominant via particularly dense targets and/or hadronic acceleration, yielding also significant low energy emission from secondaries and neutrinos, the latter with moderate fluxes and being their detection presently under debate.

The contribution from microquasars to the non thermal galactic cosmic ray spectrum is likely to be negligible in the local environment, because no microquasar is expected to be as close from the Earth as ≤ 100 pc. The microquasar non thermal cosmic ray contribution would be significant if the number of microquasars in the Galaxy were about two orders of magnitude larger than that presently known, which might be the case. However, this relies on the energetic estimates made here. The amount of jet kinetic energy going to non thermal cosmic rays is strongly model dependent, and only rough estimates can be done from the non thermal luminosities likely generated in the jets/blobs of $\sim$ 10 microquasars (accounting also for discrete ejections), too few to obtain robust statistical studies yet. Furthermore, SS 433, LS 5039 and LS I +61 303, the half of the known high mass microquasars, are strongly underluminous at X-rays when comparing with their Eddington luminosities and present powerful jets. This shows how difficult is to derive estimates of

[1]Because of the similar lifetimes and target densities for both processes.

the overall jet kinetic energy from the X-ray luminosity, even when it could come from the jet.

Although the number of known microquasars is small, it is likely that many variable γ-ray sources to be detected in the future will correspond to microquasars with faint counterparts at lower energies. Despite of being faint, the lower energy counterparts could be identified due to the arcminute angular resolution of the new γ-ray instruments. Furthermore, some non variable γ-ray sources in the galactic plane could be associated with these objects. In case microquasars were properly characterized as a γ-ray population, which seems very probable, it would be possible to study in deep all the predictions provided in this work, allowing for a far reaching step forward in modeling. Although for many of these objects the jets might not be powerful enough to produce associated surrounding emission, a substantial fraction of the whole population could be responsible of nearby radio, X-ray and γ-ray sources with little or none variability. It would be specially true for regions of matter clumping like molecular clouds, specially toward the inner spiral arms and other regions of the galactic plane.

7.2 Conclusions

- We can explain the detection of γ-rays at the fluxes detected by EGRET in LS 5039 and LS I +61 30 with a reasonable energy budget for the relativistic particles in the jet larger than that required to explain just radio emission. The high mass companions in both systems provide with the seed photons to suffer IC scattering producing the emission at the energies observed, for electron energies similar to those required for synchrotron radio emission.

- We show that, when the magnetic field is taken into account at the base of the jets, the high-energy γ-ray radiation observed in LS 5039 and LS I +61 303 can also be produced via SSC.

- The γ-ray flux variability in microquasars, at the timescales achievable by the present γ-ray instruments, can be produced via variations in the stellar photon field and the accretion rate induced by orbital eccentricity, as well as via precession.

- We conclude that microquasars could be behind a significant fraction of the unidentified variable EGRET sources in the galactic plane.

- We find that the jet could dominate at X-rays via IC radiation for systems with faint disk and corona.

- We show that significant γ-ray emission up to GeV energies could be produced when counting only the presence of disk/corona photons.

- We conclude that acceleration of the jet electrons out of the binary system appears to be necessary to explain the observed extended radio emission, provided that significant energy losses are to take place in the inner jet regions via synchrotron, star IC and SSC processes.

- We show that mildly relativistic jets are more likely in the context of cold matter dominated jet model when the accretion/ejection energy balance is considered, at least when jets are not pointing toward the observer, since the jet must carry enough matter to radiate significantly. Thus, if the matter content of the jet is large and the energy is limited by the accretion reservoir, its speed cannot be strongly relativistic.

- We find that the cold matter collimation mechanism appears to be consistent with the overall picture; this mechanism seems to be at the moment more justified from such point of view than others as external or magnetic field collimation.

- We can reproduce the overall spectrum emission detected in LS 5039 from radio up to VHE with the introduction of particle acceleration and photon-photon absorption. Some findings are that X-rays could come mainly from the jet, high-energy γ-rays would be enhanced when the compact object is in opposition to the observer, VHE γ-rays could be strongly absorbed during periastron passage, and Bremsstrahlung emission would be hardly relevant.

- We show that the introduction of an anisotropic and slow equatorial wind (as well as photon-photon absorption itself) could explain some observed variability features of LS 5039.

- We put forward that the modeling of LS 5039 points out that the optically thin nature of the radio spectrum and the relatively high VHE flux might be related to an increase of the relativistic leptons at intermediate jet scales.

- We conclude that, when the cold matter dominated jet model is applied to 1E 1740.7−2942, it can give a proper description of the detected broadband spectrum, favoring the corona as the source of hard X-rays and predicting that high-energy and VHE γ-rays might also be detectable by the new instruments working at these energies.

- We show that, in case a significant fraction of the relativistic electrons accelerated in microquasar jets left its accelerator at large distances from the compact object, extended radio emission, as well as X-ray and γ-rays for a high mass system, could be produced at detectable levels, this emission being steady for timescales shorter than ~ 1 yr.

- We find that, in case relativistic protons left the jet that interacts with the surrounding medium, the cosmic ray flux in the nearby regions would be enhanced, which shows the relevance of microquasars as cosmic ray accelerators.

- We conclude that, if dense ISM regions like molecular clouds were close to a microquasar (i.e. few pc), which could be common in the inner regions of the galactic plane, significant emission from GeV to TeV energies would be generated via neutral pion decay from proton-nuclei collisions. Furthermore, radio to X-ray synchrotron and soft γ-ray Bremsstrahlung from charged pion pairs could also be produced. These sources would be extended and steady at several yr timescales.

Therefore, the work presented in this thesis shows the richness of the physics involved on the study of microquasars, telling us that the study of the microquasar phenomenon has to cover a long way before being roughly understood in a global manner. In any case, because of the exciting prospects in both the theoretical and the observational fields, the journey toward a good understanding of these objects promises very interesting discoveries in the near future, having already provided a first taste to those who are taking the first steps in the world of the multiwavelength and the multi-particle approach to microquasars.